Informatics Control Measurement
in Economy and Environment Protection

1/2018

INFORMATYKA AUTOMATYKA POMIARY

www.e-IAPGOS.pl

W GOSPODARCE i OCHRONIE ŚRODOWISKA

ISSN 2083-0157

Kwartalnik Naukowo-Techniczny

fot. archiwum CzUN

Czerniowiecki Uniwersytet Narodowy
im. Jurija Fedkowycza
(Czerniowce, Ukraina)

1/2018

styczeń – marzec

Wydanie pod redakcją naukową
prof. dr hab. inż. Waldemara Wójcika

INFORMATYKA
AUTOMATYKA
POMIARY

W GOSPODARCE i OCHRONIE ŚRODOWISKA

Informatics Control Measurement in Economy and Environment Protection

p-ISSN 2083-0157, e-ISSN 2391-6761, www.e-iapgos.pl

INTERNATIONAL PROGRAMME COMMITTEE – RADA PROGRAMOWO-NAUKOWA

EDITORIAL OFFICE – REDAKCJA

Redakcja czasopisma
Informatyka, Automatyka, Pomiary w Gospodarce
i Ochronie Środowiska
Instytut Elektroniki i Technik Informacyjnych
Politechnika Lubelska
ul. Nadbystrzycka 38A
20-618 Lublin
tel. +48 81 53 84 309
fax: +48 81 53 84 312
www.e-iapgos.pl
iapgos@pollub.pl

PUBLISHER – WYDAWCA

Politechnika Lubelska
ul. Nadbystrzycka 38D
20-618 Lublin
tel. +48 81 53 84 100
www.pollub.pl

PRINTING HOUSE – DRUKARNIA

Agencja Reklamowa TOP
87-800 Włocławek
ul. Toruńska 148
tel. +48 54 423 20 40
nakład: 100 egzemplarzy

OTHER INFORMATION – INNE INFORMACJE

Czasopismo jest indeksowane w bazach:

BazTech:	baztech.icm.edu.pl
IC Journals Master List:	www.journals.indexcopernicus.com
Google Scholar	scholar.google.pl

Czasopismo znajduje się w wykazie czasopism naukowych opublikowanym w Komunikacie Ministra Nauki i Szkolnictwa Wyższego z dnia 9 grudnia 2016 r. – część B, pozycja 685 – z liczbą punktów przyznawanych za publikację równą 7.

Zasady publikowania artykułów, przygotowania tekstów, zasady etyczne, procedura recenzowania, wykazy recenzentów oraz pełne teksty artykułów dostępne są na stronie internetowej czasopisma:

www.e-iapgos.pl

W celu zwiększenia oddziaływania czasopisma w środowisku naukowym redakcja zaleca:

- w artykułach publikowanych w IAPGOS cytować artykuły z renomowanych czasopism międzynarodowych (szczególnie indeksowanych w bazach Web of Science oraz Scopus) używając oficjalnych skrótów nazw czasopism,
- w artykułach publikowanych w innych czasopismach (zwłaszcza indeksowanych w bazach Web of Science oraz Scopus) cytować prace publikowane w IAPGOS – zwłaszcza posługując się numerami DOI, np.:
  Kluszczyński K. *Modelowanie – umiejętność czy sztuka?* Informatyka, Automatyka, Pomiary w Gospodarce i Ochronie Środowiska – IAPGOS, 1/2016, 4–15, DOI: 10.5604/20830157.1193833.

CONTENTS – SPIS TREŚCI

DOI: 10.5604/01.3001.0010.8541

DETERMINATION OF THE EFFICIENCY FACTORS OF THE ABSORPTION AND SCATTERING OF NICKEL NANOPARTICLES

Oleksandr Machulianskyi[1], Bohdan Babych[1], Viktor Machulianskyi[2]
[1]NTUU Igor Sikorsky Kyiv Polytechnic Institute, Department of Microelectronics, [2]NTUU Igor Sikorsky Kyiv Polytechnic Institute, Institute for Applied System Analysis

Abstract. *In the dipole approximation for the spherical nickel nanoparticle with a diameter $D_0 = 2.5 \div 7$ nm in the spectral range from 0.2 to 1.1 μm at T = 300 K, efficiency factors of the absorption K_a and scattering K_s were determined with the help of the experimental values of the complex specific electrical polarizability. Numerical calculations of the K_a and K_s of the nickel nanoparticles were carried out in accordance with the theories of classical and quantum dimensional effects. It was shown that it is impossible to explain the photoabsorption of nickel nanoparticles by the intraband (Drude) type of absorption even taking into account classical or quantum dimensional effects.*

Keywords: nickel nanoparticles, optical parameters

WYZNACZANIE WSPÓŁCZYNNIKÓW EFEKTYWNOŚCI ABSORPCJI I ROZPRASZANIA NANOCZĄSTEK NIKLU

Streszczenie *Na podstawie wartości eksperymentalnych zespolonej właściwej polaryzacji elektrycznej zostały wyznaczone współczynniki efektywności absorpcji K_a i rozpraszania K_s w przybliżeniu dipolowym dla sferycznej nanocząstki niklu o średnicy $D_0 = 2{,}5 \div 7$ nm w zakresie spektralnym od 0,2 do 1,1 μm przy T = 300 K. Wykonano obliczenia numeryczne K_a i K_s nanocząstek niklu na podstawie teorii efektów klasycznego i kwantowego. Wykazano, że fotoabsorpcji nanocząstek niklu nie można wyjaśnić absorpcją wewnątrzstrefową (Drudowską), nawet biorąc pod uwagę efekty klasyczne lub kwantowe.*

Słowa kluczowe: nanocząstki niklu, parametry optyczne

Introduction

Significant interest in the metal nanoparticles, in particular nickel, arise from their use in the nanocomposite systems, which found a wide practical application in the information systems [1], switching devices of the nonlinear optics [2], power engineering [3].

The increasing need for such materials determines the necessity of the investigation of the frequency and size dependences of the electromagnetic parameters of the nanosized particles and nanocomposite systems based on them. Among them, the phenomenon of anomalous photoabsorption of such structures is essential in practical terms. Because of the limited experimental data in the literature on the size dependences of the electromagnetic parameters of the nickel nanoparticles, they are generally identified with values in the macroscopic volumes of metals or theoretical dimensional dependences [1, 4]. At the same time, information on theoretical dimensional dependences is very contradictory and, as follows from [5, 6], most of these theoretical models are not able to describe the dimensional changes in their optical parameters that are observed during the reduction of the spherical metal particles radius. In [6], we determined the complex specific electrical polarizability of nickel nanoparticles with the help of the data of the spectral and electron microscopic investigations of the island nickel films with a statistically homogeneous structure on the glass substrates and on the basis of the exact solution of the inverse problem of the spectrophotometric systems of Rosenberg's equations [7].

The properties of nanostructured materials are determined by their microstructure, processes of the absorption and scattering of the optical radiation by nanoparticles, effects caused by the dimension of the nanoparticles and their interaction with each other, as well as the influence of the external environmental factors on them, etc. [8, 9]. Analysis of the experimental information about the optical characteristics indicates the determining effect of the real distribution function of the nanoparticles by size on their properties. In connection with this, we have improved the experimental and analytical method for determining the values of the complex specific electrical polarizability of the nanoparticles taking into account the statistics of their distribution by size, which made it possible to increase the accuracy of obtaining the experimental values of optical parameters [10].

So, in this connection it is necessary to evaluate the experimental values of the photoabsorption parameters of the nanoparticles and to analyze the nature of their dimensional changes in accordance with the theories of classical and quantum dimensional effects.

The purpose of this paper is to evaluate the absorption and scattering efficiency factors of the nickel nanoparticles in the spectral range of wavelengths of 0.2 ÷ 1.1 μm on the basis of the experimental values of their optical parameters.

1. Calculation procedure

According to the Mi theory [1, 11], the efficiency factors of the absorption (K_a) and scattering (K_s) of the nanoparticle are determined by the following expressions:

$$K_a = \frac{8\pi}{3} \cdot \frac{R_0}{\lambda} \cdot \sqrt{\varepsilon_m} \cdot a_2 , \tag{1}$$

$$K_d = \frac{128}{27} \cdot \pi^4 \cdot \frac{R_0}{\lambda^4} \cdot \sqrt{\varepsilon_m} \cdot \left(\alpha_1^2 + \alpha_2^2\right), \tag{2}$$

where R_0 – particle radius, ε_m – dielectric conductivity of the medium, λ – the light wavelength, α_1, α_2 – the real and virtual parts of the specific complex electrical polarizability of the particle.

The expressions (1) and (2) are valid with the following approximations:

- particle shape is spherical;
- the particle size ($D_0 = 2R_0$) is much smaller than the length of the electromagnetic wave in the given medium ($D_0 << \lambda$) – the dipole approximation;
- metal particles are randomly distributed over the volume of the dielectric matrix;
- volume concentration of the particles is small and the distance between particles is much larger than their dimensions (a system of the non-interacting particles).

According to the classical electromagnetic theory [12], for the specified approximations the complex specific electrical polarizability of the particle can be described by the following relations:

$$\alpha_1 = \frac{3\left[(\varepsilon_1 - \varepsilon_m)(\varepsilon_1 + 2\varepsilon_m) + \varepsilon_2^2\right]}{(\varepsilon_1 + 2\varepsilon_m)^2 + \varepsilon_2^2}, \tag{3}$$

$$\alpha_1 = \frac{9\varepsilon_m \varepsilon_2}{(\varepsilon_1 + 2\varepsilon_m)^2 + \varepsilon_2^2}, \tag{4}$$

where $\varepsilon_1 = n^2 - k^2$ – the real part of the complex dielectric conductivity of the particle; $\varepsilon_2 = 2nk$ – the virtual part of the complex dielectric conductivity of the particle; n, k – respectively, the refractive and absorption indices of the particle.

According to [12], the relations (1) – (4) are valid for the values of ε_1 and ε_2 satisfying the inequality $2\pi n R_0 / \lambda << 1$. This condition, due to the phenomenological meaning of the dielectric conductivity, allows to apply the indicated expressions for the values of ε_1, ε_2, depending on D_0 for the sizes of the investigated nanoparticles D_0 < 10 nm. Analysis of the relations (1) and (4) shows that in the presence of the dispersion peaks ε_2, the corresponding bands should appear also on the spectral curves α_2 and K_a. The resonance peak in the spectra of the α_2 and K_a can also arise at $\lambda = \lambda_R$ and at the monotonic change of the ε_2 with λ, if among the values of the ε_1, the equality $\varepsilon_1(\lambda_R) = -2\varepsilon_m$ is realized for ε and ε_m measured relatively to the air. The resonance in the dispersion α_2 and K_a determined by the criterion $\varepsilon_1(\lambda_R) = -2\varepsilon_m$ is called the dipole [5, 12].

In the theories of classical [13] and quantum [14] dimensional effects in the small spherical metal particle, the dipole resonance (caused, from the phenomenological point of view, by the jump of the values of ε on the surface of the particle) is associated, at the microscopic consideration of the problem, with a surface plasma resonance of the conduction electrons.

The dimensional dependences of the real $\varepsilon_1(\omega, R_0)$ and virtual $\varepsilon_2(\omega, R_0)$ parts of the dielectric conductivity of an ultradisperse particle are approximated by the expressions:

$$\varepsilon_1(\omega, R_0) = \varepsilon_{1v}(\omega) + \varepsilon_{1s}(\omega, R_0), \tag{5}$$

$$\varepsilon_2(\omega, R_0) = \varepsilon_{2v}(\omega) + \varepsilon_{2s}(\omega, R_0). \tag{6}$$

where: $\omega = 2\pi c/\lambda$ – the cyclic frequency of the electromagnetic radiation; c – the speed of light; $\varepsilon_{1v}(\omega)$ and $\varepsilon_{2v}(\omega)$ – respectively, the values of the real and virtual parts of the dielectric conductivity of a massive (in the macroscopic volume) metal; $\varepsilon_{1s}(\omega, R_0)$, $\varepsilon_{2s}(\omega, R_0)$ – respectively, the values of the real and virtual parts of the dielectric conductivity of the particle that take into account the dimensional changes caused by the influence of the particle surface on the conduction electrons in it.

The classical dimensional effect [13] is based on the assumption about the diffuse nature of the scattering of electrons by the particle surface and the quasicontinuity of the energy spectrum of the conduction electrons. In this case, the impact of the particle size is manifested in limiting the average value of the length of the free path of conduction electrons by the surface of the particle (its diameter).

In [1] it was shown that in the case of the small particles of a spherical shape, the average length of the free path of conduction electrons is expressed through the effective length of the free path l_{eff}, which is connected to the other parameters of the particle by the relation:

$$l_{eff}^{-1} = l_\infty^{-1} + R_0^{-1}, \tag{7}$$

where l_∞ – the average length of the free path of conduction electrons in the macroscopic volumes of metals (massive metal).

In this case, it is also legitimate to establish an effective relaxation time of conduction electrons in the particle, depending on its size:

$$\tau_{eff}^{-1} = \tau_\infty^{-1} + \frac{v_F}{R_0}, \tag{8}$$

where $\tau_\infty = \dfrac{l_\infty}{v_F}$ – the relaxation time of the electrons in a massive metal; v_F – the electron velocity on the Fermi surface.

In the [13], under the assumption about the applicability of the theory of the optical properties of the Drude's metals [1] for describing the intraband absorption of a particle within the framework of the notions about the classical dimensional effect and under the condition that ω significantly exceeds the frequency of concussions of the electrons in a massive metal, the following expressions were obtained:

$$\varepsilon_{1s}(\omega, R_0) = 0, \tag{9}$$

$$\varepsilon_{2s}(\omega, R_0) = \frac{\omega_p^2}{\omega^3} \cdot \frac{v_F}{R_0}, \tag{10}$$

where ω_p – the frequency of the volume plasmous resonance for a massive metal.

$$\omega_p = \sqrt{\frac{4\pi n_0 e^2}{m_0}} \tag{11}$$

where n_0, m_0 – the number, the effective mass of the free electrons; e – the electron charge.

In the theory of the quantum dimensional effect, dimensional changes are manifested in the splitting of the continuous energy spectrum of electrons in the conduction band into the discrete states. The dependence $\varepsilon_{2s}(\omega, R_0)$ takes the form [14]:

$$\varepsilon_{2s}(\omega, R_0) = \frac{32 e^2 f(v)}{\pi \eta \omega R_0} \tag{12}$$

where

$$f(v) = v^{-3} \int_{v_0}^{1} \sqrt{x^3 (x + v)}\, dx, \tag{13}$$

where $\hbar$ – Planck constant; $v = \dfrac{\eta \omega}{E_F}$, $v_0 = 1 - v$ for $v < 1$ and $v_0 = 0$, when $v > 1$; E_F – Fermi energy.

In the [14] $\varepsilon_{1s}(\omega, R_0)$ is not explicitly represented.

2. Results and discussion

The values of the complex specific electrical polarizability of the nickel nanoparticles were determined by the improved experimental analytical method taking into account the statistics of the nanoparticle distribution by size [11] with the help of the measured transmission and reflection spectra in the wavelength range $\lambda = 0.2 \div 1.1$ μm of the island nickel films on the quartz substrates. The island films represented a morphological microstructure in the form of the monolayers of the isolated from each other spherical nickel nanoislands with a surface concentration $N_0 = (0.8 \div 2.0) \times 10^{12}$ cm^{-2} and a diameter $D_0 = 2.5 \div 7$ nm. The experimental values of α_1, α_2 of the nickel nanoparticles were determined under the condition with $\varepsilon_m = (1 + \varepsilon_0)/2$, where $\varepsilon_0 = 2.38$ (fused quartz).

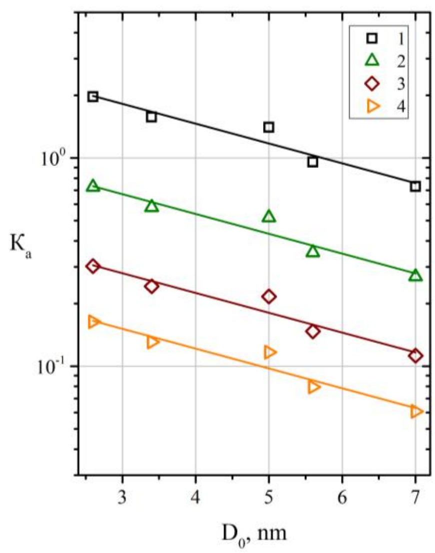

Fig. 1. Dimensional dependence of the absorption efficiency factor of the nickel nanoparticles at the different wavelengths λ: 1 – 0.2 μm, 2 – 0.4 μm, 3 – 0.6 μm, 4 – 0.8 μm

A significant increase in the absolute values of α_1 and α_2 was established during the decrease of the size of nickel nanoparticles and, in comparison with the absolute values of α_1 and α_2, also in the model spheres with optical parameters for macroscopic samples of nickel. Dispersion changes of α_2 nanoparticles of the nickel are monotonous. A comparative analysis of the spectral and dimensional dependences α_1, α_2 with the corresponding data for nanoparticles – nickel islands on a glass substrate, obtained in [7], has shown that they are qualitatively identical. Quantitatively, it was established that taking into account the real distribution function of the nanoparticles by size during the determination of α_1, α_2 with the help of the experimental-analytical method, makes it possible to increase the accuracy up to 40%.

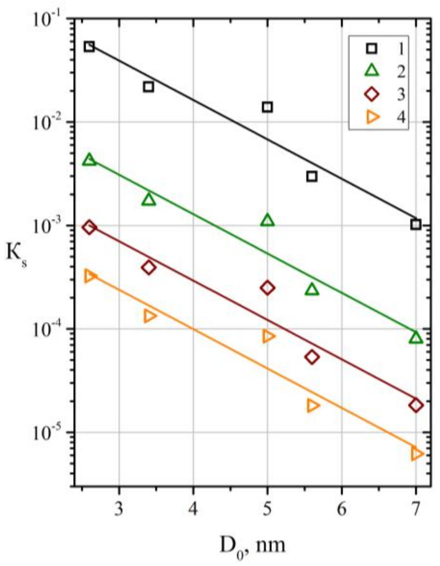

Fig. 2. Dimensional dependence of the scattering efficiency factor of the nickel nanoparticles at the different wavelengths λ: 1 – 0.2 μm, 2 – 0.4 μm, 3 – 0.6 μm, 4 –0.8 μm

The obtained experimental values of α_1, α_2 were used for estimating K_a, K_s by means of relations (1), (2). The results of the numerical calculations of the dependences of K_a, K_s on the size of the nickel nanoparticles at the different wavelengths of the electromagnetic radiation are presented in Fig. 1 and 2.

It can be seen that when the size of the nickel nanoparticle increases from 2.6 to 7 nm, the increase of the values of K_a, K_s for all λ in the investigated spectral range can be observed. It should be noted, that in the spectral interval $\lambda = 0.2 \div 1.1$ μm, the structure of the dispersion curves K_a, K_s in general repeated the regularity inherent to the spectral dependences α_1, α_2. Analysis of the data in Fig. 1 and 2 and relations (1), (2) ($K_a \sim 1/\lambda$, $K_s \sim 1/\lambda^4$) shows a faster decrease of K_a in comparison with K_s as λ increases.

The specificity of the calculations of the efficiency factors of absorption and scattering of nickel nanoparticles (with dimensions of 2.6, 3.4, 4.0, 5.0, 7.0 nm) according to the theories of classical [13] and quantum [14] dimensional effects was as follows. Firstly, $\varepsilon_1(\omega, R_0)$, $\varepsilon_2(\omega, R_0)$ were calculated with the help of the relations (5) – (13) and experimental values of $\varepsilon_{1v}(\omega)$ and $\varepsilon_{2v}(\omega)$. The last ones were estimated according to the presented in [15] dispersion dependences of the refractive index n and absorption index k of nickel in a macroscopic volume. Then with the obtained $\varepsilon_1(\omega, R_0)$, $\varepsilon_2(\omega, R_0)$ by formulas (3), (4), α_1, α_2 were calculated and, by formulas (1), (2), K_a, K_s were calculated. In order to achieve a correspondence between the calculated and experimental α_1, α_2, K_a, K_s of an individual nickel particle in an island film on a fused quartz substrate with a dielectric conductivity ε_0, according to [6], in the expressions (1) – (3) $\varepsilon_m = (1+\varepsilon_0)/2$ were used, where $\varepsilon_0 = 2.38$ of the fused quartz. Because of the ambiguity in the nature of the dimensional changes of $\varepsilon_{1s}(\omega, R_0)$, in the theory of the quantum dimensional effect, the calculation of α_1, α_2, K_a, K_s for this theory was carried out, just as in the case of the theory of the classical dimensional effect under the condition $\varepsilon_{1s}(\omega, R_0) = 0$.

The results of numerical calculations of K_a, K_s of the nickel nanoparticles $\lambda = 0.8$ μm that were determined by the theories of classical and quantum dimensional effects are presented in Fig. 3 and 4.

For comparison, the corresponding experimental (estimated with the help of the relations (1), (2) with the experimental values of α_1, α_2) dimensional dependences K_a, K_s are given in the same place. In the Fig. 3 and 4, the significant discrepancies can be observed between the experimental and calculated, with the help of the theories of classical and quantum dimensional effects, dimensional dependences of K_a, K_s of nickel nanoparticles. At the same time, the values of K_a, K_s, calculated from the theories of the dimensional effects, decrease with the decreasing of the nanoparticle size. In contrast, the experimental values of K_a, K_s increase with a reduction of the nanoparticle volume. It should be noted that this trend is preserved for all λ in the entire considered spectral interval.

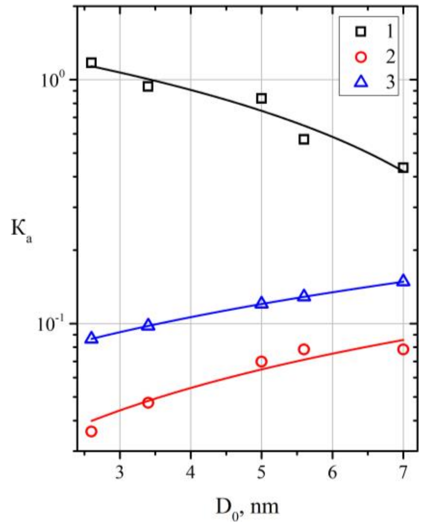

Fig. 3. Dimensional dependence of the absorption efficiency factor of nickel nanoparticles at λ = 0.3 μm. 1 – experimental curve, 2 – the results of the calculations according to the theory of the classical dimensional effect, 3 – results of the calculations according to the theory of the quantum dimensional effect

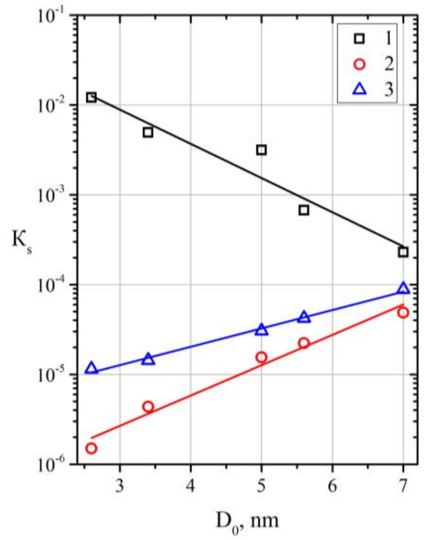

Fig. 4. Dimensional dependence of the scattering efficiency factor of nickel nanoparticles at λ = 0.3 μm. 1 – experimental curve, 2 – the results of the calculations according to the theory of the classical dimensional effect, 3 – results of the calculations according to the theory of the quantum dimensional effect

3. Conclusion

The study of the dimensional dependences of the complex specific electrical polarizability and absorption and scattering efficiency factors of the spherical nickel particles with a size from 2.5 to 7 nm with a radius of 1.5 to 8.0 nm in the spectral range from 0.2 to 1.1 μm was carried out.

The experimental values of the complex specific electrical polarizability of the nickel nanoparticles on the basis of the spectrophotometric and electron-microscopic measurements of the island nickel films on the quartz substrates were determined with the help of the improved experimental analytical method taking into account the statistics of the nanoparticle distribution by size. Such approach for the case of the inhomogeneous nanostructures made it possible to increase the accuracy of the determination of α_1, α_2 and associated with them optical characteristics (the absorption and scattering efficiency factors) up to 40%.

A significant increase (found by us [7]) up to one order of the absolute values of the real and virtual parts of the complex specific electrical polarizability of the nickel nanoparticles, during reduction of their size and as compared to the values that are typical for the macroscopic volumes of nickel was proved.

The growth of the values of the absorption efficiency factor up to one order and the scattering efficiency factor up to two orders of the magnitude of nickel nanoparticles with decreasing their size from 7 to 2.5 nm was established.

In order to clarify the nature of this phenomenon, numerical calculations of the specific dynamic polarizability, dielectric conductivity and also absorption and scattering efficiency factors of the investigated nickel nanoparticles were carried out on the basis of the theories of classical and quantum dimensional effects in the particle. It was shown that calculated in such way values of the absorption and scattering efficiency factors of the nickel particles are in 2 – 3 orders of magnitude lower compared to the experimental ones.

On the basis of these results, it can be concluded that experimental dimensional dependences of K_a, K_s, and also α_1, α_2 in the range $\lambda = 0.2 \div 1.1$ μm can be explained by manifestations of the classical or quantum dimensional effects in the dipole resonance of the nickel nanoparticle.

Thus, the results of the experimental investigations of the optical characteristics and photoabsorption parameters of the nickel nanoparticles can be used during the development of the metal-dielectric nanostructured systems for the use in the light control devices in optoelectronics, selective energy-efficient coatings in the energy-saving technologies and in the information security systems.

References

[1] Aduev B.P., et al.: Issledovaniye opticheskikh svoystv nanochastits alyuminiya v tetranitropentaeritrite s ispol'zovaniyem fotometricheskogo shara. Journal of technical physics 84(9)/ 2014, 126–131.
[2] Bondar E.A., Machulyanskiy A.V.: Spektrofotometricheskiy metod opredeleniya dinamicheskoy polyarizuyemosti ul'tradispersnykh metallicheskikh chastits. Algoritm vychisleniy. Optics and Spectroscopy 70(1)/1991, 161–163.
[3] Bondar E.A.: Razmernyye zavisimosti opticheskikh kharakteristik malykh chastits serebra v vysokochastotnoy oblasti spektrazhe. Optics and Spectroscopy 77(3)/1994, 414–420.
[4] Boren K., Hafmen D.: Pogloshcheniye i rasseyaniye sveta malymi chastitsami. Moscow 1986.
[5] Edelman I.S., et al.: Mikrostruktura i magnitooptika oksida kremniya s implantirovannymi nanorazmernymi chastitsami nikelya. Journal of experimental and theoretical physics 140(6(12))/2011, 1191–1202.
[6] Kalenskiy A.V., Ananeva M.V., Nikitin A.P.: Opticheskiye kharakteristiki nanochastits nikelya v prozrachnykh matritsakh. Modern scientific research and innovations 11-1(43)/2014, 5–13.
[7] Kawabata A., Kubo R.: Electronic properties of fine metallic particles. II. Plasma resonance absorption. J. Phys. Soc. Japan 21(9)/1966, 1765–1772.
[8] Kreibig U., Fragstein C.V.: The limitation of electron mean free path in small silver particles. Z. Physik 224(4)/1969, 307–323.
[9] Landau L.D., Lifshits E.M.: Elektrodinamika sploshnykh sred. Moscow 1982.
[10] Machulyanskiy A.V.: Razmernyye zavisimosti dinamicheskoy polyarizuyemosti ul'tradispersnykh chastits. Electronics and Communication 10/2001, 78–80.
[11] Machulyansky A., Babych B., Machulyansky V.: Modelling of electromagnetic parameters of two-dimensional nanostructural system taking into account statistics of distribution of nanoparticles on the sizes. Proceedings of the 9th International scientific conference "Functional base of nanoelectronics", Ukraine 2017, 41–44.
[12] Moulin E., et al.: Improved light absorption in thin-film silicon solar cells by integration of silver nanoparticles. Journal of non-crystalline solids 354/2008, 2488–2491.
[13] Nikitin A.P.: Effektivnost' pogloshcheniya lazernogo izlucheniya nanorazmernymi vklyucheniyami metallov v zavisimosti ot dliny volny. International scientific publication Modern fundamental and applied research 4(7)/2012, 81–86.
[14] Petrov Y.I.: Fizika malyih chastits. Nauka, Moscow 1982.
[15] Zolotarev V.M., Morozov V.N., Smirnova E.V.: Opticheskiye postoyannyye prirodnykh i tekhnicheskikh sred. Khimiya. Leningrad 1984.

Ph.D. Oleksandr Machulianskyi
e-mail: machulanske@gmail.com

Associate professor of the Department of Microelectronics of the National Technical University of Ukraine "Igor Sikorsky Kyiv Polytechnic Institute". His research area focuses on electromagnetic properties of materials with nanometer scale of sizes, synthesis of nanostructured composite systems with given complex of properties. Author of nearly 120 publications in this research area.

M.Sc. Bohdan Babych
e-mail: wvbbb@meta.ua

Ph.D. student of the Department of Microelectronics of the National Technical University of Ukraine "Igor Sikorsky Kyiv Polytechnic Institute". His research interests include electromagnetic properties of nanosized materials and development on their basis multifunctional composite structures. Author of nearly 20 publications in this research area.

M.Sc. Viktor Machulianskyi
e-mail: 4victorvictor@gmail.com

Viktor Machulianskyi received M.Sc. degree in System analysis and control from the National Technical University of Ukraine Kiev Polytechnic Institute, Kiev, in 2011. His research interests include modeling and optimization of complex inhomogeneous systems, analytical and computational tools, algorithmic support and data processing systems. Author of nearly 20 publications in this research area.

otrzymano/received: 10.10.2017 *przyjęto do druku/accepted: 15.02.2018*

DOI: 10.5604/01.3001.0010.8543

CONTROL MODEL OF DATA STREAM TRANSMITTED OVER A NETWORK BASED ON PROXYING TECHNOLOGY

Olesia Barkovska, Vitaliy Serdechnyi
Kharkiv National University of Radioelectronics, Electronic Computer Department

Abstract. *Network traffic control model is described in the work, including data mining modules transmitted in the network as well as further qualified data analysis module based on artificial intelligence methods and means, namely recursive and convolutional neural networks. The topicality of work is proved by the intensive scientific research conducted in the field of information security, big data intelligent data processing tools, and stipulated by growing necessity to limit access of children to aggressive information, which can impact on the child's psychoemotional state. Particular attention is paid in the article to proxy-server development for HTTP query receipt, search for a match in white and black lists and decision making as to data legality.*

Keywords: communication system traffic control, data transfer, access protocols, learning systems

MODEL KONTROLI DANYCH PRZEKAZANYCH PRZEZ SIEĆ W OPARCIU O TECHNOLOGIĘ PROXY

Streszczenie. *W artykule rozważono model kontroli ruchem sieciowym, który zawiera moduł do zbierania danych przesyłanych przez sieć, a także moduł do dalszej analizy przygotowanych danych w oparciu o metody i środki sztucznej inteligencji, a mianowicie rekurencyjne i splotowe sieci neuronowe. Znaczenie tej pracy jest potwierdzone przez dużą liczbę badań naukowych prowadzonych w dziedzinie bezpieczeństwa informacji, środków intelektualnych do przetwarzania dużej ilości danych, a także ze względu na rosnącą potrzebę ograniczenia dostępu dzieci do agresywnych informacji z sieci, które mogą wpływać na ich stan psychoemocjonalny. Artykuł koncentruje się głównie na opracowaniu serwera proxy do odbierania żądań HTTP, wyszukiwania dopasowań na „czarnych" i „białych" listach i podjęcia decyzji o zezwoleniu na obejrzenie.*

Słowa kluczowe: kontrola ruchu w systemie komunikacyjnym, transfer danych, protokoły dostępu, systemy uczenia się

Introduction

Control and analysis of data stream transmitted in Internet channels gains actuality every year. The World Wide Web is used for data mining, information exchange, rendering services, in particular entertainment and inconsistent with censorship. Access to the above-mentioned information is available for people of any age, gender and emotional condition. A specific instance is the information education function of electronic resources, access to which is often granted to children. When searching for valuable information, a child may encounter information, which can have a negative influence on the immature personality, e.g. bullying, aggressive images, explicit or graphic descriptions etc.

Let us call the kind of information, which causes agitation of the child's psyche, anxiety or aggression state, unwanted information (UI). Thus, limiting child's access to such kinds of information together with the creation of additional information filtration means in accordance with the set rules (filters) is considered highly relevant.

Methods of traffic classification into acceptable for viewing and inacceptable were studied by [6].

One of the methods to solve the set task is the use of the parent control function enabled by various extensions for Google Chrome, Mozilla Firefox, Opera browsers. A white list of sites authorized for lookup and a black list of certain sites unacceptable for child sessions are concurrently formed. Such popular browser extensions as Adult Blocker and TinyFilter may conduct morphological analysis of the page text content and filter pages on the basis of the downloaded content. A considerable shortcoming of the given method is their affinity to a definite browser and support of the most popular browsers only. For example, it is possible to avoid this information filtration method via the use of Internet Explorer installed on all OS Windows computers.

Limits to child's access to the content are possible via search engine tuning. Along with this, it is impossible to define the type of unwanted content – search engines usually delete only porn resources from the search results effectively.

Content filtration function can be enabled on the router. Almost all the leading manufacturers (ASUS, ZyXEL and TP-Link) provide for this capability [7]. The parent computer is identified by the router via MAC address. The functionality of filtration by the router is limited to a temporary filter (scheduled internet connection), the white and black lists of sites, incoming traffic analysis by means of verification with various unreliable resource databases.

Current control and data streams demarcation methods analysis enabled to make a conclusion that the existing methods have a number of substantial drawbacks such as the insufficient level of control and data streams demarcation methods integration, mostly passive nature of the audit processes and limited capabilities of intellectual text and image message analysis in the short run [7].

In order to eliminate the given drawback, development of a multifunctional model to control active data stream transmitted in the network as well as implementation of a proxy-server based on HTTP-requests and HTTP-responses intellectual analysis aimed at securing the child against threats from the Internet are proposed in the work.

The aim of the work is provision of inability of child's access to the information education electronic resources containing information that may cause child's psyche agitation, anxiety and aggression state, i.e. to unwanted information.

Main feature of the final software product is a primary scanning and subsequent deep analysis opened web-page content's based on existing methods of artificial intelligence. The advantage of this analysis is that the proposed approach, which is described by the control model of data stream transmitted over a network based on proxying technology [2], is able to restrict the child from viewing the site, analyzing not only the name, keywords or URL, but also the tonality of the content of the requested web page.

1. Description of the control model of data stream transmitted over a network based on proxying technology

Proceeding from the existent solutions, their advantages and disadvantages, a control model of data stream transmitted over a network based on the proxying technology was elaborated. In the given model, the proxy-server is an intermediary between the Internet and the clients, namely all Web browsers installed on a local computer. The model is presented in Fig. 1.

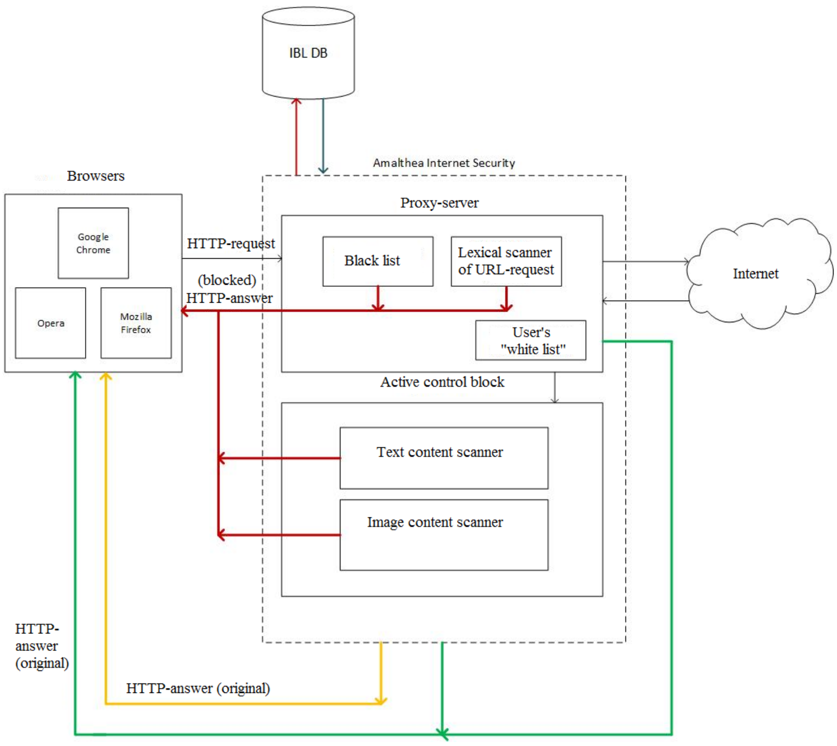

Fig. 1. Generic Control Model of Data Stream Transmitted over a Network Based on Proxying Technology

Below the description of modules in the proposed system is offered:

- the proxy server provides for the first stage of query analysis: all queries sent by any browser are received by the proxy server. Inside the server, the HTTP header is parsed and URI is distinguished, which is further compared with the white and black lists and studied by the lexical scanner. If the validation stage is successful, query analysis is accomplished and it goes to the addressee network. The response from the addressee server is also received by the proxy-server, which is compared with the white list. If a match is found, the HTTP response is sent directly to the browser avoiding the in-process control stage. Otherwise, the in-process web-page control stage begins, which presupposes intellectual content analysis;
- the black list is the list, which consists of two components: user exceptions and the exceptions generated by the system in the functioning process. If a match of the distinguished URI with the black list is found in the validation process, an HTTP-response is generated by the server to the browser with the message that the requested resource is banned. The URI further goes to the lexical query scanner;
- the lexical scanner checks on the basis of the requested URI if the page may contain forbidden materials. The procedure is based on the primitive regular expressions by means of comparison with the given letter combinations, which clearly indicate that the resource is unwanted. If this check is successful, the HTTP query is sent to the addressee;
- page content scanner conducts in-process content control via incremental intellectual analysis of the received HTTP response. Upon this, the content is divided into text content and graphic content. Text content analysis is brought to text sentiment analysis (if the text expresses a positive or a negative point of view about something) or text diversification according to topics. If the text analysis is successful, all the available images from the site received from the remote server are also analyzed for presence of the forbidden graphic information. In case of the positive analysis of the two above-mentioned content types, the response in sent to the browser and the URI of the analyzed resource is automatically added to the white list. If at least one of these stages results in the negative response, a message is formed for the browser to block the resource and the given URI is added to the black list. It should be noted that in the system being developed, a variant of partial editing of the opened Internet resource is also proposed. For example, if a web page is not a prohibited site and does not contain unwanted materials, and at the end of the page there is a comment block with obscene language, then this block will be "cut" from this page and it will be displayed in the browser without it. This approach makes it possible to safely view pages without completely blocking access to them. The criterion determining the decision to completely block or partially edit a web page can be the number of detected unwanted materials and their scatter across the page. If all of them are in one place, which is typical for comments with obscene language, then you can apply partial editing. If unwanted materials are scattered more evenly throughout the page, which is typical of a typical web resource with pornographic materials, then such a page must be completely blocked. In case the page to be opened is subject to partial editing, it is not entered either in the "white" or "black" list, so that the page is checked by the system at each visit. Automatic exceptions generation enables to minimize delays in the user’s work with regularly revisited resources and to avoid extra checks if the resource is marked unwanted;
- DBL DB (Distributed Black Lists Database) is a database to which banned sites are added. Program samples are regularly compared with this database. Thus, the more program samples function for various users, the more increased the unwanted site base, and the installed program can access the complete base from the moment of use.

2. Tasks performed by the proxy-server

The proxy-server functionality is limited by the following tasks:

- data provision for in-depth analysis;
- banning the unwanted web resources based on the analysis results.

The given tasks are performed in the function blocks of the proxy server presented in Fig. 2.

In Fig. 2, all blocks are conditionally classified into 5 groups: Configuration, Black and White Lists, SSL, Proxy kernel and Analysis. Each group contains two or more conventional function blocks.

In the Configuration group, there is the operating system and separate programs are fine-tuned for log-on via a proxy-server. Definition of the separate Firefox Proxy Configuration block is explained by the fact that Mozilla Firefox browser does not conform to the internal OS Windows proxy settings and there is the need to elaborate separate methods of its configuration.

The blocks of the Black and White Lists group put into effect work with the white and black exceptions lists. All the sites added to the black list are blocked at the request stage and the sites in the white list will be fully accessible without any time-consuming analysis.

The SSL group realizes the features for processing self-signed SSL certificates. The blocks of this group generate and manipulate such certificates as well as perform caching in order to accelerate establishment of a secured connection.

Proxy kernel is the core of the entire proxy server. Here all the necessary networking functions are realized: transport connection, establishment of a secure connection, HTTP queries / responses processing and a series of other functions, which directly provide for the work with Internet traffic.

All the features connected with data preparation for the further stage are performed by the function blocks of the Analysis group. If there is the need in analyzing a Web resource, a series of preliminary stages must be executed; formation of a “loop” on the side of the proxy-server (browser work simulation), necessary data acquisition, their decryption, transformation and formatting. Also, The Analysis group has the Preliminary Analysis function block, which verifies queries at the stage of their receipt using the set of ready regular expressions.

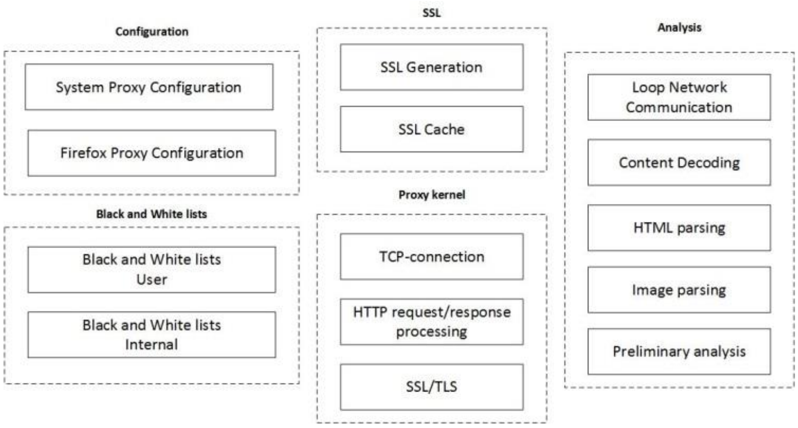

Fig. 2. Function Blocks of the Proposed Proxy Server

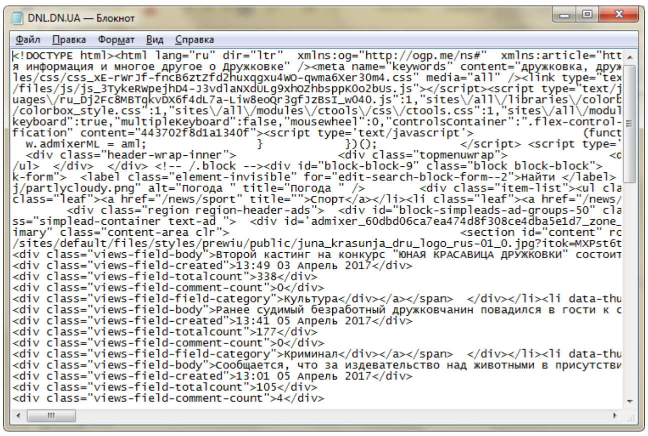

Fig. 3. Dearchived GZIP Data

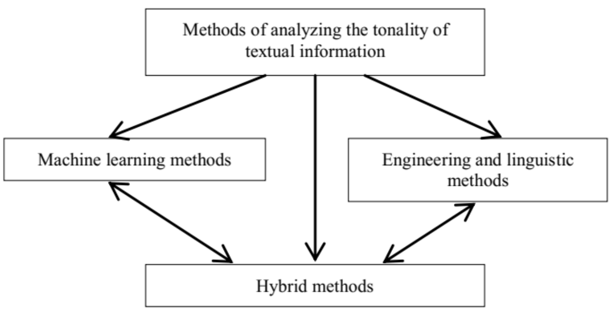

Fig. 4. The methods of analyzing the tonality of textual information

The HTML page in the HTTP response body may be transmitted by the server as clear or archived. If clear data are transmitted, their body transformation into text representation is performed after its definition. If archived data are transmitted, their decompression is needed. One of the most popular compression methods is GZIP. This method is based on the DEFLATE algorithm. Text content of the site under scrutiny after its decompression is presented in Fig. 3.

After dearchiving GZIP data and preparing input text for next group next step will be to make deep analyze of image and text content using intellectual methods. Approaches used to analyze the tonality of textual information in natural language, are divided into two main groups: engineering and linguistic methods and methods based on machine learning (Fig. 4). Machine learning methods, the list of which includes (but is not limited to) the method of conditional random fields (Condition Random Fields, CRF), Support Vector Machine (SVM) method, artificial neural networks (Artificial Neural Networks, ANN) and others. This group of methods uses mathematical models that automatically determine the optimal set of parameters for the solution of a particular problem, in this case, the definition of a key [3, 4].

Considering together the monitoring of social media and the task of automated intellectual analysis of text publications, it can be argued that today it is one of the most relevant and actively developing applied areas of sociology and computer linguistics. This fact can be confirmed by the fact that this direction has become the leading topic of international conferences in the field of computer linguistics and automatic word processing.

A number of recent works on the analysis of the tonality of English texts demonstrate the superiority of deep learning models over shallow algorithms, which include linear and logistic regressions, CRF, Bayesian classifier, and the widely used SVM method. Richard Socher has the best results in this field, in which the algorithm of machine learning for the first time, without the use of linguistic dictionaries or rules, was able to correctly recognize semantic and syntactic negations, correctly select the negative key of the phrase containing a list of positive words and denials between them. Richard Saucer, who has the best results in this field, showed that the machine learning algorithm is able to correctly recognize semantic and syntactic negations, correctly identify the negative key of the phrase containing a list of positive words and negations between them, without the use of linguistic dictionaries or rules. An additional argument in favor of methods of in-depth training (as well as methods of machine learning in general) is the ability to analyze data without an in-depth study of linguistics and/or attracting linguistic experts.

3. SSL Certificate Generation

In the elaborated proxy server, both nonsecure and secure (HTTPS) connections are realized [1].

The problem of secure connection establishment within the framework of this design lay in the field of proper SSL certificates operation. SSL functioning analysis resulted in the need to immediately generate a certificate for the requested resource and create a sort of a non-existent certification center. This is stipulated by the fact that the browsers will “know” that such certification center exists and the certificates signed by this center can be trusted.

The very mechanism of signature generation functions very simply. Equation 1 describes signature generation for *M* message.

$$SIGNATURE = M^{d} (\mathrm{mod}\, N) \quad (1)$$

where *d* and *N* are the author’s private key to the message.

M message and *SIGNATURE* can further be sent to the recipient. Signature verification on the second side is described by equation 2.

$$M = SIGNATURE^{e} (\mathrm{mod}\, N) \quad (2)$$

where *e* and *N* are the author’s public key to the message.

Thus, everybody can verify the signature of the message but it can be signed only by the person with the private key. The browser authenticates the incoming certificate by means of using the public key of the individual who signed it. Therefore, by creating and storing a certificate, it is necessary to save the private key and, then, in the proxy server work, it is possible to sign SSL certificates immediately using this key. The browser, authenticating such certificates, will verify them with the public key from the certification center, the certificate of which resides in Windows storage.

It is worth noting that at the stage of immediate SSL certificate generation by the browser, internal SSL cache is primarily checked. If the certificate for the requested host is not found, a new certificate is immediately generated. Thus, the connection system presented in Fig. 4 will be formed.

4. Conclusions

The control model of data stream transmitted over a network based on proxying technology was proposed in the work. The speed and correct operation of the proxy server currently depend on the definite browser. Proxy server test results analysis showed that 100% of the sites in the black list are successfully blocked when accessed with Opera, Internet Explorer, Google Chrome, Yandex.Browser browsers. However, the result of working in Yandex is 30% lower. This is associated with multiple queries of this browser to its servers, which results in the fact that it takes a lot of time for the site to open, or it does not open at all at the end of timeout for waiting for the response from the server set by the browser. The best result in the speed of opening Web pages when working via the elaborated proxy server was obtained with Google Chrome. Working via the proxy server in this browser enables not only to surf the Internet without any significant delay, but also to work with media traffic such as watching videos online on YouTube and listening to music.

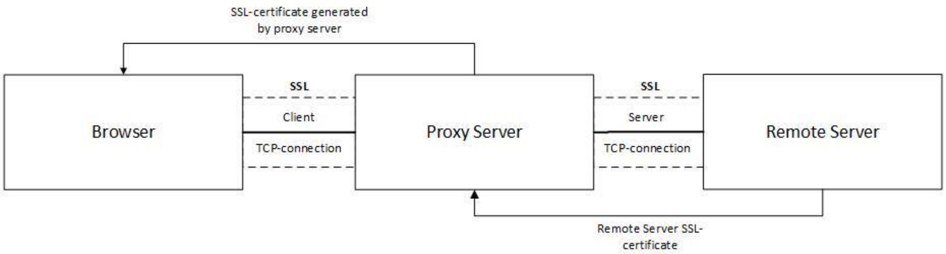

Fig. 4. Scheme of HTTPS Connection via a Proxy Server

References

[1] Barabanov A.B., Markov A.C., Cirlov B.L.: Sertifikatsiya sistem obnaruzheniya vtorzheniy. Otkrytyye sistemy. SUBD 3/2012, 31–33.
[2] Huan T.: The Application of SSL Protocol in Computer Network Communication. Intelligence Computation and Evolutionary Computation. Advances in Intelligent Systems and Computing 180/2013, 779–783.
[3] Kuznetsova E.S., Loukachevitch N.V., Chetviorkin I.I.: Testing rules for a sentiment analysis system. Computational Linguistics and Intellectual Technologies 12(2)/2013, 71–80.
[4] Pak A., Paroubek P.: Language independent approach to sentiment analysis (LIMSI participation in ROMIP ’11). Computational Linguistics and Intellectual Technologies 11(2)/2012, 37–50.
[5] Scherer S., Schwenker F., Palm G.: Emotion Recognition from Speech Using Multi-Classifier Systems and RBF-Ensembles. Studies in Computational Intelligence 83/2008, 49–70.
[6] Sentsova A.Yu., Mashkyna Y.V.: Avtomatizatsiya ekspertnogo audita informatsionnoy bezopasnosti na osnove ispol'zovaniya iskusstvennoy neyronnoy seti. Bezopasnost' informatsionnykh tekhnologiy 2/2014, 65–70.
[7] Wan S., Ren Z.: Research on Full-Proxy Based TCP Congestion Control Strategy. Advances in Intelligent and Soft Computing 133/2012, 371–378.

Ph.D. Eng. Olesia Barkovska
e-mail: olesia.barkovska@nure.ua

Senior lecturer of Electronic Computer Department of Kharkiv National University of Radioelectronics, Ph.D. in Systems and Means of Artificial Intelligence from 2011. Her research interests include data clustering, malware analysis, network security, network and server performance

B.Sc. Vitaliy Serdechnyi
e-mail: serdechny.vs@ukr.net

B.Sc. in Computer Engineering from 2017. Is currently studying for a M.Sc. degree in System Programming in Kharkiv National University of Radioelectronics. His research interests include artificial intelligence, neural networks, Internet security, .NET platform, C#

otrzymano/received: 10.10.2017 *przyjęto do druku/accepted: 15.02.2018*

DOI: 10.5604/01.3001.0010.8544

INVESTIGATION OF THE MEMRISTOR NONLINEAR PROPERTIES

Sviatoslav Khrapko, Volodymyr Rusyn, Leonid Politansky
Yuriy Fedkovych Chernivtsi National University, Department of Radio Engineering and Information

Abstract. *The study of nonlinear systems is an important research topic for scientists and researchers. Memristor, for a long time, it remained just as a theoretical element and rarely appeared in the literature because of having no simple and practical realization. In this paper, we reviewed the theoretical substantiation of the memristor and conducted a practical study of its nonlinear properties using the memristor company KNOWM of series BS-AF-W 16DIP. We also investigated the characteristics of the memristor via the LabView environment.*

Keywords: memristor, hysteresis, nonlinear system, KNOWM

BADANIE NIELINIOWYCH WŁAŚCIWOŚCI MEMRYSTORA

Streszczenie. *Badanie systemów nieliniowych jest ważnym tematem dla badaczy i naukowców. Memrystor przez długi czas pozostawał elementem teoretycznym i rzadko pojawiał się w literaturze z powodu braku prostej i praktycznej realizacji. W tym artykule zostały przedstawione teoretyczne uzasadnienie memrystora i badania jego właściwości nieliniowych na przykładzie memrystora firmy KNOWM serii BS-AF-W 16DIP. Zostały przeprowadzone badania charakterystyk memrystora w środowisku LabView.*

Słowa kluczowe: memrystor, histereza, nieliniowość, KNOWM

Introduction

In 2008 scientists were able to open a new component of electroschemes for the first time since Faraday's days and the beginning of experiments with electricity in the early 19th century. This component is called the memristor, this term was formed as a result of the fusion of words «memory» and "resistor" (electrical resistance). By this term is meant a two-pole device, the electrical resistance of which varies depending on the amount of charge flowing through it. American physicist Leon A. Chua in 1971 made an assumption about the existence of another basic element of the electrochemical system, which implements the relationship between magnetic flux and charge. It is impossible to simulate it from other passive elements, but even then it could be considered as a combination of active elements of the scheme; namely the resistor, the capacitor and the inductor [3, 6]. For example, operational amplifiers can be regarded as active elements. In this name, one of the characteristics of the element is expressed, the so-called "memory effect", that the previously applied force changes its properties, namely, the value of the resistance of the element varies depending on the amount of charge passed through it. This allows the memristor to be used as a memory cell. The resistance of the memristor was called the memresistance (*M*), which is defined as the ratio of the change in the magnitude of the magnetic field flux to the charge change, and its value depends on how long the electrical current flows through the memristor, that is, the amount of charge passed through it. Memristor is different from most types of modern semiconductor memory elements because its properties are not stored as charge. This is its main advantage, because it is not afraid of the leakage of charge, which is the main disaster, which everyone aspires to get rid of when it is transitioning to "nano chips". Another advantage of the memristor is its energy independence. These properties provide storage for memristor same time as exist materials used in its manufacturing. The same flash memory after a year of storage without connecting it to an electric current starts to lose recorded data.

Unlike the theoretical model, the memristor does not accumulate a charge like a capacitor, and does not support magnetic flux as a coil of inductance. The work of the device is provided by chemical transformations in a thin two-layer tape of titanium dioxide. One of the layers of the film is slightly depleted with oxygen, and oxygen vacancies migrate between layers under the action of the electric voltage applied to the memristor. This memristor's implementation should be attributed to the class of nanionic devices. The phenomenon of hysteresis, which we can observe in the memristor, allows us to use it as a memory cell [11].

The design of the memristors is much simpler than the flash memory. These elements represent a two-layer thin 50 nm tape placed between two 5 nm platinum electrodes. One of the layers is oxygen-depleted and the other is an insulating titanium dioxide. Under the influence of the voltage, that is applied to the electrodes, the structure of the titanium dioxide crystals begins to change – oxygen diffusion results in an increase in its electrical resistance by 1000 times. These changes in the cell do not disappear after the current is turned off. By changing the polarity of the supplied voltage, you can switch the state of the cell, and the number of these switching, according to the inventors, is not limited [10].

Another remarkable property of the memristor is that it can accept not two positions of memory: 0 and 1, as ordinary chips, but any other in the gap between zero and one, so the switch can work in the analogue, and in digital mode [12].

It is normal that memristors can be applied and give new extra highlights to simple circuits. Different simple and chaotic applications of memristor to analog, chaotic and synaptic circuits are studied in the literature [7].

1. The theoretical substantiation of the memristor

Chua came from the fact that there should be relations that connect all four main variables of electric circuits: current I, voltage *V*, charge *Q* and magnetic flux *Φ*. Total of such ratios can be six. Five of them are well known. Charge is an integral over time from the current. The connection between the voltage and the magnetic flux is determined by the law of electromagnetic Faraday's induction. Voltage and current are connected through resistance *R*, charge and voltage – through capacity C, and magnetic flux and current – through the inductance *L*. There is no the sixth ratio, which connects the flow and charge. Chua suggested that these values are connected through the "missing" element – memristor, which has "memresistance ". This statement is reflected in the formula (1) [1].

$$M(q) = \frac{d\Phi_m}{dq}, \tag{1}$$

where Φ_m is a flow coupling, generalized with current characteristics of the inductance, due to the absence of a magnetic field as such that can be regarded as an integral of voltage over time;

M(q) is a memresistance, an indicator characterized by any memristor, it relates the rate of change in flow and charge; in general, it depends on q, that is, the charge. If we consider the flow coupling as a temporary voltage integral, and the charge as a time integral of the current, then the following formula is obtained (2):

$$M(q(t)) = \frac{d\Phi_m / dt}{dq / dt} = \frac{V(t)}{I(t)} \qquad (2)$$

We see that in the case of M = *const*, the memresistance is a normal resistance, and formula (2) turns into Ohm's law for the area of circle. This equation also shows that the memresistance determines the linear relationship between current and voltage, while M does not change with charge.

Zero current means a variable over time charge. An alternating current can detect a linear dependence in the circuit if the measuring voltage is induced without changing the total charge change – until the maximum change q does not cause large changes to M. If $I(t) = 0$, then $V(t) = 0$ and $M(t)$ is constant. This is the essence of the "memory" effect.

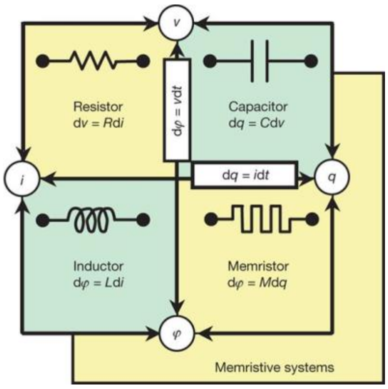

Fig. 1. Connection of the basic elements of the electric circuit

Fig.1. shows this relationship graphically [2, 5]. The voltage- or current-controlled memristor is a fundamental passive two-terminal component with resistance depending on the time history of voltage across or current through it [4].

If a variable sinusoidal voltage of a certain frequency is applied to the memristor, its voltage-ampere characteristic takes the form, which resembles a lissajous figure with center at the beginning of the coordinates: in electronics it corresponds to the assembly of two perpendicular oscillations with multiple frequencies. Normal (resistive) resistance corresponds to the slope of the curve of current dependence on voltage; here we see that at the zero current and voltage intersect such two curves. This means that the resistance may vary depending on the conditions. At the site of the sinusoid (when the voltage drops at the transition through zero) the resistance will be greater than the initial (when it increases). The figure is shown in Figure 2.

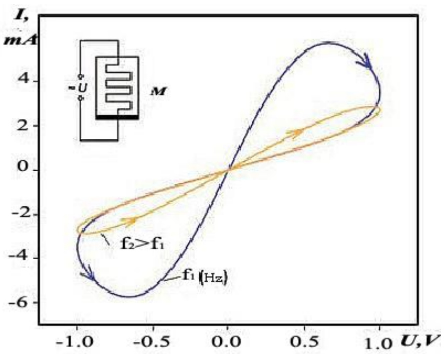

Fig. 2. The phenomenon of hysteresis of the memristor

That is, the memristor, in contrast to the resistor, has a hysteresis. The hysteresis curve turns into a straight line with an increase in the voltage frequency: the memristor is converted into a conventional resistor. This is understandable: since the change in the value of the resistance depends on the amount of charge that has passed, and with the increase in frequency for one period of charge runs less. Therefore, sufficiently short, different polar impulses of current will not affect the state of the memristor, and the magnitude of the current will show us in what state is the memristor. Thus, you can read the information without changing the state of the cell.

Hysteresis characteristics are the essential qualities of memristors [8, 9]. Hysteresis characteristics behave as multi-value mapping and memory features. Many models have been proposed to precisely depict the hysteresis phenomena, for example, Sun et al. [13] proposed a network model using the backslash operator as activation function to model hysteretic operator, Guo and Dang improved the backslash operator [8].

2. Modeling the nonlinear properties of a memristor in a LabView environment

The nonlinear element based on the memristor has a nonlinear hysteresis characteristic, which plays an important role in engineering and, in particular, in electronics. For demonstration was used one of the most advanced LabView software environment, which is a convenient tool for design and simulate various complexity of mathematical models that describe a particular devices. This environment allows creating virtual devices for generating and researching any characteristics.

Figure 3 shows a block diagram that allows generating a hysteresis characteristic.

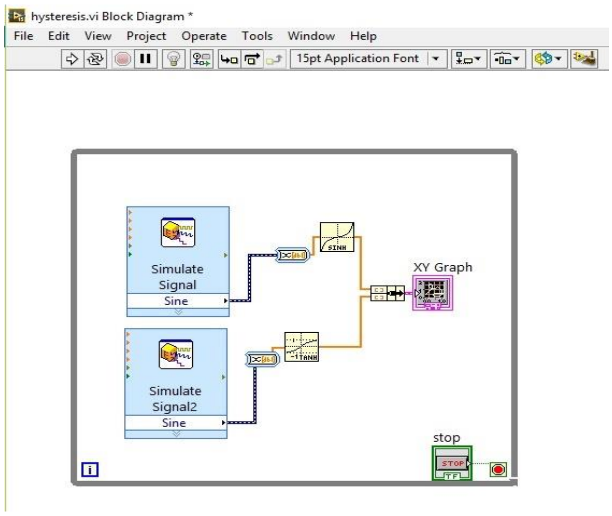

Fig. 3. Block diagram for modeling hysteresis characteristic

As sources of signals, two sources with the following parameters was selected:

1) Frequency 10.2 Hz, amplitude 2.5 V, phase -25 deq.
2) Frequency 10.1 Hz, amplitude 1 V.

Figure 4 shows interface of the program that graphically demonstrates modeling result.

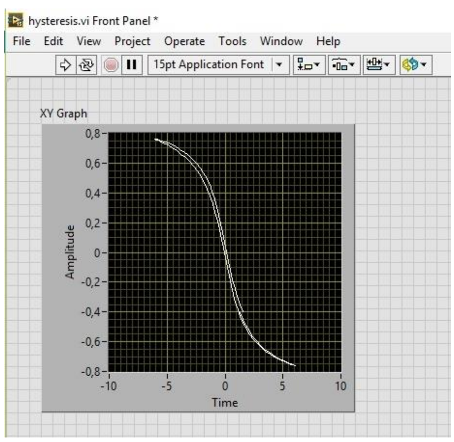

Fig. 4. Program interface that graphically demonstrates modeling hysteresis characteristic

3. Practical research of the nonlinear properties of the memristor

In this study, we use the memristor company KNOWM of series BS-AF-W 16DIP. The topological structure of the used memristor is described in detail in [13].

The memristor devices work mainly through the mechanism of the electric field of forced generation of the movement of metal ions through a multi-layer stack of chalcogenide material. The secondary mechanism of the operation is the phase change, which can be set as the main mode of operation depending on the operating conditions. The stack material is based on the mobile ionic conductivity of the metal through the chalcogenide material. Devices made from a metal layer that is easily oxidized are located near one of the electrodes. When the voltage is applied to a device with a more positive potential on the electrode near this metal layer, the metal is oxidized to form ions.

Figure 5 shows the structure of the layers of materials of the composition of the memristor [13].

After the formation of ions, the movement through the device in the direction of the lower electrode potential, these ions move through a layer of amorphous chalcogenide material (active layer) to reach the lower potential of the electrode while they decrease to their metal form and eventually form a conductive path between the two electrodes, which encompasses layer of the active material, reducing the resistance of the device. Changing the direction of the applied potential leads to the fact that the conductor channel decomposes (dissipates) and the resistance of the device increases. The devices are bipolar, cyclic between the values of high and low resistance when switching the polarity of the applied potential. Resistance is always linked with the amount of metal located within the active layer.

The memristor has two main types of work: ionic conductivity and phase change, and it can be introduced into a state consisting of a combination of two modes. The hysteresis and incremental response will vary depending on the mode in which the memristor is located at a given time.

In this paper we used a method for obtaining volt-ampere traits of the memristor.

The method we used to acquire volt-ampere characteristics is based on using sinusoidal input sign and steady increment of the amplitude of the sine wave for as long as the memristor has the properties required. Resistor *R* is a current-restricting resistor with an estimation of 51 kΩ. A sine wave from 1 to 100 Hz is applied, it is with amplitude of 0.25 V. The voltage is step by step expanded until the point when the hysteresis circle begins to be obvious. For the reason that device is working in ion-conduction mode simplest, the voltage over the load responds via following the enter waveform amid the positive cycle, the load responds and amid the negative-going erase cycle until the eradicate limit makes the gadget resistance increment.

Nonlinear characteristics of the memristor are obtained by the connection circuit presented in Figure 6.

To achieve phase-shift operation, the device is operated under high voltage and under specified conditions. In order to obtain a device from the phase transition mode, pulse, higher return voltage and pulse melting are used. Figure 7 shows the response of the phase change to a higher applied voltages in the abrasion region.

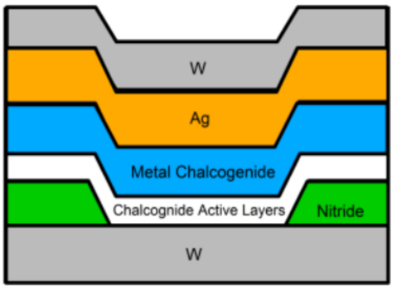

Fig. 5. Structure of the layers of the material of the memristor

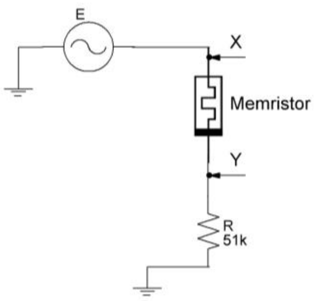

Fig. 6. The circuit of connection of the memristor to obtain I-V characteristics

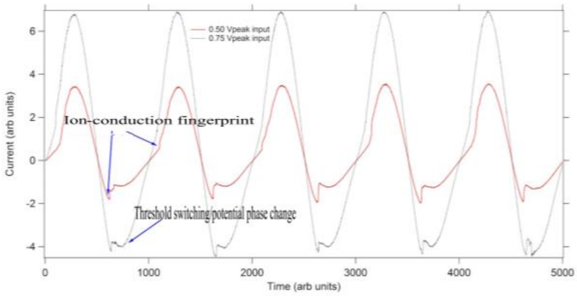

Fig. 7. Reaction of phase change from the value of the applied voltage

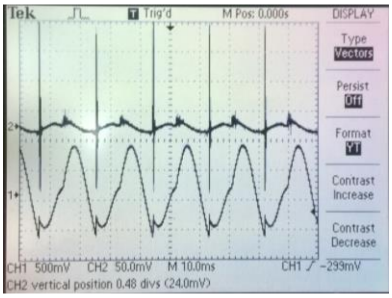

Fig. 8. Experimental phase change of the value of the applied voltage

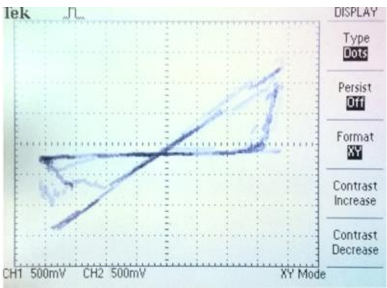

Fig. 9. I-V characteristics of the memristor at a voltage of 1.4 V and a frequency of 30 Hz

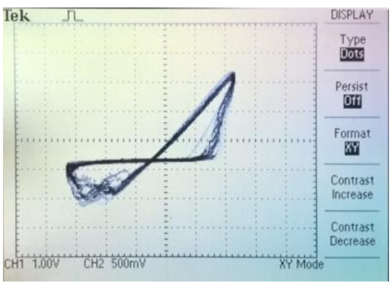

Fig. 10. I-V characteristics of the memristor at a voltage of 2 V and a frequency of 100 Hz

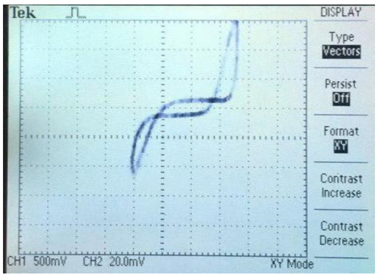

Fig. 11. I-V characteristics of the memristor at a voltage of 0.5 V and a frequency of 15 Hz

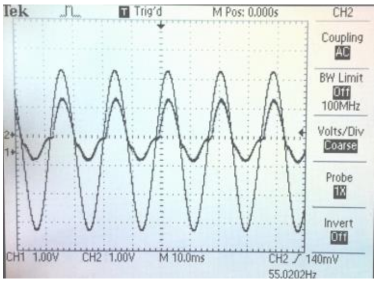

Fig. 12. Time distribution of the signal at a frequency of 50 Hz

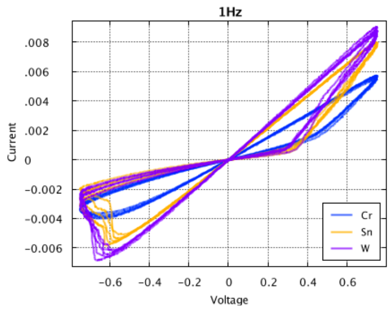

Fig. 13. Theoretical view of I-V characteristics

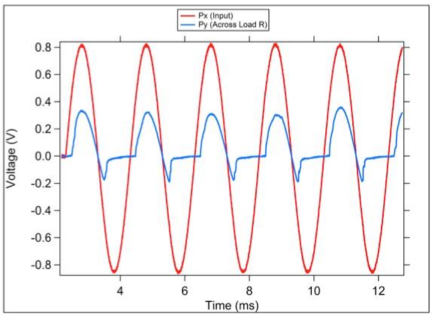

Fig. 14. The theoretical view of the time distribution

Figure 8 shows the experimental result of phase change from the value of the applied voltage.

Practically the following characteristics are obtained, according to the connection circuit shown in Figure 6, the memristor on Figure 9 at the voltage of the source E at the level 1.4 V and frequency 30 Hz.

Figure 10 shows the appearance of a hysteresis loop at a voltage of 2 V and a frequency of 100 Hz. Signals for hysteresis loops were removed from the X and Y points.

Figures 13 and 14 show the theoretical results, which are described in [13].

As can be seen from the above theoretical results coincide with the practical ones. This behavior of the memristor allows it to be used as a bipolar switch.

4. Conclusions

Nonlinear properties of volt-ampere characteristics are investigated, which makes it possible to use nonlinear properties of a memristor for constructing a oscillator of chaotic signals. It is established that in contrast to the transistor, the final state of the memristor in terms of charge does not depend on the bias voltage, that is, to support the resistance of the memristor at a certain value does not require a constant voltage, after power off the memristor retains its condition, while the resistance of the transistor depends from the presence of voltage. This indicates that the memristor can perform both the role of the memory cell and the switch.

Acknowledgments

We express great gratitude to all the staff of the Department of Theoretical Physics of Lodz University, especially to the prof. Krzysztof Kowalski and prof. Jakub Rembieliński for full support.

References

[1] Agafonov O.M.: Memristor – revolucija v mikroelektronikie. X practical-science conference 2015, 2–35.
[2] Bharathwaj M., Pracheta K.: Memristor Based Chaotic Circuits. IETE Technical Review 6/2009, 1–16.
[3] Chua L.O.: Memristor – the missing circuit element. IEEE Trans. Circuit Theory 5/1971, 507–519.
[4] Corinto F., Ascoli A.: Memristor based-element for chaotic circuits. Nonlinear Theory and Its Applications 3/2012, 336–356.
[5] Strukov D.B., Snider G.S, Stewart G.R., Williams R.S.: The Missing Memristor Found. Nature 453/2008, 80–83.
[6] Şuayb Çağrı Yener, Kuntman H.H.: Fully CMOS Memristor Based Chaotic Circuit. Radioengineering 4/2014, 1140–1149.
[7] Şuayb Çağrı Yener: Fully CMOS Memristor Based Chaotic Circuit. Radioengineering 4/2014, 1140–1149.
[8] Zhao Y., Jiang Y., Jiuchao F., Wu L.: Modeling of memristor-based chaotic systems using nonlinear Wiener adaptive filters based on backslash operator. Chaos, Solitons and Fractals 87/2016, 12–16.
[9] Zhen Y., Heng T., Chen G., Chua L.: What are memristor, memcapacitor, and meminductor. IEEE Trans. Circuits Syst-II 62/2015, 402–405.
[10] Nechaj O.: Memristor: "nedostayushchiy element". Komputerra 2011, http://old.computerra.ru/vision/591537/ [1.01.2018].
[11] Memristor, http://dic.academic.ru/dic.nsf/ruwiki/527619#.D0.9C.D0.B0.D1.82.D0.B5.D0.BC.D0.B0.D1.82.D0.B8.D1.87.D0.B5.D1.81.D0.BA.D0.B0.D1.8F_.D0.BC.D0.BE.D0.B4.D0.B5.D0.BB.D1.8C. [1.01.2018].
[12] Nikiriv A.V.: Niemnogo o memristorie, 2014 http://www.trinitas.ru/rus/doc/0023/001a/1052-nik.pdf. [1.01.2018].
[13] Knowm Memristors. Knowm Inc. Santa Fe, New Mexico 2015. http://knowm.org/downloads/Knowm_Memristors.pdf [1.01.2018].

M.Sc. Sviatoslav Khrapko
e-mail: s.khrapko@chnu.edu.ua

Yuriy Fedkovych Chernivtsi National University Department of Radio Engineering and Information Security. Ph.D. student.
Research interests: information technology, intelligent control systems and neural networks.

Ph.D. Volodymyr Rusyn
e-mail: rusyn_v@ukr.net

Yuriy Fedkovych Chernivtsi National University Department of Radio Engineering and Information Security.
Ph.D. (Engineering Sciences) Assistant of Department of Radio Engineering and Information Security.
Research interests: modeling of chaotic generators and control of chaotic oscillations.
Author of nearly 30 publications in this research area.

Prof. Leonid Politansky
e-mail: krtib1989@gmail.com

Head of department of Radio Engineering and Information Security.
Research interests: physical processes in semiconductor devices, radio engineering devices and means of telecommunications. Author of nearly 200 publications.

otrzymano/received: 10.10.2017 *przyjęto do druku/accepted: 15.02.2018*

DOI: 10.5604/01.3001.0010.8545

IMITATION MODELING OF THE ROUTING PROCESS BASED ON FUZZY LOGIC

Ivan Lesovoy, Genadij Pylypenko
Odessa National A.S. Popov Academy of Telecommunications, Infocommunication Faculty, Telecommunication systems Department

Abstract. *The paper discusses the details of modeling of the routing process according to the loading of output buffer storage. Shows the obtained dependence of the fraction of lost packets from the input intensity. It is shown that taking into account buffer occupancy increases the efficiency of their use and can significantly affect the quality of the functioning of the telecommunications network in the face of considerable.*

Keywords: fuzzy logic, routing, load, packet loss

MODEL SYMULACJI PROCESU ROUTINGU OPARTEGO NA LOGICE ROZMYTEJ

Streszczenie. *W niniejszym artykule zostały omówione cechy symulacji procesu routingu uwzględniające nośność buforów wyjściowych napędu. Otrzymano zależność frakcji zagubionych pakietów od intensywności strumienia wejściowego. Wykazano, że uwzględnienie obciążenia bufora zwiększa efektywność ich użytkowania i może znacząco wpłynąć na wydajność sieci telekomunikacyjnej w warunkach znacznego obciążenia.*

Słowa kluczowe: logika rozmyta, routing, obciążenie, utrata pakietów

Introduction

In the past telecommunication network applications have used a modest percentage of bandwidth and no one of those applictions had QoS requirements. Currently, the prevalent use of topology-driven IP routing protocols with shortest-path computations is causing serious imbalance of packet traffic distribution when least-cost paths converge on the same set of links, leading to unacceptable dela ys or packet loss even when feasible paths over less utilized links are available.

At this time, applications have been routed through network as best effort services. As we know, best effort services are not suitable for multimedia applications.

Congestion occurs when the telecommunications network uses network resources unevenly, there is blocking, or when the number of packets received by the network to transport between users exceeds a certain threshold.

In the process of controlling the queue for hypothetical traffic, the waiting time in the queue and the probability of an overflow of the input buffer are calculated [2]. If the probability of buffer overflow and buffer overflow corresponds to the desired QoS, then a new traffic packet is received.

The search for the best route is carried out in a network with indistinctly defined parameters since switching units and transmission channels parameters used to determine the metrics in routing protocols may change. Telecommunications network load is not a uniform and it changes through time.

In the loading buffer management system based on a rigid logic, excessive requirements for limited resources telecommunication network by one or more users can reduce the quality of service for other users. Additionally, there are some problems that can occur during this transmission, especially in aspect of delays, bandwidth and packet losses. Therefore it is desired to design some intelligent controlling mechanisms for solving different problems in a network. In order to design the above mention intelligent mechanisms in network platform we have used theory of fuzzy sets. Solve the problem of designing an adequate metric allows fuzzy logic based on the theory of fuzzy sets.

In this paper, we propose a fuzzy-logic based algorithm for routing under traffic engineering constraints. The proposed Fuzzy Routing Algorithm (FRA) modifies the well known protocol EIGRP [4], by using fuzzy-logic membership functions in the – buffer load control process.

1. Routing based on fuzzy logic

With the development of telecommunication networks, there are more and more additional factors that must be considered in routing algorithm, which points to the need to improve routing protocols through analysis and evaluation performance. To improve the routing algorithm adequacy, the metric should take into account some more factors. An important factor in choosing a route is the degree of utilization of the output buffer, which determines, or discard of the packet or redirection of it by a longer route whose buffers are less loaded. However, as a rule, the degree of buffer loading in determining the metric is not taken into account. The switching nodes and transmission channels used to calculate the metric may vary due to the fact that:

- the buffer space of routers is restricted;
- the reliability of lines and equipment transport network is limited;
- signals distributed to the network are exposed to random nature noise;
- to handle packet in router need some time;
- the length of the messages are independent.

Thus, finding the optimal route is in a network with fuzzy parameters or sets of parameters. In a network with fuzzy parameters to describe the inaccurate category, ideas and knowledge to operate them and make appropriate conclusions we used fuzzy logic the theory it is based on fuzzy sets.

Fuzzy logic is tolerant in imprecise data, nonlinear functions and can be used with other techniques for different problems solving. The main principle of fuzzy logic is using fuzzy groups which are without crisp boundaries.

In particular the fuzzy logic controllers is useful in two special cases:

- when the control processes are too complex to analyze by conventional quantitative techniques;
- when the available sources of information are interpreted qualitatively or uncertainly.

When choosing the best route the routing algorithm based on fuzzy logic allows set factors considered. In this case the most acceptable for systems for control the traffic is linguistic fuzzy decision-making model. Given that traffic control is carried out in real time, and hassle formalization information on the procedures and conditions for their use, with the description of knowledge, it is advisable to use productive model (a set of fuzzy production rules).

The concept of "fuzzy logic" was introduced by Zadeh (1965). He proposed the theory of "fuzzy sets", which can be used to construct fuzzy analogs of all mathematical concepts and to create necessary formal techniques for simulation of human reasoning and human way of solving problems. The theory of "fuzzy sets" deals with "human knowledge" which is called "expert information".

Fuzzy logic introduces a simple, rule-based IF X AND Y THEN Z approach to solving the management problem, rather than trying to model the system mathematically. Fuzzy logic describes the behavior of the operator during control. Fuzzy logic is based on the empiricist (experience) of the operator, and not on understanding the insides of the system. Fuzzy logic uses some numerical parameters to estimate the load and the rate of change in the load, but exact values of these quantities are usually not required.

For example, instead of using the exact values of buffer loading, we are dealing with rules like "IF (the download is small) AND (rate of change in the load is small) THEN (increase the number of packets for transmission through this interface)" or "IF (large buffer loading) AND (the load increases rapidly) THEN (redistribute packages on alternative routes)".

These statements are inaccurate and at the same time describe what really happens. Usually fuzzy logic allows the system to work from the first time without any adjustment.

A Fuzzy Logic Controller is a rule based system in which fuzzy rule represents a control mechanism. In this case, a fuzzy controller uses fuzzy logic to simulate human thinking.

A fuzzy control is characterized by immediate application of qualitatively formulated expert knowledge for generation of control actions on the controlled object (process) is represented by rules of the form: if (initial situation), then (response). Such rules correspond to the elementary form of human interactions.

In order to get a traffic control system on the base fuzzy logic, need to describe the states and actions of the system using fuzzy rules in natural language.

The concepts of "a linguistic variable", "linguistic quantity" and "membership function" $\mu(x)$ play the central role in the theory of fuzzy sets. The function $\mu(x)$ determines the degree of membership of an element (linguistic variable) x to a fuzzy set (to a term) X in the form of a numerical value within the range [0, 1] (this numerical value is called "the degree of truth" of a linguistic variable). A fuzzy set is described completely by its membership function. For example, representing the linguistic quantity (fuzzy subsets) "negative", "positive", "large" and "small" by the linguistic variable "an error" through their membership function, the ranges of variation in the qualitatively described physical quantity. The membership function of linguistic quantities, as a rule, overlap each other; therefore, these functions can inform of different nonzero values of "degree of truth".

In Ukraine, the concept of "fuzzy-logic" introduced by Zadeh means the illegible logic; therefore, illegible controllers are named also fuzzy-controllers, and control systems with fuzzy-controllers the fuzzy-systems.

Fuzzy logic controller consists of: fuzzifier, rule base, fuzzy inference and defuzzifier. A fuzzifier operator has the function of transforming crisp value input variable to fuzzy set. Rule-Base (Linguistic Rules): Contains IF-THEN rules that are determined through fuzzy logic. Fuzzy Inference is a process of converting input values into output values using fuzzy logic. Converting is essential for decision making. Fuzzy Inference process includes: membership functions and logic operation. Defuzzifier identifies crisp value of control action. Converting process of fuzzy terms in crisp values is called defuzzification.

The use of fuzzy controllers (regulators, operating on the basis of fuzzy logic) to control the various (in particular, nonlinear and non-stationary) objects shows their high efficiency and in a number of cases their significant advantages over digital linear regulators [3].

The functional diagram of the router based on fuzzy logic is shown in Fig. 1

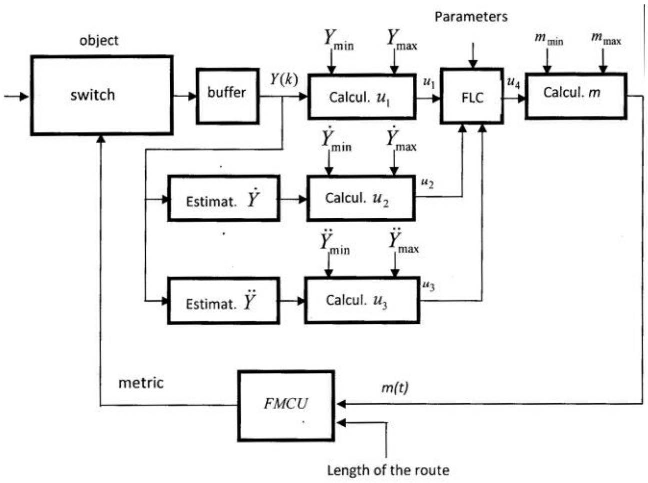

Fig. 1. Structure of the router based on fuzzy logic unit (FLC – fuzzy logic controller, FMCU – fuzzy metric calculate)

The most acceptable systems control the flow of burden is linguistic fuzzy decision-making model. Given that load control is carried out in real time, and hassle formalization information on the procedures and conditions for their use, with the description of knowledge, it is advisable to use productive model (a set of fuzzy production rules). Each fuzzy production rules allows of matching situation that has developed an action.

The conversion of current values of the input variables of a fuzzy-controllers into linguistic variables of the degree of truth is called fuzzyfication. In a fuzzy-controller, a logic decision is formed on the basis of IF-THEN rules (a rulebase). Deriving a control action at the output of a fuzzy-controller in the form of a resulting membership function (in the form of the fuzzy set) and the generation of the output variable of a fuzzy-controller (of a control action on a controlled object) are called de fuzzyfication.

The conversion of current values of the input variables of a fuzzy-controllers into linguistic variables of the degree of truth is called fuzzyfication. In a fuzzy-controller, a logic decision is formed on the basis of IF-THEN rules (a rulebase). Deriving a control action at the output of a fuzzy-controller in the form of a resulting membership function (in the form of the fuzzy set) and the generation of the output variable of a fuzzy-controller (of a control action on a controlled object) are called de fuzzyfication.

As input variables are proposed to use value-load buffer Y, utilization rate of change (first derivative) $\dot{Y}$, and acceleration (second derivative) $\ddot{Y}$ workload. Output variable controls action on the object of control m.

The main parameters of digital fuzzy controllers in which their synthesis and calculation were performed, are, firstly, the number and shape of membership functions $\mu^T(u)$ of linguistic variables and, secondly, ranges of input and output linguistic variables load buffer, the first derivative of load buffer, the second derivative load buffer control action on the switch, i.e.

$$[Y_{\min}, Y_{\max}],\ [\dot{Y}_{\min}, \dot{Y}_{\max}],\ [\ddot{Y}_{\min}, \ddot{Y}_{\max}],\ [m_{\min}, m_{\max}]. \quad (1)$$

Number of functions of MF (the number of terms that describe the input and output variables) limits, if possible, the least number [3]. For each linguistic variable you can use your membership functions. Thus, there is a fairly large number of options for assigning membership functions when optimizing the parameters of the fuzzy controller.

Membership functions take triangular. Correction of triangular MF to expert data, is performed by exponentiation, where the exponent determines the change in the form of MF.

In universal set of given two fuzzy sets, membership function which is monotone for each linguistic value (terms positive -1, negative -2)

$$\mu^1(u) = 1 - u; \quad \mu^2(u) = u; \quad u \in [0, 1].$$

Fig. 2 shows the triangular membership functions of the device for controlling the load output buffer of the router functioning on the basis of fuzzy logic.

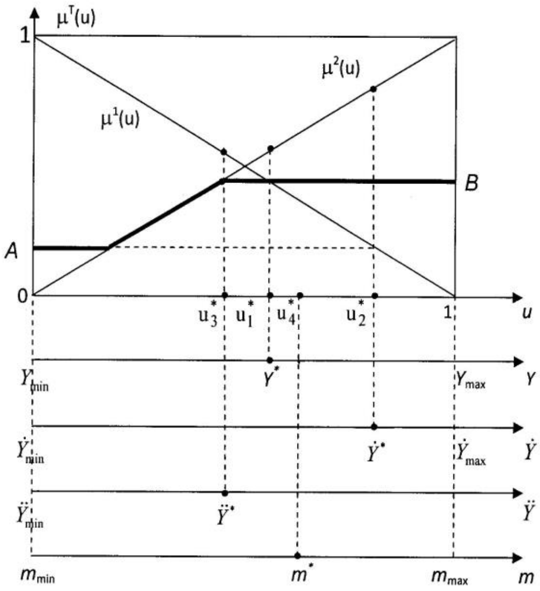

Fig. 2. The triangular membership functions of the device for controlling the load of the output buffer

In order to gain better results at the output of the FLC, one important role plays selection of defuzzification method. There are some defuzzification methods: COG (Centre of Gravity), COGS (Centre of Gravity for Singletons), COA(Centre of Area), LM (Left Most Maximum) and RM (Right Most Maximum).

Three most important methods are: COG, MOM and LOM. It is important to find which method gives better results in aspect of routing.

Centre of Gravity method determines the centre of resultant shape that is gained from membership functions with AND and OR logic operators. Formula with which we can calculate the defuzzified crisp output U is given:

$$U = \frac{\int_{Min}^{Max} u\mu(u)du}{\int_{Min}^{Max} \mu(u)du},$$

where: U is defuzzification result; u – output variable; μ – membership function; *Min* – minimum limit for defuzzification, *Max* – maximum limit for defuzzification.

With formula we can calculate the surface of resultant shape and also we can find central point. Projecting this point in the abscissa axis determines the crisp value after defizzification.

The resulting membership function was obtained by the Mamdani method.

The abscesses center of gravity $s_c = S(u_c, \mu_c)$ calculation in resultant shape (MF) $\mu(u)$ within the range of the variable u from $u = U_1$ to $u = U_2$, are determined using numerical integration the trapezoids method

$$u_c = \frac{\frac{U_1\mu_1}{2} + \sum_{i=1}^{M-1} u_i\mu_i + \frac{U_2\mu_M}{2}}{\frac{\mu_0}{2} + \sum_{i=1}^{M-1} \mu_i + \frac{\mu_M}{2}},$$

where: $(U_2 - U_1)/M = u_0$ sampling step; M – the number of readings on the interval $U_2 - U_1$, i = 1, 2, 3, ..., M–1.

To test and analyze the effectiveness of the algorithm, experimental studies were performed.

2. Modeling process routing based on fuzzy logic

Routing metrics have a significant role, not just in complexity of route calculation but also in QoS, especially when we have to deliver triple play services. The use of multiple metrics is able to model the network in a more precise way, but the problem for finding appropriate path can become very complex.

Thus, it is important to take into consideration some metrics that play a key role in offering those services. Those metrics play a direct role in for delivering triple play services over packet network. In order to consider multiple metrics simultaneously, we will use the main component of soft computing, so called fuzzy logic.

Controller based on fuzzy logic is called fuzzy logic controller (FLC). FLC is intelligent technique that can manipulate with two or more input parameters simultaneously without any problem.

The process of passing packets flow through the node distribution information is random and similar processes in queuing systems. Routers serviced packet flows received from subscribers and transmission channels of adjacent units. Streams of incoming packets and processing time are random, so the entrance formed network processor queue for service. To maintain the router packages that may not serve the currently prescribed buffer storage. That inlet distribution unit sold procedure information service with expectations.

After processing processor packages are sent to one of the transmission channels adjacent node. The time depends on the transmission capacity of the selected path and the length of the package and is a random variable. So at the entrance of each transmission path also implemented the bulk of service expectations. So is a two-phase model of router queuing system.

An important factor is the degree of choice route congestion source junction that determines the appropriateness or drop packet forwarding it more extended route, which buffers are not loaded. However busy junction buffer storage in determining metrics is usually not taken into account.

In the process of routing expediently to consider not only the distance but also dynamic load corresponding output buffer drive interface and a number of other factors. It should be considered that when choosing the best route factors influence the set allows routing algorithm based on fuzzy logic. Research methods of load control based on fuzzy logic executed for the most common protocol EIGRP.

For study the efficiency of EIGRP routing protocol based on fuzzy logic, is developed simulation model, under such assumptions: packets entering the router are characterized by priority, length and the remainder of life-time.

The remainder of the packet lifetime in the model is given by the random variable with exponential distribution. Packet loss simulated router sending the package to the clipboard is full, so the request is not served and the number of counter requests is not granted, it is incremented.

Sometimes service packages in the router and eventually spread signal transmission path are ignored and the router queue is not limited. The length of the packet is a random variable with exponential distribution and average value $\overline{l_n}$. The main input stream is a Poisson with intensity λ_0. The capacity of all output channels of 10 Mbit/s. Functional circuit simulation model is shown in Fig. 3.

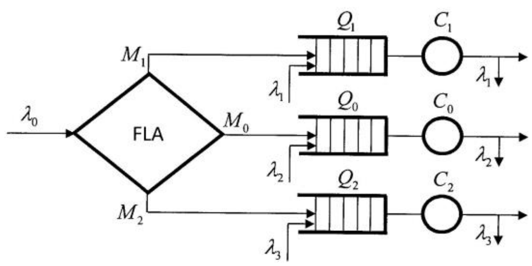

Fig. 3. Functional diagram simulation model of network processor

Model network processor consists of a fuzzy implement routing algorithm (FLA) and three output buffers to drive the main (M_0) and two alternative routes (M_1, M_2).

The direction of the packets to the appropriate buffer storage is carried out in accordance with a modified protocol EIGRP based on fuzzy logic. $Q_0, Q_{1,} Q_2$ – the queue in output buffer router joints.

Loading telecommunications network to network processor is simulated by introducing into each output buffer more incoming flow Poisson intensity λ_i ($i = 1, \ldots, 3$). After passing through the flow further paths are removed.

The proposed model of the network processors uses "soft" computing [3]. With fuzzy production rules, a linguistic approximation of the process of selecting transmission channels is performed based on their bandwidth and dynamic load output buffers drives.

In the simulation efficiency of routing it was estimated the ratio of lost packets to the total number of packets transferred [4]. Lost packets dependence on the intensity of the input stream is given in the table.

Table 1. Dependence Lost packets on the intensity of the input stream of packets.

Intensity of the input stream, Mbit/s		0	15	30	45	60	90	120	150
Lost packets dependence	EIGRP	0	0,1	0,33	0,48	0,62	0,69	0,75	0,76
	EIGRP with FLA	0	0	0	0,29	0,47	0,59	0,73	0,76

The traffic control system for "hard" logic takes a decision to route only alternative route in case of exceeding a certain value workload output buffer. Network processor based on fuzzy logic controlling the dynamic load output buffers of the first manifestations of the increase in their workload, which have no effect on the efficiency of the telecommunications network in advance direct flow of packets alternative routes.

Routing algorithm based on fuzzy logic would reduce the share of lost packets by 30 percent if the intensity of the input stream equal to the total throughput capacity of output channels and 10 percent if the intensity of the input stream exceeds the total bandwidth output channels doubled. This shows at improving the quality of routing since packets are not lost, and sent to alternative routes are not loaded, providing efficient use of the resource router [1].

3. Conclusions

The analysis methods of design metrics in different routing protocols not found profound reflection in the metric of all aspects of the network. Despite the complexity of routing algorithms, the number of factors is taken into account in the metric remains low (1–4 factors).

To improve the adequacy of the routing algorithm, the metric should consider more factors. Solve the problem of designing a new metric based on fuzzy sets theory allows and it is based on fuzzy logic.

The results reported in this paper show that FRA achieves traffic distribution at higher loads without increasing the path-request blocking probability. The analysis of the results shows that when using a fuzzy set of routing algorithms, the average queue length and waiting time in the packet in the queue is somewhat increasing, indicating a more complete use of the router's resources.

The use of fuzzy logic is easily possible to create a scalable system routing logic which makes it easy to build and change the structure of metrics on a systematic basis by expanding the (changing) rules base for route selection. Studies have shown that with the use of fuzzy sets in problems routing opens up new possibilities of management based on simple heuristic rules and adaptation to extreme and non-stationary traffic.

Taking into account the dynamics of load buffers increases the efficiency of their use, contributing to the optimization of the network (reducing time distribution packages, reducing the share of lost packets, simplifying the requirements for buffer memory and storage interfaces.). Given the significant workload resources telecommunications network may significantly affect the quality of operation.

Optimizing the parameters of the regulator during the design and implementation of the router does not take much time. Automation of the process of debugging the router based on fuzzy logic will significantly reduce the development and commissioning time of routers based on fuzzy logic.

References

[1] Kleynrok L., Hrushko Y.Y., Neyman V.Y.: Teoriya massovogo obsluzhivaniya. Mashinostroyeniye. Moscov 1979.

[2] Lozhkovskyy A.H., Verbanov O.V.: Pydvyshchennya tochnosty rozrakhunku kharakterystyk yakosty obsluhovuvannya pry samopodyvnomu trafyku merezhy. Naukovi pratsi ONAZ im. O.S. Popova 1/2015, 36–41.

[3] Pospelov D.A.: Sytuatsionnoe upravlen′ye: Teoriya i praktyka. Nauka, Moscov 1986.

[4] Vrublevskyy A.R., Lisovyy I.P., Pylypenko H.V.: Modelyuvannya protsesu marshrutizatsii na osnove nechetkoy logiko za protokolom EIGRP. Modelyuvannya ta informatychni tekhnolohiyi 77/2016, 145–147.

Prof. Ivan Lesovoy
e-mail: ur5fo55@gmail.com

Lesovoy Ivan Pavlovich Doctor of Technical Sciences (2005), Professor (2008). Professor of the Department of Telecommunication Systems, Institute of Information and Communication Technologies and Computer Engineering of Odessa National Academy of Telecommunications the name of A.S. Popov. Author of more than 100 scientific works, including 10 monographs, 5 textbooks. Research interests: fuzzy logic in telecommunications, digital processing and signal generation in telecommunication systems.

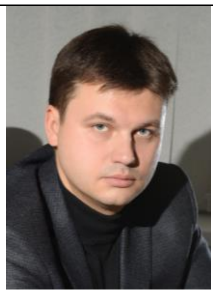

M.Sc. Genagij Pylypenko
e-mail: gvpilipenko@gmail.com

Pylypenko Genadij Viktorovych postgraduate student of the department of Telecommunication Systems, Institute of Information and Communication Technologies and Computer Engineering of Odessa National Academy of Telecommunications, the name of A.S. Popov. Author of 8 scientific works. Research interests is packet network traffic management on the fuzzy logic base.

otrzymano/received: 10.10.2017 *przyjęto do druku/accepted: 15.02.2018*

DOI: 10.5604/01.3001.0010.8569

INVARIANT PIEZORESONANCE DEVICES BASED ON ADAPTIVE MULTIFREQUENCY SYSTEMS WITH A PREDICTIVE STANDARD

Sergey Pidchenko, Alla Taranchuk
Khmelnitsky National University, Department of Telecommunication and Computer-Integrated Technologies

Abstract. *The paper presents conceptual provisions for the construction of invariant multi-frequency piezoelectric resonance devices with a predictive reference model. The law of the optimal control of the system in real time is formulated, aimed at minimizing energy costs to ensure the trajectory of the system. The results of piezoelectric resonance system mathematical modelling in the conditions of temperature and vibration perturbations are presented.*

Keywords: invariant multi-frequency piezoelectric resonance system, optimal control, mathematical model

NIEZMIENNE URZĄDZENIA PIEZOREZONANSOWE NA PODSTAWIE ADAPTACYJNYCH WIELOCZĘSTOTLIWOŚCIOWYCH SYSTEMÓW Z PROGNOZOWANYM STANDARDEM

Streszczenie. *W artykule przedstawiono koncepcyjne zasady konstruowania niezmiennych wieloczęstotliwościowych piezoelektrycznych urządzeń z predykcyjnym modelem odniesienia. Zostało sformułowane prawo optymalnego sterowania systemem w czasie rzeczywistym, aby przy minimalnych stratach energii zapewnić trajektorię ruchu systemu. Przedstawiono wyniki matematycznego modelowania układu piezorezonansowego w warunkach zaburzeń temperatury i drgań.*

Słowa kluczowe: niezmienne wieloczęstotliwościowe układy piezoresonansowe, optymalne sterowanie, model matematyczny

Introduction

Modern piezoelectric resonance devices as part of infocommunication systems operate in considerable variation of temperature and vibrational-mechanical environment. This obstacle substantially complicates a problem of providing the invariance under a condition of parametrical non-stationarity and it requires special approaches to be solved.

Effective solving the problem dedicated to providing technical invariance of a piezoelectric resonance device (PRD) requires the transition to multi-frequency mode of oscillatory system excitation and representation of PRD like dynamic object. It allows formulating a novel algorithmic approach to problem-solving concerning providing the PRD invariance in respect to destabilizing and perturbation factors (DPF) by using a combination of the main, i.e. frequency defining and stabilizing the function of quartz resonator (QR) and additional measurement function that allows performing flowing PRD identification [1, 2].

1. Invariant PRD model in the form of adaptive system with the predictive standard

Let us consider a model of multi-frequency invariant PRD having controlled dynamics (IPRD/CD). Such model is represented in the form of an adaptive self-adjusting control system having predictive standard model (see Fig. 1). The main element of the system is the PRD core, i.e. multi-frequency oscillatory piezoelectric resonance system (MOPS) contained additional circles for control, matching, thermo- and vibro-stabilization and operating according to predictive standard model (see Fig. 1). The main element of the system is the PRD core, i.e. MOPS contained additional circles for control, matching, thermo- and vibro-stabilization influenced by destabilizing and perturbation factors (PF) [2, 3].

Optimal or suboptimal estimation and identification system forms the estimate of vector state $\hat{\mathbf{X}}_S$ and vector parameter estimate $\hat{\mathbf{X}}_P$ for mathematical model PRD on the basis of signal vector observation $\mathbf{Y}$. This approach corresponds to parametrical identification. Optimal control system forms the vector of controlling influences $\mathbf{u}$ on the basis of the standard mathematical model and a current estimate of the state vector PRD. It provides optimal system operating mode performed both at the stage of exit to the multi-frequency stable oscillation (terminal task) mode and at the stage of system state stabilization (technical invariance) according to given optimization criterion and limitations for $\mathbf{L}$ caused by a specific physical realization of the MOPS. Expanded vector of controlling influences $\mathbf{u}'$ also is used by optimal estimation and identification system.

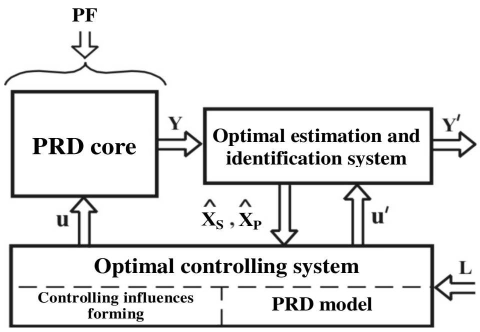

Fig. 1. Generalized structure of multi-frequency IPRD/CD

System operating is defined by standard predictive PRD model. The model allows defining the end time t_{set} and the exit trajectory $y_{mi}(t)$ for each oscillation excitation mode $\hat{y}_i(t)$ with given accuracy ε_i on the basis of a priory and current information about IPRD/CD as:

$$\left| y_{mi}(t) - \hat{y}_i(t) \right| \le \varepsilon_i\,;\; i = \overline{1,n} \tag{1}$$

according to minimum time criterion necessary for reconstruction of multi-frequency oscillations:

$$\tau_{\text{set}}^{\text{opt}} = \min_{\mathbf{L}\in\mathbf{D}} \max_{1\le i\le n} \tau_{\text{set}_i}\,, \tag{2}$$

$$\mathbf{D} = \left\{ \mathbf{L} \in \Re^{\mathrm{N}} : l_{j\min} \le l_j \le l_{j\max}, 1 \le j \le N \right\},$$

where τ_{set_i} is the set time for i-th oscillation mode which defined by given long-time frequency instability parameter δ_i; $\mathbf{L}_{\min} = \{ l_{1\min},...,l_{\mathrm{N}\min} \}$, and $\mathbf{L}_{\max} = \{ l_{1\max},...,l_{\mathrm{N}\max} \}$ are the vectors of minimum and maximum permissible values of core parameters given in IPRD/CD.

IPRD/CD structure comes near to optimal mode. It corresponds to the separation theorem and gives a possibility of separate optimization for estimation, identification and control system [2].

2. The basic equivalent circuit of multi-frequency core MOPS

The basic core architecture represents multi-frequency MOPS to have principles of creating filtering schemes implemented (Fig. 2). It incorporates passive multi-frequency quartz quadripole unit (MQU) on the base of quartz resonator with m-frequencies generating z_{qj} and n excitation channels embedding the generalized non-linear component (NLC) and phasing selective feedback circuit (FBC). The automatic bias circuits with complex equivalent resistance z_{b_i} are used for stabilizing NLC$_i$ operational mode. The selective non-linear circuits FBC with gain $K_{ji}(j\omega, u_\Sigma, \tau)$, $j=\overline{1,m}$, $i=\overline{1,n}$, except for their function to set required amplitude-phase ratio in excitation channels, provide significant reducing competition in oscillations due to their own selective properties $K_{ji}(j\omega)$ and also automatic adjustment $K_{ji}(u_\Sigma)$ of oscillation amplitudes for fixing the specified (ultimately acceptable) power dissipation on QR.

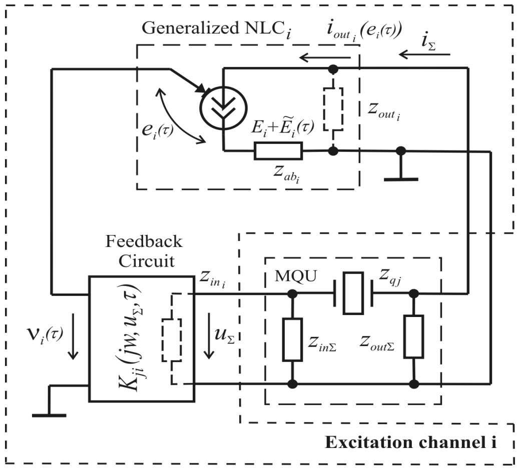

Fig. 2. The basic equivalent circuit of multi-frequency core MOPS

Figure 2 has the following symbols' identifications: $z_{\text{in}\Sigma} = R_{\text{in}\Sigma} \Big/ \left(1 + j\omega\tau_{\text{in}\Sigma}\right)$, $R^{-1}_{\text{in}\Sigma} = \sum_i R^{-1}_{\text{in}_i}$, $C_{\text{in}\Sigma} = \sum_i C_{\text{in}_i}$ – the complex equivalent total resistance of partial FBC input circuits; $z_{\text{out}\Sigma} = R_{\text{out}\Sigma} \Big/ \left(1 + j\omega\tau_{\text{out}\Sigma}\right)$, $R^{-1}_{\text{out}\Sigma} = \sum_i R^{-1}_{\text{out}_i}$, $C_{\text{out}\Sigma} = \sum_i C_{\text{out}_i}$ – the complex equivalent total resistance of output NLCi circuits; $z_{\text{ab}_i} = R_{\text{ab}_i} / \left(1 + j\omega\tau_{\text{ab}_i}\right)$ – complex resistance of auto-bias circuit i; $\tau_{\text{ab}_i} = R_{\text{ab}_i} C_{\text{ab}_i}$, $\tau_{\text{in}\Sigma} = R_{\text{in}\Sigma} C_{\text{in}\Sigma}$, $\tau_{\text{out}\Sigma} = R_{\text{out}\Sigma} C_{\text{out}\Sigma}$ – time constants; $i_\Sigma = \sum_i i_{\text{out}_i}(e_i)$ – total current of NLCi; $e_i(\tau) = \sum_j v_i(\tau) + E_i + \tilde{E}_i(\tau)$ – control voltage in NLCi input, where E_i, $\tilde{E}_i(\tau)$ – constant and variable components of auto-bias voltage;

$u_\Sigma(\tau) = U_0(\tau) + \sum_j U_j(\tau) \cdot \cos[\omega_j t + \varphi_j(\tau)]$ – the total voltage in FBC circuit input, where $U_j(\tau)$, ω_j and $\varphi_j(\tau)$ – envelope, frequency and phase of oscillation j correspondently, $\tau = t - t_0$ – time interval from initial moment t_0 (MOPS start up moment).

3. General formulation of the task of the temperature and vibration measuring

Multi-frequency excitation of MPOS is necessary for combining the function of stabilizing the frequency with measuring function, which allows the simultaneous identification of influence factors (temperature, vibration) and allows defining MPOS as multi-dimensional object, in the model of which the controlled perturbations appear:

$$y_i(p) = y_{s_i}(p) + \Delta y_{c_i}(p) + \Delta y_{nc_i}(p) = W_{ii}(p) x_{s_i}(p) + \\ + \sum_{j=1,\, j\neq i}^{m} W_{ij}(p) x_{s_j}(p) + \sum_{k=1}^{n} A_{i_c}(p) x_{c_k}(p) + \Delta y_{nc_i}(p), \tag{3}$$

where $\mathbf{X}_s(p) = \{x_{s_i}\}_{j=1}^{m}$ – is the vector of control which is set; $\mathbf{X}_c(p) = \{x_{c_k}\}_{k=1}^{n}$ – is the vector of controlled perturbations; $\mathbf{W}(p)$, $\mathbf{A}(p)$ – are the transmission functions of direction channels and the channels of perturbations accordingly; $\Delta y_{nc_i}(p)$ is the additional movement by means of non-controlled perturbations.

Dependence of QR frequencies from temperature T and vibration acceleration G are presented as:

$$f_{REF} = f^0_{REF} + a_{1T} T + a_{1G} G; \tag{4}$$

$$f_T = f^0_T + a_{2T} T + a_{2G} G; \tag{5}$$

$$f_G = f^0_G + a_{3T} T + a_{3G} G, \tag{6}$$

where f^0_{REF}, f^0_T, f^0_G are nominal meanings of frequencies; a_{1T}, a_{2T}, a_{3T} – are coefficients of temperature sensitivity; a_{1G}, a_{2G}, a_{3G} – are the coefficients of vibration -sensitivity.

On the exit of Mixers the oscillations of difference frequencies are distinguished:

$$F_T = f_T - f_{REF} = \left(f^0_T - f^0_{REF}\right) + a^*_1 T + a^*_2 G = F^0_T + \Delta F_T; \tag{7}$$

$$F_G = f_G - f_{REF} = \left(f^0_G - f^0_{REF}\right) + a^*_3 T + a^*_4 G = F^0_G + \Delta F_G, \tag{8}$$

where $a^*_1 = (a_{2T} - a_{1T})$, $a^*_2 = (a_{2G} - a_{1G})$, $a^*_3 = (a_{3T} - a_{1T})$, $a^*_4 = (a_{3G} - a_{1G})$ are difference coefficients.

Solving together (7) and (8) we get a possibility of synchronous identification of temperature T and vibrational acceleration G [3]:

$$T = \frac{a^*_4 \Delta F_T - a^*_2 \Delta F_G}{a^*_1 a^*_4 - a^*_2 a^*_3}; \; G = \frac{a^*_1 \Delta F_G - a^*_3 \Delta F_T}{a^*_1 a^*_4 - a^*_2 a^*_3}. \tag{9}$$

3. Strategy of optimal control for software trajectory motion of PRD with predictive model

The designed concept for invariant PRD like adaptive system with predictive standard requires solving inverse dynamics problem. It requires determination of the dynamic system motion and its parameters under a condition of performing of the motion corresponding to given trajectory. In accordance to specificity of development and exploiting IPRD/CD control process is performed by two stages.

The first stage is the oscillation forming. Control impacts are formed in each exciting channels. The impacts provide the output to the stationary mode under a minimum time of set of stable multi-frequency oscillatory mode.

Second stage is the oscillation stabilization. Control of IPRD/CD is directed to support of generated oscillations stability under influence of destabilizing factors, i.e. providing technical invariance [2].

We will carry out the construction of optimal or sub-optimal control law according to generalized work criterion that has good results at the stage of analytical construction during a designing period. Using this approach allows not only simplifier the procedure of obtaining the optimal control laws, but often do not obtain the functional dependences due to the cumbersomeness and complexity related to control laws. In such case, solving a problem comes to an end with an algorithm which performs optimization during system functioning and it is convenient from the point of view of a realization of microprocessor control.

Let us consider controlled process in the form of

$$\dot{y}_i + f_i(x_1, \ldots, x_n, y_1, \ldots, y_m, t) = 0, \; \dot{x}_j = u_j, \tag{10}$$

where f_i is differentiable or piecewise differentiable functions; $\mathbf{x} = (x_1, \ldots, x_n)$ is the state vector of the control elements; $\mathbf{y} = (y_1, \ldots, y_m)$ is the state vector of the control object; $\mathbf{u} = (u_1, \ldots, u_m)$ is the control vector, $i = \overline{1,n}$, $j = \overline{1,m}$.

In considered case, the control of the rates related to the variations of controlled elements is performed. Object non-stationarity can be taken into account by extension its state vector.

Equation of system free movement (3) can be written as

$$\dot{\mathbf{y}} + f(\mathbf{x}, \mathbf{y}, t) = 0, \; \dot{\mathbf{x}} = 0, \tag{11}$$

e.g. free system movement is the movement under fixed locations of the control elements.

For the task formulated by using an expression (3), we have expanded state vector $(\mathbf{x},\mathbf{y})$. According to optimal controlling the minimum of the functional

$$I = V_{\text{set}}(\mathbf{x}(t_2),\mathbf{y}(t_2)) + \int_t^{t_2} Q(\mathbf{x},\mathbf{y},t)dt + \frac{1}{2}\int_t^{t_2}\sum_{j=1}^{m}\frac{u_j^2+u_{jopt}^2}{k_j^2}dt \quad (12)$$

provides the control of the form of

$$u_j = u_{jopt} = -k_j^2\frac{\partial V}{\partial x_j}, \quad (13)$$

where $V = V(y,t)$, is the solving the following equation

$$\frac{dV}{dt} - \sum_{i=1}^{n} f_i\frac{dV}{dy_i} = -Q, \quad (14)$$

under boundary condition of $V_{t=t_2} = V_{\text{set}}$; f_i, Q, where V_{set} are given uninterrupted functions; $k_j^2 > 0$ are given coefficients.

In order to provide prediction of object behavior, model of free movement must operate in faster mode as $t' = t/\chi$, where $\chi = \text{const} >> 1$. Then, the equation of prediction model can be written as

$$\frac{d\mathbf{y}_{\text{M}}}{dt'} + \chi\cdot f(\mathbf{x}_{\text{M}},\mathbf{y}_{\text{M}},\chi t') = 0, \quad \frac{d\mathbf{x}_{\text{M}}}{dt'} = 0. \quad (15)$$

A prediction model has to provide the integration of free movement during total optimization interval from $t = t_1$ till to t_2 by using faster rate under initial conditions given by control (estimation) system. Integration rate that defined by χ value is selected in such a manner that for each cycle of Δt_c (in many times less than $t_2 - t$) several runs of a free movement were performed during the interval of $t_2 - t$. The latter procedures are necessary for numerical evaluation the partial derivations $\partial V/\partial y_i$. Because of this, the values χ in real-life control of a process must be of the value equal to dozens, hundreds and even thousands units.

The beginning of each cycle coincides with current time moment t with accuracy equal to Δt_c. At the beginning of each cycle, control and estimation system operating with real-life controlled process defines the state vector $\mathbf{x}(t)$ and gives initial conditions for free movement model (13). As a result, the following equality is provided for beginning of each cycle

$$\mathbf{y}_{\text{M}}(t) = \mathbf{y}(t). \quad (16)$$

Under free movement of the system, the left part of (7) transforms to the total derivative under time as

$$\dot{V} = -Q. \quad (17)$$

Therefore, we obtain

$$V(\mathbf{y}_{\text{M}}(t_2)) - V(\mathbf{y}_{\text{M}}(t_1)) = -\int_{t_1}^{t_2} Q(\mathbf{y}_{\text{M}},t)dt, \quad (18)$$

and for a terminal task:

$$V(\mathbf{y}_{\text{M}}(t_2)) = V_{\text{set}}(\mathbf{y}_{\text{M}}(t_2)). \quad (19)$$

Thus, for free movement system mode under predictive model, the following computations must be performed

$$V = V_{\text{set}}(\mathbf{x}_{\text{M}}(t_2'),\mathbf{y}_{\text{M}}(t_2')) + \chi\int_{t'=t/\chi}^{t_2'=t_2/\chi} Q(\mathbf{x}_{\text{M}},\mathbf{y}_{\text{M}},\chi t')dt'. \quad (20)$$

In order to evaluate by using numerical technique the partial derivations $\partial V/\partial x_j$, the variability of initial requirement related to $\mathbf{x}_{\text{M}}$ is performed for each run of the model (15).

Let us consider the features necessary for selection of integrand for minimizing functional $Q(\bullet)$ given in the form (12). The features depend on the difference between output vector $\mathbf{y}_{\text{M}}$ contained in the model (8) and the estimate of the control process state $\hat{\mathbf{y}}$:

$$Q = Q\left(\mathbf{y}_{\text{M}} - \hat{\mathbf{y}}\right). \quad (21)$$

Let us introduce the square functional as:

$$Q = \left(\mathbf{y}_{\text{M}} - \hat{\mathbf{y}}\right)^{\text{T}}\boldsymbol{\beta}\left(\mathbf{y}_{\text{M}} - \hat{\mathbf{y}}\right), \quad (22)$$

where $\boldsymbol{\beta}$ is the diagonal matrix contained the elements that are proportional to the maximum errors related to the corresponding coordinates (principle of the contribution of the errors).

By exploiting the optimal Kalman filter or suboptimal estimation procedure, it is necessary to define the following

$$\boldsymbol{\beta} = \hat{\mathbf{R}}^{-1}, \quad (23)$$

where $\mathbf{R}$ is the error covariance matrix or their estimates $\hat{\mathbf{R}}$.

It is also interesting an approach to forming the sequence of quality functional which describes the energy of system movement, for example, the minimum of acceleration energy as

$$Q = \left(\ddot{\mathbf{y}}_{\text{M}} - \hat{\ddot{y}}\right)^{\text{T}}\boldsymbol{\beta}\left(\ddot{\mathbf{y}}_{\text{M}} - \hat{\ddot{y}}\right). \quad (24)$$

This approach allows improving the dynamic accuracy for control of transmission processes in IMPRD/CD on the stage of oscillation reconstruction.

Several limitations exist for solving the task (10) – (15) according to physical peculiarities and functional assignment of PRD, particularly, for oscillation magnitude U_i, initial frequency run-out $\Delta\omega_i$, total power of quartz resonator excitation $P_{\text{osc}\Sigma}$ in multi-frequency mode and rate of its variations [2, 5]:

$$U_{\min} \le U_i \le U_{\max};$$
$$\Delta\omega_i \le \Delta\omega_{\max}, \ i = \overline{1,n}; \quad (25)$$
$$P_{\text{osc}\Sigma} \le P_{\max}; \ \frac{dP_{\text{osc}\Sigma}}{dt} \le K_{\text{dyn}}^{(P)}$$

In order to give limitations, expanded state vector $(\mathbf{x},\mathbf{y})$ can be represented in the form of some space state domain G, which we will consider as enclosed and simply-connected. Let us give the penalty function $Q_{\text{f}}(\mathbf{x},\mathbf{y})$, which is equal to zero inside and on the borders of the domain G and rather fast accrue in given domain. Assuming that the domain G is described by the equation $Q_{\text{f}}(\mathbf{x},\mathbf{y})$=0, we represent the integrand function of the functional of quality related to generalized work (12) as

$$Q = Q_{\text{opt}} + Q_{\text{f}}, \quad (26)$$

for what inside the domain of limitations $Q = Q_{\text{opt}}$. The function Q_{opt} is determined by the limitations of (22) – (24) given inside the domain G, and the limitations of (25) are given for the minimized functional (19) with help of the penalty function Q_{f} (26).

It should be noted that described above algorithm corresponds to the terminal (quasi-terminal) control state $V_{t=t_{\text{set}}} = V_{\text{set}}$ which is related to the first control stage, e.g. forming stable and multi-frequency oscillating mode in IMPRD/CD. However, it can be simply transformed to the non-terminal algorithm of control by using transition to "sliding" optimization interval for which optimization interval is given as $t_2 = t + T_{\text{set}}$, where T_{set} is the given optimization interval. According to that, predictive model performs integration of the equations (15) within the interval from t/χ till to $(t+T_{\text{set}})/\chi$. As the function of V_{set} can be selected, an arbitrary function, including $V_{\text{set}} \equiv 0$.

After achievement the terminal state (19), stabilization of location of the system relatively given state is performed $V_0 \equiv V_{\text{ST}}$. For this reason, transition to the "sliding" optimization interval T_{ST} is executed.

Let us define productivity of control microprocessor system necessary for realization of technical invariance principle in PRD using adaptive system with predictive standard. If under condition of single-entry numerical integration for optimization interval equal to T_{ST} necessary N operations, then performance of microprocessor device can be approximately estimated as follows

$$n_M = \frac{m+1}{2\Delta t_c} N . \tag{27}$$

It was assumed here that number of components of influence vector which give control process is equal to m and binary system of numerical differentiation is exploited. Value of Δt_c is defined by a necessary velocity of the update for given influences. For example, for $m = 3$, $\Delta t_c = 0.5\,\mathrm{s}$, $N = 2 \cdot 10^5$ microprocessor device must provide productivity in the level of $n_M = 8 \cdot 10^5$ operations per one second [2].

4. Experimental result

The main contribution to the dynamic of variations of oscillation frequency is made by the Quartz Resonator self-heating up, here at the thermo-dynamic component of instability of QR can exceed the meaning $(0.5 \ldots 1)\cdot 10^{-5}$. At the same time the vibration instability on this stage of oscillations is one or two degrees less. After establishing the temperature balance of Quartz Resonator for $t > (80\ldots100)$ s the dynamics of frequency shifts is defined mainly by vibration-dynamic component.

The similar character of dependences can be observed also for the third harmonic component of QR oscillations, which is determined by the localization of mechanic oscillations of resonator in one capacity and proves high correlation dependence between the oscillations of the first and third mechanic frequency of QR. Temperature and vibration components of instability of QR frequency in the form of difference dependences is shown in Fig. 3.

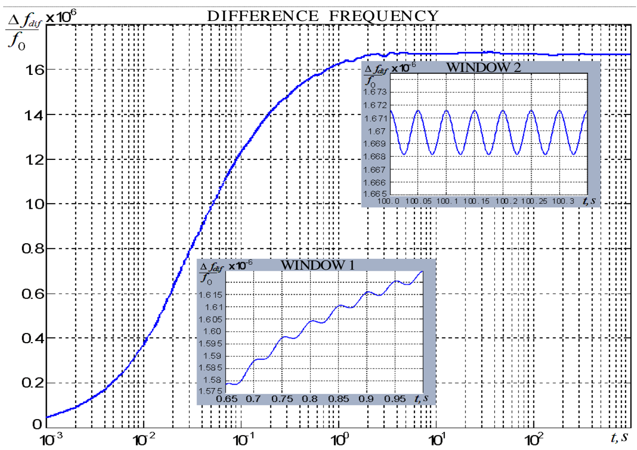

Fig. 3. Difference frequency in POS

It can be seen that for the difference component δf_{dif} because of high correlation of shifts of oscillation frequencies f_1, f_3 the sharp shortening of the process of establishing the frequency of difference oscillation f_{dif} (approximately by a degree) with synchronic decrease of vibration-dynamic instability to a value $(0.3 \ldots 0.5)\cdot 10^{-8}$ can be observed (Fig. 3, Window 2).

On the basis of frequencies of difference oscillations ΔF_T (7), ΔF_G (8) the scheme of formation the signal of compensation (Fig. 1) provides the currant identification of temperature and vibration influences onto Quartz Resonator in accordance with (9) and the formation of correcting code $N(T,G)$ for Digital Synthesizer of Direct Synthesis in accordance with (4) [4, 5].

5. Conclusion

Using of suggested conceptual states related to design invariant multi-frequency piezoelectric resonance devices with controlled dynamics (IMPRD/CD) in the form of adaptive-self-tuning systems with the fast operating predictive standard provided creation of novel class invariant PRD which accuracy performance is of maximum close to potentially possible level. Control the trajectory operating in a real-time environment is performed on the basis of predictive numerical analysis of the core dynamics in MOPS. Model parameters are given corresponding to the results of identification of current state QR under multi-mode excitation and taking into account the constructive peculiarities of PRD concrete type.

In order to provide given system operation mode under its incomplete parametrical distinctness (robustness), two-stage interval-approximation control law has been developed. The law provides dividing the process into the sequence interval-local approximation tasks within the limits of two stages for restoration and stabilization of multi-mode oscillation mode. During the first stage, adaptive control task is solved for each separate mode of MOPS in order to provide operating the system under stationary oscillation mode in minimum time. During the second stage, control influences are formed. The latter ones are directed to the system stabilization under influence of destabilizing factors, i.e. providing technical invariance. Criteria for an optimal control in IMPRD/CD are analytically designed. That provides for each stage the minimization of energy expenses for optimal system operating trajectory. Local and global stability of interval-approximation control technique IMPRD/CD is demonstrated. Estimate of productivity of digital control system in IMPRD/CD confirms opportunity of physical realization of given conception by using wide spread ARM processes.

References

[1] Lam C.: A review of the recent development of MEMS and crystal oscillators and their impacts on the frequency control products industry. IEEE Ultrasonics Symposium 2-5 Nov 2008, Beijing, China, 694–704.
[2] Pidchenko S., Taranchuk A.: Principles of Quartz Multifrequency Oscillatory Systems with Digital Compensation of Temperature and Vibrational Instability Frequency. Int. Conf. Radio Electronics & Info Communications (UkrMiCo): 11-16 Sept. 2016, Kiev, Ukraine, 281–284.
[3] Pidchenko S.: Dual-frequency temperature-compensated quartz crystal oscillator CriMiCo. 23rd Int. Crimean Conf. Microwave and Telecommunication Technology 8-14 September 2013, Sevastopol, Ukraine, 669–670.
[4] Pidchenko S.: Theory and fundamentals implementation of invariant piezoresonance devices and systems. KNU, Khmelnytskyi 2014.
[5] Taranchuk A., Pidchenko S., Khoptinskiy R.: Dynamics of temperature-frequency processes in multifrequency crystal oscillators with digital compensations of resonator performance instability. Radioelectronics and Communications Systems 58(6)/2015, 250–257.

D.Sc. Sergey Pidchenko
e-mail: sergpchn@gmail.com

Associate professor in Department of Telecommunication and Computer-Integrated Technologies at Khmelnytsky National University. Research field covers of problems of generation and formation of multi-frequency highly stable signals, as well as to solving the problems of stabilizing and formation the frequency of piezoelectric resonance communication devices. Author of nearly 120 publications in this research area.

Ph.D. Alla Taranchuk
e-mail: allatr@ukr.net

Associate professor in Department of Telecommunication and Computer-Integrated Technologies at Khmelnytsky National University. Research field covers of problems of generation and formation of highly stable signals, as well as to solving the problems of stabilizing the frequency of piezoelectric resonance communication devices. Author of nearly 80 publications in this research area.

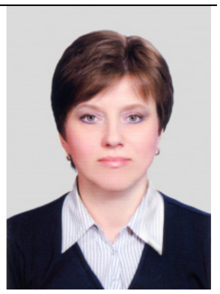

otrzymano/received: 10.10.2017 *przyjęto do druku/accepted: 15.02.2018*

DOI: 10.5604/01.3001.0010.8638

DEVELOPMENT AND RESEARCH OF CRYPTOGRAPHIC HASH FUNCTIONS BASED ON TWO-DIMENSIONAL CELLULAR AUTOMATA

Yuliya Tanasyuk[1], Sergey Ostapov[2]

[1]Yuriy Fedkovych Chernivtsi National University, Department of Computer Systems and Networks, [2]Yuriy Fedkovych Chernivtsi National University, Computer Systems Software Department

Abstract. *Software solution for cryptographic hash functions based on sponge construction with inner state implemented as two-dimensional cellular automata (CA) has been developed. To perform pseudorandom permutation in round transformation function several combinations of CA rules 30, 54, 86, 150 and 158 have been proposed. The developed hashing mechanism provides effective parallel processing, ensures good statistical and scattering properties, enables one to obtain hash of a varying length and reveals strong avalanche effect.*

Keywords: cryptographic hash functions, cellular automata, cryptographic sponge, pseudo-random permutations

OPRACOWANIE I BADANIA KRYPTOGRAFICZNYCH FUNKCJI SKRÓTU (HASH) NA PODSTAWIE DWUWYMIAROWYCH AUTOMATÓW KOMÓRKOWYCH

Streszczenie. *Za pomocą oprogramowania zostały opracowane kryptograficzne funkcje skrótu (hash) na podstawie gąbki kryptograficznej, której stan wewnętrzny został zrealizowany w postaci dwuwymiarowych automatów komórkowych (KA). W celu implementacji permutacji pseudolosowych zaproponowano kombinację zasad obróbki CA 30, 54, 86, 150 i 158 w celu realizacji funkcji transformacji rundy. Opracowany mechanizm haszowania pozwala na skuteczne przetwarzanie równoległe, zapewnia jakościowe charakterystyki statystyczne i rozproszenia, pozwala na otrzymanie skrótu o zmiennej długości i ujawnia stabilny efekt lawinowy.*

Słowa kluczowe: kryptograficzne funkcje skrótu, automaty komórkowe, gąbka kryptograficzna, przekształcenia pseudolosowe

Introduction

Hash functions have many applications in modern cryptography, including Internet Security Protocol (IP Sec), digital signature schemes, password storage and key derivation. Among all, these cryptographic primitives are probably best known for the important role they play in the practical use for data integrity and message authentication. Hash functions are considered to be efficient with respect to energy consumption and computations needed to produce a concise fixed-size signature of the message of arbitrary length. A computed fingerprint should be highly sensitive to all input bits. Finally, the hash functions must be secure, since they are normally used without keys and deal with a plaintext. A robust hash function possesses one-wayness, i.e. given a fingerprint it's infeasible to derive a matching message. Another security property of the hash functions, desirable for digital signature, is their collision resistance. It's essential that two different messages do not hash to the same value and it should be computationally infeasible to find such messages [6].

In order to evaluate the cryptographic level of security, provided by a hash function, it's a good practice to analyze its statistical properties. A hash function that behaves like a pseudorandom function and satisfies the avalanche effect is generally considered to be secure and can be used safely for cryptographic purposes. The avalanche effect reflects the sensitivity of the hash function to elementary changes in the hashed message: a little change in the input message (flipping one single bit) produces a significant change of the output (the final hash) [2].

A large number of hash functions have been proposed over the last three decades. The most popular algorithms of MD5 and SHA-1 are based on compression mechanism that is reported to cause the collision occurrence. Moreover, they appear to be incompatible with the algorithms of AES and 3DES, due to insufficient level of security. This drawback was eliminated in four existing versions of the SHA-2 algorithm, each providing the message digest of the fixed length (224, 256, 384 and 512 bits), yet falling under a threat of being compromised [7]. However, in 2012 through public competition, initiated by NIST, a new hashing algorithm named Keccak was adopted as a novel standard of SHA-3 to provide a backup for the existing hashing mechanisms in case of any further vulnerabilities revealed. The selected algorithm possesses many admirable properties. In particular, it is praised for the ability to run well on different platforms of computing devices, including embedded and smart ones, and for higher performance in hardware, comparing to SHA-2.

It should be stressed that Keccak has a quite different internal structure than the hash functions that belong to the MD4 family, including SHA-1 and SHA-2. It doesn't rely on a compression approach of its predecessors, but is based on a sponge construction. The sponge is an interactive framework, which utilizes pseudorandom permutation functions and provides the output close to that of random oracle [1, 6].

In order to achieve such an effect in programmable way, the use of cellular automata and their transformation rules seem to be appealing.

Cellular automata (CA) have several properties that favor their use as a basis for the design of hash functions. Their chaotic, complex and unpredictable behavior for some types of the applicable rules promotes their effective use to design safe and reliable hash functions. In addition, CA are very appropriate to design hash functions with low hardware and software complexity because of the involved logical operations, parallelism and extreme sensitivity to initial conditions alterations [2].

According to the results of investigations, reported in [5] linear CA, evolving with the use of various transformation rules, provide efficient means of creating high-performance key stream generators, block ciphers and hash functions with reasonable statistical properties. It is suggested, that deployment of multi-dimensional structures may bring about some additional opportunities for their parallel processing and performance enhancement.

The purpose of the given paper is to create and study cryptographic hash functions based on two-dimensional CA, with elaborated combinations of the processing rules, underlying permutation function of the sponge construction.

1. Cryptographic sponge: parameters and details of operation

In terms of SHA-3 standard Keccak the hash function supports the message digest lengths of 224, 256, 384 and 512 bits. Last three hash values provide an attack complexity of approximately 2^{128}, 2^{192} and 2^{256}, respectively, corresponding to the cryptographic strength that the three key lengths of AES provide against brute-force attacks. Similarly, 224-bit output shows the same collision resistance as 3DES with a cryptographic strength of 2^{212} [6].

The construction of sponge, used in Keccak algorithm, has its inner state − the binary array with a width of $b = 1600$ bits, divided into two parts: r and c, $b = r + c$. A parameter of r is called a bit rate. This very part is combined with the blocks of input message, for which the hash value is to be calculated. A second parameter of c, known as a capacity, doesn't interact directly with the portions of the input message, being involved only in the permutation process. Capacity is said to be responsible for the security level and with proven mathematical stability needs to be twice as large as the desired hash value. The security level denotes the number of computations an attacker has to perform to break the hash function. Table 1 gives recommended values of the sponge parameters for inners state of 1600 bits with respect to the hash length.

Table 1. The parameters of Keccak hash function [6]

Sponge state b, bits	Hash length, Z, bits	Rate r, bits	Capacity $c = b\text{-}r$, bits	Security level, $Z/2$, bits
1600	224	1152	448	112
1600	256	1088	512	128
1600	384	832	768	192
1600	512	576	1024	256

It's noteworthy, that Keccak function is not confined to the hash lengths, listed in Table 1. One may generate a message digest of any arbitrary number of bits, holding corresponding correlation of the parameters and security level [6].

In Keccak algorithm the sponge state is arranged as three-dimensional array of 5×5 64-bit words. The operation of sponge construction consists of two stages: absorbing and squeezing (Fig. 1). Prior to the actual processing by the hash function an input message undergoes preprocessing, which implies its padding to the length of a multiple of r bits [1]. Further the complimented string is divided into the equal portions of r length.

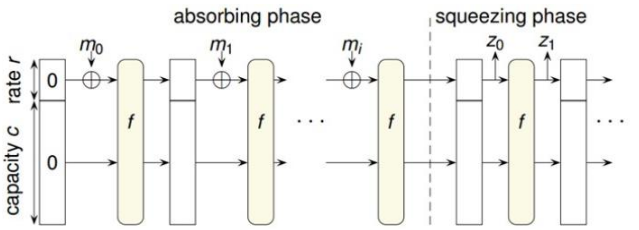

Fig. 1. Operating phases of the cryptographic sponge [1]

At each step of absorbing sponge intakes a message block, combines it with the r portion of the sponge state through XOR operation and further processes the whole state with round permutation function.

The squeezing stage begins after loading of all message blocks. It also includes permutation, followed by extracting a predetermined number of bits from r portion and their appending to the output hash string, until a message digest of the desired length is obtained.

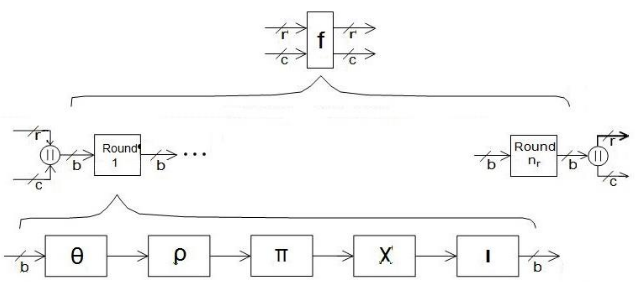

Fig. 2. The steps of the round function of Keccak-f permutation [9]

The Keccak-*f* permutation function is at the heart of the hash algorithm and is used in both phases of the sponge construction. The function includes n rounds. Each round has an input of $b = r+c$ bits. The number of rounds is defined as $n = 12+2log_2k$, where $k = b/25$, and for $b = 1600$ bits, $n = 24$. As shown in Fig. 2, each round consists of a sequence of five steps denoted by Greek letters: θ (theta), ρ (rho), π (pi), χ (chi) and ι (iota). The named functions include various combinations of bitwise operations, and are claimed to be relatively hardware friendly resulting in high performance of the Keccak algorithm [1, 6].

2. Hash functions with the use of processing rules of two-dimensional CA

Our experiments were aimed at creating a software model of Keccak-like hash function based on two-dimensional CA. Cellular automata can be viewed as a collection of cells organized in a grid, when each cell has a corresponding current state. The states of the cells evolve over time, depending on their current states and the states of the neighboring cells, according to a local and identical interaction rule in the case of uniform CA, or different interaction rules in the case of non-uniform or hybrid CA [3, 9].

The paper presents the results on the hash functions implemented as a sponge construction with the two-dimensional CA inner state, processed by the following transformation rules:

$$\text{rule 30: } C[i]' = C[i-1] \oplus (C[i] \vee C[i+1]) \quad (1)$$

$$\text{rule 54: } C[i]' = (C[i-1] \vee C[i+1]) \oplus C[i] \quad (2)$$

$$\text{rule 86: } C[i]' = (C[i-1] \vee C[i]) \oplus C[i+1] \quad (3)$$

$$\text{rule 150: } C[i]' = C[i-1] \oplus C[i] \oplus C[i+1] \quad (4)$$

$$\text{rule 158: } C[i]' = C[i-1] \oplus C[i] \oplus C[i+1] \vee C[i] \wedge C[i+1] \quad (5)$$

where $C[i]$ is a current cell, $C[i]'$ is the value of the current cell after the rule application, $C[i-1]$, $C[i+1]$ are previous and next neighbor cells, and $\oplus$, $\wedge$, $\vee$ denote the bitwise XOR, AND, and OR operations, respectively.

The permutation functions under investigation assumed utilization of several CA processing rules, both linear and nonlinear, to provide collision resistance and nonlinearity to the hashing mechanism [4].

2.1. Interaction scheme of two-dimensional CA

In two-dimensional representation the sponge state is arranged as an array of 25 vectors of 64 bits, making 1600 bits in total. The cells are localized according to the Moore neighborhood [9], when two cells are considered adjacent if they have either a common edge or a vertex. Therefore, each cell interacts with its eight direct neighbors, denoted as parts of the world (Fig. 3).

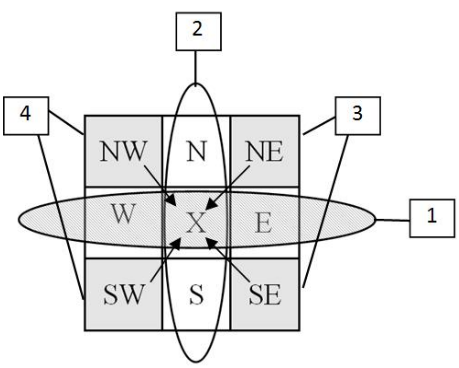

Fig. 3. The notation of the cells in two-dimensional 8-neighbor CA, used in the permutation function, where 1, 2, 3 and 4 are index numbers of possible interactions of cells

Cells, represented by N, W, NW, NE are considered as previos, while S, E, SW and SE participate as the next neighbours. Extreme cells are connected in tor with their counterparts on the opposite edge (row/column) of the array. In order to enhance performance, selected rules were applied to the entire rows concurrently, rather than to single bits. In particular, to implement transformation within one row two copies of it were created: one-bit cyclically shifted to the right instance represented all previous cells (W), while one-bit cyclically left-shifted one contained all next cells (E). Similarly, cyclically shifted to the right previous and next rows correspond to NW and SW vectors, respectively while their one-step cyclic shift to the left produces NE and SE bit strings, correspondingly.

Table 2. The developed permutation functions based on the CA processing rules, corresponding to the index numbers of interactions, given in Fig. 3

id	Notation of the permutation function	Interaction number	CA rule	Cell's interaction
1.	Rule_30_150_86	1	rule 30	X' = W⊕(X∨E)
		2	rule 150	X' = N⊕X⊕S
		3	rule 86	X' = (NE∨X)⊕SE
		4	rule 86	X' = (NW∨X)⊕SW
2.	Rule_54_150_86	1	rule 54	X' = (W∨E) ⊕X
		2	rule 150	X' = N⊕X⊕S
		3	rule 86	X' = (NE∨X)⊕SE
		4	rule 150	X' = NW⊕X⊕SW
3.	Rule_54_158_150_86	1	rule 54	X' = (W∨E)⊕X
		2	rule 158	X' = N⊕X⊕S∨X∧S
		3	rule 86	X' = (NE∨X)⊕SE
		4	rule 150	X' = NW⊕X⊕SW

To ensure effective permutation, combinations of adjacent cells were processed with different CA transformation rules for a number of times successively. In general, we'll consider three types of permutation functions, the notations and related CA rules of which are given in Table 2.

2.2. Implementation of sponge construction on two-dimensional CA

The software solution for the cryptographic sponge with the use of processing rules of CA has been developed in C++ programming language. The sponge state is implemented as a two-dimensional binary array of 25×64 bits, which consists of two parts of r and c. The values of the parameters are aligned with those proposed in the original Keccak algorithm. A number of vectors that belong to r portion of the state can be defined as $r/64$. E.g. for hash length of 512, r equals 576 (Table 1) and spans first nine 64-bit rows of two-dimensional array. These vectors are initialized with binary 1s. For better diffusion, a bit corresponding to a vector's index is inverted. The rows of capacity portion are set to 0 s. The whole sponge state is preliminary processed by application of one of the mentioned permutation function for 25 times.

At the absorbing phase r vectors of the sponge are loaded with equally divided blocks of the padded input message. Then, the whole state undergoes consecutive permutation for a number of times according to the deterministic rule combination.

In course of squeezing, on completion of permutation rounds, the content of the first vector is appended to the output message digest. When the hash string of the initially defined length is obtained, it is output to a user in hexadecimal representation.

3. Statistical properties and avalanche effect

Pseudorandom behavior and avalanche effect are generally considered as good indicators of a secure hash function, the output of which should resemble that of the random oracle. We've used a technique of NIST STS statistical testing in order to check randomness properties of the developed permutation functions.

In the performed experiment the implemented hash functions with the parameters (bits): $b = 1600$, hash length $Z = 512$, $r = 576$, $c = 1024$, have been utilized in the mode of a generator of pseudorandom numbers to create a binary file of 100 MB. The statistical suit of NIST STS v.2.1.2 divided generated binary sequences into 100 equal parts of 10^6 bits each. The bit strings were tested against 16 statistical tests with different parameters. The randomness properties were assessed in terms of probability of the tests being passed. As a result, a vector of 189 values of probability was formed. Ideally, only one sequence of a hundred can be rejected. This means that a coefficient of test passing equals 99%. However, this requirement is rather strict. In most cases the evaluation is carried out based on the confidence interval, the lower limit of which is assumed to be at the level of 96%. Fig. 4 shows the results of the conducted statistical testing.

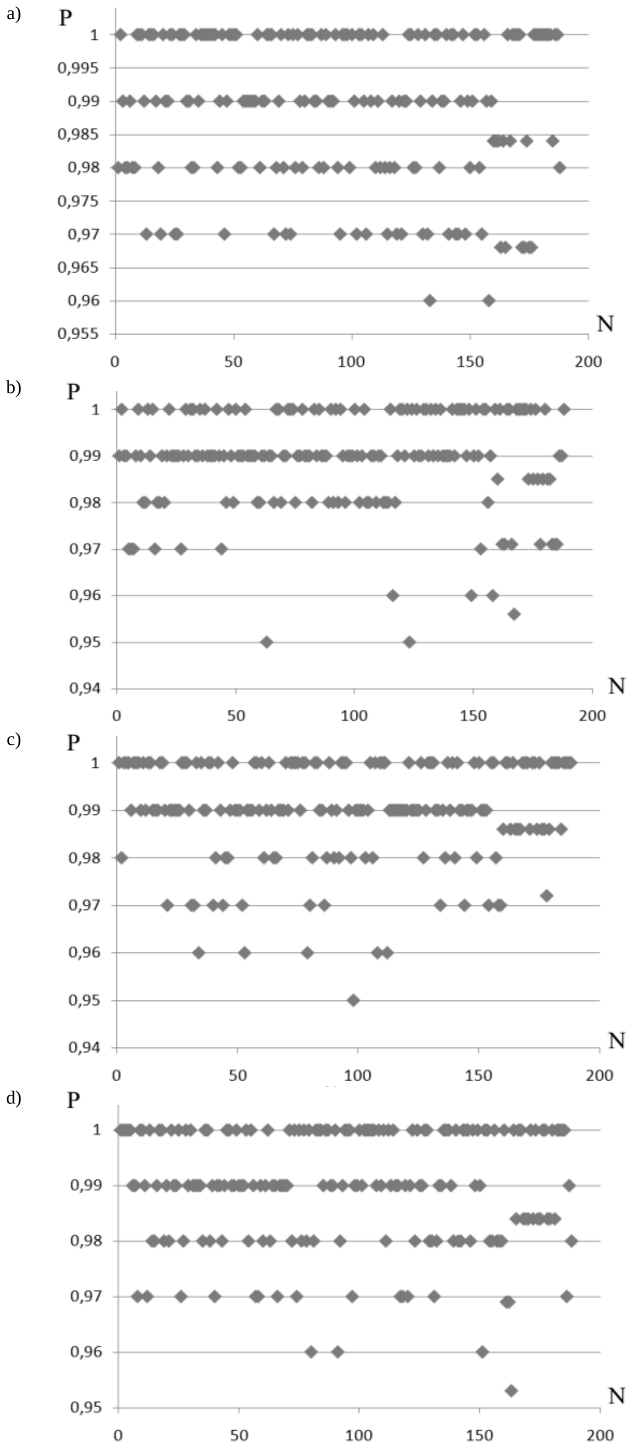

Fig. 4. Statistical portraits of the cryptographic hash functions, based on two-dimensional CA processing rules (Table 2), applied for a number of permutation rounds: a) RULE_30_150_86, 5 rounds; b) RULE_54_150_86, 5 rounds; c) RULE_54_150_86, 10 rounds; d) RULE_54_158_150_86, 5 rounds, where N is a number of a test, P is he portion of tests sequence that passed the test

According to the obtained statistical data, on average, up to 99% of all tested bit sequences have successfully passed the tests, with only a few of them revealing values at the level of 95%. The overall results of NIST STS testing for the proposed permutation functions at different number of processing rounds are listed in Table 3. The investigation revealed that with inclusion of rules 54 and 158 and at greater number of permutations the body of sequences, which passed the tests is slightly increased.

Table 3. Results of NIST STS testing of the hash functions based on the proposed permutation mechanisms of two-dimensional CA (see Table 2) at different number of processing rounds

Permutation function ID	Number of rounds	NIST STS testing results				
		0.95	0.96	0.98-0.97	1-0.99	Average
1	5	0	2	66	121	0.9889
2	5	2	4	48	135	0.9897
2	10	1	5	34	149	0.9907
3	5	1	3	57	128	0.9893
3	10	1	4	52	132	0.9896

The application of the developed permutation functions for obtaining a hash image revealed occurrence of strong avalanche effect. Namely, for the same input message a distinct hash string was obtained when changing hash length (224, 256, 384, 512 bits), applying permutation functions of various types, and modifying the number of processing rounds. Moreover, very small alterations of the input string produced significant changes in the output. The hexadecimal hash strings of 512 bits, resulting from 5-round application of RULE_30_150_86 permutation function, for the test vectors, are given below.

1) Empty file
   baf53bbea29e4bb458aac3df56c023c55bf8ac117cfdabbcbc2e1
   e2a069363cd453cba9c2468dd0389aef8630ae3e14b9461236e8
   430388f9435fb529c3a9dbf
2) The quick brown fox jumps over the lazy dog
   116312e16c3e9cf29c58687ed40f18e06ca478b64ae4c52e7ce4
   e3a5dfacdc111f8cc6d97cfb5f1cb24d1ccb30edb8dd9a9ec4f1e
   6deb2acb4517aa93d52709c
3) The quick brown fox jumps over the lazy **dog.**
   48a4f612dfae9c2583923f0c5a03528f86c50386fff5958021635
   d5a678be53c9f0d9e552468cb99c49e820da3376295928f37ae5
   5e9d22516447f5379681126
4) The quick brown fox **jump** over the lazy dog.
   e87efd05456a290eacb516f2c17f8a24c32ca5920f3f866b213d3
   2d4ae42e0f67ee931537a5a09d420ffc485aae41e4f9760bb3c1e
   a70bc7c7b3b99c8c7751bc

It should be outlined that the use of the two-dimensional CA and the designed combinations of the processing rules enabled us to considerably reduce the number of processing rounds. As reported in [8], for hash functions on the basis of one-dimensional CA, processed with combination of rules 30, 86, 150 and cyclic shift operations, the avalanche effect was achieved after 50 rounds of permutation. While a full change of hash image occurs for the designed two-dimensional hash functions starting from 5 processing rounds.

4. Conclusions

Thus, summarizing the investigations carried out the following conclusions can be made:

1) For the first time two-dimensional cellular automata, which evolve according to a series of processing rules, have been studied with respect to their utilization as a permutation function of the cryptographic sponge.
2) The developed permutation approach, which includes concurrent processing of two-dimensional CA and application of various interaction rules, provides good statistical properties and can be considered as a promising candidate for cryptographic purposes.
3) The designed hash functions on the basis of two-dimensional CA reveal strong avalanche effect, pointing out non-linearity and pseudorandom properties of the developed permutation schemes.

References

[1] Bertoni G. et al.: The Keccak sponge function family. http://keccak.noekeon.org/ [1.01.2018].

[2] Eddine A., Belfedhal K., Faraoun M.: Building secure and fast cryptographic hash functions using programmable cellular automata. J. of Computer and Information Technology CIT 4/2015, 317–328.

[3] Jamil N., Mahmood R., Z'aba R., Udzir N.I. Zukarnaen N.A.: A new cryptographic hash function based on crllular automata rule 30, 134 and omega-flip network. ICICN 27/2012, 163–169.

[4] Jeon J.Ch.: Analysis of hash functions and cellular automata based schemes. International Journal of Security and Applications 7(3)/2013, 303–316.

[5] Ostapov S., Val O., Yanushevsky S., Chyzhevsky D.: Cryptography on the Base of Cellular Automata. Internet in the Information Society – Chapter 6, Scientific Publishing University of Dabrowa Gornicza 2015.

[6] Paar Ch., Peltz J.: Understanding cryptography. Springer-Verlag, Berlin Heidelberg 2010.

[7] Robshaw M.J.B.: MD2, MD4, MD5, SHA, and Other Hash Functions. Technical Report TR-101/1994.

[8] Tanasyuk Yu., Melnychuk Kh., Ostapov S.: Development and research of cryptographic hash functions on the basis of cellular automata. Information Processing Systems 4(150)/2017, 122–127.

[9] Wolfram S.: A New Kind of Science Wolfram Media Inc., 2002, 1197 http://www.wolframscience.com/ nksonline/toc.html [1.01.2018].

Ph.D. Yuliya Tanasyuk
e-mail: y.tanasyuk@chnu.edu.ua

Associate professor at Department of Computer Systems and Networks, Physical, Technical and Computer Sciences Institute, Yuriy Fedkovych Chernivtsi National University, Chernivtsi, Ukraine.
Research interests and academic activities: programming, network information technologies, cryptography.

Prof. Sergey Ostapov
e-mail: s.ostapov@chnu.edu.ua

Head of Computer Systems Software Department, Physical, Technical and Computer Sciences Institute, Yuriy Fedkovych Chernivtsi National University, Chernivtsi, Ukraine.
Research interests and academic activities: cryptography, information security, big data analysis
The author of more than 150 publications in the given research field.

otrzymano/received: 10.10.2017 *przyjęto do druku/accepted: 15.02.2018*

DOI: 10.5604/01.3001.0010.8639

GENERALIZED APPROACH TO HURST EXPONENT ESTIMATING BY TIME SERIES

Lyudmyla Kirichenko[1], Tamara Radivilova[2], Vitalii Bulakh[1]

[1]Kharkiv National University of Radioelectronics, Deptartment of Applied Mathematics, [2]Kharkiv National University of Radioelectronics, Deptartment of Infocommunication Engineering

Abstract. *This paper presents a generalized approach to the fractal analysis of self-similar random processes by short time series. Several stages of the fractal analysis are proposed. Preliminary time series analysis includes the removal of short-term dependence, the identification of true long-term dependence and hypothesis test on the existence of a self-similarity property. Methods of unbiased interval estimation of the Hurst exponent in cases of stationary and non-stationary time series are discussed. Methods of estimate refinement are proposed. This approach is applicable to the study of self-similar time series of different nature.*

Keywords: self-similar stochastic process, time series, Hurst exponent

UOGÓLNIONE PODEJŚCIE DO ESTYMACJI WYKŁADNIKA HURSTA NA PODSTAWIE SZEREGÓW CZASOWYCH

Streszczenie. *W pracy przedstawiono uogólnione podejście do analizy fraktalnej samopodobnych procesów losowych przedstawianych w krótkich szeregach czasowych. Zaproponowano kilka etapów analizy fraktalnej. Wstępna analiza szeregów czasowych obejmuje eliminację krótkoterminowej zależności, identyfikację prawdziwej długoterminowej zależności oraz weryfikację hipotezy o istnieniu własności samopodobieństwa. Uwzględniono metody bezstronnej oceny przedziału czasowego wykładnika Hursta w przypadku stacjonarnych i niestacjonarnych szeregów czasowych. Zaproponowano metody walidacji uzyskanego oszacowania wykładnika Hursta. To podejście ma zastosowanie do badania samopodobnych szeregów czasowych o różnym charakterze.*

Słowa kluczowe: samopodobny proces stochastyczny, szeregi czasowe, wykładnik Hursta

Introduction

The tasks of modern nonlinear physics, radio electronics, control theory and image processing require the development and application of new mathematical models, methods and algorithmic support for data analysis. In recent decades, it has been discovered that many stochastic processes in nature and technology have long-term dependence and fractal structure. The most suitable mathematical apparatus for studying the dynamics and structure of such processes is fractal analysis.

Stochastic process $X(t)$ with continuous real time is called to be self-similar of parameter *H*, 0 <*H*<1, if for any value $a > 0$ processes $X(at)$ and $a^H X(t)$ have same finite-dimensional distributions:

$$\text{Law}\left\{X(at)\right\} = \text{Law}\left\{a^H X(t)\right\}. \tag{1}$$

The notation Law{*} means finite distribution laws of the random process. Parameter *H* is called Hurst exponent. It is a measure of self-similarity. Along with this property, Hurst exponent characterizes the measure of the long-term dependence of stochastic process, i.e. the decrease of the autocorrelation function $r(k)$ in accordance with the power law: $r(k) = k^{-\beta}$, $H = 1 - \beta / 2$.

For values 0.5 <*H*< 1 the time series demonstrates persistent behaviour. In other words, if the time series increases (decreases) in a prior period of time, then this trend will be continued for the same time in future. The value *H* = 0.5 indicates the independence (the absence of any memory about the past) of time series values. The interval 0 <*H*< 0.5 corresponds to antipersistent time series: if a system demonstrates growth in a prior period of time, then it is likely to fall in the next period.

Information data flows in telecommunication networks were among the first real stochastic processes, where self-similar properties were discovered. For self-similar traffic, calculating methods of computer network characteristics (channel capacity, buffer capacity, etc.) based on classical models do not conform to necessary requirements and do not adequately assess the network load. Many publications are devoted to the analysis of the fractal traffic properties and their impact on the functioning and quality of service of the telecommunications network [7, 21–24].

Typical examples of fractal stochastic structures are the modern financial markets. The hypothesis of fractality of financial series assumes that the market is a self-regulating macroeconomic system with feedback, using information about past events that affect decisions in the present, and containing long-term correlations and trends. The market remains stable as long as remains its fractal structure. Analyzing the occurrence of time intervals with the different fractal structure, it is possible to diagnose and predict unstable market conditions (crises) [6, 18, 20].

Numerous studies have shown that many bioelectrical signals have a fractal structure. Distinct changes of the fractal characteristics of cardio- and encephalograms appear in various diseases, with changes in mental and physical stress on the body. Fractal analysis of bioelectric signals can be the basis for conducting statistical studies, what will allow to formulate methods that will be significant for clinical practice [3, 4, 10].

Obviously, that the evaluation of the Hurst exponent for experimental data plays an important role in the study of processes having self-similarity properties. There are many methods for estimating the self-similarity parameter, each of which bears the imprint of that area of scientific applications where it was originally developed [5, 13, 21, 23]. In practice, the methods of rescaled range, variance-time analysis and the detrended fluctuation analysis are most often used to estimate the Hurst exponent. Methods based on wavelet transform are particular important among the research methods of fractal non-stationary processes. The basic ideas of wavelet-fractal methods of analysis are formulated in [1, 9].

In recent years, fractal time series analysis has become very popular. However, at the present time, there is no universal approach to estimating fractal characteristics based on a preliminary study of the time series structure. The major drawbacks in the application of fractal analysis methods are absence of a preliminary study of the correlation structure of the process, the use of only one method of analysis, a weak study of the statistical properties of estimates obtained from time series of short length.

The goal of the work is to present generalized use of fractal analysis techniques to study the time series of small length, using special methods of preliminary data research.

1. The main methods of estimating the Hurst exponent

Moments of the q-th order of the self-similar random process (1) can be expressed as follows:

$$\mathrm{M}\left[\left|X(t)\right|^{q}\right] \propto t^{qH} . \qquad (2)$$

In fact, all methods of estimating the self-similarity parameter at the time series, are based on relation (2) with the value $q = 2$. The method of rescaled range (R/S-analysis) was proposed by H.Hurst [11] and it is still one of the most popular in the study of fractal series of different nature [8]. It is based on scaling relationship

$$M\left[R(\tau)/S(\tau)\right] \propto \tau^{H} ,$$

where $R(\tau)$ is the range of the cumulative deviate series $x^{cum}(t,\tau)$, $S(\tau)$ is standard deviation of the initial series.

Variance-time analysis is most often used to processes researches in telecommunication networks [21, 22, 24]. It is based on the fact that the variance of the aggregated time series

$$x_k^{(m)} = \frac{1}{m}\sum_{t=km-m+1}^{km} x(t),\ k = 1,...,N/m \qquad (3)$$

satisfies scaling relation

$$Var(x^{(m)}) \propto \frac{Var(x)}{m^{\beta}} ,$$

where $H = 1 - \frac{\beta}{2}$.

The method of detrended fluctuation analysis (DFA), originally proposed in [19], is currently the main method for determining self-similarity by non-stationary time series [12, 13]. In the DFA method, the fluctuation function $F(\tau)$ is calculated:

$$F^2(\tau) = \frac{1}{\tau}\sum_{t=1}^{\tau}(y(t) - Y_m(t))^2 ,$$

where $Y_m(t)$ is the local m-polynomial trend. The averaged on the whole of the time series function $F(\tau)$ have scaling dependence on the length of the segment:

$$F(\tau) \propto \tau^{H} .$$

The wavelet estimation of the Hurst exponent is based on the properties of the detailing wavelet coefficients, which at each decomposition level j also have self-similarity. The method of wavelet estimation [2] is based on the fact that the wavelet energy E can be written as the scaling relation.

$$E_j \propto 2^{(2H+1)j} .$$

2. Generalized approach to Hurst exponent estimation

In [15, 16] a comparative analysis of the statistical characteristics of the Hurst parameter estimates by time series of short length was performed. Summarizing the results of the research, we can suggest the following scheme for fractal analysis of some random process, represented by a time series of length N. In the main stages of fractal analysis, the methods of the rescaled range, DFA, and wavelet estimation are used. Since the application of the wavelet transform requires the appropriate software and work experience, the use of wavelet estimation methods is desirable, but not an obligatory element. However, the use of the DFA method is necessary for two reasons: this method has sufficient accuracy and it is designed to non-stationary time series. Consider step-by-step implementation of generalized approach to estimating the fractal properties of self-similar time series.

2.1. Preliminary study of the time series

1. Before starting the fractal analysis of time series, it is necessary to find out from a priori known information whether the series is cumulative $X_k^{cum} = \sum_{i=1}^{k} x_i$, for example, the currency rate in Fig. 1 (top) or it is a series of increments, for example, data traffic in Fig. 1 (bottom). If, by its nature, the series is cumulative, the following stages of fractal analysis refer to the corresponding series of increments $x_i = X_{k+1}^{cum} - X_k^{cum}$.

2. Determination of intervals of different scaling.

If the self-similar process has several scales that depend on time intervals, then on each such interval the series dynamics is determined by the corresponding Hurst exponent. To determine such intervals, it is necessary to consider the Hurst exponent as a function of time $H(\tau) = f[\log\frac{R}{S}(\tau)]$. This approach is possible in applying the rescaled range method, when time intervals change in small increments [17, 20].

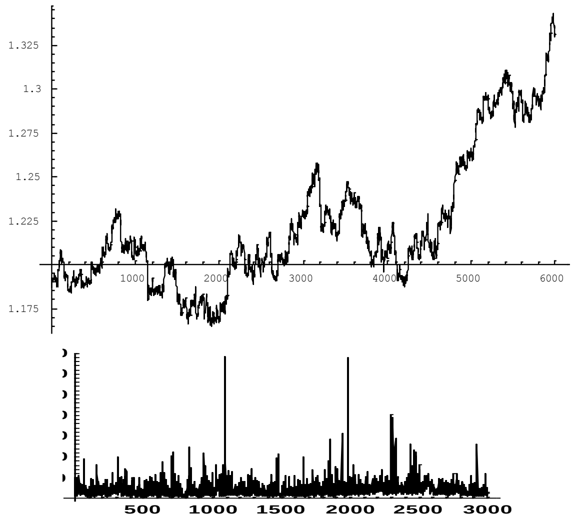

Fig. 1. Cumulative time series: currency rate (top), increments series: data traffic in telecommunication network (bottom)

Fig. 2 shows the dependence $H(\tau)$ for hourly data of the exchange rate. The time intervals which have presence ($0.5 < H < 1$) and absence ($H = 0.5$) of long-term dependence are distinctly different.

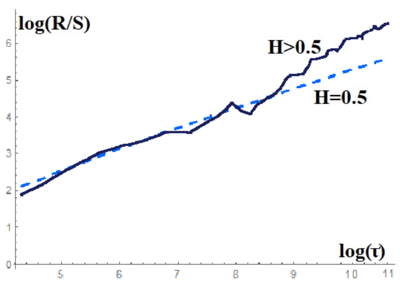

Fig. 2. Hourly data of the exchange rate: time intervals, where there are presence and absence of long-term dependence

In addition to the rescaled range method, it is possible to use the DFA method to get the fluctuation function $F(\tau)$ to determine the intervals of different scales. If there are several scales, the function changes the angle of slope. However, unlike the rescaled range method that investigates the long-term dependence along the entire length of the time, the fluctuation function can be correctly constructed only on the interval of values $N/4$ [12].

3. Identification and removal of short-term autoregressive dependence.

R/S-analysis and DFA allow to discover and eliminate the short-term dependence which is characteristic of autoregressive processes. The autoregressive dependence increases value of the Hurst exponent and demonstrates a false long-term memory [17, 20]. Therefore, when clarifying the fractal structure of the time series, it is first necessary to find out the existence of a short-term correlation. To do this, we need to regress the values $x(t)$ as the dependent variable against $x(t-1)$ and find linear dependence between them: $S(t) = x(t) - (a + b \cdot x(t-1))$. The significance of the coefficient b indicates the presence of short-term dependence. To resolve it, the residual series is determined: $S(t) = x(t) - (a + b \cdot x(t-1))$.

After this, fractal analysis of the residual series $S(t)$ is carried out. If the initial series $x(t)$ has a long-term dependence, then it remains, while the short-term dependence is eliminated. If the autoregressive correlation is significant, then all of the above fractal analysis steps relate to the residual time series.

The fluctuation functions $F(\tau)$ of the EEG realization obtained before and after the removal of the autoregressive dependence are shown in Fig. 3. In this case $H_1 = 0.78,\ H_2 = 0.63$.

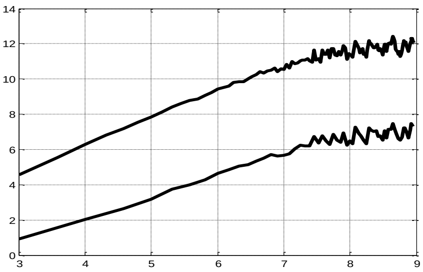

Fig. 3. Fluctuation functions before the removal of the autoregressive dependence (on top) and after the removal (bottom)

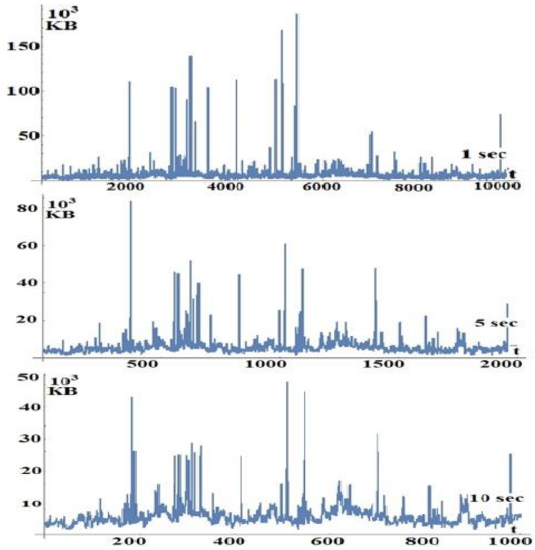

Fig. 4. Aggregated time series of telecommunication traffic

4. Testing the hypothesis about the presence of self-similarity.

If the Hurst parameter H is close to 0.5, it is necessary to test the self-similarity hypothesis. As a null hypothesis, it is usually postulate that random increments are independent. In [20], the criteria and areas for accepting this hypothesis are presented.

A qualitative test of the existence of the properties of statistical self-similarity is the construction of aggregated time series (3), for which sample distribution functions are calculated. In the case of the self-similarity of the time series $x(t)$ the aggregated series have the same distribution, confirmed by statistical criteria. Fig. 4 demonstrates the aggregated time series of telecommunication traffic. It is obvious that at all levels of aggregation the distribution functions of time series have heavy tails.

2.2. Estimation of the Hurst exponent of a stationary series

To estimate the Hurst exponent it is necessary to determine whether the series $x(t)$ is stationary by known statistical methods. If the series is stationary, then the Hurst exponent and confidence interval estimation of the H can be determined by the above or others methods.

The results of the researches [2, 12, 15] showed that the estimates of the Hurst parameter are biased. For each method, the bias and the mean square deviations of estimates depend on the time series length and decrease with increasing series length. Fig. 5 shows the values of the mean estimate bias for each method, depending on the length of the time series. Estimates calculated by the DFA and wavelet transform methods have the minimum bias. The estimates obtained by the wavelet method have a much smaller deviations than others. Wavelet estimates significantly depend on the mother wavelet [2, 14].

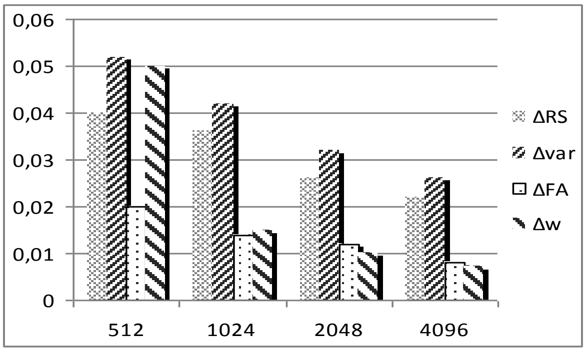

Fig. 5. Mean estimate bias for each method

The sample distribution laws of estimates of the Hurst parameter were investigated and it was shown that they have a normal distribution [2, 12, 15, 16, 20]. In this way, estimate of the Hurst exponent can be represented by confidence interval within which the true value H is found:

$$\hat{H} + \Delta - t_\alpha S < H < \hat{H} + \Delta + t_\alpha S \,, \tag{4}$$

where $\hat{H} = \hat{H}(N,\ method)$ is obtained evaluate of H; N is the time series length; *method* is the chosen method of estimation; $\Delta = \Delta(N,\ method)$ is the calculated mean bias of the estimate, $S = S(N, method)$ is the calculated standard deviation; α is required significance level; t_α is the quantile of the simple normal distribution [15].

2.3. Estimation of the Hurst exponent of a nonstationary series

If the series $x(t)$ is non-stationary, then the correct estimate of the Hurst parameter can be determined by the DFA method or by wavelet estimation.

1) First it is necessary to study the structure of the series using the correlation function, spectral density or spectrum of wavelet energy, which allow to identify the trend and cyclic components of the initial series.
2) When evaluating the Hurst exponent by method of DFA, it is necessary at first to make rough estimate using local polynomial trends of increasing degree and determine the smallest polynomial degree from which the Hurst parameter

estimate stops to change [12]. After this, to evaluate the self-similarity of the time series it is necessary to delete the local polynomial trend of the found degree. Fig. 6 presents the fluctuation functions $F(\tau)$ for a model fractal series with quadratic trend. After removing the local polynomial trend of the order of the larger two, the values of the Hurst index estimates cease to change.

3) The wavelet estimation of a non-stationary time series can be carried out according to the methods presented in [1, 2]. In this case, the evaluation of the exponent H depends essentially on the chosen mother wavelet.

2.4. Refinement of the evaluate of Hurst parameter

The analysis of the correlation dependence between the Hurst parameter estimates obtained by different methods showed that the sample correlation coefficients have absolute values less than 0.5. The correlation of wavelet estimates with ones calculated by other methods is insignificant. Therefore, the arithmetic mean of unbiased estimates obtained by several estimation methods can be used to increase the accuracy of the estimation.

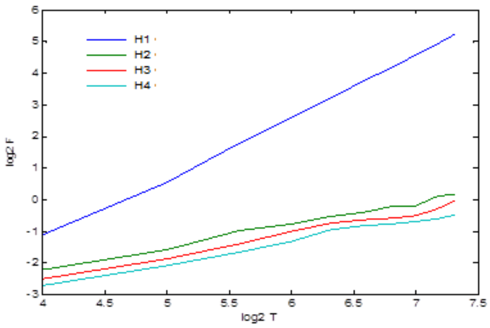

Fig. 6. Fluctuation functions with different local polynomial trends

To improve the accuracy of wavelet estimation, the comparative analysis of the statistical characteristics of the estimates calculated using different wavelet functions was carried out [2, 14]. The correlation analysis of the wavelet estimates of the Hurst exponent, obtained using different wavelets, showed that the more accurate estimation of the Hurst parameter is the arithmetic average of the estimates calculated through several different wavelet functions.

3. Conclusion

The paper offers the generalized approach to the analysis of fractal properties of time series. The proposed method involves a preliminary study of the structure of the time series, unbiased interval estimation of the self-similarity parameter and the joint use of several methods of fractal analysis. This makes it possible to increase the reliability of the Hurst exponent estimates. This approach is applicable to the study of self-similar time series of different nature: telecommunication traffic, financial indicators, biomedical signals, etc.

References

[1] Abry P., Flandrin P., Taqqu M.S., Veitch D.: Self-similarity and long-range dependence through the wavelet lens. Theory and applications of long-range dependence, Birkhäuser 2003.
[2] Abry P., Veitch D.: Wavelet analysis of long-range dependent traffic. IEEE/ACM Transactions Information Theory, Vol. 1(44), 1998.
[3] Bassingthwaighte J.B., Liebovitch L.S., West B.J.: Fractal Physiology. Oxford University Press, New York 1994.
[4] Ching E.S.C., Tsang Yue-Kin : Multifractality and scale invariance in human heartbeat dynamics. Physical Review E, Vol. 76, 2007, 041910.
[5] Clegg R.G.: A practical guide to measuring the Hurst parameter. Computing science technical report 2005. Vol. CS–TR–916.
[6] Cont R., Tankov P.: Financial modelling with jump processes. Chapman & Hall CRC Press, 2004.
[7] Czarkowski M., Kaczmarek S., Wolff M.: Influence of Self-Similar Traffic Type on Performance of QoS Routing Algorithms. INTL Journal of electronics and telecommunications, Vol. 62, no. 1, 2016, 81–87.
[8] Feder J.: Fractals. Plenum, New York 1988.
[9] Flandrin P., Gonzalves P., Abry P.: Scaling, Fractals and Wavelets. John Wiley & Sons, London 2009.
[10] Harikrishnan K.P., Misra R., Ambika G: Can the multifractal spectrum be used as a diagnostic tool? Chaotic Modeling and Simulation, Vol. 1, 2013, 51–57.
[11] Hurst H.E., Black R.P., Simaila Y.M.: Long-Term Storage: An Experimental Study. Constable, London 1965.
[12] Kantelhardt J.W., Koscielny-Bunde E., Rego H.H.A., Havlin S., Bunde A.: Detecting long-range correlations with detrended fluctuation analysis. Physica A 295, 2001, 441–454.
[13] Kantelhardt J.W.: Fractal and Multifractal Time Series. 2008. http://arxiv.org/abs/0804.0747 (available: 12.10.2017).
[14] Kirichenko L., Deineko Zh.: Estimation of the self-similarity of stochastic time series by the wavelet analysis method. Radio-electronic and computer systems, Vol. 4 (38), 2009, 99–105.
[15] Kirichenko L., Radivilova T., Deineko Zh.: Comparative Analysis for Estimating of the Hurst Exponent for Stationary and Nonstationary Time Series. Information Technologies & Knowledge, Vol. 5, No 4, 2011, 371–388.
[16] Kirichenko L., Radivilova T.: Comparative analysis of statistical properties of the Hurst exponent estimates obtained by different methods. Information Models of Knowledg. ITHEA, Kiev–Sofia 2010.
[17] Kirichenko L., Radivilova T.: Investigation of long-term dependence of network traffic using R / S-analysis. Automated control systems and automation devices, Vol. 135, 2006, 51–55.
[18] Meléndez G.R.: The fractal nature of bitcoin: evidence from wavelet power spectra. Fundacion Universidad de las Americas Puebla 39, 2014. http://ssrn.com/abstract=2547281 (available: 12.10.2017).
[19] Peng C.-K., Buldyrev S.V., Havlin S., Simons M., Stanley H.E., Goldberger A.L.: Mosaic organization of DNA nucleotides. Phys. Rev. E 49, 1994, 1685–1689.
[20] Peters E.E.: Fractal Market Analysis: applying chaos theory to investment and economics. Wiley, 2003.
[21] Sheluhin O.I., Smolskiy S.M., Osin A.V.: Self-similar processes in telecommunications. JohnWiley & Sons Ltd, Chichester 2007.
[22] Stollings W.: High-speed networks and Internets. Performance and quality of service. New Jersey 2002.
[23] Tsugawa S., Ohsaki H.: Emergence of Fractals in Social Networks: Analysis of Community Structure and Interaction Locality. 38th Annual Computer Software and Applications Conference, 2014
[24] Willinger W., Taqqu M.S., Erramilli A.A.: Bibliographical guide to self-similar traffic and performance modeling for modern high-speed network in ″Stohastic networks: theory and applications″. Claredon Press (Oxford University Press), Oxford 1996.

D.Sc. Lyudmyla Kirichenko
e-mail: lyudmyla.kirichenko@nure.ua

D.Sc., professor of Department of Applied Mathematics in Kharkiv National University of Radioelectronics. Major fields of scientific research: self-similar and multifracta time series analysis, wavelet analysis, chaotic systems. Author of nearly 150 publications in this research area.

Ph.D. Tamara Radivilova
e-mail: tamara.radivilova@gmail.com

Ph.D., associated professor of Department of Infocommunication Engineering in Technical Sciences at Kharkiv National University of Radioelectronics. Major fields of scientific research: self-similar and multifracta time series analysis, telecommunication network, cybersecurity. Author of nearly 100 publications in this research area.

M.Sc. Vitalii Bulakh
e-mail: bulakhvitalii@gmail.com

Graduate student at Kharkiv National University of Radioelectronics. Major fields of scientific research: self-similar and multifractal time series analysis, machine learning, data mining, chaotic systems.

otrzymano/received: 10.10.2017 *przyjęto do druku/accepted: 15.02.2018*

DOI: 10.5604/01.3001.0010.8641

SPECTRAL SENSITIVITY OF HUMAN VISION TO THE LIGHT PULSES

Volodymyr Brailovsky[1], Ivan Pyslar[1], Margaryta Rozhdestvenska[1], Magdalena Michalska[2]
[1]Chernivtsi National University, Department of Radio Engineering and Information Security, [2]Lublin University of Technology, Institute of Electronics and Information Technology

Abstract. *In the paper we represent experimental results of the research of human vision sensitivity to pulsed radiation of discrete light emitting diodes (LEDs) of different colors when their dissipated electrical power was the same. We used color components of RGB LED matrix and determined the values of the dissipated power at which resultant LED radiation was perceived as white light. These power values were used to investigate sensitivity of human eye to radiation of each color of RGB matrix. Spectral characteristic of RGB LED under investigation was checked for presence of additional spectral components. The results we obtained give the possibility to develop information systems with concealment of the data transfer process using white light which color components are informative.*

Keywords: RGB LED, light pulse, human vision, information system

CZUŁOŚĆ WIDMOWA WZROKU LUDZKIEGO NA IMPULSY ŚWIATŁA

Streszczenie. *W artykule zostały przedstawione wyniki badań eksperymentalnych czułości wzroku ludzkiego na promieniowanie impulsowe diod LED o różnych kolorach światła przy jednakowych rozpraszanych na nich mocach elektrycznych. Za pomocą macierzy RGB określa się wielkości mocy rozpraszanej na diodach LED macierzy, przy których wynikające promieniowanie diod LED jest odbierane jako białe. W tak określonych mocach elektrycznych została zbadana czułość ludzkiego widzenia na pulsacyjne promieniowanie każdej z diod LED matrycy RGB. Charakterystyka widmowa badanej diody RGB LED została sprawdzona pod kątem obecności dodatkowych składowych widmowych. Uzyskane wyniki umożliwią opracowanie systemów ukrytej transmisji informacji za pomocą światła białego, którego składowe widmowe mają charakter informacyjny*

Słowa kluczowe: dioda RGB LED, impuls świetlny, ludzki wzrok, system informacyjny

Introduction

Subjective human perception of light pulses is widely used in medicine for diagnostics of diseases of human vision. These methods are based, in particular, on the Talbot-Plateau law [1] and the Ferry-Porter law [2]. The reaction of human eye to sequences of light pulses is described by Talbot-Plateau law. According to this law when flashes (light pulses) effect on observer's eye with frequency higher then critical fusion frequency F_{limFFT} (flicker fusion threshold) its sensation becomes continuous. The effect of light pulses fusion causes a visual sensation identical to created by the light of constant brightness. The effective luminance L_{ef} will be the average luminance during a period:

$$L_{ef} = L \cdot t_1 /(t_1 + t_2), \quad (1)$$

where t_1 is duration of light pulses, t_2 is time interval between two adjacent pulses, L *is* luminance of light pulses.

Flicker fusion threshold F_{limFFT} can be calculated after the Ferry-Porter law:

$$F_{\lim FFT} = a \cdot \mathbf{lg} L_{ef} + b, \quad (2)$$

where L_{ef} is effective luminance, parameter $a = 12.5$ for cone (day) vision and $a = 1.5$ for rod (night) vision, $b = 37$.

Appearance of powerful LED light sources gives the opportunity to expand the application of these laws beyond the scope of diagnosing human illness. They can be applied to develop information systems with concealment of the data transfer process.

Previous research shown that at nonzero background lighting level there is fairly wide interval of frequencies of pulse sequence, when human eye does not see light pulses. The investigations were carried out in the cases of direct and peripheral fields of view. Such sequence of light pulses can not be detected by traditional methods of photo and video recording.

This is connected with the problem of spectral distribution of frequencies of invisibility for white light. To solve this problem two experiments different in their approach were carried out. The essence of the first one was to find the frequencies of invisibility of three separate LEDs (red, green, blue) when the power, supplied to them, was the same.

In the second experiment we used RGB LED matrix and controlled the power given to each colour LED component. The value of the power was chosen so that resultant (total) radiation of LEDs was perceived by human vision as white light. The electrical power value, determined in such way remain permanent. In the experiment only the character of the radiated by colour LED components was changed: from continuous light it was transformed into pulsed light with adjustable frequency and duration.

Information systems of visual light are being actively developed [3] and offered on the market. In developing of such systems, it should be taken into account that human brain extremely negatively responds to action of two and more light stimuli operating with different frequency rhythms (for example, computer monitor, lighting system, etc.) [4]. At the same time ensuring the concealment of the data transfer process is also an important aspect of functioning of light information systems [5, 6].

It should be noted that the main task in this experiment was not the determination of colour. The main task of this experiment was the determination of light impulse from LED.

1. Spectral components of RGB LEDs matrix under investigation

Preliminary we studied radiation spectra of light emitting diodes which are parts of LED matrix with diameter 5 mm. Spectrum of LED radiation light flux was analysed using the spectrophotometer SF-4. The spectrophotometer sent the signal to photoelectronic multiplier (PEM). PEM transformed poor light flux to electrical signal. PEM output signal was measured by the voltmeter M95 in which there is no possibility of the sensitivity change. So RGB LED current was set to such a value that for maximum of LED spectral characteristic the voltmeter readings did not exceed 0.9 of voltmeter scale range.

Using this algorithm, we determined electrical current for all LEDs:

$$I_{green} = 0.10 \text{ mA}; I_{red} = 0.13 \text{ mA}; I_{blue} = 0.04 \text{ mA}.$$

Low level of the current of blue LED shows its highest efficiency of conversion of electrical energy to the light. Red LED is characterized by the lowest efficiency of conversion.

Experimental results of spectral distribution of relative intensity of light flux from every RGB matrix LED are represented in Fig. 1. In this figure you can see that RGB LED radiation spectrum consists of wavelengths of red (RED curve in Fig. 1); green (GREEN curve) and blue (BLUE curve) colours and has similar width of radiation spectra. Radiation spectrum width was determined at 0.707 level of radiation maximum. For blue and red components of matrix it is equal 13 nm, and for green one the radiation spectrum width is 15.6 nm.

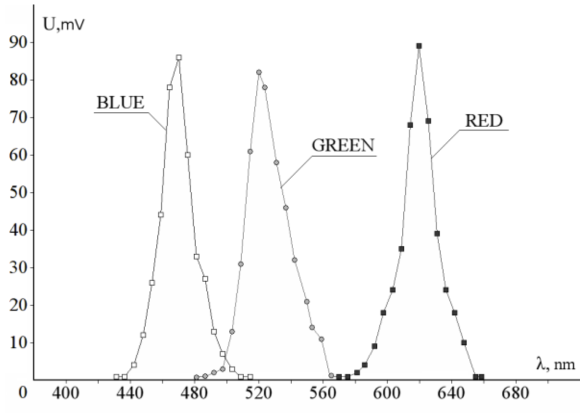

Fig. 1. Spectral distribution of relative intensity of light flux for different LEDs of RGB matrix

Experimental results could be changed under influence of any additional light source. Therefore, the experiments were conducted in dark room. There were no other light sources in this room. Background light also was formed using LED matrices Epistar 5730 (Fig. 2).

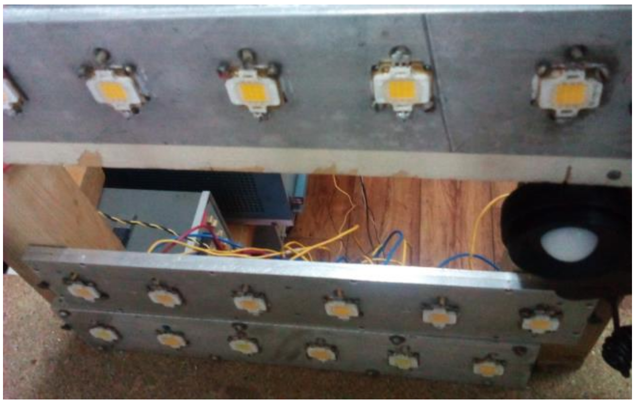

Fig. 2. Panels for forming background lighting

Radiation of these LED matrices is similar to white light spectrum. Background lighting level was controlled by changing the voltage on LED matrices. The distance between observer and LED (called as test-target) was 1 m. The experiment was conducted in the case of direct vision (4-7°) and constant duration of pulses (5 μs). Pulses of the same duration but different power were given to RGB LED leads. Mixing of colored LED radiation (switches S1, S2, S3 in Fig.3 were closed) formed the white light [7, 8]. Electrical pulses with the required parameters were formed using the pulsed generator G5-54. Output signal parameters of the generator were controlled by the digital oscilloscope TDS1012. Regulation of the current and consequently LED luminescence brightness was provided by the potentiometers R5, R6, R7 (Fig. 3). Resulting flux of radiated light was formed, as aforementioned, according to the criterion that the total emitted radiation is perceived as a white light. To meet this criterion the pulse power supplied to the LED must have the values represented in Table 1.

Table 1. The power of pulses supplied to RGB LED matrix components

Type of LED component	Power, W
Red	0.045
Green	0.017
Blue	0.016

Sizes of the LED under investigation are much more than for example sizes of monitor pixels of modern computers [9, 10, 11]. Therefore, mixing radiated LED light was less effective. To solve this problem the light radiated by LEDs was directed to a light-scattering screen.

Due to a significant own capacity of p-n junction (C_{pn}) of the LEDs we observed a post-emitting effect. To speed up the process of dissipating electrical power accumulated on p-n junction capacity we used the parallel load resistors R11, R12, R13 (Fig. 3) with resistance of 27 Ohm. Such value of resistance was chosen due to the condition that discharging time constant would be less than duration of electrical and consequently light pulses:

$$\tau_{dis.} << \tau_{pulse},$$

where $\tau_{dis.} = C_{pn}R_L$, R_L is load resistance.

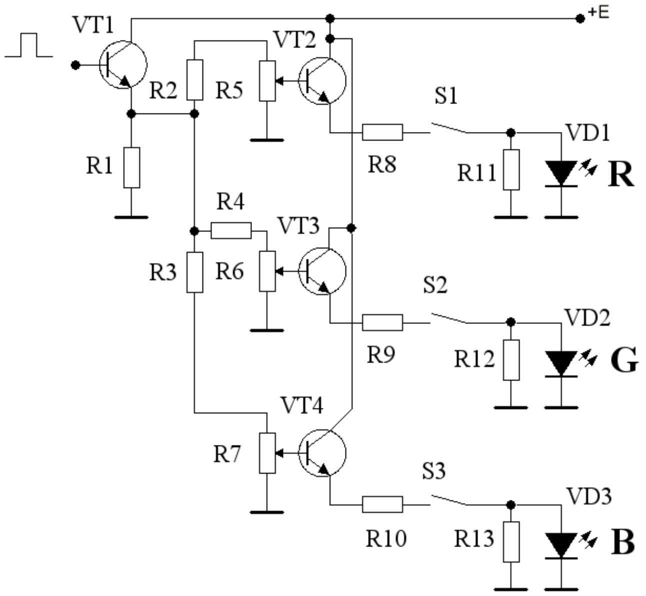

Fig. 3. Schematic circuit diagram of light pulses former

This allowed to obtain the form of the pulses radiated by LED as rectangular form of electrical pulses given to the LED.

During the experiment the RGB LED was studied to reveal the presence of “invisible” frequency ranges for every its spectral component. Electric energy brought to the LED was constant during the experiment. Its value allowed formation of white light after mixing of radiated colored light (switches S1, S2, S3 were closed). The results are represented in Fig. 4. White areas in all parts of small Fig. 4 correspond to the frequency range when human eye see the light radiation. Gray areas in all parts of small Fig. 4a correspond to the frequency range when human eye doesn't see the light radiation. It was found that the largest frequency range of "invisibility" among R, G, B LEDs under consideration is observed for a blue LED (Fig. 4c).

Light pulses threshold frequency above which light pulses are perceived by human vision as continuous radiation (white area in Fig. 4) significantly depends on background lighting level. For example, at E = 100 lx for green LED component this frequency is $F_{lim.green}$ = 3 kHz. In the case of the same background lighting level for red and blue LED components we obtained values $F_{lim.red}$ = 1.6 kHz and $F_{lim.blue}$ = 5.5 kHz, respectively. In the case of synthetic white light, formed by mixing color radiation of RGB LED all components, $F_{lim.white}$ = 7.1 kHz.

Threshold frequencies for background lighting level E = 160 lx are the following: $F_{lim.green}$ = 4.9 kHz, $F_{lim.red}$ = 2.7 kHz, $F_{lim.blue}$ = 7.7 kHz. At the same conditions for mixing (white) light the threshold frequency is $F_{lim.white}$ = 10 kHz.

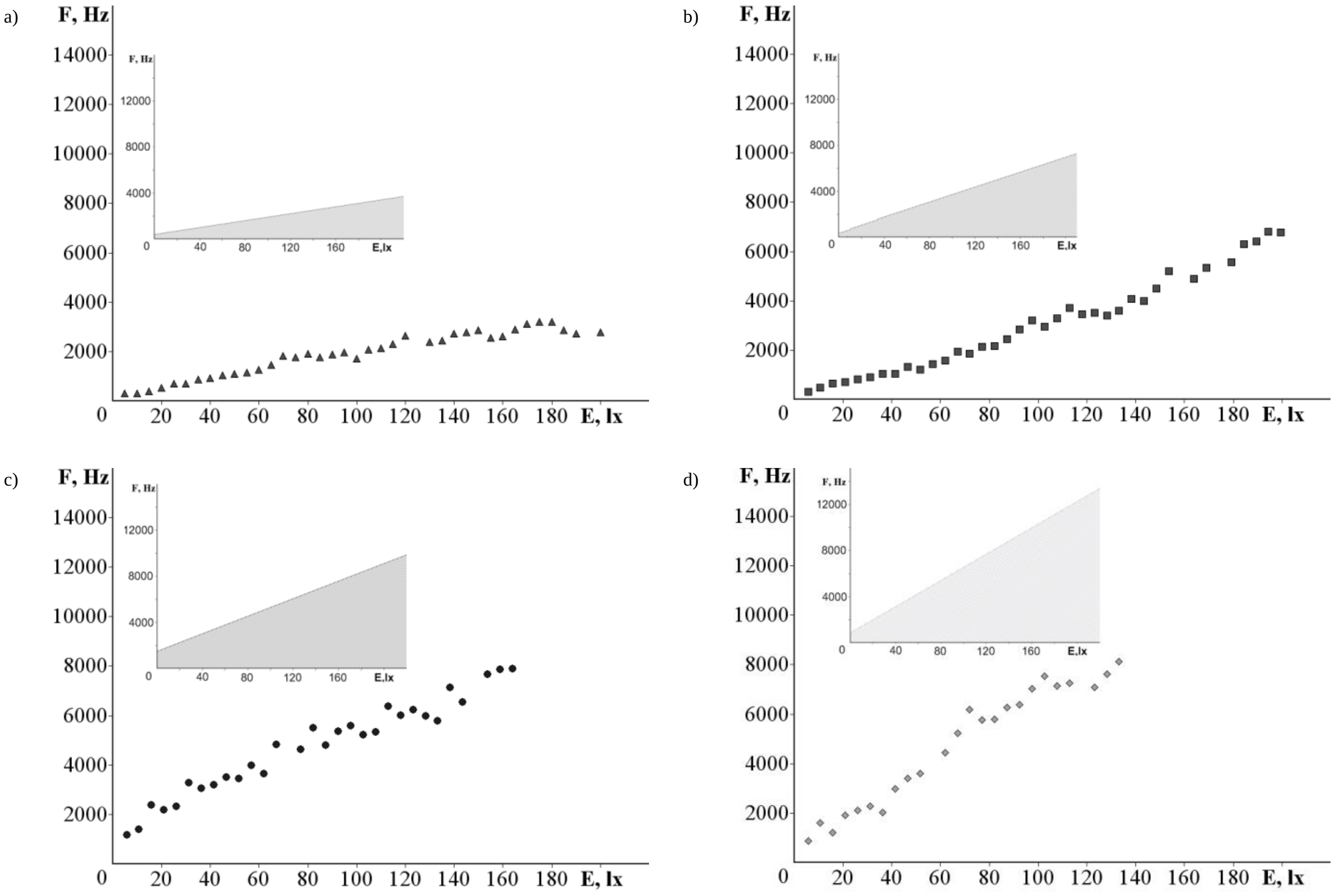

Fig. 4. Averaged experimental intensity of illumination – frequency dependencies of "invisible" radiation of green (a), red (b), blue (c) components of the RGB LED and their simultaneous radiation (white light) (d) (Approximation lines for experimental results, respectively. Gray areas correspond to "invisible" frequency range)

The rate of the change of the threshold frequency with the change of intensity of illumination varies for spectral components. Mark this parameter as $k = \Delta F/\Delta E$, where F is frequency (in Hz) at given level of background lighting (in lx). Table 2 presents k values for spectral components of artificially formed white light.

Table 2. The parameter k (at the level of background lighting E = 160 lx) for different spectral components of white light of the investigated LED

component	k, Hz / lx
Red	17
Green	30
Blue	48

2. Separate color LEDs study

Each separate LED was supplied by the power of 0.06 W, duration of the pulses in this experiment was 5 µs. In Fig. 5 intensity of illumination – frequency characteristics of "invisible" light pulses are represented.

It was determined that at background lighting level E = 100 lx average observer did not see light pulses from green LED when their frequency achieved the threshold 216 Hz. In the cases of red and blue LEDs threshold frequencies were 54 Hz and 72 Hz, respectively.

Consequently frequency threshold of 'invisibility' of green light LED is 4 times and 3 times greater than the threshold frequency of the red and blue LEDs, respectively.

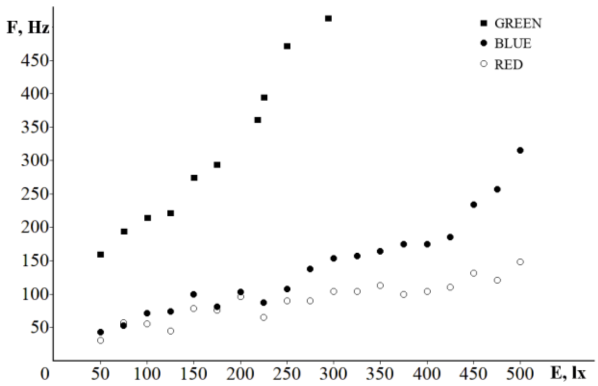

Fig. 5. Intensity of illumination -frequency dependence of radiation of green, red, blue LEDs

3. Summary

The lowest threshold frequencies were obtained for the green spectral component. This can be explained by the high sensitivity of human vision to green light.

The highest threshold frequencies were determined for the blue LED. Using the correlation between frequency of pulse sequence and bit rate one can say that for blue component this parameter is limited approximately to 7 kbit per second for background light level of 160 lx. Variable level of background lighting requires the development of smart control module for the information systems with concealment of data transfer.

The results of the research show that application of green and red spectral components of visible light in the information systems under consideration is ineffective.

References

[1] Fedyukyna H.V., Rokhmyn H.N.: Spravochnaya kniga po svetotekhnike. Rokhmyn, 2006.
[2] www.britannica.com/science/human-eye/The-work-of-the-retina#ref531589 (18.11.17)
[3] Gagandeep K.V.: Li-Fi. A new Communication Mechanism. International journal of Computer Applications, Vol. 118, No 15, 2015.
[4] Il'ina E.I., Chastuhina T.N.: Pochemu ne prinimayutsya mery dlya snizheniya pul'satsii osveshchennosti. Vol. 4, Svetotehnika, Moscov 2005.
[5] Brailovsky V.V., Pyslar I.V., Rozhdestvenska M.G. Poshak O.V.: Fiziologicheskiye aspekty proyektirovaniya sistem skrytoy peredachi informatsii na opticheskom izluchenii vidimogo diapazona. Tekhnologiya i konstruirovaniye v elektronnoy apparature, Vol. 1, 2015, 13–16.
[6] Brailovsky V.V., Pyslar I.V., Rozhdestvenska M.G.: Zavadostiyka informatsiyna systema na svitlovykh promenyakh. Vymiryuvalʹna ta obchyslyuvalʹna tekhnika v tekhnolohichnykh protsesakh, Vol. 3, 2013, 157–160.
[7] Kolokol'cev M.M., Solovev V.A.: Malogabaritnyy pribor dlya issledovaniya porogov svetorazlicheniya i kolichestvennoy otsenki anomaliy tsvetovogo zreniya cheloveka. Opticheskiy zhurnal, Vol. 81, No 10, 2014, 42–45.
[8] Tal'nishnih N.A., Chernjakov A.V., Aladov A.L., Zakgejm A.L.: Issledovaniye svetodiodnykh istochnikov sveta na printsipe RGB smeshchevaniya s vysokim indeksami tsvetoperedachi. Izvestiya Samarskogo nauchnogo tsentra Rossiyskoy akademii nauk, Vol. 16, No 4(3), 2014, 631–635.
[9] Doroshhenkov G.D., Kozhemyako V.P., Pavlov S.V.: Systemy telebachennya ta tekhnichnoho zoru. Navchalʹnyy posibnyk. VNTU, Vinnytsya 2014.
[10] Groshev F.V., Golubcov K.V., Trunov V.G., Ajdu Je.A.: Komp'yuternaya sistema dlya issledovaniya labil'nosti zritel'noy sistemy. Sbornik trudov 31-zh konferentsii molodykh uchenykh i spetsialistov IPPI RAN ″Informatsionnyye tekhnologii i sistemy″. Gelendzhik, 2008, 259–261.
[11] Golubinov K.V., Kuman I.G., Hejls T.S., Shigina V.G., Trunov V.G., AjduJe. A.I., Bykova T.A., Sofronov P.D., Rjabceva A.A.: Mel'kayushchiy svet v diagnostike i lecheniye patologicheskikh protsessov zritel'noy sistemy cheloveka. Informatsionnyye protsessy, Vol. 3, No 2, 2003, 114–122.

M.Sc. Ivan Pyslar
e-mail: i.pyslar@chnu.edu.ua

Ph.D. student at the department of Radio Engineering and Information Security in Institute of Physics-Technology and Computer Science at Yu. Fedkovych Chernivtsi National University, Chernivtsi, Ukraine. Research field covers wide variety of radio engineering and information security. Author of 3 publications in this research area.

Ph.D. Volodymyr Brailovsky
e-mail: brailovsky@ukr.net

Lector at the department of Radio Engineering and Information Security in Institute of Physics-Technology and Computer Science at Yu. Fedkovych Chernivtsi National University, Chernivtsi, Ukraine. Research field covers wide variety of radio engineering and information security. Author of nearly 100 publications in this research area.

Ph.D. Magharyta Rozhdestvenska
e-mail: m.rozhdestvenska@chnu.edu.ua

Lector at the department of Radio Engineering and Information Security in Institute of Physics-Technology and Computer Science at Yu. Fedkovych Chernivtsi National University, Chernivtsi, Ukraine. Research field covers wide variety of radio engineering and information security. Author of nearly 20 publications in this research area.

M.Sc. Magdalena Michalska
e-mail: magdalena.michalska@pollub.edu.pl

Ph.D. student, Institute of Electronics and Information Technology, Lublin University of Technology.
Recent graduate Warsaw University of Technology The Faculty Electronics and Information Technology. Since 2017 member of IEEE Students Poland Section Branch Lublin University of Technology. Research field covers wide variety of 3D modeling, medical image processing, spectrophotometry, human brain atlases.

otrzymano/received: 10.10.2017 *przyjęto do druku/accepted: 15.02.2018*

DOI: 10.5604/01.3001.0010.8643

ORGANIZATION OF IMPLEMENTATION OF UBIQUITOUS SENSOR NETWORKS

Sergey Toliupa[1], Yuriy Kravchenko[2], Aleksander Trush[2]
[1]Kyiv National Taras Shevchenko University, Department of Cybersecurity and Information Protection, [2]Kyiv National Taras Shevchenko University, Department of Network and Internet Technologies

Abstract. *The article deals with the implementation of one of the most promising technologies of the 21st century – the permeable sensor networks of the USN. The features, architecture, organization and routing algorithms of sensory networks are described. It is determined that further improvement of the work of such networks requires standardization of the development process and implementation process. USN's Vertical Sensor Networks is one of the most promising technologies of the 21st century. Cheap and "smart" sensors, in large quantities combined into a wireless network connected to the public communications network, today provide an unprecedentedly wide range of control and management services for buildings, businesses, cars, and so forth. USN networks, depending on the type of sensors, can be deployed on the ground, in the air, under and over water, in buildings and, finally, on the skin and inside living organisms, including humans. They are also widely used in such important areas as military affairs, crisis and emergency management, and the fight against terrorism.*

Keywords: ubiquitous sensor networks USN, network architecture, touch-route routing algorithms

ORGANIZACJA IMPLEMENTACJI WSZECHOBECNYCH SIECI SENSOROWYCH

Streszczenie. *Artykuł dotyczy implementacji jednej z najbardziej obiecujących technologii XXI wieku – wszechobecnej sieci sensorowej USN. Opisano funkcje, architekturę, organizację i algorytmy routingu sieci sensorowych. Ustalono, że dalsza poprawa takich sieci wymaga standaryzacji procesu rozwoju i procesu wdrażania. Pionowe sieci sensorowe USN to jedna z najbardziej obiecujących technologii XXI wieku. Tanie i "inteligentne" czujniki w dużych ilościach w połączeniu z siecią bezprzewodową podłączoną do publicznej sieci komunikacyjnej zapewniają obecnie niespotykany dotąd szeroki zakres usług zarządzania budynkami, przedsiębiorstwami, samochodami i tak dalej. Sieci USN, w zależności od rodzaju czujników, mogą być rozmieszczone na ziemi, w powietrzu, pod wodą i nad wodą, w budynkach, a wreszcie na skórze i wewnątrz organizmów żywych, w tym ludzi. Są również szeroko stosowane w tak ważnych obszarach, jak sprawy wojskowe, w sytuacjach kryzysowych i zarządzania kryzysowego oraz w walce z terroryzmem.*

Slowa kluczowe: wszechobecne sieci sensorowe USN, architektura sieci, algorytmy routingu sieci sensorowych

Introduction

USN's Vertical Sensor Networks (Ubiquitous Sensor Networks) is one of the most promising technologies of the 21st century. Cheap and "smart" sensors, in large quantities combined into a wireless network connected to the public communications network, today provide an unprecedentedly wide range of control and management services for buildings, businesses, cars, and so forth. USN networks, depending on the type of sensors, can be deployed on the ground, in the air, under and over water, in buildings and, finally, on the skin and inside living organisms, including humans. They are also widely used in such important areas as military affairs, crisis and emergency management, and the fight against terrorism. To support the specified characteristics, each sensor must correspond to a specific architecture in which the main elements are: directly the touch device, memory, antenna, power supply.

1. Vertical Sensor Networks USN

An important aspect of the efficient functioning of the network is its scalability. However, today it is impossible to ignore the mobile all-pervading sensory networks, the use of which also covers all aspects of human activity and society. Other important features of the networks are:

- Low energy consumption. Due to the fact that quite a large part of the USN deployment scenarios involves the presence of sensors in hard-to-reach places, their maintenance may become an unrealistic task. That is why the life cycle of the sensor is often limited by the time the power source is operating.
- Self-organization of the network. Deployment of the sensor network is significantly different from the deployment of traditional networks. Often, sensors are distributed randomly in a given area, and further such a "set" of sensors should be self-organized into the network. Then it will not be possible to control them from the outside. Self-organization should be dynamic - the failure of the components of the network due to, for example, their physical destruction, or the discharge of power sources, should be determined operatively [4]. Otherwise, the effective functioning of the USN will be under threat.

Standardization of such networks is dealt with by the IEEE 802.15.6 working group. Taking into account the all-pervading nature of sensor networks and their use in various spheres of life, it is advisable to name the society that uses them - ubiquitous. This corresponds to the previous name of the WSN (Wireless Sensor Networks) network. The urgency of the network and its viscidity, as reflected by standards and draft standards of the International Telecommunication Union, allowed the use of the USN abbreviation.

Wireless sensor networks are just such examples of special networks that do not have a common infrastructure other than gateways to other networks. Each of the nodes of the sensor network must be able to function as both a terminal and a transit node. Transmission of data in sensory networks is carried out by means of their redirection to the nearest node step by step.

Such networks are called multi-step (with repeaters). It should be noted that more sophisticated routing algorithms may exist when the next node is selected based on an analysis of its characteristics, such as energy costs, reliability, etc. In the presence of mobile sensor nodes, the architecture of the sensor network becomes more and more dynamic.

Sensor networks are defined as "distributed networks consisting of small wireless nodes of narrow specialization in a large number distributed on a certain surface (Fig. 1). Thus, the sensor network is a large number of wireless sensors, distributed in some area with a high density. In the area of signal, coverage of each of the sensors must be at least another sensor; in this case, the sensor will be called neighboring. The more "neighbors" of each of the sensors, the higher the accuracy and reliability of the sensor network [1].

A cluster organization is considered efficient and scalable for solving similar problems (Figure 2), but only if the cluster network's main site is rational and at the appropriate time.

Indeed, at the time of the T1 time, the sensor node does not necessarily have to be at another time, since the existing main node can already spend a fairly large amount of energy for transmitting messages from all sensory cluster nodes to the time T2. Therefore, at the moment of time T2, the main node in the cluster can be assigned another sensor node, which has by this time retained the largest energy supply.

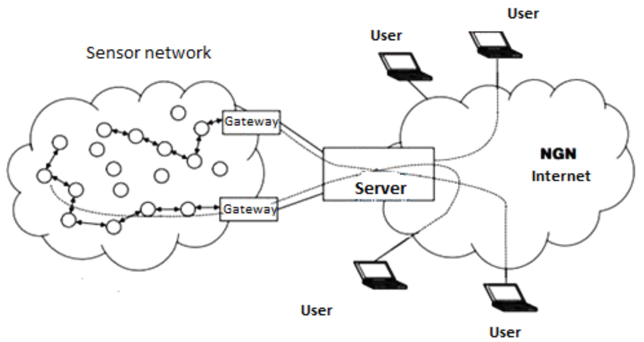

Fig. 1. An example of connecting the sensor network to the public communications network

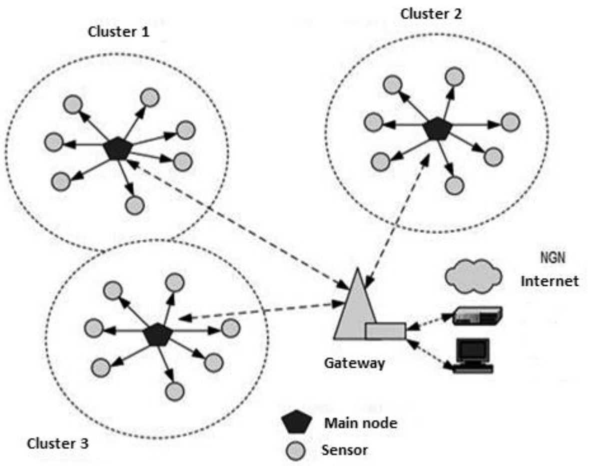

Fig. 2. USN Cluster Architecture

One of the most well-known mechanisms that provide the functioning of sensor networks and the selection of main nodes is the Low Energy Adaptive Cluster Hierarchy (LEACH) algorithm.

The LEACH algorithm involves the probable selection of the sensor node for the role of the main at the beginning of the functioning of the sensor network, and subsequently rotation of the main energy characteristics of other sensor nodes. Such a solution increases the duration of the functioning of sensor nodes and the network as a whole, but does not solve the problem of providing better coverage for a sufficiently long time. And this is natural, since when creating a LEACH such a task was not raised. There are quite a few algorithms that are one way or another trying to improve LEACH. These are algorithms used as a criterion for the amount of residual energy; the location of the candidate node for the main cluster node in relation to other nodes; information about the topology of the network at the current time. For example, the HEED (Hybrid Energy – Efficient Distribution) algorithm uses a mixed criterion for choosing a host based on the analysis of residual energy and the location of adjacent nodes. All these algorithms are used to maximize the duration of the functioning of sensor nodes and the network as a whole. However, with the development of sensor networks, there were additional tasks that require close attention. For example, the problem of quality of service, which is the most important metric for any network, including the sensory one [6].

The problem of extending the life of the sensor network is very important. However, if this network does not perform its functions to the extent necessary, then the task itself to increase the life of the sensor network does not meet the requirements for quality of service. In monitoring systems, one of the most important requirements is the continuity, that is, the monitoring of parameters throughout the space or throughout the process. Proceeding from the above, it is necessary to develop such an algorithm for selecting the main node of the cluster, which would provide better coverage of the area of two-dimensional area (area) for monitoring over a sufficiently long period of time. This approach means optimizing the life of the sensor network, as well as optimizing the performance of the sensory network of its functional tasks with a given quality of service over a sufficiently long period of time.

2. Sensor architecture

The sensor, like any telecommunication node or terminal, consists of hardware and software. In general, the sensor consists of the following subsystems: monitoring and perception, data processing, as well as communication subsystem and power supply. The subsystem of monitoring and perception allows the sensor to collect such data on the environment as temperature, light intensity, vibration, acceleration, magnetic field, chemical composition of air, acoustics, etc. It is this subsystem that defines the area or implementation in which the sensor can be used. The sensor can optionally be supplemented by other subsystems, such as positioning, power generator, etc. (Figure 3)

The monitoring and perception subsystem contains an analogue device that directly removes certain statistics, and an analog-to-digital converter that converts analog data into digital for further processing. The data processing subsystem includes memory and a central processing unit, allows you to store and process both sensor-generated data and the service data necessary for the correct and efficient operation of the communication subsystem.

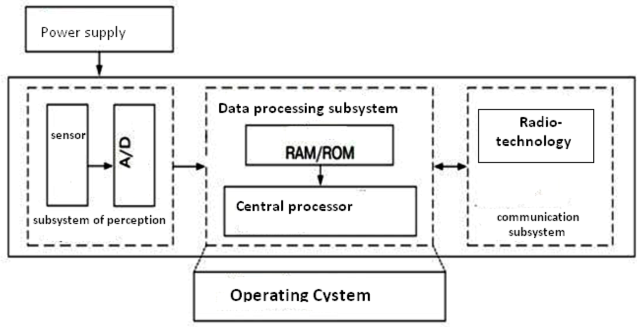

Fig. 3. Sensor architecture

The most important technical aspects of the sensor implementation are the small size of a telecommunication device with complex functions. Today, the minimum requirements for the hardware part of the sensor can be as follows: the frequency of the central processor is 20 MHz, the amount of RAM is 4 KB, the transmission rate is 20 kbit/s. Hardware optimization allows you to reduce the size of the sensor, however, as a rule, it causes an increase in its price. Optimization of the operating system (OS), taking into account the architecture of the used CPU is necessary. Today's most popular is the open source Tiny OS, which allows you to flexibly handle the sensors of various developers. Power requirements impose significant limitations on radio technologies that can be effectively applied in sensor networks. Moreover, the limited performance of the CPU does not allow the use of standard routing protocols for IP networks, but the high complexity calculation of the algorithm of the optimal path overload the central processor of the sensor. A large number of special routing protocols for sensor networks have been developed. In addition to the classical architecture of the sensor node, others are possible, due to the need not only to monitor or control the measured characteristics, but also to influence the objects of measurements. Such an element that has the ability to influence the object is called an actor.

One of the most important parameters when constructing sensory networks is energy consumption. Given that the sensor node can serve as both a terminal and a transit node, increasing the life of the power supply is one of the priority tasks, which is solved not only by increasing the life of the power source, but also through its efficient use.

Taking into account the known classical energy consumption ratio by the mobile node, which indicates that the ratio of energy consumption in the "transmission; receptions; standby mode; sleeping mode "is given in the ratio" 13:9:7:1", intensified attention is paid to reducing the time of transmission and reception of information and increasing the proportion of time when the sensor is in standby or hibernation mode. This should be taken into account when designing routing algorithms.

3. Sensor architecture

Since the sensor network may not have a permanent infrastructure, it is hardly possible to use classic routing algorithms for sensor networks. In addition, in USN, data traffic can be generated so that the same information is obtained from different sensor nodes operating in any zone. In addition, sensor sizes and costs are limited in the same way as their resources: energy, memory, computing capabilities. Therefore, it's impractical to transmit the same information across the network from many sensor nodes. Proceeding from the above, when developing routing algorithms in wireless sensor networks, the following factors should be taken into account:

Self-organization. Sensory networks should be able to self-organize. Proceeding from this, computing capabilities, communication and management capabilities should be sufficient to ensure autonomous existence.

Energy efficiency. Sensor nodes are designed, as a rule, with the provision of battery power and, accordingly, the term of their operation is primarily determined by the power supply system. Minimization of power consumption is one of the most important research tasks in the field of wireless sensory networks.

Flexibility. Sensory network algorithms should be flexible enough to allow them to adapt to different USN implementations. The operating environment, the environment and the capabilities of the sensor node itself vary widely, although some conditions may be pre-predicted or even identified before the network is created.

Scalability. In wireless sensor networks, the number of sensor nodes depending on the task being solved can vary from a few hundred to thousands. It is no coincidence that in the Zig-Bee specifications, the number of sensor nodes located in the same zone can reach 64,000. The large-scale and high-bandwidth networks with a bandwidth limit should, moreover, provide services with a certain level of service quality.

Tolerance to failures. Unlike traditional networks, wireless sensor networks are organized randomly, and the interconnections of sensory nodes in them are also random in time. Sensory nodes may fail due to insufficient power supply, the emergence of critical conditions in the environment, the failure of the hardware, etc.

Accuracy and quality. Ensuring sufficient accuracy and actualization of information in real time is one of the most important tasks for a large number of USN implementations. The algorithms must ensure that the data is transmitted in the wireless sensor network at the right time and with a given probability. The ideal algorithm should ensure the timely transmission of information with a given accuracy and minimum power consumption.

4. Classification of routing algorithms in USN

At the development stages of the USN, various solutions were proposed for constructing network routing algorithms, taking into account the necessary features outlined above. The proposed USN routing algorithms can be grouped into different groups according to the criteria. In tabl. 1 shows a simple classification of routing algorithms in USN using a typical approach.

In a one-level network, all nodes play the same role and have the same functionality. The collected data is transmitted to the network using multi-directional routing. The algorithms in the one-level network should ensure the transfer of large amounts of transit information through the network and, of course, they are application-oriented. Basically, the algorithms for a one-level network are centralized, since their main task is to ensure the transit of data through a homogeneous touch network. In many cases, the algorithms for a one-level network are quite complex, since there is both a scaling and a dynamic change in the USN topology.

Table 1. Simple classification of routing algorithms

Criterion	Category	Examples
Network structure	One-level	SPAN
	hierarchical	ILEACH
Knowledge about resources	Based on residual energy	HEED
	On the basis of accuracy Location	Directed Diffusion
Management protocols	Centralized	SPAN
	Geographic	GFG
	Based on QoS	SAR
	Based on the theory of queues	COUGAR

The SPIN (Sensor Protocols for Information viaNegotiation) and DD (Direct Diffusion) algorithms are basic for a one-level wireless sensor network, and all the subsequent one-level algorithms are developed on their basis.

In hierarchical networks, sensor nodes play different roles, and there are two categories of sensor nodes: the main cluster node CH (Cluster Head) and members of the cluster. A higher level of sensory nodes collects information from cluster members and controls a lower level. After aggregation of data, nodes of a higher level, if necessary, direct it to the next level. The main nodes of the clusters interact with the nodes of the public communications network. Each main node collects data from the nodes of its cluster, aggregates them and passes on. All hierarchical routing algorithms should provide the choice of the best CH. Since the cluster's main nodes are responsible for gathering, aggregation, and transmitting data over quite long distances, they should be more energy independent than just cluster members. The algorithms for selecting the master cluster node assume rotation and redistribution of the cluster main node periodically depending on the distribution of the load as a whole through the wireless sensor network and other factors such as power consumption, coverage, etc.

At the development stages of the USN, various solutions were proposed for constructing network routing algorithms, taking into account the necessary features outlined above. The proposed USN routing algorithms can be grouped into different groups according to the criteria. In a one-level network, all nodes play the same role and have the same functionality. The collected data is transmitted to the network using multi-directional routing. The algorithms in the one-level network should ensure the transfer of large amounts of transit information through the network and, of course, they are application-oriented. Basically, the algorithms for a one-level network are centralized, since their main task is to ensure the transit of data through a homogeneous touch network. In many cases, the algorithms for a one-level network are quite complex, since there is both a scaling and a dynamic change in the USN topology. The SPIN (Sensor Protocols for Information viaNegotiation) and DD (Direct Diffusion) algorithms are basic for a one-level wireless sensor network, and all the subsequent one-level algorithms are developed on their basis [4, 7].

Consider algorithms for hierarchical wireless sensor networks. The main problem in creating algorithms for such networks is the choice of the main node of the cluster. There are two approaches to choosing the main cluster node: random choice and preference choice.

Let's consider the algorithm of random selection of the main node, using which the rotation of the main nodes can be performed among all members of the cluster, taking into account their characteristics at the current time. The LEACH (Low-Energy Adaptive Clustering Hierarchy) hierarchical low-energy clustering algorithm involves ensuring the balance of energy consumption of the wireless sensor network. The LEACH algorithm is basic. There are many algorithms based on it. The basic idea behind LEACH is to: touch nodes can be randomly selected as the main ones based on information about their functioning at a pre-emptive point in time. In this case, in the cluster, each sensor node generates a random number from the interval [0, 1]. Each sensor node has a threshold Th (LEACH) corresponding to a predetermined number of main sensor nodes in the network. If the integer random number is less than Th (LEACH), then the touch node may become the main one; otherwise this node remains only a member of the cluster. The Th (LEACH) calculation is a key task in implementing the LEACH algorithm.

LEACH is a very effective algorithm. It reduces power consumption by 7 and more times compared with the direct interaction of sensor nodes and 4 to 8 times in comparison with other routing algorithms.

In hierarchical networks, sensor nodes play different roles, and there are two categories of sensor nodes: the main cluster node CH (Cluster Head) and members of the cluster. A higher level of sensory nodes collects information from cluster members and controls a lower level. After aggregation of data, nodes of a higher level, if necessary, direct it to the next level. The main nodes of the clusters interact with the nodes of the public communications network. Each main node collects data from the nodes of its cluster, aggregates them and passes on. All hierarchical routing algorithms should provide the choice of the best CH. Since the cluster's main nodes are responsible for gathering, aggregation, and transmitting data over quite long distances, they should be more energy independent than just cluster members. The algorithms for selecting the master cluster node assume rotation and redistribution of the cluster main node periodically depending on the distribution of the load as a whole through the wireless sensor network and other factors such as power consumption, coverage, etc.

Comparing the one-level and hierarchical routing algorithms, it can be noted that hierarchical algorithms provide more possibilities for the introduction of USN. The research noted the following characteristics of hierarchical algorithms:

- hierarchical network routing is an effective way of reducing energy costs;
- hierarchical routing allows you to flexibly solve various tasks based on the capabilities of sensor nodes. Hierarchical routing allows you to balance network load;
- hierarchical routing allows you to simply implement a schedule and avoid collisions;
- hierarchical routing is easy to implement.

Although one-level routing can use optimal routes, its implementation is usually quite complicated. The limited capabilities of sensor nodes can be a problem for the implementation of complex algorithms and schemes. Hierarchical routing involves the division of compounds into the internal cluster and external ones. Only the main node of the cluster is responsible for the external connections, while the cluster members interact only on the internal cluster level. This simple routing reduces the number of messages in the cluster [5].

5. Conclusion

The article deals with the architecture and routing algorithms of sensor networks. It is determined that further improvement of the work of such networks requires standardization of the development process and implementation process.

References

[1] Akyildiz I.F.: Key Wireless Networks Technological in the Next Decade. NEW2AN 2006, St. Petersburg, Russia June 2006.
[2] Berkman L.N., Tolupa S.V.: The architectural concept of construction, the principle of implementation, the efficiency of the application of intelligent telecommunication network. Problematic sciences works of VITI NTUU-KPI 3/2007, 9–17.
[3] Burov E.: Computer networks. Baku, Lviv 1999.
[4] Golishko A.: IMS: useful recommendations. CONNECT 5/2009, 2–6.
[5] Retana A., Slice D., Ras U.: Principles of Designing Corporate IP Networks. Williams Publishing House 2002.
[6] Steklov V.K, Kilchytsky Ye.V.: Fundamentals of management of networks and telecommunication services. Technique, Kiev 2002.
[7] Tikhvin O.V., Terentyev S.V.: SV LTE mobile communication networks and architecture. Moscow, Eco-Trend Publishing House 2010.
[8] Ujukha T.: Prospects of SDN on a telecom. Market. Technologies and media 2(107)/2015, 52–54.

Prof. Sergey Toliupa
e-mail: tolupa@i.ua

Scientific and practical interests are related to such areas as intelligent control systems, the direction of improving the efficiency of information technology, information security systems, cybersecurity and cyber defense. He is the author of 5 monographs and over 150 scientific and methodological works, 16 textbooks and manuals.

Prof. Yuriy Kravchenko
e-mail: kr34@ukr.net

The branch of scientific interests is the functional stability of computer and other complex technical systems. The author of more than 100 scientific works and inventions.

Ph.D. Aleksander Trush
e-mail: trush.viti@gmail.com

Scientific and practical interests are related to such areas as information and communication systems and networks, systems of technical protection of information, cyber defense. He is the author of over 35 scientific and methodological works, 2 textbooks.

otrzymano/received: 10.10.2017 *przyjęto do druku/accepted: 15.02.2018*

DOI: 10.5604/01.3001.0010.8645

PECULIARITIES OF THE RADIO SIGNALS AND HINDRANCES IN THE NAVIGATION SYSTEM OF THE REMOTE-PILOTED VEHICLES

Mykola Mykyjchuk, Volodymyr Markiv
Lviv Polytechnic National University, Department of Measuring Information Technologies

Abstract. *The article dwells upon the peculiarities of radio signals concerning the use of remote-piloted vehicles. It is highlighted that it is important take into consideration the fractal analysis of remote-piloted vehicles based on diverse fractal dimensions. The significance of remote-piloted vehicle control system investigation based on radio signals is presented. Also it is highlighted that there are many hindrances during the remote-piloted vehicle flight and it is important to take them into consideration and develop methods in order to omit them. Also the vital role of remote-piloted vehicles in different spheres of life, for example, in environment research is depicted..*

Keywords: radio signals, fractal analysis, remote-piloted vehicle, fractal dimension

CHARAKTER SYGNAŁÓW RADIOWYCH I UTRUDNIEŃ W SYSTEMACH NAWIGACJI W BEZZAŁOGOWYCH STATKACH POWIETRZNYCH

Streszczenie. *W artykule został poruszony temat cech sygnałów radiowych w przypadku ich zastosowania w bezzałogowych statkach powietrznych. W pracy podkreśla się istotność bazowania na fraktalnych wymiarach podczas analizy fraktalnej bezzałogowych statków powietrznych. Podkreślono znaczenie sygnałów radiowych w systemach sterowania. Przedstawiono istnienie wielu utrudnień podczas lotów bezzałogowych statków powietrznych oraz wskazano na konieczność uwzględniania i opracowania metod uniknięcia tych utrudnień. Podkreślono również istotną rolę bezzałogowych statków powietrznych w różnych sferach życia, na przykład w badaniach środowiska.*

Slowa kluczowe: sygnały radiowe, analiza fraktalna, bezzałogowy statek powietrzny, wymiary fraktalne

Introduction

Nowadays, remote-piloted vehicles are widely used in different spheres of life, particularly in the area research. They have a lot of advantages: high economic efficiency; low altitude of aerial photoshooting; aerial photoshooting exactness.

But also here are some hindrances at any height, in particular, if take into account low-level remote-piloted vehicles. Then the flight is complicated due to the high turbulence of the atmosphere and the inability to track the change in the altitude, as on small unmanned aerials, the device for measuring the relative altitude is used for landing or absent altogether. Therefore, it is necessary to increase the height of the automatic flight and thus reduce the efficiency of the accomplishment of the tasks [1, 6].

However, using ultrasonic ultrasound, which is small, consumes little energy and inexpensive, and vertical load data can stabilize the relative altitude of the flight. To increase the range of measurements, a satellite navigation system signal and a barometric altimeter are used [1, 7].

The remote-piloted vehicle may lose contact with the control panel as a result of the operation of a small interference jammer of the corresponding power. The GPS spoofer intercepts the drone without destroying it, with the help of the false signal of the Global Positioning System, namely by silencing the positioning signal and flashing a signal. In the result, the user of the spoof can send a drone to where he wants [2].

The main component of the spoofer is the GPS simulator. This device is used to test navigation systems. The GPS signal simulator is low-power and operates within a radius of ten meters. Therefore, the second component of the spoofer are amplifiers that increase the power of the wrong GPS signal tens of times.

Also remote-piloted vehicles during flight are under the influence of a variety of factors [6, 7]:

- weather (temperature, wind direction, humidity);
- the level of radio barriers;
- region relief;
- atmospheric pressure.

So, it is extremely important to improve the control and localization of remote-piloted vehicles by improving metrological measurements and the reduction of the metrology errors.

Also it is not simple to recognize remote-piloted vehicles with the help of infrared means due to low-powered and almost noiseless engines. An experimental study of reflected signals from moving objects shows that different complexity of motion leads to different forms of the signal, that is, the analyzed signal has fluctuations due to change in frequency, phase and amplitude of the reflected signal.

Recently, fractal time series analysis has been used to in order to analyze signals having a complex form have been used fractal method of time series analysis. The nature of the fluctuations of the reflected signal is determined by the nature of the motion of the object. The degree of fluctuations can be described with the help of the characteristic coefficient, so called fractal dimension [9, 10].

1. Remote-piloted vehicle control and navigation systems

It is necessary to make the further researches by analyzing the existing problems regarding the control of remote-piloted vehicles. Also, it is important to develop metrology supply mathematical model and to improve metrology supply indices measurement of remote-piloted vehicles control based on the practical realization.

The main remote-piloted vehicle equipment consists of: angular velocity sensor; accelerometer; magnetometer; altimeter; inspection device, GPS tracker etc.

Especially, GPS tracker it is a receiving and transmitting device designed for remote monitoring of the location of a mobile object. The GPS tracker is located on the object under observation (monitoring) and determines the location of the object using the GPS receiver, location data is transmitted to the GPS monitoring system, or directly to the user's computer.

The tracker provides the ability constantly to observe the movement of the object everywhere, where there is coverage of GSM networks. Most modern trackers have the ability to store traffic data in the event of a temporary lack of a GSM network and transmit the march-rout record after the connection is restored.

The main device in the GPS-monitoring system is the GLONASS / GPS / GSM-terminal, which performs functions of determining the coordinates with the help of a satellite receiver, collecting information from on-board equipment and additional sensors, transmitting information by channels of GSM communications, control of on-board equipment for commands received from the operator [2–4].

The collected information is then transmitted to the processing server in the form of a binary AVL package containing the "snapshot" of the data received by the terminal – time, coordinates, values of internal and external parameters. The user then receives information from the server using the client software clock, or, in some cases, directly through the browser, using the WEB-system interface [2, 3].

The navigation system of remote-piloted vehicle is depicted in the Fig. 1 [5, 8].

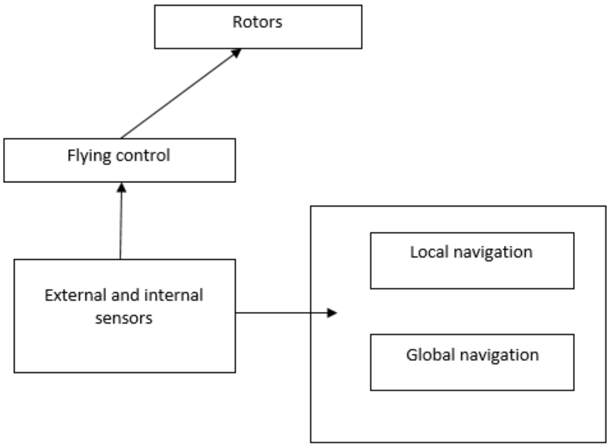

Fig. 1. Navigation system of remote piloted vehicle

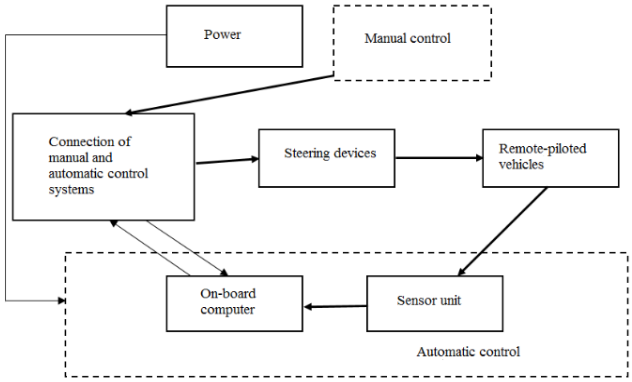

Fig. 2. Control system structure of remote-piloted vehicle

Self-positioning and modeling of environment relative to the local coordinate system is under control of local navigation. 3D information is formed based on a set of flat images, forming 3D map of the studied surface. Block "Global navigation" presents the positioning of the remote-piloted vehicle by using the constructed 3D model of the external environment.

This technique allows to solve the problem of positioning in the condition of absence of GNSS signals. Local positioning system takes into consideration the onboard sensors indices, external sensors and position change data from the camera, which after processing by the filter solve the problem of orientation in space of dense urban development [6].

The high speed of errors accumulation in inertial systems of positioning is caused by error of measurements of the used integrated accelerometers and the need to calculate the integral, leads to the multiplication of errors and does not allow to obtain positioning accuracy comparable with the accuracy of GNSS.

The positioning of remote-piloted vehicle is made on the basis of the analysis of the location of ground objects and pre-designed models of environment. The block "Flying task and control" is responsible for the collection and processing of the 2D images obtained through the onboard camera, and solves such important tasks:

- adjustment of coordinates of an inertial positioning system;
- stabilization with respect to a predetermined position;
- safe landing of remote-piloted vehicle.

There are various types of remote-piloted vehicles control system:

1) manual control when remote-piloted vehicle is under the control of a pilot;
2) automated control when the control is made based on the telemetric data;
3) automatic control when the control is made based on the system chosen parameters.
4) It is presented in the Fig. 2 [6].

Figure 2 depicts the overall structure of the control system for drone. In particular, the sensor unit contains an inertial module, a tri-axial magnetometer, a receiver of satellite navigation signals, receivers of static and dynamic pressure, an ultrasound altimeter.

In order to use remote-piloted vehicles in appropriate way it is also important to understand the control system structure. It is presented in Fig. 3 [6, 7].

Such scheme demonstrates that the control system of remote piloted vehicles consists of radio signal receiver and transmitter, terrestrial control and remote piloted vehicle operator. Also, such control is based on the engines controllers.

Nowadays radio signals fill all frequency ranges and it is extremely important to protect the signal from accidental and non-accidental interferences. One of the most effective method is fractal analysis based on fractal dimensions. That is why it is necessary to investigate it taking into consideration different conditions of remote-piloted vehicles.

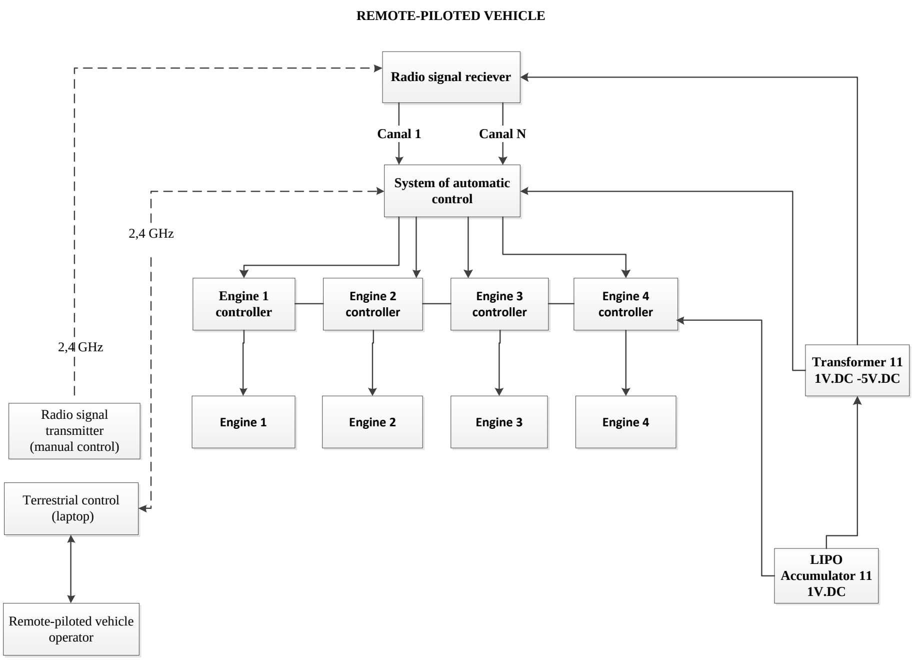

Fig. 3. Control system of remote-piloted vehicles

2. Fractal analysis in the process of remote-piloted recognition

To solve the problem of analyzing background signals, it is expedient to calculate the fractal dimension and to estimate the complexity of the reflected signals. Thus, the difference in the values of the fractal dimensions of the signals from the output of the headphones during background and remote-piloted vehicle sounding can be used as a sign of remote-piloted vehicle recognition [9, 10].

Fractal dimension it is a positive non-integer number that displays, to some extention, the complexity of the signal form. A large degree of filling of the plane corresponds to a large value of the fractal dimension. Fractal dimension is close to 1 (practically coincides with the topological dimension of the line) in case of smooth signals and for the cut-off signals it is close to 2 (practically coincides with the topological the dimension of the whole area).

The calculation of the fractal dimension of the initial time series allows to analyze the complexity form of the reflected signals. The forms of the reflected signals from moving objects have different complexity. So the value of the fractal dimension, which characterizes this complexity, also depends on the type of the moving object, which can be used when recognizing them.

It is expedient to analyze signal during the move of remote-piloted vehicle. It is revealed that the signal structure is not homogeneous as in the case of remote-piloted vehicle hanging.

The values of the fractal dimension signals obtained during the hanging of the remote-piloted vehicle and during its move in the direction to and from the radar are practically the same. It is impossible to determine the type of remote-piloted vehicle move by the size of the fractal dimension. This is because the modulation of the signal is mainly due to the rotation of the screws, and not because of the flight speed of the remote-piloted vehicle, which during the experiments was not high [9, 10].

Thus, the difference in the nature of the remote-piloted vehicle move (entrainment or movement in the direction to and from the radar) can be determined by the extent and periodicity of the appearance of the smallest fractal dimensions.

In the modern conditions, remote piloted vehicles are widely popular in different spheres. It helps to solve various tasks of the territory observation. Remote-piloted vehicles have a lot of advantages.

They are mobile, effective, convenient and cheap means of exploration in the form of photos, videos. However, it is difficult to recognize them by the means of radiolocation due to theirs relatively small dimensions and materials that weakly reflect electromagnetic waves.

3. GPS-spoofing and hindrances concerning remote-piloted vehicles

The use of the Global Positioning System (GPS) is very popular nowadays, especially concerning the use of remote-piloted vehicle. GPS it is a set of radio electronic means that allows to determine the position and speed of the object on the Earth's surface or in the atmosphere. The position of the object is calculated by using a GPS receiver that receives and processes the signals of the satellites of the global positioning system.

However, the phenomenon of GPS spoofing, attack that tries to cheat the GPS receiver by transmitting a more powerful signal than received from GPS satellites is widespread today. As a result, the location is incorrectly determined.

The GPS systems work by measuring the time taken for the signal to reach from the satellite to the receiver. So the simulating signal must be designed with allowable time delay [3, 4].

The spoofing system operates in such a way that the GPS signal generator transmits the simulation of the signal of several satellites through the antenna at the GPS frequency. In case that the level of the simulating signal is slightly higher than the signal level of real satellites, the GPS receiver will perceive the simulated signal and calculate the position on its basis.

A separate problem is the creation of a field of spoofing in the conditions of urban development, where the reflection of the signal interferes with the buildings, as well as radios, the configuration of which for a real signal coming from satellites, and signal interference is very different [2, 3].

There are different methods to detect GPS spoofing. For example, the allocation of an erroneous signal may be based on the direction of the source. It is possible to determine the direction by comparing the phase of the signal on several antennas.

Consequently, the main problem of using remote-piloted vehicles is the accuracy of long-range data management and data transmission. The most important task is to carry out research where it is difficult to obtain information using other methods and means. To do this, it is necessary in the future to consider in detail the specialties of the management of different types of drone.

The work of the radar station occurs under the conditions of various types of interference, which cause a decrease in the efficiency of the functioning. The degree of reduction of the efficiency is directly related to the change in the characteristics of the radar image under the influence of various obstacles.

The degree of interference is significantly dependent on the nature of the interaction of noise and signal. On this basis, the hindrances are divided into two types: multiplicative and additive. The effect of multiplicative interferences leads to parasitic amplitude and phase modulation of a useful signal. Aditive obstacles create a masking noise, against which there are useful signals. By its nature, the noise is divided into regular (deterministic) and random (statistical), the methods of filtering which are different.

For the effective operation of the radar system installed on the remote-piloted vehicle, it is crucially important accurately to determine the flight parameters of the remote-piloted vehicle, since, due to the relatively low mass and speed of the flight, they essentially change under the influence of turbulence of the atmosphere, vibration of the engines, errors of on-board equipment [2–4].

The main hindrances causing errors in determining the parameters of the remote-piloted vehicle flight are the following: the trajectory instability of the remote-piloted vehicle, elastic variations of the structure, errors in the control system and the errors of inertial meters.

In the formation of the radio image in the radar station the control of both real and synthesized directional diagrams of the antenna are important. The laws of management are determined by the given type of survey of the earth's surface. In this case, the scanning of the synthesized directional diagrams is carried out using appropriate supporting functions.

However, regardless of the type of inspection, the character and parameters of control signals are determined either by a priori data on the flight mode, or by the a posteriori values of the parameters of the remote-piloted vehicle movement. If the type of trajectory of the phase center of the antenna for which the reference function (reference trajectory) is calculated is fixed and known then the reference function can be pre-introduced into the memory of the processing system.

With an arbitrary reference trajectory, when it varies from one correction interval to another, the reference function is calculated for each interval separately during the flight based on the determination of the parameters of the remote-piloted vehicle movement.

As a fixed trajectory of the remote-piloted vehicle flight is usually used a straight line trajectory. In the simplest case of side examination with uniform rectilinear flight for the formation of the radio image, in principle, it is only necessary to measure the velocity of the remote-piloted vehicle.

However, really, no flying machine can fly quite evenly and straightforwardly. And first of all, this statement relates to the remote-piloted vehicle. The fact is that during the remote-piloted vehicle flight in the atmosphere there is a continuous change in the direction and speed of wind, pressure and air density, etc., in connection with which there are random deviations of the remote-piloted vehicle flight mode from the given.

The remote-piloted vehicle control system, on the one hand, does not always have time to react to all these changes and maintain a given flight mode, on the other hand, it introduces accidental elements in the remote-piloted vehicle movement itself. The most typical example in this regard is the piloting errors on the part of the remote-piloted vehicle operator.

Any random deviations from the given flight mode are called trajectory instabilities. Trajectory instabilities include deviation of the remote-piloted vehicle from the program flight trajectory, its angular oscillations, random modifications of the module and direction of the velocity vector.

Trajectory instability is the reaction of the remote-piloted vehicle as a solid body to the influence of the turbulent atmosphere and noise of the control system. At the same time, it should be borne in mind that the design of the remote-piloted vehicle is flexible.

Elastic shifts of the remote-piloted vehicle design elements under the influence of aerodynamic forces during a flight in a turbulent atmosphere are called elastic structural variations. In real-life conditions, trajectory instabilities and elastic structural variations operate on the radar station simultaneously and cause random deviations of the trajectory of the phase center of the antenna from the reference, which is illustrated in the Fig. 4 [3, 4].

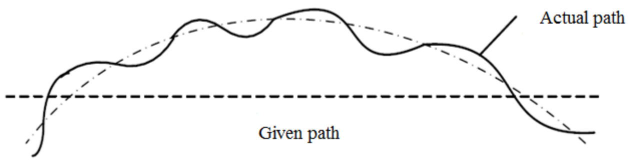

Fig. 4. Lines of given and actual path

In the figure, the dashed line shows the line of the given path, the dash-dotted line - the deviation from it through the trajectory instabilities, and the solid line is the actual path, taking into account the trajectory instabilities and the elastic structural variations. Random deviations from the given flight mode are inherent to all aircraft.

In the conditions of flight through the trajectory instability and elastic structural variations, the fuselage of the carrier is bent, which leads to errors in the definition of the module and the angular orientation of the vector.

In order to compensate trajectory instabilities and elastic oscillations of the structure affecting the synthesis of apertures, a modern system of compensation is provided in modern radar station, which is created using inertial meters.

4. Conclusions

Nowadays information society develops very fast. New scientific prospects become visible and acceptable. One of the perspectives is the use of remote-piloted vehicles in different spheres of life. It is really justified. Many countries use remote-piloted vehicles for different purposes concerning aerial photoshooting and terrestrial researches. It is the effective mean of reconnaissance. Modern remote-piloted vehicles use new technologies, cameras, radars, infrared detector and others.

So, there is a need for new methods of intelligence in areas where information is difficult to obtain using other methods. It is important to provide protection against unauthorized encroachments on location information. It is necessary to create new means of electronic combat on the basis of the phase-frequency theory of the measurement and transformation of radio signals.

Modern countermeasures are often energy-poor, with a low radius of signals and high value. That is why it is necessary to develop mobile systems of electronic warfare against modern types of radio communications by measuring and generating radio signals, with radio control channels and shooting video information.

It is necessary to improve the accuracy of metrological measurements, obtaining research indicators through the analysis and improvement of control systems for drone taking into consideration radio handrances.

The difference in the values of the fractal dimensions of the signals from the output of the headphones during sounding of the background and the remote-piloted vehicle can be used as a sign of the remote-piloted vehicle recognition.

The fractal dimensions of the signals during the remote-piloted vehicle hanging and its movement at a low speed practically are the same and it is impossible to determine the type of remote-piloted vehicle movement based on the size of fractal dimension.

References

[1] Barton J.: Fundamentals of Small Unmanned Aircraft Flight. Johns Hopkins APL Technical Digest. V. 31, No. 2, 2012, 132–149.
[2] Bond L.: Overview of GPS Interference Issues. GPS Interference Symp., Volpe National Transportation System Center, 1998, 28–32.
[3] Forssel, B. Olsen T.: Jamming Susceptibility of Some Civil GPS Receivers. GPS World No. 1, 2003, 54–58.
[4] Key E.: Technique to Counter GPS Spoofing. Int. Memorandum. MITRE Corporation. 1995.
[5] Martin, M.: Non-linear DSGE Models and The Optimized Central Difference Particle Filter, 2010, 2–45.
[6] Markiv V.: Analysis of remote-piloted vehicles use and control system description. Computer sciences and information technologies No. 843, 2016, 347–351.
[7] Markiv V.: Justification of remote-piloted vehicles use and metrology supply improvement. 5th Int. Scientific Conf. ICS-2016, 2016, 20–21.
[8] Neitzel, F., Klonowski, J.: Mobile 3d mapping with a low-cost UAV system. Int. Archives of the Photogrammetry, Remote Sensing and Spatial Information Sciences. Vol. XXXVIII-1/C22, 67–70.
[9] Roach. D.: Dimensionality analysis of patterns: fractal measurements, Computers Geosciences, 1993, 849–869.
[10] Sandau K.: Measuring fractal dimension and complexity – an alternative approach with an application. 1993, 164–176.

D.Sc. Mykola Mykyjchuk
e-mail: mykolam@ukr.net

Director of Computer Technologies, Automation and Metrology Institute, Professor at the Department of Measuring Information Technologies. Research field covers wide variety of methods and means of metrology supply improvement based on metrology indices, development of methods and means of operational control of industrial errors. Author of nearly 120 publications in this research area.

M.Sc. Volodymyr Markiv
e-mail: vovamarkiv6230@gmail.com

Ph.D. student at the Department of Measuring Information Technologies in speciality 05.01.02 "Standardization, certification and metrology supply". Research field covers development of theoretical and methodical bases of the quality characteristics of products and services and the development of metrological supply for measurement and monitoring of certification. Author of nearly 10 publications in this research area.

otrzymano/received: 10.10.2017 *przyjęto do druku/accepted: 15.02.2018*

DOI: 10.5604/01.3001.0010.8646

DISTORTIONLESS SIGNALS TRANSFER THROUGH A WIRE MEDIA METASTRUCTURE

Dmytro Vovchuk, Serhii Haliuk, Leonid Politanskyy
Yuriy Fedkovych Chernivtsi National University, Department of Radio Engineering and Information Security

Abstract. *In the paper the development of the components of communication means is considered based on the wire metastructures. This approach is novel and quite promising due to the metamaterials provides new opportunities for the radio engineering devices such as antennas, absorbers etc. First of all it makes possible decreasing of the dimensions of devices while the characteristics stay the same or better. Here the artificially created metastructure that consists of parallel metallic wires and characterizes by a negative electric permittivity was investigated. The possibility of broadband power transfer of electromagnetic waves was demonstrated. Also, at first time, the investigation of possible signal distortions due to wave propagation through the wire medium (WM) slab was performed via analyzing of spectral characteristics. The obtained results allow applying of WM to power transfer in wide frequency range (not only at frequencies of Fabry-Perot resonant) and enhancement of weak source propagation as well as to antennas constructions due to the absence of signal distortions. One of the promising applications of such structures is the possibility of realizing of flexible screens with nanometer thickness and high resolution.*

Keywords: wire medium, signal transfer

TRANSMISJA SYGNAŁÓW BEZ ZNIEKSZTAŁCEŃ PRZEZ METASTRUKTURĘ PRZEWODOWĄ

Streszczenie. *W artykułe omówiono rozwój komponentów komunikacyjnych opartych na metastrukturach przewodowych. Proponowane podejście jest nowe i obiecujące, ponieważ metamateriały zapewniają nowe możliwości dla urządzeń radiotechnicznych, takich jak anteny, pochłaniacze itp. Przede wszystkim dotyczy to możliwości zmniejszenia zasięgu urządzeń, podczas gdy ich charakterystyki pozostają niezmienione, a nawet się poprawiają. W artykule badana jest sztucznie wytworzona metastruktura, składająca się z równoległych przewodników metalowych i charakteryzująca się wartościami ujemnymi stałej dielektrycznej. Została opisana możliwość jej wykorzystania do szerokopasmowego przesyłania fal elektromagnetycznych. Ponadto, po raz pierwszy zbadano obecność możliwych zniekształceń sygnałów przesyłanych przez strukturę za pomocą analizy charakterystyk widmowych. Uzyskane wyniki pozwalają na wykorzystanie struktury równoległych przewodników do przesyłania sygnałów w szerokim zakresie częstotliwości (nie tylko na częstotliwościach rezonansowych Fabry-Perot) oraz do poprawy sygnałów o niskiej mocy, a także w konstrukcjach antenowych z powodu braku zniekształceń sygnałów. Jednym z obiecujących zastosowań takich konstrukcji jest możliwość ich zastosowania do elastycznych ekranów o grubości kilkudziesięciu nanometrów o wysokiej rozdzielczości.*

Słowa kluczowe: środowisko przewodowe, transmisja sygnałów

Introduction

Metamaterials are one of the most perspective materials to the development of the modern devices, such as waveguides and antennas, radio locators, transmission lines, absorbers, reflectors, metamirrors, lenses [2, 9, 13] etc. In general, metamaterials are effectively homogeneous artificial materials with unusual and useful electromagnetic properties [8]. This class of materials characterizes by negative value of electric permittivity and/or magnetic permeability [10, 11] and includes a large group of artificial electromagnetic structures. One of them is the wire metamaterials that present optically dense array of aligned metal wires or rods embedded into dielectric matrices [5, 7].

Wire medium (WM) is one of the kinds of the wire metamaterials consisting of a two- or three-dimensional rectangular lattice of low-loss wire grids and in the case of 2D WM this structure is the array of parallel metal wires with length L, diameter $2r$ and lattice period a (Fig. 1).

The WM structure is known for the effective energy transfer at the frequencies of Fabry-Perot resonances which wavelengths are corresponds to the length of structure wires. This property is very useful for modifications of antennas [1] and near-field imaging [3, 6] whereas the case of operation in wide frequencies range was impossible. However, in the case of narrow band electromagnetic wave propagation a signal source was directly placed in front of an interface of the WM slab. Therefore, in the works [4, 12] the possibility of broadband power transfer using WM slab was considered and the idea was that an embedded source of electromagnetic signal into the WM construction (between wires) provides the damping of Fabry-Perot resonances and supports expanding of operation frequencies.

Therefore, the goal of this paper is to demonstrate the possibility of broadband power transfer of electromagnetic energy the wire media construction and investigate the possible distortions of propagation harmonic and complex signals.

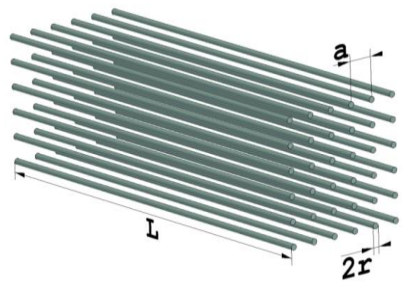

Fig. 1. The metamaterial that consists of parallel metallic wires with length L, wires diameter 2*r and lattice period a, so-called wire medium*

1. Broadband power transfer through the wire media slab

The schematic structure of the investigated system is shown in Fig. 2a. The system consists of two rectangular (164 by 82 mm) metallic waveguides (input and output) separated by an air gap l = 90 mm. The experiment included both the power transfer of electromagnetic energy through the empty space and using WM slab (length of wires is L = 100 mm) between waveguides.

To provide the broadband regime the WM slab was inserted inside each waveguide into a certain depth (5 mm from each side) that supported near-field interaction of the WM slab with source and the WM slab with transmitter. Thus, the aim of the performed investigation was the comparison of two kinds of power transfer without and with using of the metastructure.

The effectiveness of broadband power transfer was proven by the simulation (Fig. 3) and experimental (Fig. 4) investigations that were performed in [4, 12] via scattering S_{21}-parameters estimation. The averaged values of enhancement 2.5 and 2.0 in the frequency range from 1 to 2 GHz were reached for simulated model and experimental setup respectively.

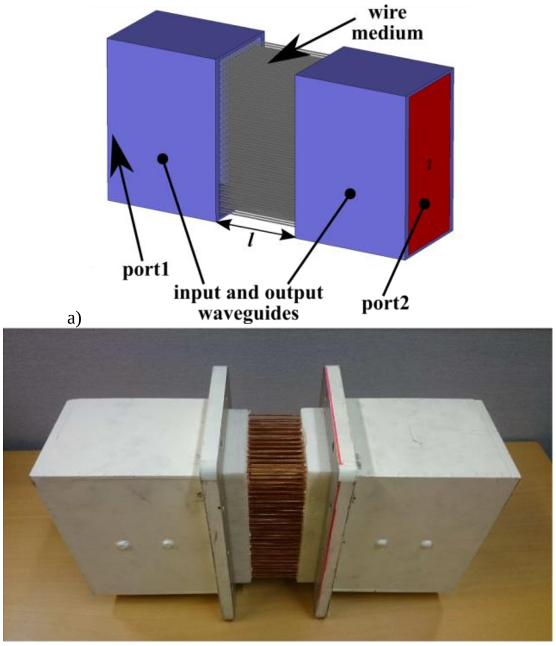

a) b)

Fig. 2. The investigated system of two waveguides separated by an air gap that is filled by a copper WM structure: a – simulated and b – experimental setups

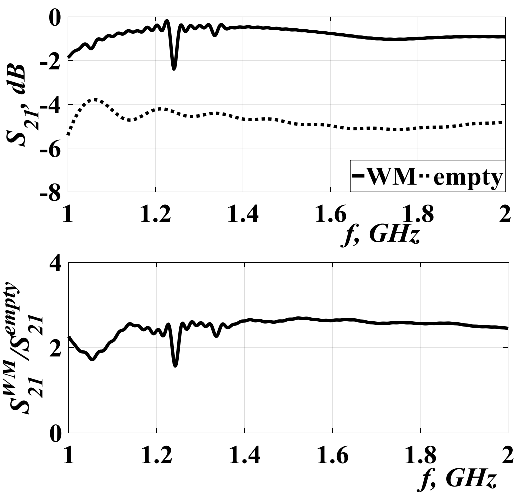

a) b)

Fig. 3. The simulated reflection parameters (S_{21}) (a) and obtained enhancement (S_{21}^{WM} / S_{21}^{empty}) (b) without (dashed plot) and with (solid plot) using WM structure

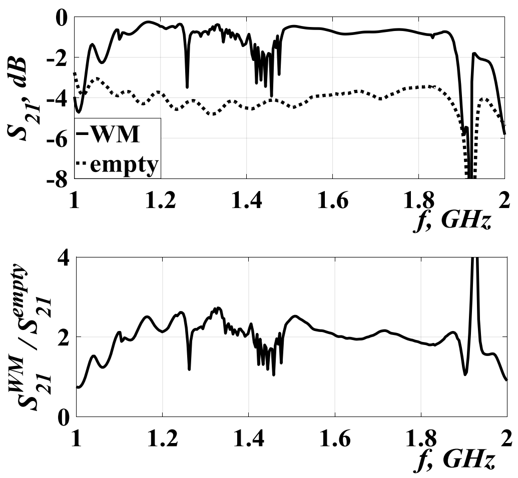

a) *b)*

Fig. 4. The experimentally obtained reflection parameters (S_{21}) (a) and achieved enhancement (S_{21}^{WM} / S_{21}^{empty}) (b) without (dashed plot) and with (solid plot) using WM structure

2. Spectra characteristics of transferred signals through the WM metastructure

However, from obtained results can be only concluded about the possibility of the power transfer of electromagnetic waves with different modes. In this case we cannot say exactly about the waveform and the response of the WM slab to the input signal but that is very important when the signal accuracy must be satisfied. For example, in the deterministic chaos theory both the broadband and accuracy are required.

For the purpose of possible signal distortions that can be introduced by the WM structures the investigation of the harmonic and chaotic signals transfer through the WM slab were carried out and their spectra characteristics were analyzed by simulation and experiment.

2.1. Simulation results

The simulation investigation was performed using already introduced system in Fig. 2a. Port 1 was used as a signal generator and port 2 as a receiver. For the first experiment the transfer of harmonic signal was investigated. The operation signal frequencies were picked up beyond the Fabry-Perot frequencies of the WM slab. Therefore, for presentation in this work for harmonic signals propagation with frequency 2 GHz were shown as the results. As one can see from Fig. 5a and b the spectra characteristics of input and output signals contains only one spectral component. It confirms that the investigated metamaterial is a linear structure.

For the next simulation the complex signal was used as the input signal of Port 1. The spectra characteristic of the input signal includes five components at 1.7, 1.75, 2, 2.1 and 2.3 GHz. As a conferment of the previous simulation investigation, the output signal was not distorted that is confirmed by comparison of spectra characteristics of input and output signals (Fig. 6a and b). The obtained results show the broadband effect without nonlinear distortions.

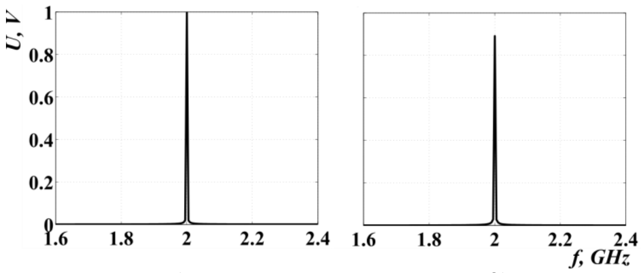

a) b)

Fig. 5. The simulated spectral characteristics of the input (a) and output (b) harmonic signals transferred through the WM metastructure

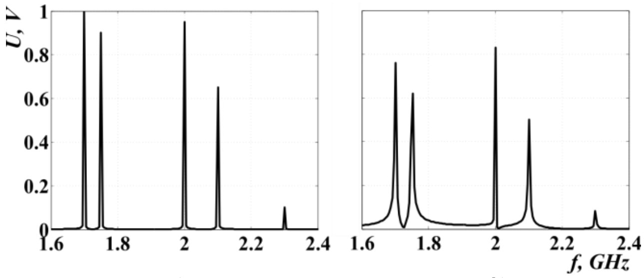

a) b)

Fig. 6. The simulated spectral characteristics of the input (a) and output (b) complex signals transferred through the WM metastructure

2.2. Experimental results

For the experimental investigation the system displayed in Fig. 2b was realized but in spite of the S-parameters investigation in the previous section the signal generator was used as the source of harmonic signal and the spectrum analyzer was exploited for the received signal analysing. The investigation was separated into two stages which included harmonic signal transfer through the closed waveguide transmission line (it allows to estimate the possible distortions from the WM construction) and through the air gap between two waveguides coupled by the WM structure as is shown in Fig. 2b (it allows to confirm the obtained in [4, 12] results for the possibility of the enhancement power transfer).

Since the transfer of the electromagnetic signals via a waveguide line is almost lossless and without distortions it is possible to investigate the influence of the WM slab on wave propagation and possible wave degradation.

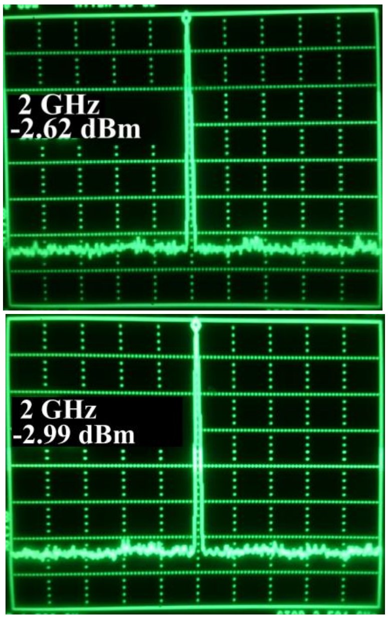

Fig. 7. The spectral characteristics of the harmonic signals received by the output waveguides in the case of: a – empty waveguide and b – embedded WM slab

To perform this kind of experiment the manufactured WM slab of 30 mm length 10 mm lattice period of copper wires was embedded inside the closed waveguide line as shown in Fig. 2. The investigated frequencies of the harmonic signals were picked up different from the Fabry-Perot resonances of the used WM slab. Therefore, the experimental spectral characteristics of the received harmonic signals for the propagation through the empty waveguide and in the case of using of the WM structure are shown in Fig. 7a and b respectively at the frequency 2 GHz. One can see that in the first case the signal power has decreased from 1 (the initial power of harmonic signal) to 0.55 mW (the power of received harmonic signal) which correspond on 0 and -2.62 dBm. In the case when the WM structure is embedded into the waveguide the power of the received signal is 0.50 mW (-2.99 dBm) and any additional spectral components are absent. It means that the structure does not impact on signal propagation and waveform.

For the next experiment the metal grid with mesh period 10 mm was manufactured and inserted into the input waveguide in front of the WM slab interface in order to imitate the evanescent wave propagation (Fig. 8). Using the WM metastructure allows enhancing the signal power from 0.0047 mW (-23.26 dBm) to 0.32 mW (-4.94 dBm) that are shown in Fig. 9a and b respectively. It means that using the WM slab it is possible to recover the propagation signal without distortions almost to the initial shape.

Fig. 8. Metallic grid with mesh period 10 mm embedded into the input waveguide to provide the enhancement wave propagation

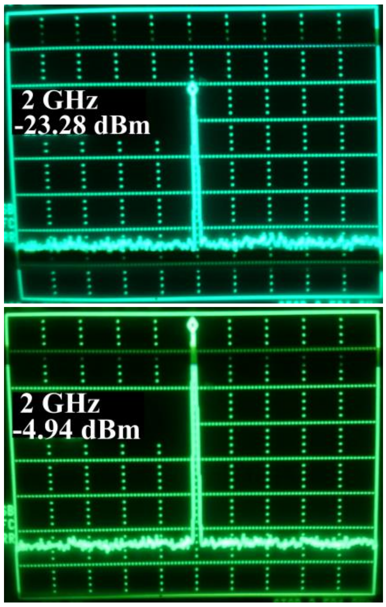

Fig. 9. The same plot as in Fig. 7 for the case when the metallic grid is embedded into input waveguide Port1

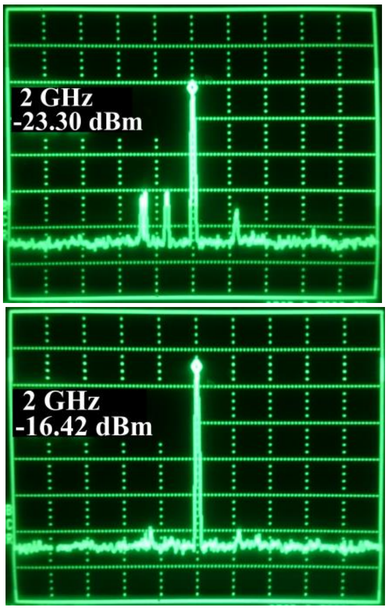

Fig. 10. The same plot as in Fig. 7 and 9 for the case when the waveguides is located one in front of another with distance 90 mm between their apertures

To investigate the enhancement of harmonic signal transfer through the air gap between the transmitter and receiver two waveguides were placed one in front of another with distance 90 mm between their apertures as shown in Fig. 2b. The air gap causes the scattering of electromagnetic energy that correspond the low value of the signal power 0.0047 mW (-23.3 dBm) and the presence of additional spectral components at the frequencies 1.87, 1.93 and 2.12 GHz due to wave reflection from the output waveguide edges as well as wave interference (Fig. 10a).

The usage of the WM slab allows to enhance the harmonic signal power transfer in approximately 4.85 times (-16.42 dBm) as well as the additional spectral components are absent due to the near-field interaction between the metastructure and the waveguides (Fig. 10b). It proves the obtained result in [4, 12] and demonstrates the possibility of the evanescent harmonic signal transfer via the suggested WM metastructure without any distortions at the frequencies different from the Fabry-Perot ones.

Conclusion

The WM structure that consists of parallel metallic wires (Fig. 1) was considered to show the possibility of broadband power transfer. For simulation and experimental studying the system that consists of two waveguide ports allocated one in front of another with air gap between them was carried out for this purpose (Fig. 2). As a result the enhancement approximately 2.0…2.5 times was achieved for the frequency range 1…2 GHz.

For the investigation of possible distortions from the WM structure the same setup was exploited and two cases were considered. To study the structure impact to the signal propagation the WM structure was embedded inside the closed waveguide line and it was found that the nonlinear distortions are excluded. The investigation of signal transfer through the free space using WM slab has proven the ability of the metastructure to enhance the evanescent signals and prevent the distortions due to possible reflections, wave interference etc.

The results of our investigation can be useful for the applications of enhancing and controlling heat radiation in thermophotovoltaic devices, signal transfer without nonlinear distortions, broadband communication systems including deterministic chaos signals and, as a main perspective application, flexible screens with high resolution.

References

[1] Burghignoli P., Lovat G., Capolino F., Jackson D.R., Wilton D.R.: Radiation from Elementary Sources in the Presence of Wire-Medium Slabs: Physical Mechanisms and Full-Wave Analysis. Proceedings of XVI Riunione Nazionale di Elettromagnetismo, Genova 2006, 113–116.

[2] Engheta N., Ziolkowski R.W.: Metamaterials: Physics and Engineering Explorations. John Wiley & Sons Inc. 2006.

[3] Kalteneker K.J. et al.: Ultrabroadband Perfect Imaging in Terahertz Wire Media Using Single-Cycle Pulses. Optica 3(5)/2016, 458–464.

[4] Kosulnikov S., Vovchuk D., Nefedov I., Tretyakov S., Simovski C.: Broadband Power Transfer through a Metallic Wire Medium Slab. Proceedings of URSI International Simposium on Electromagnetic Theory (EMTS) 2016.

[5] Mirmoosa M.S.: Wire Media for Enhancement of Radiative Heat Transfer and Spontaneous Emission. PhD Thesis at Aalto University, 2017.

[6] Pendry J.B.: Negative Refraction Makes a Perfect Lens. Physical Review Letters 85 (18)/2000, 3966–3969.

[7] Rotman W.: Plasma simulation by artificial and parallel plate media. IRE Transactions on Antennas and Propagation 10 (1)/1962, 82–95.

[8] Sihvola A.: Metamaterials in electromagnetic. Physical Review Letters 85 (18)/2000, 3966–3069.

[9] Simovski C.R., Belov P.A., Atrashchenko A.V., Kivshar Yu.S.: Wire Metamaterials: Physics and Applications. Advanced Materials 24/2012, 4229–4248.

[10] Smith D.R., Padill W.J., Vier D.C., Nemat-Nasser S.C., Schultz S. Composite medium with simultaneously negative permeability and permittivity. Physical Review Letters 84/2000, 4184–4187.

[11] Veselago V.G.: Electrodynamics of substances with simultaneously negative electrical and magnetic permeabilities. Sov. Phys. Usp. 10/1968, 5–13.

[12] Vovchuk D., Kosulnikov S., Nefedov I., Tretyakov S., Simovski C.: Multi-Mode Broadband Power Transfer through a Wire Media Slab. Progress in Electromagnetics Research 154/2015, 171–180.

[13] Zheludev N.I., Kivshar Yu.S.: From metamaterials to metadevices. Natural Materials 11/2012, 917–924.

Ph.D. Dmytro Vovchuk
e-mail: dimavovhuk@gmail.com

Assistant of professor at Radio Engineering and Information Security Department of Yuriy Fedkovych Chernivtsi National University. Research field includes metamaterials for the radio devices applications. Author of more than 10 publications.

Ph.D. Serhii Haliuk
e-mail: galiuk@inbox.ru

Assistant of professor at Radio Engineering and Information Security Department of Yuriy Fedkovych Chernivtsi National University. Research field covers the development of the different components of hidden communication systems. Author of more than 20 publications.

Prof. Leonid Politanskyy
e-mail: rt-dpt@chnu.cv.ua

Yuriy Fedkovych Chernivtsi National University. D.Sc. (technical), Professor, Head of the Department of Radio Engineering and Information Security. Research interests: physical processes in semiconductor devices, radio engineering devices and means of telecommunications. Author of nearly 200 publications in this research area.

otrzymano/received: 10.10.2017 *przyjęto do druku/accepted: 15.02.2018*

DOI: 10.5604/01.3001.0010.8649

THE USE OF ARTIFICIAL INTELLIGENCE IN AUTOMATED IN-HOUSE LOGISTICS CENTRES

Tomasz Rymarczyk[1,2], Grzegorz Kłosowski[3]
[1]Research and Development Center, Netrix S.A., Lublin, [2]University of Economics and Innovation in Lublin,
[3]Lublin University of Technology, Faculty of Management, Department of Organization of Enterprise

Abstract. *The paper deals with the problem of works transport organization in logistic center with the use of artificial intelligence algorithms. The presented approach is based on non-changeable path during travel along a given loop. The ordered set of containers requesting transport service was determined by fuzzy logic, while the sequence of containers in a loop was optimized by genetic algorithms. A solution for semi-autonomous transport vehicles wherein the control system informs the driver about optimal route was presented. The obtained solution was verified by a computer simulation.*

Keywords: logistics, fuzzy logic, intelligent transportation systems, genetic algorithms

ZASTOSOWANIE SZTUCZNEJ INTELIGENCJI W ZAUTOMATYZOWANYCH CENTRACH LOGISTYCZNYCH

Streszczenie. *Artykuł dotyczy problematyki sterowania transportem wewnątrzzakładowym w zautomatyzowanych centrach logistycznych z zastosowaniem metod sztucznej inteligencji. Zaprezentowane podejście zakłada predykcję niezmiennej trasy przejazdu środka transportu. Kolejność zbioru regałów wymagających obsługi transportowej jest determinowana przez logikę rozmytą, natomiast do optymalizacja trasy przejazdu wykorzystano algorytmy genetyczne. Zaprezentowano koncepcję środka transportu, w którym system sterowania informuje kierowcę dokąd ma jechać. Uzyskane rozwiązanie zostało zweryfikowane z wykorzystaniem metod symulacji komputerowej.*

Słowa kluczowe: logistyka, logika rozmyta, inteligentne systemy transportowe, algorytmy genetyczne

1. Introduction

Technological progress is an inherent feature of the evolution of economic and social systems [4]. One of the main trends accompanying the ongoing change is globalization [6, 7]. In turn, this phenomenon entails the need to improve logistics systems and processes. The consequence of this necessity is the emergence of modern logistic centers which due to their complex organizational complexity require sophisticated management methods [1]. With the development of information systems, the role of artificial intelligent (smart) systems has grown considerably, taking over more and more human tasks [3]. The systems of works transport control can be included to this set of logistic tasks [5]. Transport control within the logistics center is a continuous process. Due to its high complexity, many problems are NP-hard [2]. For this reason, IT systems using optimization and decision support algorithms work well in this problem. This article presents the concept of works transport control in a large logistics center. The presented concept uses fuzzy logic, evolutionary algorithms and deep learning (convolutional neural network).

2. Smart warehouse concept

The method presented in this paper concerns the operation of the works transport system at a large logistic center. Organization of the logistics center takes into account the division of the entire area into zones. The number of zones is selected so that one zone is handled by one mean of transport. Each zone contains dozens of shelves on which containers are stored. Each container has an RFID identifier. Parts stored in containers may also be tagged. It depends on the organization of given warehouse. Individual parts may also be stored in individually or collectively tagged packages. The logistics center is in fact a large warehouse that has to handle multiple deliveries and pick-up operations. A lot of transportation vehicles are moved within the logistics center, which, due to the zonal organization of the warehouse, does not collide with each other. Transporters can both deliver and receive parts (parcels).

Transporters perform loop-through rides. They leave the switching station and return there at the end of each loop. Transporters are driven by drivers, but drivers have their smartphones equipped with the right application in front of them. The application is dedicated to a specific, intelligent transport system. A ready to start new route vehicle receives assigned to it an ordered tasks vector. The tasks vector is fixed during whole loop execution. In the switching station, the transportation vehicle is loaded according to the delivery tasks waiting for it. When driving a loop, the conveyor goes by the planned route (ordered containers) shown on the smartphone. Transportation vehicle bypasses shelves with containers to which it either add parts or take them out in appropriate quantities. All details that should be done are visible on the smartphone screen. The system discreetly (e.g. by each second) receives the following information:

- current storage status of all containers,
- vector of parts that need to be delivered (what part and which container),
- vector of parts that need to be picked-up (what part and which container),
- information about which transport tasks have already been assigned to the mean of transport and which are not yet.

In addition to container metering (tagging), the system uses two subsystems:

- The genetic algorithm-based subsystem that optimizes the vehicle route (loop prediction) by minimizing the distance (the traveling salesman problem).
- The fuzzy logic subsystem assigns priority to the transport operation assigned to each container requiring service (delivery or pick-up). For example, if a container has already reached its maximum capacity or is approaching it, then the fuzzy logic subsystem automatically raises the pick-up priority for this container (real number from 0 to 1) and decreases the delivery priority. Where there are two or more containers that are designed to hold one type entity, the delivery will be directed to a container with a lower current fulfill level. In case of pick-up operation, higher priority container should have higher fulfill level.
- Convolutional neural networks for identifying (classifying) parts and selecting the best way of gripping parts during automated loading and unloading operations between the transport vehicle and containers.

3. Fuzzy logic to determine the hierarchy of transport tasks

In the described transportation system, each container in seconds intervals generates two types of information: delivery priority and priority of pick-up. This activity is realized because of the Fuzzy Logic based unit. The outline of the fuzzy logic system is shown in Fig. 1. It can be observed that the system has the following inputs:

x_1 – capacity [%] $0 \le x_1 \le 100$
x_2 – waiting time for pick up [%] $0 \le x_2 \le 100$
x_3 – risk $0 \le x_3 \le 10$

Variable x_1 reflects the current fill level of the container. Variable x_2 is estimated by comparing waiting times for receiving parts from a given container with similar times for other containers of a given zone. Variable x_3 specifies the level of due time risk associated with a part within given container. The level of risk can depend on many factors. For example, transport tasks involving parts with expire date or designated as priority may have an increased level of risk. Those parts should be handled prior to other transport tasks.

The fuzzy inference system has two following outputs:

y_1 – Delivery $-1 \le y_1 \le 1$, when $y_1 > 0$ then delivery
y_2 – Pick-up $-1 \le y_2 \le 1$, when $y_2 > 0$ then pick-up

In order to use the fuzzy inference system, each container should be metered and should be equipped with its own fuzzy controller unit. The sensor system together with the driver units operate in a discrete system with a sampling time of one second. At second intervals the fuzzy controller of the container receives input data that, after processing, generates an output signals. The received (output) information will be used to decide whether a container needs transport handling, what kind of handling it is and what is its priority.

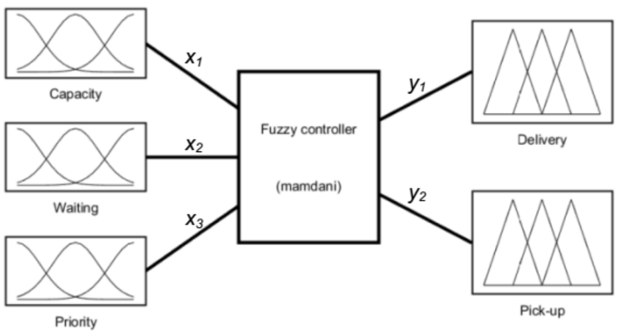

Fig. 1. Fuzzy inference system

The fuzzy controller performs the process of transferring the input vector into output based on the heuristics that are described by the following six linguistic rules:

1) If (Capacity is Low) or (Waiting is Short) or (Priority is Low) then (Delivery is Urgent)(Pick-up is Redundant).
2) If (Capacity is Average) or (Priority is Average) then (Delivery is Advisable)(Pick-up is Advisable).
3) If (Capacity is High) or (Waiting is Long) or (Priority is High) then (Delivery is Redundant)(Pick-up is Urgent).
4) If (Capacity is Average) or (Waiting is Short) or (Priority is Average) then (Delivery is Advisable)(Pick-up is Advisable).
5) If (Capacity is High) or (Waiting is Short) or (Priority is Average) then (Delivery is Redundant)(Pick-up is Advisable).
6) If (Capacity is Low) and (Waiting is Long) and (Priority is High) then (Delivery is Urgent)(Pick-up is Urgent).

The fuzzy controller performs the process of transferring the input vector into output based on the heuristics that are described by the following six linguistic rules:

1) If (Capacity is Low) or (Waiting is Short) or (Priority is Low) then (Delivery is Urgent)(Pick-up is Redundant)
2) If (Capacity is Average) or (Priority is Average) then (Delivery is Advisable)(Pick-up is Advisable)
3) If (Capacity is High) or (Waiting is Long) or (Priority is High) then (Delivery is Redundant)(Pick-up is Urgent)
4) If (Capacity is Average) or (Waiting is Short) or (Priority is Average) then (Delivery is Advisable)(Pick-up is Advisable)
5) If (Capacity is High) or (Waiting is Short) or (Priority is Average) then (Delivery is Redundant)(Pick-up is Advisable)
6) If (Capacity is Low) and (Waiting is Long) and (Priority is High) then (Delivery is Urgent)(Pick-up is Urgent)

The way of operation of the rules mentioned above, together with sample runs of the membership functions, is presented in Fig. 2. Each of the six rows of membership functions corresponds to one fuzzification rule. The first three columns of the membership functions correspond to the three input variables of the controller. The last, fourth and five, columns reflect the output parameters. The values of those parameters are computed through the determination of the centroid of a plane figure which is the result of compilation of several inference rule graphs (left right bottom corner of Fig. 2).

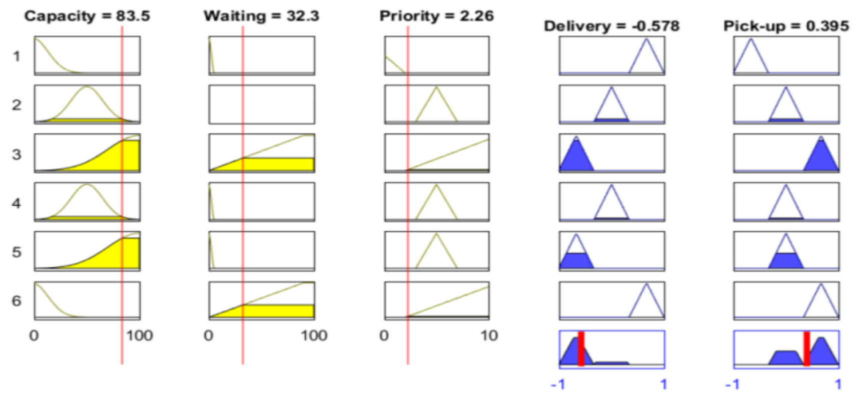

Fig. 2. Functioning of inference rules

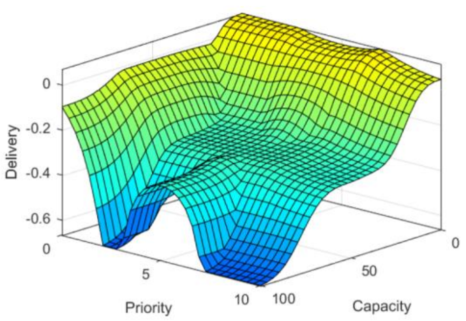

Fig. 3a. Response surface of the fuzzy controller

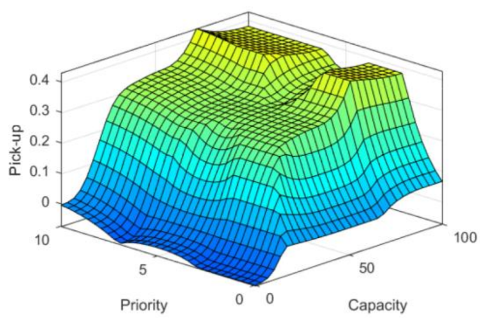

Fig. 3b. Response surface of the fuzzy controller

In the presented example, the Delivery variable is -0.578, Pick-up 0.395. It can be seen that a given container in a given second has much higher Pick-up priority than the Delivery. This is mainly due to the fact that given container is already fully filled up (Capacity 83.5%).

Figures 3a and 3b show the spatial diagrams illustrating relationships between two selected input variables (Priority and Capacity) and parts delivery and pick-up from the container. The irregular shape of both surfaces indicates a complex function which maps inputs as outputs. Therefore, it can be obvious that the task of describing these relationships with a mathematical formula would be very difficult. This fact explains to a high extent the sense and benefits of using fuzzy logic to solve decision problems connected with control processes.

4. Genetic algorithms for optimizing the route of a transport vehicle

One of the key elements of the vehicle transport control process is the choice of an optimal route. This is a problem known as the "symmetrical salesman problem". The solution to this problem is a structured vector of workstations that should be handled by the vehicle in a single pass loop. Because the salesman problem is a class of NP-hard problems, there is no deterministic method to solve this problem in polynomial time. That means that to solve the mentioned problem it is necessary to check all possible solutions, compare them and choose the best ones. The number of possible routes is permutation *1,2,3, ..., n* points (containers) lying on each route (n!).

The considered case of transportation problem has some characteristic features and limitations that distinguish it from the classical problem of the traveling salesman. Firstly, the transport vehicle always starts from one point - the switching station. It also has a pre-determined position (container) with the lowest priority that should be handled last. So it remains a problem to determine the order of services for the rest containers, that is, to properly sort the vector of containers requiring transport service between the switching station *n(1)* and the lowest priority container *n(i)*. The objective function is represented as an equation (1). Optimization is subject to the distance function that the transport vehicle must drive through in one loop of passage.

$$S(s_0, \mathbf{x}) = c_{s,l} \sum_{i=0}^{N} \left(s_{n(i)}, n(i), n(i+1) \right) \tag{1}$$

where: $c_{s,l}$ – unit operating cost of l-th vehicle for distance s [PLN/m], N – total number of all containers, $n(i)$ – i-th container serviced by vehicle n, $S(s_0, \mathbf{x})$ – function of distance; s_0 is the distance of the beginning; $\mathbf{x}$ is the vector of containers that must be serviced in next loop, $s_{l,n(i)}, n(i), n(i+1)$ – distance of l-th vehicle between containers *n(i)* and *n(i+1)*.

Fig. 4 shows a single loop of a transport vehicle optimized with genetic algorithm. The distance value obtained by optimizing the objective function was 284 meters. The resulting optimization was achieved after 200 iteration epochs.

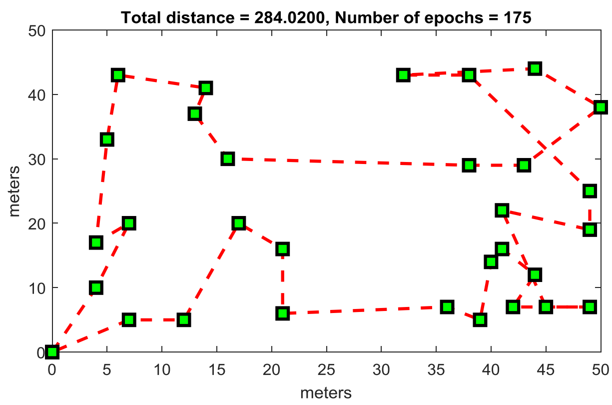

Fig. 4. Arrangement of containers in the zone in question

Fig. 5 shows the process of optimization. The falling curve reflects the decreasing value of the objective function that was obtained after the successive iterations. In this example we are dealing with the minimization of distance function, so the shape of the curve demonstrates the high efficiency of the applied genetic algorithm. The iteration process ends after 200 epochs. This is a parameter that has been set permanently to avoid too long conversion times.

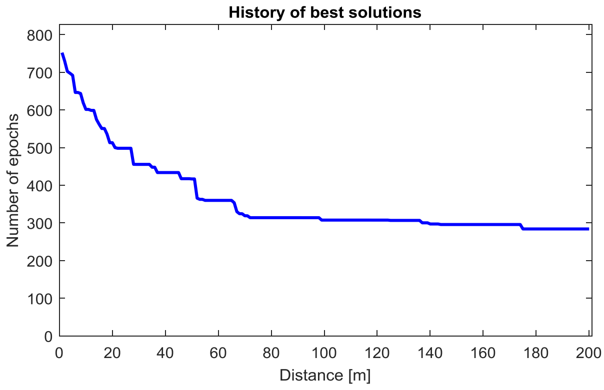

Fig. 5. Process of optimization

5. Simulation experiment

In order to verify control concepts using artificial intelligence algorithms, a simulation model of the logistics center was developed. The model incorporates elements such as a transport vehicle, a dedicated logistic zone consisting of 32 containers equipped with 32 fuzzy logic controllers.

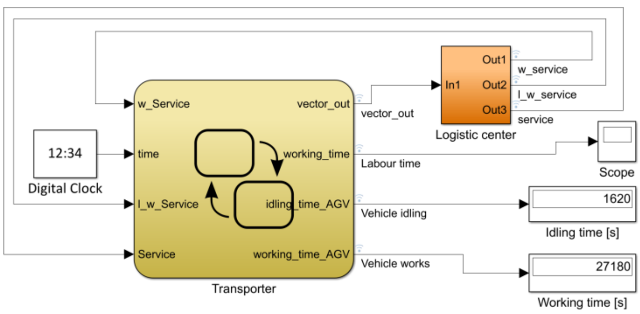

Fig. 6. Simulation model of transport system

Thanks to the above-mentioned controllers, the control system receives on-line, up-to-date information on the state of the containers. At the moment of completing the transport tasks vector, the control system makes a prediction of the next loop for the transport vehicle.

This is done on the basis of information about delivery and pick-up tasks. It also optimizes the route and current information on container occupancy, their priorities and risk. Fig. 6 shows a model of a developed transport system with its main components.

Based on the model, a number of simulation experiments have been performed. The eight hour shift divided into 28800 seconds was simulated. Results of one simulation run are presented in the figures below. Fig. 7 shows the Delivery signals distributed over time generated by the fuzzy controller. The horizontal axis is the time in seconds. Along the vertical axis the value of the Delivery parameter are presented. It can be seen that during the working shift there were seven deliveries (seven peaks) to the considered container.

Fig. 8 illustrates the distributed demand pick-up signals generated by the fuzzy controller of the given container during the shift. The horizontal axis is the time in seconds. The vertical axis is the Pick-up value. It can be seen that in case of given container there were eight pick-up operation during the 8-hours shift.

Fig. 9 shows the pick-up times for a given container from the time the shipping order occurred. It can be seen that the longest wait times ranged in 900 seconds. In addition, the moments in which subsequent transport operations follow are in line with Fig. 8.

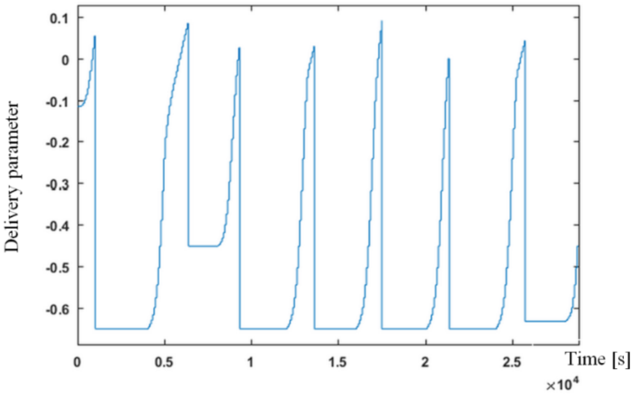

Fig. 7. Delivery tasks in time for given container

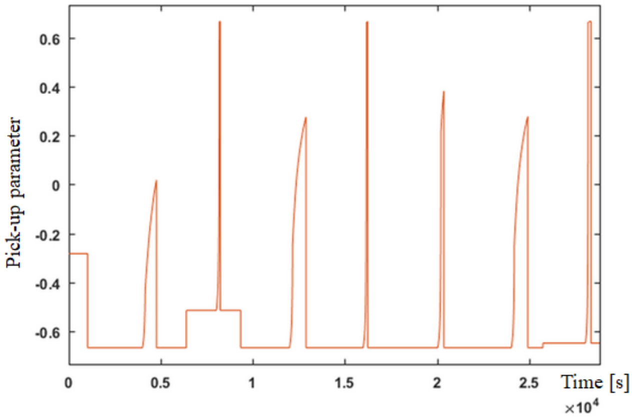

Fig. 8. Pick-Up tasks in time for given container

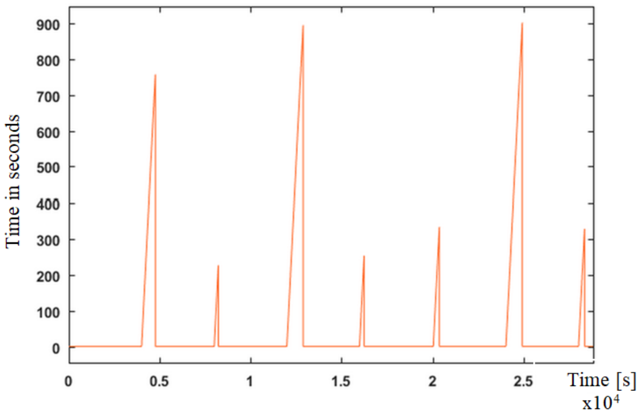

Fig. 9. Waiting times of pick-up services for given container

6. Deep learning for handling parts

In the case of automated transport systems important role play gripping robots and automatic manipulators allowing for proper grasping of parts for loading or unloading. Good grip problem is important because the operations of carrying parts and parcels are crucial from a safety point of view (protection against collapse or parts destruction) and time minimization of transport operations.

To automate mentioned above handling operations convolutional neural networks (CNN) can be used. For this purpose, it would be useful to gather the appropriate image database for the parts together with the correct ways to capture them. Conventional neural networks, thanks to their ability to extract important images, are suitable for classifying objects. In this case, CNN's first step would be to make a proper classification of the part. Then, knowing what kind of parts is being handled, the network should match the grip parameters such as approach angle, grip position and thrust.

7. Conclusions

This paper presents the original concept of artificial intelligence in handling the smart logistics center. A fuzzy inference system was developed to generate signals to assign priority to each container in the warehouse. A genetic algorithm was used to optimize the route of means of transport operating at the logistics center. A simulation model was developed, consisting of: a mean of transport, 32 containers equipped with 32 fuzzy logic units and a genetic algorithm unit. Simulation experiments were conducted because of which the behavior of the transport system during the 8-hour shift was investigated. The obtained results confirmed the effectiveness of the presented smart control concept.

References

[1] Atzori L., Iera A., Morabito G.: The internet of things: a survey. Computer Networks 54/2010, 2787–2805.
[2] Bai L., et al.: Centralized and optimal motion planning for large-scale AGV systems: A generic approach. Advances in Engineering Software 106/2017, 33–46.
[3] Barton D., Court D.: Making advanced analytics work for you. Harvard Business Review 90/2012, 79–83.
[4] Hofmann E., Rüsch M.: Industry 4.0 and the current status as well as future prospects on logistics. Computers in Industry 89/2017, 23–34.
[5] Neradilova H., Fedorko G.: Simulation of the Supply of Workplaces by the AGV in the Digital Factory. Procedia Engineering 192/2017, 638–643.
[6] Tsan-Ming C., Chun-Hung C., Hing-Kai C.: Risk management of logistics systems. 2016.
[7] Xanthopoulos A., Vlachos D., Iakovou E.: Optimal newsvendor policies for dual-sourcing supply chains: a disruption risk management framework. Comput. Oper. Res. 39/2012, 350–357.

Ph.D. Eng. Tomasz Rymarczyk
e-mail: tomasz.rymarczyk@netrix.com.pl

He is the director in Research and Development Center in Netrix S.A. He also is assistant professor in the University of Economics and Innovation, Lublin, Poland. His research area focuses on the application of non-invasive imaging techniques, electrical tomography, image reconstruction, numerical modelling, image processing and analysis, process tomography, software engineering, knowledge engineering, artificial intelligence and computer measurement systems.

Ph.D. Eng. Grzegorz Klosowski
e-mail: g.klosowski@pollub.pl

Assistant Professor in Department of Organization of Enterprise at the Faculty of Management of Lublin University of Technology. The research interests of the author include artificial intelligence, simulation and modeling of engineering and business processes. Leader and participant in several implementation projects. Chairman of the Board of the Special Purpose Vehicle of POLLUB-Invest Ltd., whose purpose is indirect commercialization.

otrzymano/received: 10.10.2017 *przyjęto do druku/accepted: 15.02.2018*

DOI: 10.5604/01.3001.0010.8652

USING MICROSERVICES ARCHITECTURE AS ANALYTICAL SYSTEM FOR ELECTRICAL IMPEDANCE TOMOGRAPHY IMAGING

Tomasz Cieplak[1], Tomasz Rymarczyk[2,3], Grzegorz Kłosowski[1]
[1]Lublin University of Technology, Faculty of Management, Department of Organization of Enterprise
[2]Research and Development Center, Netrix S.A., Lublin, [3]University of Economics and Innovation in Lublin

Abstract. *An image reconstruction with use of EIT method has been found useful in many areas of medical, industrial and environmental applications. Papers show that computational systems used for image reconstructions are utilizing parallel and distributed computations and multi-tier architecture, as well as monolithic architecture. The aim of our research is to define an analytical system architecture that will be able to combine a variety of image reconstruction algorithms with their representations in different programming languages. Based on examples described in different proceedings and research papers, a microservices architecture seems to be an interesting alternative to the monolithic one.*

Keywords: electrical impedance tomography, microservices, Internet of Things, image reconstruction

ZASTOSOWANIE ARCHITEKTURY MIKROUSŁUG W ANALITYCZNYM SYSTEMIE REKONSTRUKCJI OBRAZÓW ELEKTRYCZNEJ TOMOGRAFII IMPEDANCYJNEJ

Streszczenie. *Zaprezentowano postępy prac związanych z budową system analitycznego służącego do rekonstrukcji obrazów obiektów badanych za pomocą elektrycznej tomografii impedancyjnej. Celem system jest elastyczność pozwalająca na integrację wewnątrz jednego system modułów analitycznych bazujących na różnych algorytmach rekonstrukcji obrazu identyfikowanego obiektu. Kolejnym ważnym wymaganiem jest możliwość oprogramowania modułów analitycznych za pomocą najczęściej wykorzystywanych w tej dziedzinie językach programowania. System zapewnia komunikację z urządzeniem za pośrednictwem łączy internetowych, co pozwala na zdalne sterowanie i pobieranie wyników pomiarów. Dodatkowym założeniem stawianym aplikacji jest możliwość korzystania z dowolnego źródła danych (urządzenie typu tomograf, baza danych, systemy plików) poddawanych analizie, a wyniki rekonstrukcji mają być dostępne dla każdego urządzenia komputerowego. Zaprezentowano dwa rodzaje architektury aplikacji, monolityczną i opartą o mikro usługi.*

Słowa kluczowe*: elektryczna tomografia impedancyjna, mikro usługi, Internet rzeczy, rekonstrukcja obrazów*

Introduction

Electrical Tomography is a relatively mature imaging method that can be useful in medical, industrial and environmental applications to discover the inner structure of an investigated object [11, 16, 23–27].

The image reconstruction in EIT is a highly ill-posed inverse problem [2, 7–9, 17–21]. To solve the EIT inverse task, several algorithms are well known and used. They can be split into two categories: direct algorithms and iterative ones. There are few recognized as ready to use for commercial applications (e.g. GREIT) [1] and many that are in continuous development, therefore risky to use. Every case of an image reconstruction consists of almost the same number of steps beginning from data acquisition, data analysis by means of different methods, and ending with a visualization. Using such assumption and combining information about similar researches carried out on analytical systems applications on different research fields [4, 12, 13], a thesis was formulated, that it is possible to use architecture based on microservices to combine various image reconstruction methods in one analytical system.

1. Monolithic approach to analytical system design

Till now, the natural way to create analytical system was to build a monolithic web application.

That design was used to create a prototype of system for tomography analysis. The basic assumption was made to build an application which will gather data from devices, preserve and analyze them, and accomplish basic visualizations. Additionally, application could monitor tomographic device status.

The system consisted of four layers, as shown in Figure 1. The data was acquired from tomographic devices as time series datasets. In this stage MQTT protocol was used to pass the data from the source to the analytical system.

The data flow (Figure 2) was replicated into two flows: the first one was sent to the database system (for this purpose NoSQL Cloudant database system was used) and the second one was sent to the analytical system for further analysis. The aim of such operation was to process data in real time as well as to keep raw historical data for additional offline analysis.

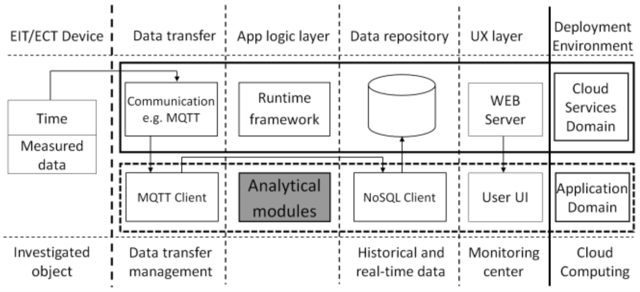

Fig. 1. Model of monolithic web application

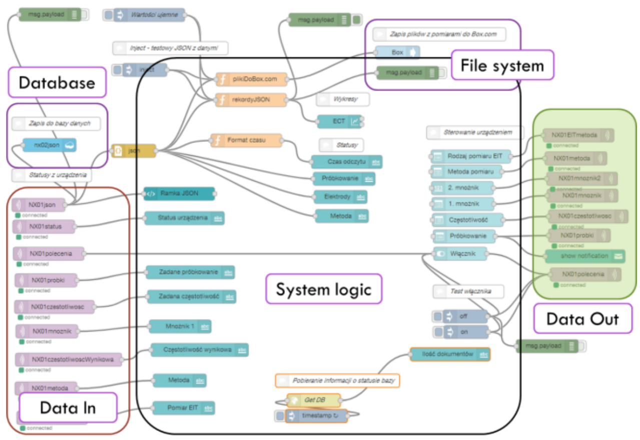

Fig. 2. Data flow inside of the system

The analytical system in form of web application (Figure 3) was built on top of IBM Bluemix PaaS platform. The advantage of this platform is easy integration with other analytical services like IBM Data Scientist Experience, which allows to use additional analytical methods from Apache Spark framework for further data analysis.

Monolithic application is a good approach, however, it had certain limitations. It was quite difficult to combine in one analytical stage few different algorithms written in different languages, which could be very useful for image reconstruction.

Fig. 3. Web application – device's control page

The structure of such system also caused difficulties in extending analytical layer with additional methods, because it involved rewriting these methods in supported language or doing plumbing between system and additional methods libraries. The solution was scalable in means of adding additional application instances, memory, CPU etc. but it affected whole system due to monolithic nature, so there wasn't possible to scale only a part of the system (e.g. analytical resources). General problems with monolithic architecture:

- code becomes harder to maintain and test as it grows larger,
- coupling between modules causes random bugs when changes are made,
- deployments and upgrades require application downtime,
- if part of a service crashes then entire site goes down,
- difficulty in application scaling,
- incorporating new technologies is rather difficult.

2. Modular approach to analytical system design

The analytical system should easily deal with a variety of data sources, analytical methods, as well as many different types of users' applications. Taking into consideration the use cases and requirements of different analytical systems applications, the common features can be summarized as: need of easy deployment and monitoring, possibility of replacement of system components (if they are malfunctioned or a new version appears), reliability, flexibility and fault-tolerance. Experience brought from an industry (a good example is Netflix service) shows rapid change in applied, distributed systems architecture from building monolithic applications to adopting microservice architecture [5, 6, 14]. While the fundamental concepts of microservices are not new, sometimes they can be wrongly treated as SOA architecture, but in fact they are something different [5]. The aim of creating microservices concept was to eliminate unnecessary complexity and implement single functionality in one small and independent service. They can communicate with each other using mechanisms such as HTTP-based RESTful APIs. The adoption of microservices is driven by scalability challenges, lack of efficiency, slow development and difficulties with adoption of new technologies that arise in case of complex software systems, constructed as one huge monolithic application. After Martin Flower, it can be said that microservices are not only philosophy of designing systems but also a new way to cooperate with clients [10].

Microservices mean not only easiness and lack of problems caused by monolithic architecture. In case of heavily distributed system, developers need to follow strictly the design assumptions and keep standardization of the architecture. There are many patterns telling how the system should be built and decision of choosing one best for the designed system could be problematic. Adding to the bucket the variety of technology – languages, frameworks, deployment solutions – can cause the design process of a system based on microservices complicated [15]. On the other hand, the simplicity in the scaling of an application can repay a hard work. The deployment on microservices can be done easily with use of containerization technologies like a Docker [3]. Docker container contains everything required to run a software – code, runtime environment, system tools, libraries and settings. This ensures that the software will run the same way, regardless of where it's deployed. When the solution is divided into microservices and deployment procedure operates on containerization it is one step away from moving such system to a cloud computing environment [22].

3. The work aim

Nowadays, during a development stage of analytical systems, there are few requirements for the designed systems that should be taken into consideration:

- they should be reachable for every researcher,
- they are supposed to be scalable and easy extendable.

Analytical systems are utilized in every kind of business and industry. In case of the research on electrical tomography, one of the main parts of the system is an images reconstruction system. The measurement system and analytical system are separated in natural way. Also, modules of computational system can be divided into layers and analytical layer can be split into smaller parts including image's reconstruction methods. Each reconstruction method module should be easy to use and to replace.

Additionally, the system must be scalable in various ways. Need of scalability depends on a size of measurement system – microscale can consist of one measurement device but the same reconstruction system should be able to work with hundreds measurement sets. Such assumptions conduct one to look for the solution in a set of distributed systems architectures.

The summarization of system requirements gives a conclusion that all properties of building systems will be achieved with application of microservices architecture. Benefits of incorporating to the system the microservices architecture is as follows:

- if microservice crashes, the rest of the system will keep going,
- deployment doesn't require downtime of any part of the system,
- each microservice can be scaled individually according to its needs,
- services can use different technical stacks (i.e. programming language, runtime engine, operating system)
- code complexity is reduced.

This new approach is focused on analytical engine, as seen in Figure 4. Every single functionality is contained within one separated microservice – that is the premise and goal for the rebuilt system. In the case the system's rebuild one can assume several scenarios:

- adding new microservices when development is moving forward with application,
- breaking pieces of functionality into microservices over time,
- refactoring the entire system into microservices at once.

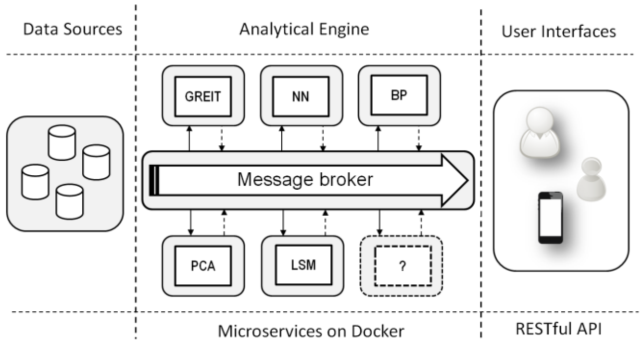

Fig. 4. System context diagram of the analytical system based on microservices

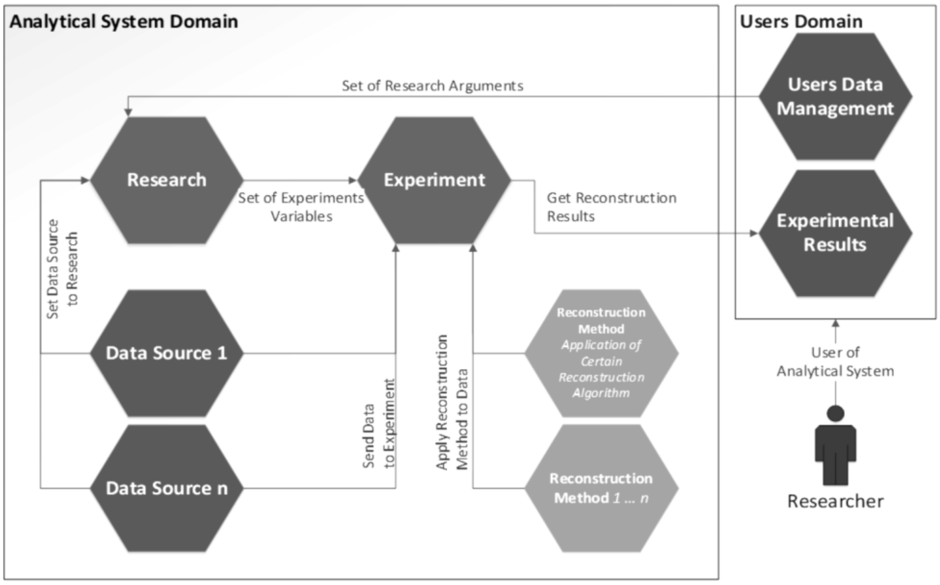

Fig. 5. Container diagram of analytical system

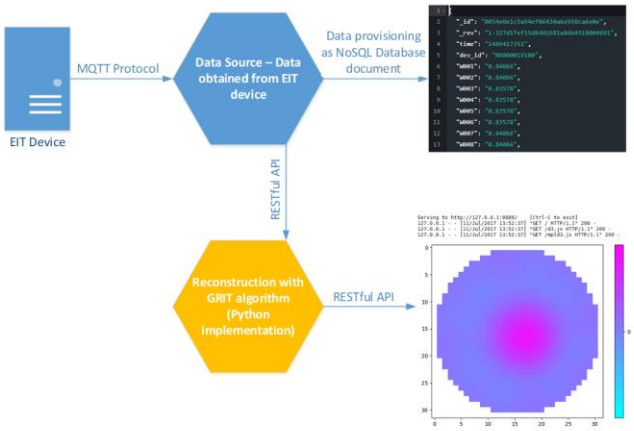

Fig. 6. Component diagram of image reconstruction case with application of GREIT algorithm

While the first two approaches are feasible, the latter was not appropriate in case of the presented research.

Ultimately, microservices are communicating with each other and the rest of the system using message broker, which accept messages, queue them up and route them to destination(s). These analytical modules have they own APIs which expose calculation results to the system clients. In fact, the calculation result may be an image reconstruction matrix, which can be used by such libraries, like D3.js, to visualize a reconstruction image (in this case MPLD3 library was used). More detailed diagram of the system is shown in Figure 5. The core of the system is included in analytical system domain and user functionality is located inside users' domain.

Those two subsystems communicate with each other using RESTful API and data is exchanged in JSON format. To use the system, first, user must create a unit called Research. It is used as a container to store different researches carried by the same user. Each research can consist of many different experiments with different properties, like different source of data as well as variety of reconstruction methods. After setting research arguments and experiment properties user can run the experiment. As a result of the experiment, reconstruction of an image is ready for further processing. The final step is displaying the reconstruction image on the user's application on the device. User decides about the form in which the reconstruction data will be depicted (e.g. in web or mobile application) due to RESTful API. Modular system design allows to rebuild system easily, providing that the RESTful API and data format stays the same. Application of microservices permits using of polyglot programming, i.e. multiple programming languages inside one computational system.

Taking into consideration more detailed data flow, which is shown in Figure 6 (see page below), one can see some example of data analysis procedure. In the simplest case, data is gathered from EIT device and then stored in database (i.e. NoSQL database). Next, reconstruction algorithm consume data brought from data source and produce the reconstruction image. The image is presented on a web page. In this case only two microservices are used: one as data source and one for image reconstruction. The data source microservice is written in JavaScript using Node.js framework and the other is implemented in Python with Flask library.

4. Conclusions

The difference between monolithic and modular approaches to build an analytical system was shown. One comes to conclusion that monolithic application is good for research starting point, but quickly it becomes very restrictive in many areas.

An important factor in the use of architecture is the ability to verify the operation of different reconstruction algorithms running at the same time. To date, such experiences have been difficult.

An important feature of the analytical system based on microservices is its resistance to failures due to faulty analysis modules. In this case, failure of one analytical module does not cause the entire system to shutdown. What in the case of a monolithic system leads to the closure of the entire system.

This solution works with IBM Bluemix cloud computing system. By using the PaaS model, each microservice can receive virtually unlimited hardware resources. The number of running micro-instances and resources such as memory, processor type can be dynamically changed during system operation. In the case of a monolithic applications, such operations are difficult to carry out.

In the presented research, the main problem with a monolithic application was a lack of easy extensibility in adoption of analysis algorithms written in different programming languages. What, as shown, can be bypassed by changing the application architecture and use of microservices.

References

[1] Adler A., Arnold J.H., Bayford R., Borsic A., Brown B., Dixon P., Grychtol B.: GREIT: a unified approach to 2D linear EIT reconstruction of lung images. Physiological measurement 30(6), 2009, 35–55, [DOI: 10.1088/0967-3334/30/6/S03].

[2] Borcea L.: Electrical impedance tomography. Inverse Problems 18, 2002, 99–136.

[3] Amaral M., Polo J., Carrera D., Mohomed I., Unuvar M., Steinder M.: Performance evaluation of microservices architectures using containers. Network Computing and Applications (NCA), IEEE 14th International Symposium, 2015.

[4] D'Agostino D., Roverelli L., Zereik G., De Luca A., Salvaterra R., Belfiore A., Tiengo A.: A microservice-based portal for X-ray transient and variable sources. PeerJ Preprints, No. e2519v2, 2017.

[5] Dragoni N., Giallorenzo S., Lafuente A. L., Mazzara M., Montesi F., Mustafin R., Safina L.: Microservices: yesterday, today, and tomorrow. arXiv preprint arXiv:1606.04036, 2016.

[6] Dragoni N., Lanese I., Larsen S. T., Mazzara M., Mustafin R., Safina L.: Microservices: How to make your application scale. arXiv preprint arXiv:1702.07149, 2017

[7] Duda K., Adamkiewicz P., Rymarczyk T.: Nondestructive Method to Examine Brick Wall Dampness. International Interdisciplinary Phd Workshop 2016, 68–71.

[8] Filipowicz S.F., Rymarczyk T.: Measurement Methods and Image Reconstruction in Electrical Impedance Tomography. Przeglad Elektrotechniczny 88(6), 2012, 247–250.

[9] Filipowicz S.F., Rymarczyk T.: The Shape Reconstruction of Unknown Objects for Inverse Problems. Przeglad Elektrotechniczny 88(3A), 2012, 55–57.

[10] Fowler M.: Microservices. ThoughtWorks, http://martinfowler.com/articles/microservices.html, 2014 [06.09.2017].

[11] Holder D.S.: Electrical Impedance Tomography: Methods, History and Applications. Series in Medical Physics and Biomedical Engineering, London 2005.

[12] Johanson A., Flögel S., Dullo C., Hasselbring W.: OceanTEA: Exploring Ocean-Derived Climate Data Using Microservices. 6th International Workshop on Climate Informatics, National Center for Atmospheric Research in Bloulder, 2016.

[13] Kapusta P., Majchrowicz M., Sankowski D., Jackowska-Strumiłło L., Banasiak R.: Distributed multi-node, multi-GPU, heterogeneous system for 3D image reconstruction in Electrical Capacitance Tomography–network performance and application analysis. Przegląd Elektrotechniczny 89(2B), 2013, 339—342.

[14] Kim M., Mohindra A., Muthusamy V., Ranchal R., Salapura V., Slominski A., Khalaf R.: Building scalable, secure, multi-tenant cloud services on IBM Bluemix. IBM Journal of Research and Development 60(2-3), 2016.

[15] Richardson C.: Pattern: Microservices Architecture, Microservices.io. http://microservices.io/patterns/microservices.html [06.09.2017].

[16] Rybak G., Chaniecki Z., Grudzień K., Romanowski A., Sankowski D.: Non–invasive methods of industrial process control. Informatyka, Automatyka, Pomiary w Gospodarce i Ochronie Środowiska 3, 2014, 41–45 [DOI: 10.5604/20830157.1121349].

[17] Rymarczyk T.: Using electrical impedance tomography to monitoring flood banks. International Journal of Applied Electromagnetics and Mechanics 45, 2014, 489–494.

[18] Rymarczyk T.: New Methods to Determine Moisture Areas by Electrical Impedance Tomography. International Journal of Applied Electromagnetics and Mechanics 37(1–2), 2016, 79–87.

[19] Rymarczyk T., Tchórzewski P., Sikora J.: Monitoring of Flood Embankment System by Nondestructive Method with Infinite Boundary Element. Studies in Applied Electromagnetics and Mechanics 40, 2015, 176–183.

[20] Rymarczyk T., Tchórzewski P.: Topological methods to determine damages of flood embankments. Przegląd Elektrotechniczny 92(12), 2016, 153–156.

[21] Sankowski D., Sikora J.: Electrical capacitance tomography: Theoretical basis and applications. IEL, Warsaw 2010.

[22] Sousa G., Rudametkin W., Duchien L.: Automated Setup of Multi-Cloud Environments for Microservices-Based Applications. 9th IEEE International Conference on Cloud Computing, San Francisco, USA, 2016.

[23] Sikora J., Wójtowicz S.: Industrial and Biological Tomography: Theoretical Basis and Applications. IEL, Warsaw 2010.

[24] Smolik W.: Forward Problem Solver for Image Reconstruction by Nonlinear Optimization in Electrical Capacitance Tomography. Flow Measurement and Instrumentation 21, 2010, 70–77.

[25] Tai C., Chung E., Chan T.: Electrical impedance tomography using level set representation and total variational regularization. Journal of Computational Physics 205(1), 2005, 357–372.

[26] Wajman R., Fiderek P., Fidos H., Jaworski T., Nowakowski J., Sankowski D., Banasiak R.: Metrological evaluation of a 3D electrical capacitance tomography measurement system for two-phase flow fraction determination. Meas. Sci. Technol. 24(6), 2013, 065302.

[27] Wang M.: Industrial Tomography: Systems and Applications. Elsevier, 2015.

Ph.D. Tomasz Cieplak
e-mail: t.cieplak@pollub.pl

Doctor of Engineering, acting assistant professor in the Department of Enterprise Organization in the Faculty of Management, Lublin University of Technology. He has research experience gained in the prepared doctoral dissertation at Saga University, Japan. The area of research interest is the use model of cloud computing in the enterprise, creating systems based on SOA and the cloud computing model.

Ph.D. Eng. Tomasz Rymarczyk
e-mail: tomasz@rymarczyk.com

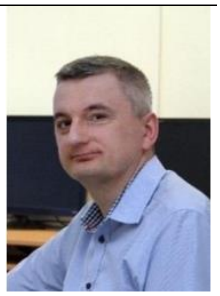

He is the director in Research and Development Center in Netrix S.A. He also is assistant professor in the University of Economics and Innovation, Lublin, Poland. His research area focuses on the application of non-invasive imaging techniques, electrical tomography, image reconstruction, numerical modelling, image processing and analysis, process tomography, software engineering, knowledge engineering, artificial intelligence and computer measurement systems.

Ph.D. Eng. Grzegorz Kłosowski
e-mail: g.klosowski@pollub.pl

Assistant Professor in Department of Organization of Enterprise at the Faculty of Management of Lublin University of Technology. The research interests of the author include artificial intelligence, simulation and modeling of engineering and business processes. Leader and participant in several implementation projects. Chairman of the Board of the Special Purpose Vehicle of POLLUB-Invest Ltd., whose purpose is indirect commercialization.

otrzymano/received: 10.10.2017 *przyjęto do druku/accepted: 15.02.2018*

DOI: 10.5604/01.3001.0010.8654

OPTIMIZATION OF DATA PROCESSING FOR REQUESTING OBSERVATION SYSTEMS

Iryna V. Svyd[1], Andrij I. Obod[1], Oleksandr S. Maltsev[1], Daria B. Pavlova[2], Bridel V. Mongo[2]
[1]National University of Radio Electronics, Department of Radiotechnologies Information and Communication Systems,
[2]National Technical University "KhPI", Department of Information Systems

Abstract. *The article discusses how to optimize the data when it detects air targets by requesting observation systems. Two schemes for the detection of air objects, differing in the order of the operation of deciphering the aircraft responders' response signals, were investigated. It is shown that performing the operation of decoding the signals of the aircraft responder after the operation of detecting the air object makes it possible to improve the quality of data processing of the requesting observation systems. The influence of the aircraft responder readiness coefficient and the probability of suppression of signals in the answer channel on the probability of detection of air objects was researched.*

Keywords: data processing optimization, requesting observation systems

OPTYMALIZACJA PRZETWARZANIA DANYCH DLA ZAPYTAŃ SYSTEMÓW OBSERWACJI PRZESTRZENI POWIETRZNEJ

Streszczenie. *Artykuł dotyczy optymalizacji przetwarzania danych podczas wykrywania obiektów powietrznych poprzez żądanie systemów nadzoru. Zbadano dwa schematy wykrywania obiektów powietrznych, różniące się kolejnością operacji odczytywania sygnałów odpowiedzi statków powietrznych. Pokazano, że wykonanie operacji deszyfrowania sygnałów transponderów statku powietrznego po uruchomieniu wykrywania obiektów powietrznych pozwala poprawić jakość przetwarzania danych zapytań systemów nadzoru. Zbadano wpływ współczynnika gotowości statku powietrznego i prawdopodobieństwa tłumienia sygnałów w kanale odpowiedzi na prawdopodobieństwo wykrycia obiektów powietrznych.*

Słowa kluczowe: optymalizacja przetwarzania danych, systemy przesłuchań, transpondery lotnicze

Introduction

The article presents the results of research as a joint optimization of signal processing and primary data processing data of the requesting observation systems. [20], as well as improving the quality of data processing of the requesting airspace observation systems by changing the algorithm for processing joint data.

Using a sequential procedure for processing surveillance system data, due to the functionally completed processing steps, allowed to formalize the data processing procedure [5, 12, 20].

However, this significantly limited, and in some cases excluded, the opportunities for inter-stage data processing optimization [5, 12].

The lack of inter-stage optimization of data processing of modern radar observation systems leads to a decrease in the quality of information services for decision-makers in the airspace control system.

In this paper, the main focus is on the joint optimization of the detection signals phase and the airborne objects detection phase by requesting observation systems which belong to the major information resources of the airspace control system.

1. Data processing structure of airspace observation systems

The airspace control system as an information supervision and information management system must provide the following functions:

- conducting continuous exploration of airspace (in real time);
- collecting, accumulating and data processing of all from means of active and passive electronic surveillance and intelligence;
- development the data map of air situation basis on this data;
- informational sufficiency for functioning of the airspace control system;
- high accuracy and non-distortion of information;
- exclusion of intervention and organized counteraction.

Observation systems are the information resource of the airspace control system.

Observation systems represent the following data:

- detecting an air object;
- definition of their coordinates;
- estimation of parameters of motion;
- classification by state.

Data about horizontal and vertical velocities identifying characteristics or intentions may also be presented.

The necessary data and parameters of the technical characteristics depend on the specific types of application.

That is, in most cases, surveillance systems give the user information about where the air object is and who it is.

As a rule, the primary observation systems [2, 5, 7, 10, 12, 15, 21] correspond to the first question, and on the other – requestioning (identification) observation systems [1–4, 6–8, 10, 12, 13, 15–21].

Processing of observation system data is a process of bringing information received from observation systems into a suitable form for further transmission to users.

The data processing of observation systems is impossible without wide use of information technologies, which allows to realize the automatic collection, processing, storage, transmission and delivery of information to consumers, while increasing practically all quality indicators.

The data processing system of the observation systems is directly related to the signal sources and provides the solution of the following tasks:

- detecting useful signals received from airborne objects, and removing obstacles;
- determination of parameters of received signals;
- detection of airborne objects;
- measurement of coordinates and parameters of airborne objects movement;
- receipt of flight information from the airspace;
- identification of the airborne object on the basis of "Friend or foe";
- correlation of detected airborne objects in the trajectory and determination of parameters of these trajectories;
- calculation of smoothed and ahead of certain time interval of coordinates of air objects;
- the formation of a generalized air environment in the control zone from several sources.

The solution of these tasks leads to a variety of functions performed by the system related to the staged processing of large streams of information. At each stage of processing, certain operations are performed on the input data of individual devices of varying complexity. Thus, the system of processing modern observing systems can be represented as a set of elementary subsystems with complex interconnections. Naturally, the complexity of the processing system does not allow formalization and analysis of its work in general, so it is necessary to pre-break the system into elements and study their functioning. In this regard, it is expedient that the elements of the processing system have a clearly defined purpose, as well as what they could be described with rather general mathematical positions. This approach allows the process of data processing of airspace observation systems to be divided into the following functionally completed stages, which are performed sequentially:

- signal processing of observation systems;
- primary data processing;
- secondary data processing.

It should be noted that the first stage is performed in the monitoring system using the signal processor. The second and third stages are performed using the data processor [5, 12]. Such an order of data processing leads to the impossibility of inter-segment (compatible) optimization of data processing [5], which, as a result, leads to a decrease in the quality of information users provision.

Indeed, the components of data processing are detecting a signal in the first stage and detecting an air object in the second stage. The optimization of detection is usually carried out using the Neumann-Pearson criterion, which reduces to maximizing the probability of correct detection with restrictions on the likelihood of false detection. Thus, at the first and second stages, the following procedures are carried out

$$D_0 = f(z_0, q) \text{ when } F_0 = f(z_0) = const;$$

$$D_{01} = f(k, N) \text{ when } F_0 = f(k) = const,$$

where z_0 – analog signal detection threshold, q – signal/noise ratio (SNR), k – digital threshold for detecting airspace, N – number of received signals from an air object in one review.

The structure of data processing observation systems clearly shows that providing optimization of processing is possible only with centralized data processing.

It should be noted that only the analog control threshold, which can be optimized for detection at all stages of data processing, is the threshold for detecting signals. This circumstance clearly determines that only in systems with centralized processing of data processing stages can a joint optimization of detection of air objects.

The foregoing allows to form the structure of the data processing of airspace data, which includes a single structure of signal processing and primary data processing.

2. The airborne detection quality assessment of requesting observation systems

Consider the possibilities of compatible optimization of detection of air objects by requesting observation systems. Requesting observation systems represents dual-channel data transmission systems formed by the request channel and the response channel. Airplane responder is an open system of mass service with failures. The presence of intra-system and intentional correlated obstacles leads to the fact that the probability of a response by an airplane responder to a specific request signal is always less than one, that is $P_0 < 1$, where P_0 – the readiness factor of the aircraft's responder.

As query and answers signals, requesting observation systems use interval-time codes. Since for requesting observation systems a high signal-to-noise ratio is characteristic, it is possible to achieve the required quality indicators when processing single pulses of interval-time codes. The processing of received signals by the receiver, in this formulation of the question, consists in decoding the received signal and its result of the decision.

Various methods of processing, in particular, methods for inter-period processing of coded signals, can be used to increase the probability of a decision taken in the processing of encoded signals, as well as to protect the requesting observation systems from inter-system interference.

In this regard, it is interesting to consider the characteristics of detecting response signals in different processing methods, as well as the influence of the aircraft's responder readiness factor and the probability of response detection suppressing an airborne object.

Let's consider the joint optimization of the airborne object detection. We obtain comparative characteristics of air objects detection with different methods of response signals processing under the influence of fluctuation and impulse noise in the radio channel. Calculations will be made for the criteria and features of the construction of the equipment for processing interval-time codes in existing requesting observing systems.

Suppose that the response factor is equal to one and there is no suppression in the response radio channel. At the output of the receiver, binary quantization of signals is carried out, that is, at a fixed signal/noise ratio (q) and the chosen threshold limit from below (z_0) the uncertainty of probability is uniquely determined – P_{11} (probability of detecting a single pulse of the response signal) and P_{01} (probability of occurrence of noise emission at a given time position).

Let's also assume that the decoder performs the logic n/n, where n – the value of the response code, and in the airborne object detection device, the logic is used k/N, where k – the digital threshold of the detection of the air object, N – the length of the packet of received response signals, at which fixing the signal of the decision to detect an air object occurs in the presence of any K signals in N positions

We will compare the characteristics of the detection of air objects of both treatment methods using the Neumann-Pearson criterion, that is, at a fixed level of false alarms, we will find the detection characteristic (the probability of detecting the coded signal), depending on the SNR for the moment of the first detection of the object (fulfillment of the detection criterion beginning of the information package).

When decoding with the next inter-period processing (I method of processing) received signals, the probability of passing n of pulse interval-time codes and false signals through a decoder are defined as

$$D_d = (P_{11})^n;\ F_d = (P_{01})^n.$$

The probabilities P_{01} and P_{11} are determined by the following relationships

$$P_{01} = \exp\left(-z_0^2/2\right);\ P_{11} = \int_{z_0}^{\infty} x \exp\left[-\left(x^2 + q^2\right)\right] I_0(qx)\,dx,$$

where $I_0(qx)$ – is the modified Bessel function of the first kind of zero order.

The probability of detecting useful signals and false alarms at the output of devices interperiod processing are calculated respectively as

$$D_{2d} = \sum_k^N C_k^N D_d^k (1 - D_d)^{N-k};\ F_{2d} = \sum_k^N C_k^N F_d^k (1 - F_d)^{N-k}. \quad (1)$$

For the method of decoding with the previous inter-period processing of the response signals (II method of processing), the probability of passing coded signals and false alarms through the inter-period signal processing device can be written, respectively, as

$$D_1 = \sum_k^N C_k^N P_{11}^N (1 - P_{11})^{N-k};\ F_1 = \sum_k^N C_k^N P_{01}^N (1 - P_{01})^{N-k}. \quad (2)$$

Probability of passing useful and false signals through decoder can be defined as either:

$$D_{1d} = D_1^n;\ F_{1d} = F_1^n. \quad (3)$$

Given (3), the expression (2) can be written as

$$D_{1d} = \left[\sum_k^N C_k^N P_{11}^N (1-P_{11})^{N-k}\right]^n;\ F_{1d} = \left[\sum_k^N C_k^N P_{01}^N (1-P_{01})^{N-k}\right]^n. \quad (4)$$

In Fig. 1 shows the dependence of the probability of detecting an air object on the SNR for two- and three-pulse interval-time codes under different logic of processing and the probability of false alarms $F = 10^{-3}$, calculated from expressions (1) and (4).

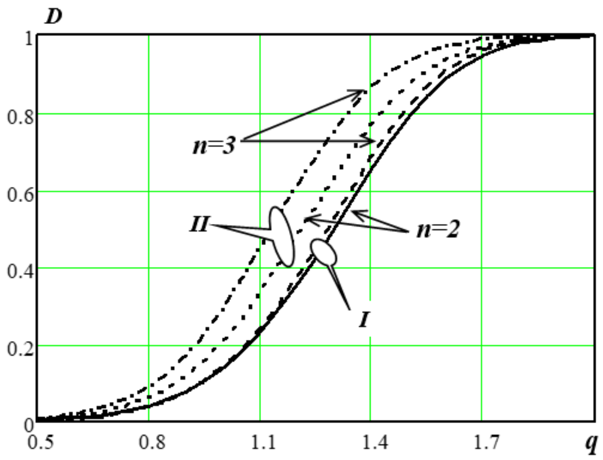

Fig. 1. The airborne detection characteristics

The analysis of the above dependencies shows that the characteristics of the detection of an air object for a decoding method with a pre-inter-period processing exceed the characteristics of detecting an air object for a decoding method with subsequent inter-period processing. Certainly, for $q = 1.25$ and $n = 3$ the probability of detecting an air object for the first processing method is 0.4, and for the second processing method it is 0.7. An increase in the value of time interval intervals leads to an increase in the probability of a proper detection of an airborne object.

2.1. Assessment of the impact of the airplanes responder readiness factor and the probability of suppressing response signals to airborne detection characteristics

The presence of interruptions (intersystem or intentional correlated) in the query channel of the requesting observation systems leads to the fact that the responder will receive a response signal not for each request signal. Certainly, an airplane responder is characterized by a readiness factor (P_0) of an airplane responder that is nothing like the probability of a response to a request signal. Thus, the readiness rate of the aircraft responder is always less than one ($P_0 < 1$). In addition, the presence of intra system interference in the response channel, which is typical for the systems under consideration, leads to suppressed individual pulses of the response signal, which can be taken into account as the probability of suppressing the response signals.

Let's obtain the comparative characteristics of an air object detection probability for the considered methods of processing response signals, taking into account the actual readiness factor of the aircraft responder and the probability of the response signals suppression (P_p). In doing so, we assume that the probability of response signals suppressing the does not affect the formation of false alarms. In this regard, we will only determine the probability of an air object detecting.

When decoding with the next interperiodal processing of the received response signals, the probability of passing of interval-time codes through a decoder, taking into account the effect of the response factor of the readiness of the aircraft and the probability of suppressing the response signals, can be determined as

$$D_d = P_0 P_p P_{11}^n.$$

The probability of detecting useful signals at the output of the interperiodic processing device of response signals in this case is defined as

$$D_{2d} = \sum_{i=0}^{N-k} C_i^N \left[P_0 P_p P_{11}^n\right]^{N-i} \left[1 - P_0 P_p P_{11}^n\right]^i. \quad (5)$$

For the second method of decoding, the probability of passage of coded signals through the device interperiod processing, taking into account the airspeak response factor and the probability of suppressing the response signals, can be determined from the following relationships

$$D_1 = \sum_{i=0}^{N-k} C_i^N \left[P_0(1-P_p)\right]^{N-i} \left[1 - P_0(1-P_p)\right]^i \sum_{j=0}^{N-k-i} C_j^{N-i} P_{11}^{N-j-i} (1-P_{11})^j.$$

The probability of detecting the coded signal at the output of the decoder in this case can be written as

$$D_{1d} = \sum_{i=0}^{N-k} C_i^N \left[P_0(1-P_p)\right]^{N-i} \left[1 - P_0(1-P_p)\right]^i \left[\sum_{j=0}^{N-k-i} C_j^{N-i} P_{11}^{N-j-i} (1-P_{11})^j\right]^n. \quad (6)$$

Expressions (5) and (6) are obtained for the general case, when both P_p and P_0 variables. This is $P_p = 1$ – a special case when only obstacles are taken into account. This is $P_0 = 1$ – another special case when only the effect of the probability of suppressing the response signals is taken into account.

In Fig. 2 shows a family of characteristics of airspace detection at two- and three-pulse interval-time codes for both methods of processing at $P_p = 0.01$ and $P_0 = 0.95$.

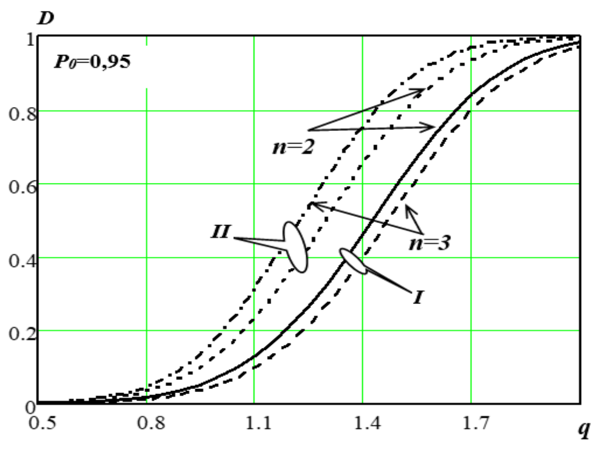

Fig. 2. Characteristics of the of airborne objects detection

The analysis of figs. 1 and 2 shows that the reduction of the readiness factor of the aircraft responder by 0.05 and the probability of suppressing signals leads to a decrease in the likelihood of detecting an air object. So, with $q = 1.4$ and $n = 3$ the probability of detecting an air object for the second processing method, decreases from 0.88 to 0.76. Reducing the readiness factor of the aircraft responder leads to the fact that, at a certain value of the airplane responder's readiness factor, the best detection characteristics provide a method of decoding with subsequent inter-period processing.

Figure 3 shows the calculations of the air objects detection probability by a requesting observing system with a fixed SNR $q = 1.9$ and the probability of suppressing the response signals

$P_p = 0.01$ as a function of the airplane response readiness factor, the significance of the interval time codes, and the data processing methods under consideration.

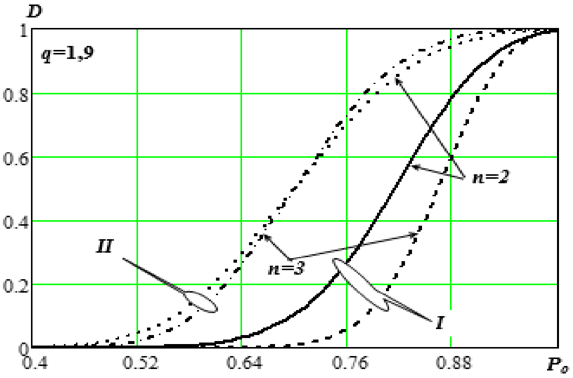

Fig. 3. Characteristics of the of airborne objects detection

3. Summary

The conducted research allowed to determine the structure of data processing of requesting observation systems at the stages of detection of signals and detection of an air object in which it was possible to conduct a joint optimization of data processing at the specified stages of processing. The method of data processing is proposed, which, unlike the one used, decodes the response signals by the interprocess processing of the response signals. The indicated calculations of the probability of detecting an air object by inquiry systems have shown a sufficient improvement in the quality of data processing and the reduction of the impact of the airplane response readiness factor and the probability of suppressing response signals by intra systemic impediments to the quality of data processing.

References

[1] Ahmadi Y., Mohamedpour K., Ahmadi M.: Deinterleaving of Interfering Radars Signals in Identification Friend or Foe Systems. Proc. of 18th Telecommunications forum TELFOR 2010, Belgrade, 2010.
[2] Bagad V.S.: Radar System. Technical Publications 2009.
[3] Bouwman R.: Fundamentals of Ground Radar for Air Traffic Control Engineers and Technicians. SciTech Publishing, 2009 [DOI: 10.1049/SBRA008E].
[4] Eaves J., Reedy E.: Principles of Modern Radar. Springer Science & Business Media 2012.
[5] Farina A., Studer F.: Digital radar data processing. Radio i svyaz, Moscow 1993.
[6] Garcia M.L.: Test For Success: Next Generation Aircraft Identification System RF Simulation. IEEE ICNS '07, 007.
[7] Harman W.H., Wood M.L.: Triangle TCAS Antenna, Project Report ATC-380. MIT Lincoln Laboratory, Lexington, MA, 2011.
[8] Honold P.: Secondary radar: fundamentals and instrumentation, Siemens-Aktiengesellschaft, Hardcover 1976.
[9] Kim E., Sivits K.: Blended secondary surveillance radar solutions to improve air traffic surveillance. Aerosp. Sci. Technol. 45/2015, 203–208.
[10] Kovalyov F.N.: The target location precision in bistatic radiolocation system. Radioengineering 8/2013, 56–59.
[11] Lynn P.A.: Radar Systems. Springer, Boston 1987, [DOI: 10.1007/978-1-4613-1579-7].
[12] Obod I.I., Strelnitskyi O.O., Andrusevich V.A.: Informational network of aerospace surveillance systems. KhNURE, Kharkov 2015.
[13] Obod I.I., Svyd I.V., Shtyh I.A.: Interference protection of questionable airspace surveillance systems: monograph. KhNURE, Kharkiv 2009.
[14] Otsuyama, T., Honda, J., Shiomi, K., Minorikawa, G., Hamanaka, Y.: Performance evaluation of passive secondary surveillance radar for small aircraft surveillance. Proc. of 12th European Radar Conference (EuRAD), New York, 2015, 505–508.
[15] Raju G.S.N.: Radar Engineering. I.K.International Pvt Ltd 2008.
[16] Ray P.S.: A novel pulse TOA analysis technique for radar identifications. IEEE Transactions on Aerospace and Electronic systems, vol. 34, No. 3, 1998, 716–721.
[17] Richards M.A., Holm W.A., Scheer J.: Principles of Modern Radar: Basic Principles. Institution of Engineering and Technology 2010.
[18] Richards M.A., Melvin W.L., Scheer J., Scheer J.A., Holm W.A.: Principles of Modern Radar. Radar Applications, Institution of Engineering and Technology 2014.
[19] Shiomi, K., Senoguchi, A., Aoyama, S.: Development of mobile passive secondary surveillance radar. Proc. of 28th International Congress of the Aeronautical Sciences, Brisbane 2012.
[20] Stevens M.C.: Secondary Surveillance Radar, Artech House, Norwood 1988.
[21] Thompson S.D., Flavin J.M.: Surveillance Accuracy Requirements in Support of Separation Services. MIT Lincoln Laboratory Journal, Volume 16, Number 1, 2006.
[22] Ueda T., Shiomi K., Ino M., Imamiya K.: Passive Secondary Surveillance Radar System for Satellite Airports and Local ATC Facilities. Proc. of 43rd Annual Air Traffic Control Association, Atrantic City, NJ, USA 1998.

Ph.D. Iryna V. Svyd
e-mail: iryna.svyd@nure.ua

Scientific work: methods to improve the noise immunity of data transmission channels; information support of control systems; management of information networks, management of quality of service in communication networks; neural technologies in telecommunications; design and optimization of communication networks; renewable energy engineering.

M.Sc. Andrij I. Obod
e-mail: andrii.obod@gmail.com

Postgraduate Department of Radiotechnologies Information and Communication Systems on the specialty 05.13.06 – Information Technology.

Scientific work: methods of improving the quality of information provision for consumers of information networks of airspace surveillance systems.

M.Sc. Oleksandr S. Maltsev
e-mail: aleksandr.maltsev@nure.ua

Postgraduate Department of Radiotechnologies Information and Communication Systems on the specialty 05.12.17 – Radio and Television Systems.

Scientific work: increase the efficiency of using many frequency signals in next generation communication systems.

B.Sc. Daria B. Pavlova
e-mail: d_rics@nure.ua

Magistrate Department of Information Systems on the specialty 172 Telecommunications and radio engineering.

B.Sc. Bridel V. Mongo
e-mail: bridelviel@gmail.com

Magistrate Department of Information Systems on the specialty 172 Telecommunications and radio engineering.

otrzymano/received: 10.10.2017 *przyjęto do druku/accepted: 15.02.2018*

DOI: 10.5604/01.3001.0011.6005

METHODS OF PRODUCING APODIZED FIBER BRAGG GRATINGS AND EXAMPLES OF THEIR APPLICATIONS

Łukasz Zychowicz, Jacek Klimek, Piotr Kisała
Lublin University of Technology, Institute of Electronics and Information Technology

Abstract. *The paper presents the principle of operation, the structure, applications and methods of producing uniform, chirped and blazed fiber Bragg gratings as well as long period gratings. Finally, several selected methods used to make apodized gratings are listed and described.*

Keywords: apodized fiber Bragg grating, uniform Bragg grating, chirped Bragg grating, long-period grating, blazed Bragg grating

METODY WYTWARZANIA I ZASTOSOWANIE APODYZOWANYCH SIATEK BRAGGA

Streszczenie. *W artykule omówiono zasadę działania, budowę i zastosowania apodyzowanych siatek Bragga: równomiernych, o zmiennym okresie, długookresowych i skośnych oraz wpływ apodyzacji na te siatki. Na koniec wymieniono i opisano kilka wybranych metod stosowanych do wytworzenia apodyzowanych siatek.*

Słowa kluczowe: apodyzowane siatki Bragga, równomierna siatka Bragga, siatka Bragga o zmiennym okresie, siatka długookresowa, skośna siatka Bragga

Introduction

At the end of the 1970s, it was noticed that the creation of periodic structures in glass fibers can significantly expand the field of applications of fiber optics [10]. In the 1980s, the first proposals for the use of Bragg gratings began to appear [19], and it was only in the 1990s that their manufacturing technology was sufficiently advanced to apply the gratings practically [6, 21]. The first publications regarding the apodized gratings were published in 1995–1996 [26, 29]. Since then, these gratings have been intensively researched and developed (including uniform, chirped and blazed gratings, and long-period gratings, discussed in detail in the further part of the paper), as evidenced by the large number of published articles, that are mentioned in the following paragraphs.

1. Principle of operation of the Bragg gratings

The optical fiber Bragg gratings feature periodic changes in the refractive index of the optical fiber core. They are produced by removing the coating of the optical fiber, resulting in the jacket being exposed. On the fiber prepared in this way, the fringes are inscribed with laser light at appropriate distances from each other. The grating acts as a selective mirror – it reflects the light of a specific wavelength (the so called Bragg wavelength), while the light with other wavelengths (which do not meet the Bragg condition, defined by equation 1 – the case of the uniform grating) passes practically without losses.

$$\lambda_B = 2n_{eff} \cdot \Lambda, \tag{1}$$

where n_{eff} is the effective refractive index of the optical fiber core, and Λ is the period of the grating.

2. Apodization profiles

It was noted that the functionality of the optical fiber Bragg gratings can be significantly improved by using apodization. There is a true apodization and a non-true apodization. Apodization is a technique of eliminating the unfavorable features of the spectrum – the true apodization can effectively eliminated side-lobes in the reflected spectrum [7]. In addition, it was noted improvement of a group delay (GD) responses of the apodized chirped FBG [31] and a shaping of efficiency of the Bragg wavelength harmonics reflection (i.e. reflections at wavelength that satisfy the higher order Bragg condition) [22, 24]. Apodization consists in forcing a suitable, spatial distribution of light intensity from the laser writing the grating. Many apodizing functions are known. Gaussian, cosine, raised cosine, sinc function are the ones most commonly used. In order to obtain an apodized T(z) profile, one uses a particular transformation [34]:

Gaussian profile: $$T(z) = \exp\left\{-a\left[\frac{\left(z-\frac{L}{2}\right)}{L}\right]\right\}^2 \tag{2}$$

Sinc profile: $$T(z) = \left\{\frac{sin\left[\frac{2\pi\left(\frac{L}{2}\right)}{L}\right]}{\frac{2\pi\left(\frac{L}{2}\right)}{L}}\right\}^{n} \tag{3}$$

Hamming profile: $$T(z) = n\left\{\frac{1+Hcos\left[\frac{2\pi\left(\frac{L}{2}\right)}{L}\right]}{1+H}\right\} \tag{4}$$

Sin profile: $$T(z) = sin^m\left(\frac{\pi z}{L}\right) \tag{5}$$

Cauchy profile: $$T(z) = \frac{1-\left[\frac{2\left(z-\frac{L}{2}\right)}{L}\right]^2}{1-\left[\frac{2C\left(z-\frac{L}{2}\right)}{L}\right]^2}, \tag{6}$$

where L is the length of the grating. Reflection characteristics for selected types of apodized variable period grating profiles are shown in Figure 1.

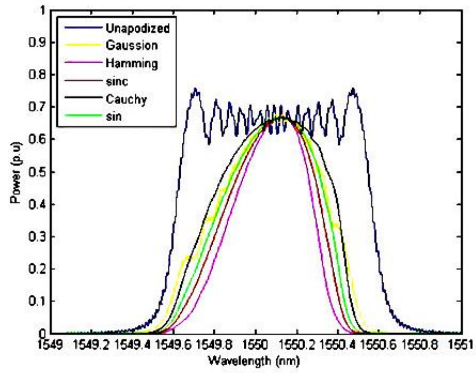

Fig. 1. Comparison of the refraction spectrum of an unapodized chirped Bragg grating with spectra of apodized gratings [34]

In Figure 1, it can be seen that the spectrum of the grating without apodization takes on a rectangular shape, which makes finding the maximum power very difficult. In the case of a grating with any apodization applied, the maximum of the spectrum can be easily determined.

3. Uniform Bragg gratings

Uniform Bragg gratings (gratings with a constant period and amplitude) are the simplest and most common gratings. The scheme of such grating is shown in Figure 2. It can be seen that the plane of the grating is perpendicular to the axis of the optical fiber. The light (corresponding to Bragg wavelength) is partially reflected at each grating period, forming a beam reflected in the opposite direction to the introduced light.

These gratings are most often produced using the phase mask method, featuring high repeatability.

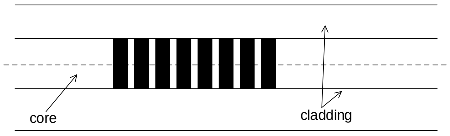

Fig. 2. Scheme of a uniform Bragg grating structure

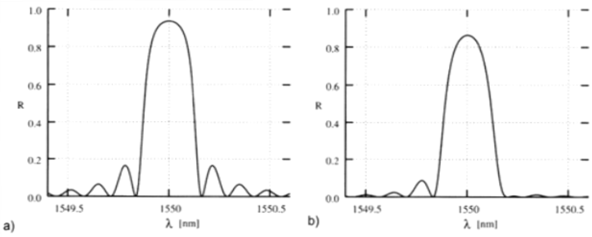

Fig. 3. Power reflection spectrum for a 6 mm grating: a) no apodization, b) with apodization [13]

In Figure 3, it can be observed that apodization has reduced the reflectivity by a small extent, but for that it has minimized the so-called sidebands resulting from multiple reflections from the opposite ends of the grating, which in selected applications turns out to be more important than the reduced reflectivity. The uniform Bragg gratings have found applications in optical telecommunications (dispersion compensation, optical filtering), measurement (especially strain sensors, where the whole spectrum (without sidebands) contains information about the strain distribution [2, 33]), as well as shock wave transducers [27].

4. Chirped Bragg gratings

Non uniform or chirped gratings feature a variable period along the axis of the optical fiber. Waves with shorter lengths are reflected in the segments of the grating where the period is smaller, while longer waves are reflected in segments with larger periods (in accordance with the Bragg's law).

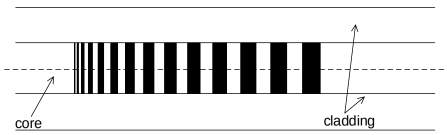

Fig. 4. Scheme of the chirped Bragg grating structure

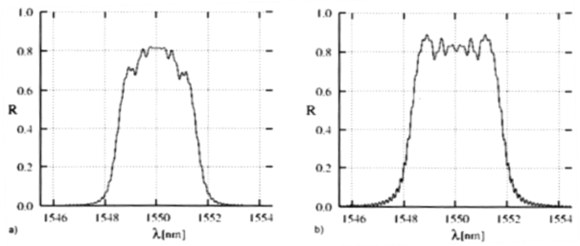

Fig. 5. Power reflection spectrum for a grating: a) with apodization, b) without apodization [13]

The resulting spectrum of a chirped Bragg grating is closer to a rectangular one for a grating without apodization than for a grating with apodization (as shown in Figure 5). Apodized chirped Bragg gratings are widely used in telecommunications and sensor technology, i.e. in spectrum analyzers [30], chromatic dispersion compensators, where apodization has a positive effect on ripples in group delay response [1, 8, 16], linear edge filters [4].

5. Long period gratings

Long Period Bragg gratings (LPG) feature only transmissive properties, i.e. coupling of core modes with cladding modes [17]. Because of this, LPGs do not have a reflection spectrum, therefore the transmission spectrum is shown in Figure 7. In the case of LPGs the period is much longer, compared with the other types of FBGs – for the grating in Figure 6, numerically calculated using the OptiGrating environment, the period is 150 µm.

Based on Figure 7, it can be noted that the grating with apodization features less sidebands, but low dynamic range of peaks (dips). If it is necessary to obtain a higher dynamic range of peaks, similar to an unapodized grating, another "*a*" factor should be used but the increase of index modulation changes can be a better concept. The full width at half maximum (FWHM) is much larger for the apodized grating. In the transmission spectrum of both gratings, further resonance peaks can be seen, which correspond to the subsequent mode couplings of the core mode with the modes in the fiber cladding. In reference [28] it was shown that apodization in the case of LPG makes the most sense for spectral measurements in the range (of spectrum changes) corresponding to higher cladding modes, because there is the greatest noise reduction there, and the disadvantage of apodizing is the decrease in the attenuation of waves with resonance wavelengths.

LPGs are used in sensors of non electrical quantities (strain, temperature, bending) [11], where changes in the wavelengths, at which the power minimum occurs, are measured, as well as in ultrafast optical signal processing [3].

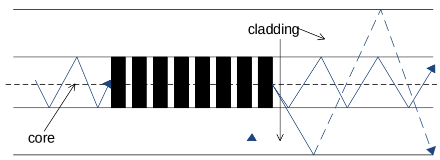

Fig. 6. Scheme of the structure and the method of coupling of the LPG modes

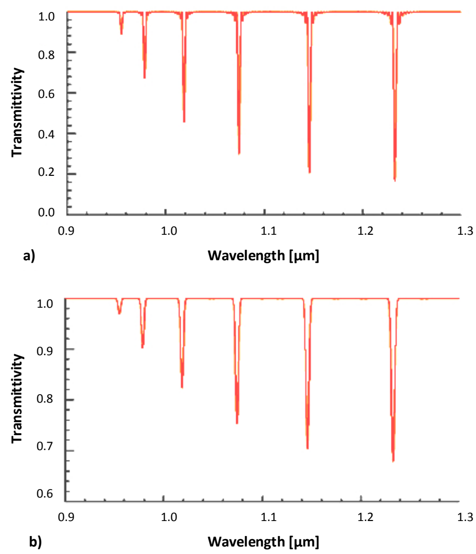

Fig. 7. Transmittivity as a function of wavelength for an LPG: a) without apodization, b) with the Gaussian apodization profile and the coefficient a = 0.5

6. Blazed Bragg gratings

Blazed Bragg gratings feature an angle between the longitudinal axis of the fiber and the planes of the grating of less than 90°. The light introduced into the core undergoes partial reflection to the outside of the fiber, which results in the passage of a relatively small amount of light through all planes of the grating.

In the Divison of Optoelectronics and Teleinformatic Networks of the Institute of Electronics and Information Technology of the Lublin University of Technology many types of apodized Bragg gratings are being produced – figure 9 shows the spectrum of a chirped grating with a blaze angle of 0°, and figure 10 – the spectrum of a chirped grating with a blaze angle of 2.5°. Apodization was imposed by the excimer laser beam distribution (it is approximately a Gaussian profile), and the beam distribution profile is measured using a beam profiler with a BC 106 VIS camera.

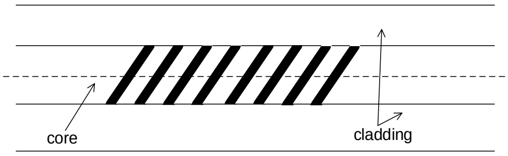

Fig. 8. Scheme of the structure of a blazed Bragg grating

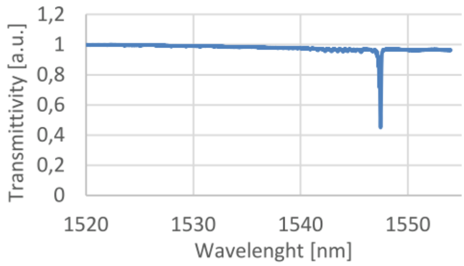

Fig. 9. Transmittivity as a function of wavelength for a 0.1 nm/cm chirp grating and 0° write angle

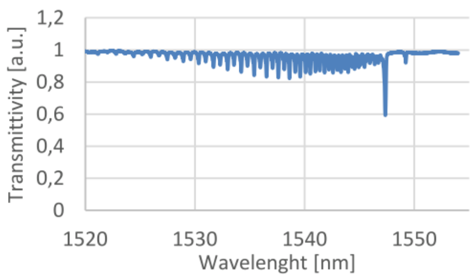

Fig. 10. Transmittivity as a function of wavelength for a 0.1 nm/cm chirp grating and 2.5° write angle

Based on the figures above, it can be seen that in the second case, the transmission of the deepest dip is higher than in the first case, and for the smaller wavelengths there are numerous peaks with transmittivity close to twice the transmittivity of the main dip.

Blazed Bragg gratings are used to build spectrometers, erbium doped fiber amplifiers (EDFA) [14]. Bragg gratings are also known to be used for bending sensors [5], spectrum analyzers [30], polarization discriminators [18].

7. Methods of producing apodized Bragg gratings

Apodized fiber optic Bragg gratings are produced using the phase mask method, multiple printing of in-fiber gratings, the moving fiber/phase mask technique, the symmetric stretch apodization method, using phase mask with variable diffraction efficiency method. Furthermore point-by-point method [32] using a CO_2 laser [9] or a UV laser [12] is used to LOG inscription.

The phase mask method is the simplest and most effective technique for producing gratings. It consists in directing a beam of UV light onto a diffraction structure made of quartz glass. For a grating with a particular period Λ, a phase mask with a period of 2Λ is required. In order to move the beam of light on the surface of the optical fiber, precise positioning mechanisms are created. This method works very well in the production of uniform and blazed gratings. The selected apodization profile is created by using a properly designed and manufactured lens that focuses the light beam on the fiber [25].

The multiple printing of in-fiber gratings (MPF) consists in writing short (4 mm) gratings that overlap each other, so after each print several new grating periods are created. A pulse generating UV laser is used for this. The segment of the fiber where the grating is supposed to be inscribed is placed in a V-shaped glass groove. Precise movement the fiber forward and backward is controlled by a computer. The light source – an interferometer is in a fixed position [15].

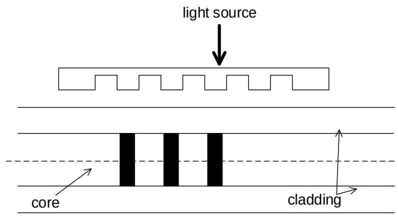

Fig. 11. Scheme of the setup for producing gratings using the phase mask method

In the moving fiber/phase mask technique (MPM), the fiber and phase mask are fixed in a holder, moved by a precision piezoelectric device. The UV beam remains stationary. During the creation of the grating, the fiber is being moved forward and backward, thus creating a "blur" effect of the grating. MPM allows to create an apodized gratings with a variable period. Figure 12 shows the scheme for writing gratings with this method.

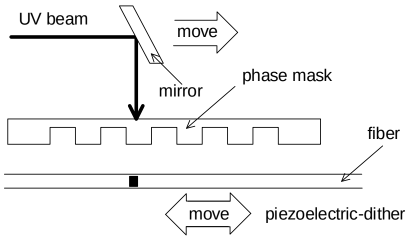

Fig. 12. Scheme of the setup for producing gratings using the MPM method

Similar to MPM apodization technique, where phase mask is dithered instead of optical fiber is presented in [20].

The symmetric stretch apodization method (SAM) is a combination of the MPF and MPM methods, so strict synchronization of the fiber and UV beam positioning systems is required. This allows the writing of two gratings in the same place, with the correct phase relation between them. First, the grating is written on an non-deformed fiber and then on a deformed one. The stretching and loosening of the fiber is carried out using a piezoelectric transducers [15]. Figure 13 shows the SAM scheme using a phase mask, which can be replaced with an interferometer.

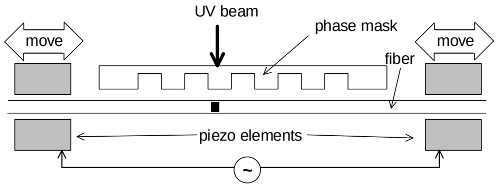

Fig. 13. Scheme of the setup for producing gratings using the SAM method

The phase mask with variable diffraction efficiency is the most reproducibility method. There is constant effective refractive index along the whole grating, so short-wavelength side broadening of spectral characteristic is avoiding in this method. The change of duty cycle and groove depth causes variable diffraction efficiency of the phase mask. The coherent UV laser beam lights up the phase mask and the interference pattern is writing in the fiber core. The technique is working in the case of sources with low coherence, because there is a small distance between the optical fiber and the phase mask [23].

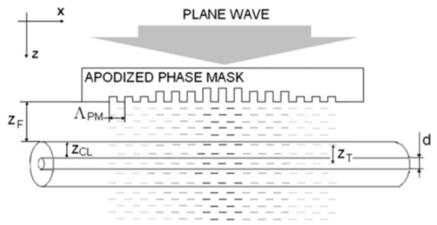

Fig. 14. Scheme of the setup for producing gratings using the phase mask with variable diffraction efficiency, where where: z_F is the distance between phase mask and the optical fiber, z_T is the Talbot distance [23]

8. Conclusions

The apodization minimizes the side bands of the transmission spectrum for all types of gratings described above. An undeniable disadvantage of apodization is the reduction in the reflectivity of the transmission spectrum, whereas in the majority of applications of Bragg gratings, it is more important to minimize the side bands than to obtain the highest possible main peak, which is still high even for apodized gratings. There are several methods for producing apodized Bragg gratings that are constantly being improved due to the increasingly precise devices used to produce the designed gratings. The use of a phase mask considerably speeds up the process of formation of periodic structures and contributes to their mass production. Nevertheless, for the production of some types of gratings, it is more convenient to use an interferometer (interference method).

Literature

[1] Aladadi Y.T., Abas A.F., Alresheedi M.T.: Performance Optimization of an Apodized-Chirped Fiber Bragg Gratings Based Chromatic Dispersion Compensator. IEEE ICTON 2016, 1–5.
[2] Ashik T.J. et al.: Analysis of simultaneous measurement of temperature and strain using different combinations of FBG. AIP Conf. Proc. 1849, 2017, 020031-1–020031-8.
[3] Ashrafi R., Asghari M.H., Azana J.: Ultrafast Optical Arbitrary-Order Differentiators Based on Apodized Long-Period Gratings. IEEE Photonics Journal, vol. 3, no 3, 2011, 353–364.
[4] Bandyopadhyay S. et al.: Empirical Relations for Design of Linear Edge Filters Using Apodized Linearly Chirped Fiber Bragg Grating. Journal of Lightwave Technology, vol. 26, no. 24, 2008, 3853–3859.
[5] Beak S., Jeong Y., Lee B.: Characteristics of short-period blazed fiber Bragg gratings for use as macro-bending sensors. Optical Society of America, vol. 41, no. 4, 2002, 631–636.
[6] Campbell R.J., Kashyap R.: Optically written Bragg gratings in photosensitive fibre. IEE Colloquium on Non-Linear Effects in Fibre Communications, 1990, 4/1–4/3.
[7] Dziubiński G. et al.: Optymalizacja parametrów światłowodowych czujników do pomiaru temperatury. Annual Set The Environment Protection 18/2016, 309–324.
[8] Faiyaz N.M., Omi A.I., Faisal M.: Optimization of Apodization Profile of Chirped Fiber Bragg Grating for Chromatic Dispersion Comensation, Dispersion Compensation Using Chirped Apodized FBG. International Conference on Electrical Engineering and Information & Communication Technology (ICEEICT) 2014, 1–5
[9] Gu Y., Chiang K. S., Rao Y. J.: Writing of Apodized Phase-Shifted Long-Period Fiber Gratings With a Computer-Controlled CO2 Laser. IEEE Photonics Technology Letters, vol. 21, no. 10, 2009, 657–659.
[10] Hill K.O., Fujii Y., Johanson D.C., Kawasaki B.S.: Photosensivity in optical fiber waveguides: aplication to reflection filter fabrication. Appl. Phys. Lett. 32, 647, 1978, 647–649.
[11] James S.W., Tatam R.P.: Optical fibre long-period grating sensors: characteristics and application. Meas. Sci. Technol. 14, 2003, 49–61.
[12] James S.W., Topliss S.M., Tatam R.P.: Properties of Length-Apodized Phase-Shifted LPGs Operating at the Phase Matching Turning Point. Journal of Lightwave Technology, vol. 30, no. 13, 2012, 2203–2209.
[13] Kaczmarek Z.: Światłowodowe czujniki i przetworniki pomiarowe. PAK, Warszawa 2006.
[14] Kashyap R., Wyatt R., Campbell R.J.: Wideband gain flattened erbium fibre amplifier using a photosensitive fibre blazed grating. Electronics Letters 21st, vol. 29, no. 2, 1993, 154–156.
[15] Kashyap R.: Fiber Bragg Gratings. Academic Press, 1999.
[16] Khan S.S.A., Islam M.S.: Chromatic Dispersion Compensation Using Linearly Chirped Apodized Fiber Bragg Grating. ICECE 2010, 9–12.
[17] Kisała P.: Periodyczne struktury światłowodowe w optoelektronicznych czujnikach do pomiaru wybranych wielkości nieelektrycznych. Monografie – Politechnika Lubelska 2012.
[18] Labidi H., Debarros C., Letteron R., Riant I.: Slanted Bragg grating with ultra-low polarization dependant loss. Optical Fiber Communication Conference and Exhibit 2002, 113.
[19] Lam D.K.W., Garside B.K., Hill K.O.: Dispersion cancellation using optical-fiber filters. Optical Society of America, vol. 7, no. 6, 1982, 291.
[20] Markowski K., Perka A., Jędrzejewski K., Osuch T.: Custom FBGs inscription using modified phase mask method with precise micro and nano-positioning. Proc. SPIE vol. 10031, 2016, 100311H [doi: 10.1117/12.2249381].
[21] Morey W.W., Meltz G., Weiss J.M.: Separation Of Temperature And Strain Measurands In Fiber Bragg Grating Sensors. LEOS '92 Conference Proceedings IEEE Lasers and Electro-Optics Society, 1992, 454–455.
[22] Osuch T., Jaroszewicz Z.: Influence of optical fiber location behind an apodized phase mask on Bragg grating reflection efficiencies at Bragg wavelength and its harmonics. Opt. Commun. 382, 2017, 36–41.
[23] Osuch T., Jaroszewicz Z.: Numerical analysis of apodized fiber Bragg gratings formation using phase mask with variable diffraction efficiency. Optics Communications, vol. 284, 2011, 567–572.
[24] Osuch T.: Numerical analysis of harmonic components of the Bragg wavelength content in spectral responses of apodized fiber Bragg gratings written by means of phase mask with variable phase step height, J. Opt. Soc. Am. A 33 (2), 2016, 172–178.
[25] Otto M. et al.: Flexible Manufacturing Method For Long-Period Fibre Gratings With Arbitrary Index Modulation Profiles. Fibre and Optical Passive Components, 2002, 6–11.
[26] Pastor D. et al.: Design of Apodized Linearly Chirped Fiber Gratings for Dispersion Compensation, Journal of Lightwave Technology, vol. 14, no. 11, 1996, 2581–2588.
[27] Sikora A.: Apodyzowane siatki Bragga o stałym okresie jako przetworniki odkształceń impulsowych. Analiza numeryczna. PAK, vol. 56, nr 12, 2010, 1436–1438.
[28] Stepniak P., Kisała P.: Analisys of impact long period Bragg gratings parameters on their special transmission characteristics. Proc. SPIE 10445, 2017, 104450G [doi: 10.1117/12.2280868].
[29] Theriault S. et al.: Effect of phase mask stitching errors on the spectral response of uniform and apodized fiber Bragg gratings. 8th Annual Meeting Conference Proceedings, vol. 1, 1995, 77–78.
[30] Wagner J.L. et al: Fiber Grating Optical Spectrum Analyzer Tap. Integrated Optics and Optical Fibre Communications, 11th International Conference on, and 23rd European Conference on Optical Communications, no. 448, 1997, 65–68 [doi: 10.1049/cp:19971613].
[31] Wang L. et al.: Impact of apodisation functions on group delay and reflectivity ripple of chirped fiber Bragg gratings. Optoelectronics Letters, vol. 2, no. 6, 2006, 430–432.
[32] Williams R. et al.: Modeling of apodized point-by-point fiber-Bragg gratings. 2011 International Quantum Electronics Conference (IQEC) and Conference on Lasers and Electro-Optics (CLEO) Pacific Rim incorporating the Australasian Conference on Optics, Lasers and Spectroscopy and the Australian Conference on Optical Fibre Technology, 133–135.
[33] Wójcik W., Kisała P.: Modelowanie struktur światłowodowych siatek Bragga wykorzystywanych w układach czujnikowych. PAK vol. 53, no.11, 2007, 10–14.
[34] Yu Y., Zhenhong Y.: Performance optimization of chirped fiber Bragg gratings by asymmetrical apodization. Proc. of the SPIE 10250, 2017, 1025003–6.

M.Sc. Łukasz Zychowicz
e-mail:lukas.zychowicz@gmail.com

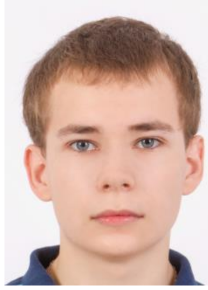

Łukasz Zychowicz is currently Ph.D. student in the Institute of Electronics and Information Technology of Lublin University of Technology (LUT). He is working as telecommunication networks designer. In 2016, he graduated from Mechatronics at LUT. His main scientific interests are apodized Bragg gratings.

M.Sc. Jacek Klimek
e-mail: j.klimek@pollub.pl

Jacek Klimek – assistant in the Electrical Engineering and Computer Science Faculty of the Lublin University of Technology, author of many publications on fiber-optic topics. His research focuses on the production and testing optical periodic structures known as Bragg gratings. Current scientific interests focus on issues related to bistable optical systems and complex periodic structures.

D.Sc. Piotr Kisała
e-mail: p.kisala@pollub.pl

Piotr Kisała is currently a professor in the Institute of Electronics and Information Technology of Lublin University of Technology (LUT), Lublin, Poland. He received the Ph.D. degree in 2009 and habilitation degree in 2013 from LUT. He is currently head of Optoelectronic & ICT Department at LUT. His research interests include optical sensors projects, fabrication and testing as well as designing and developing of unconventional FBG sensors. He has authored over 70 journal publications and conference contributions and 2 patents.

otrzymano/received: 10.10.2017 *przyjęto do druku/accepted: 15.02.2018*

DOI: 10.5604/01.3001.0011.6007

DEAD TIME MEASUREMENT BY TWO-SOURCE METHOD – OPTIMIZATION OF MEASUREMENT TIME DIVISION

Grzegorz Domański, Bogumił Konarzewski, Robert Kurjata, Krzysztof Zaremba, Janusz Marzec, Michał Dziewiecki, Marcin Ziembicki, Andrzej Rychter, Waldemar Smolik, Roman Szabatin, Piotr Brzeski
Warsaw University of Technology Institute of Radioelectronics and Multimedia Technology

Abstract. *The article presents the analysis of the dead time measurement using two sources for a non-paralyzable detector. It determined the optimum division of count rate measurement time between both source measurement and a single source one. Results of the work can be used to optimize dead time measurement for systems which count photons or particles.*

Keywords: dead time, count rate, two-source method

POMIAR CZASU MARTWEGO METODĄ DWÓCH ŹRÓDEŁ – OPTYMIZACJA PODZIAŁU CZASU POMIARU

Streszczenie. *W artykule zaprezentowano analizę pomiaru czasu martwego detektora nieparaliżowalnego metodą dwóch źródeł. Wyznaczono optymalny podział czasu pomiaru częstości zliczeń dla pomiaru jednym i dwoma źródłami. Wyniki pracy mogą być wykorzystane do optymalizacji systemów zliczających fotony lub cząstki.*

Słowa kluczowe: czas martwy, częstość zliczeń, metoda dwóch źródeł

Introduction

In many problems of nuclear techniques it is important to determine the detector dead time. In practice, there are two types of detectors: non-paralyzable and paralyzable (Chapter 4 in [1]). For the measurement of the dead time, there are two methods: two-source method [2, 3] and the method of short-lived single-source [1].

1. Theory

Two-source method of detector dead time measurement involves measuring the count rates for two radioactive sources separately, and then measuring the count rate from both radioactive sources together. For non-paralyzable detector it allows to easily determine the dead time.

Symbols:
m – count rate recorded by a detector of dead time τ,
n – count rate recorded by an ideal detector with zero dead time.

The following relationships occur:

$$m = \frac{n}{1 + n\tau} \qquad n = \frac{m}{1 - m\tau} \tag{1}$$

The following indexes are added for the count rate symbols: 1 – measurement for the first source, 2 – measurement for the second source, 12 – measurement for both sources together. For the measurement procedure used to measure the dead time one can write equation:

$$n_1 + n_2 = n_{12} \tag{2}$$

The count rate *n* can be replaced by expressions dependent on the respective count rate *m*:

$$\frac{m_1}{1 - m_1\tau} + \frac{m_2}{1 - m_2\tau} = \frac{m_{12}}{1 - m_{12}\tau} \tag{3}$$

After simple transformations quadratic equation form can be obtained:

$$m_1 m_2 m_{12}\tau^2 - 2m_1 m_2\tau + (m_1 + m_2 - m_{12}) = 0 \tag{4}$$

The solution to this equation are the two roots:

$$\tau' = \frac{1 - \sqrt{\left(1 - \frac{m_{12}}{m_1}\right)\left(1 - \frac{m_{12}}{m_2}\right)}}{m_{12}} \qquad \tau'' = \frac{1 + \sqrt{\left(1 - \frac{m_{12}}{m_1}\right)\left(1 - \frac{m_{12}}{m_2}\right)}}{m_{12}} \tag{5}$$

Due to the physical interpretation, only the first root is correct. It can be represented as

$$\tau = \frac{m_1 m_2 - \sqrt{m_1 m_2 (m_{12} - m_1)(m_{12} - m_2)}}{m_1 m_2 m_{12}} \tag{6}$$

Equation (6) allows to determine the dead time of the detector based on the count rate measurements m_1, m_2 and m_{12}.

To estimate the uncertainty of the dead time (the random error) the variance of the random variable τ need to be determined. However, use of a strict equation (6) leads to a very complex expression. Therefore, to evaluate the random error simplified formula is used:

$$\tau = \frac{m_1 + m_2 - m_{12}}{2m_1 m_2} = \frac{1}{2}\left(\frac{1}{m_1} + \frac{1}{m_2} - \frac{m_{12}}{m_1 m_2}\right) \tag{7}$$

obtained by assuming that in quadratic equation (4) the component τ_2 can be neglected.

The all above count rate values are mean values. To estimate the dead time uncertainty (the random error) the variances of the count rates m_1, m_2 and m_{12} presented in formula (7), will be required. Count rate m can be expressed depending on the number of registered pulses *M* and the measurement time *t*:

$$m = \frac{M}{t} \tag{8}$$

Then the variance of the random variable m is:

$$\sigma^2 m = \frac{\sigma^2 M}{t^2} = \frac{\overline{M}}{t^2} \approx \frac{M}{t^2} = \frac{m}{t} \tag{9}$$

with the obvious assumption that the number of registered pulses *M* is subject to the Poisson distribution, and the best approximation of its average value (for single measurement) is measured value M. In fact, the variance of registered counts, with non-zero dead time is less than that resulting from the Poisson distribution, but we accept this approximation in view of the establishment of a short dead time. We assumed here that dead time is short compared to the average time between successive counts. In the case that the above assumption is not fulfilled the full formula for the variance of the variable m should be used:

$$\sigma^2 m = \frac{m}{t(1+n\tau)^2} \tag{10}$$

The variance of the random variable τ is

$$\sigma^2\tau = \left|\frac{\partial\tau}{\partial m_1}\right|^2 \sigma^2 m_1 + \left|\frac{\partial\tau}{\partial m_2}\right|^2 \sigma^2 m_2 + \left|\frac{\partial\tau}{\partial m_{12}}\right|^2 \sigma^2 m_{12} \tag{11}$$

where the partial derivatives are respectively:

$$\frac{\partial\tau}{\partial m_1} = \frac{1}{2}\frac{m_{12}-m_2}{m_2 m_1^2} \qquad \frac{\partial\tau}{\partial m_2} = \frac{1}{2}\frac{m_{12}-m_1}{m_1 m_2^2} \qquad \frac{\partial\tau}{\partial m_{12}} = -\frac{1}{2m_1 m_2} \tag{12}$$

The formula (11), after using the necessary numerical values of variables, estimates the variance of the random variable τ (that is, the random error of measurement).

However, in addition to the knowledge of τ dispersion, it is useful to be able to select optimal partition of count rate measurement time. If the measurement times t_1 and t_2 will be equal it raises the question of what the relationship should be between these times and t_{12} measuring time to get the minimum random error of measurement dead time for the total measurement time equal to t = const.

Symbols:

$$\begin{aligned} & t_1 = t_2 = t_0 \\ & t_1 + t_2 + t_{12} = t = const \\ & 2t_0 + t_{12} = t = const \\ & t_0 = kt \\ & t_{12} = (1-2k)t \end{aligned} \tag{13}$$

where k is a constant with a value in the range of (0,0.5).

Using the above designations variance of the random variable τ can be written as:

$$\sigma^2 m = \frac{m}{t(1+n\tau)^2} \tag{14}$$

Differentiating expression for the variance of the random variable τ with respect to k one can determine the division of the measurement time t, which will provide the minimum value of the measured random error of dead time τ. To further transformations there will be adopted the following substitutions that can simplify equations:

$$A = \frac{(m_{12}-m_2)^2}{4m_2^2 m_1^3}, B = \frac{(m_{12}-m_1)^2}{4m_1^2 m_2^3}, C = \frac{m_{12}}{m_1^2 m_2^2} \tag{15}$$

After using these substitutions the optimum allocation of given measurement time t can be determined by solving the equation of the form:

$$\frac{\partial\sigma^2\tau}{\partial k} = -\frac{A}{k^2 t} - \frac{B}{k^2 t} + \frac{2C}{(1-2k)^2 t} = 0 \tag{16}$$

After simple transformations one can obtain the quadratic equation form:

$$[2C - 4(A+B)]k^2 + 4(A+B)k - (A+B) = 0 \tag{17}$$

The solution to this equation are the two roots:

$$k' = \frac{-1 - \frac{1}{2}\sqrt{\frac{2C}{A+B}}}{\frac{C}{A+B} - 2} \qquad k'' = \frac{-1 + \frac{1}{2}\sqrt{\frac{2C}{A+B}}}{\frac{C}{A+B} - 2} \tag{18}$$

Due to the physical interpretation, only the second root is valid – it can be represented as:

$$k = \frac{-1 + \frac{1}{2}\sqrt{2x}}{x-2}, \quad x = \frac{4m_1 m_2 m_{12}}{(m_{12}-m_2)^2 m_2 + (m_{12}-m_1)^2 m_1} \tag{19}$$

2. Results of measurements

Measurements of dead time in the spectrometric system that uses radiation detector type Ge(Li). A block diagram of the measurement system is shown in Figure 1.

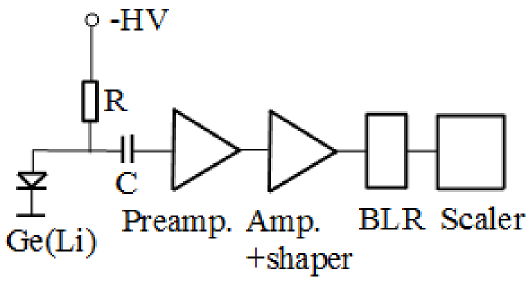

Fig. 1. The block schema of measurement system

It consists of a detector powered by the high voltage -1000V, preamplifier, shaping amplifier, base line restorer and scaler type PT-72. Three series of measurements using two Am-241 radioactive sources were made. The first series consisted of 10 measurements using the first source during 10 s, 10 measurements using the second one during 10 s and 10 measurements using both sources during 20 s. The second series consisted of 10 measurements using the first source during 1 s, 10 measurements using the second one during 1 s and 10 measurements using both sources during 40 s. The third series consisted of 10 measurements using the first source during 20 s, 10 measurements using the second one during 20 s and 10 measurements using both sources during 1 s. Mean count rates are presented in the Table 1.

The Table 2 shows the determined values of dead time and relative standard deviations for the three measurement series.

Table 1. The results of measurements of the count rates for the three measurement series

Serie	Source	Time [s]	Mean count rate [cps]
1	No. 1	10	12881
1	No. 2	10	6930
1	No. 1 + No. 2	20	15004
2	No. 1	1	12859
2	No. 2	1	6864.8
2	No. 1 + No. 2	40	14988
3	No. 1	20	12868
3	No. 2	20	6918.7
3	No. 1 + No. 2	1	14959

Table 2. The results of the determined values of dead time and relative standard deviation for the three measurement series

Serie	Total time [s]	Ratio k	Mean dead time τ [μs]	Relative standard deviation δ(τ)/τ
1	40	0.2500	37.437	0.0036
2	42	0.0238	37.185	0.0095
3	41	0.4878	37.792	0.0075

For the measured count rates and Poissonian approximation the optimum split of the time is determined by the ratio $k = 0.15$. For non-Poisson approximation the optimal value of k is about 0.28. The dependence of the relative standard deviation of the random variable τ with respect to the ratio k is shown in Figure 2 (assuming total measurement time of 40 s). Two curves – the first (solid line) calculated according to the formula (9) and the second (dashed line) calculated according to the formula (10) are shown. Location of the minimum on the first curve corresponds to the value calculated from the formula (19). The second curve was calculated using numerical approximation of derivatives for full accuracy formula (6). The relative standard deviation tends to infinity for two extreme cases, the parameter k close to zero or value of 0.5. In the first case, the measurement time for a single source tends to zero, and the relative error of count rate for a single source tends to infinity. In the second case, the value of the parameter k tends to 0.5 and the time of the measurement by both sources tends to zero, so the relative error of count rate for both sources also tends to infinity. The measured relative standard deviation values of the dead time are generally higher than predicted by the formula (11). This may be caused by instability of the measuring equipment.

3. Conclusions and discussion

The analysis of the dead time measurement uncertainty of non-paralyzable detector indicates the existence of an optimal allocation of measurement time between both sources. The formula for the optimal allocation of measurement time was derived assuming that the dead time is short compared to the average time between successive counts. Experimentally confirmed the existence of the optimal allocation of time. Results of the work can be used to optimize dead time measurement for systems which count photons or particles.

Bibliography

[1] Knoll G.F.: Radiation Detection and Measurement (4th ed.). Willey, 2010.

[2] Meeks C., Siegel P.B.: Dead time correction via the time series. Am. J. Phys. 76 (6), 2008, 589–590 [DOI: 10.1119/1.2870432].

[3] Myers R.T.: Dead Time of a Geiger-Mueller Tube by the Double-Source Method. Journal of Chemical Education 33(8), 1956, 395–396 [DOI: 10.1021/ed033p395].

Ph.D. Grzegorz Domański
e-mail: g.domanski@ire.pw.edu.pl

M.Sc. (1994), Ph.D. (2001); nuclear and medical electronics; Assistant Professor, Nuclear and Medical Electronics Division, Institute of Radioelectronics and Multimedia Technology, Faculty of Electronics and Information Technology, Warsaw University of Technology. Faculty Coordinator of Radiological Protection (2002-); Tutorial assistance of Biomedical and Nuclear Engineering Students Scientific Group (2013-).

Ph.D. Eng. Bogumil Konarzewski
Ph.D. Eng. Robert Kurjata
Prof. Krzysztof Zaremba
Prof. Janusz Marzec
Ph.D. Eng. Michał Dziewiecki
M.Sc. Eng. Marcin Ziembicki
Ph.D. Eng. Andrzej Rychter
Prof. Waldemar Smolik
Ph.D. Eng. Roman Szabatin
Ph.D. Eng. Piotr Brzeski

otrzymano/received: 15.06.2015 *przyjęto do druku/accepted: 15.02.2018*

DOI: 10.5604/01.3001.0010.8655

ANALYSIS OF THE BENDING STRAIN INFLUENCE ON THE CURRENT--VOLTAGE CHARACTERISTICS OF HTC SUPERCONDUCTING TAPES

Jacek Sosnowski
High Power Department, Electrotechnical Institute, Warsaw

Abstract. *Analysis of the influence of the bending strain on the electric properties of the HTc superconducting tapes is presented. The results of experimental investigations in liquid nitrogen temperature of the current-voltage characteristics and critical current of Bi-based tape are given for various bending strain values. Theoretical model of obtained dependences is proposed, while results of numerical calculations are in qualitative agreement with experimental data.*

Keywords:bending strain, current-voltage characteristics, HTc superconductors, capturing effects

ANALIZA WPŁYWU ODKSZTAŁCENIA PRZY ZGINANIU NA CHARAKTERYSTYKI PRĄDOWO-NAPIĘCIOWE WYSOKOTEMPERATUROWYCH TAŚM NADPRZEWODNIKOWYCH

Streszczenie*. Przeprowadzono analizę wpływu odkształcenia przy zginaniu na elektryczne własności wysokotemperaturowych taśm nadprzewodnikowych. Zaprezentowano wyniki badań doświadczalnych w temperaturze ciekłego azotu charakterystyk prądowo-napięciowych i prądu krytycznego taśm nadprzewodnikowych opartych na bizmucie, w funkcji wartości odkształcenia przy zginaniu. Teoretyczny model otrzymanych zależności został zaproponowany, którego numeryczne rezultaty są w dobrej jakościowej zgodności z wynikami doświadczalnymi.*

Słowa kluczowe: odkształcenie przy zginaniu, charakterystyki prądowo-napięciowe, nadprzewodniki wysokotemperaturowe, efekty zakotwiczenia

Introduction

Continuous growth of the critical temperature of the HTc superconductors bringing now the value of 203 K in sulfur hydride system [1] leads to the rapid increase of the interest in the applications of these materials in electric engineering. However we should remember that applications of them is dependent on the technical parameters of the HTc superconducting tapes, which are influenced by the subtle structure of ceramic superconductors, expressed for instance in sensitivity of their properties to bending strain. In paper is given electromagnetic analysis of the influence of this effect on the current-voltage characteristics of the HTc tapes. This model deals to both, the first and second generation HTc tapes, in which appear superconducting elements in the form of thin filaments or superconducting films stabilized by silver sheath. This topic is further important from scientific and technical point of view, investigated recently among other in [2, 4, 6], in which papers are presented changes of the electric properties of BSCCO, DI-BSCCO and YBCO tapes subjected to strain.

1. Experimental data

For verifying proposed in the next chapter theoretical model of the creation in the bending strain process of the micro-cracks in HTc superconducting tapes and influence of this effect on the electric properties of tapes, the experimental measurements have been performed. Four contacts method has been used for measuring current-voltage characteristics. Superconducting tape has been folded in room temperature up to required value of the bending strain, on the especial form and then this setup was cooled in the cryostat filled with liquid nitrogen. Direct electric current flowed through the high temperature superconducting tape and current-voltage characteristics have been measured using sensitive micro-voltmeter. The results of measurements current-voltage characteristics as the function of the bending strain are presented in the Fig. 1. Dots indicate the experimental data, while solid line is approximation by power function. The bending strain is defined according to the relation:

$$e\,(\%) = 100\ t/R \tag{1}$$

where e is value of the bending strain in percent, t half-thickness of the tape, R bending radius. Received on the base of these measurements, the influence of the bending strain on the critical current of the HTc superconducting tape is given in Fig. 2. It is seen, according to the Fig. 2 that for low values of the bending strain occurs reversible, elastic process, which does not influence significantly the critical current, while for higher bending strains there appear not reversible, destructive mechanical processes, creating micro-cracks, which lead to the decrease of the critical current. In the present case this decrease of the critical current with bending strain has been described by the linear approximation, fitted to the experimental data presented in Fig. 2.

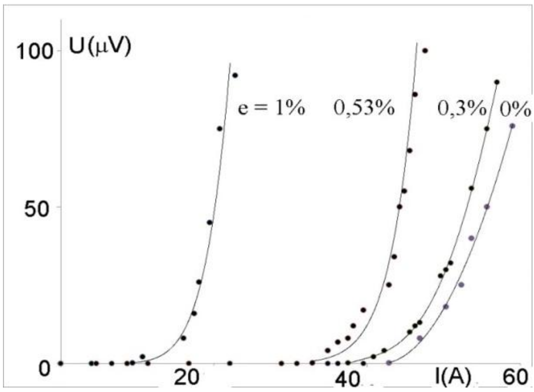

Fig. 1. Experimental current-voltage characteristics at liquid nitrogen temperature of high temperature superconducting BSCCO tape, as a function of the bending strain parameter e

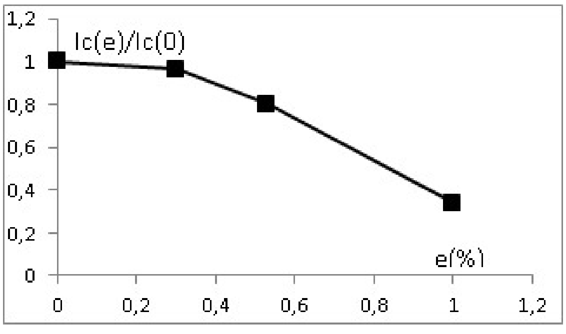

Fig. 2. The experimental (squares) and linearly approximated (solid line) dependence of the critical current of the HTc superconducting tape on the bending strain at liquid nitrogen temperature

In this paper it has been taken into account too in details geometrical effect indicating, that it will be slightly different bending strain value acting on the individual filament in the first generation tape or film in second generation, in comparison to bending strain applied to total superconducting tape. Schematically such bending strain geometrical effect is shown in Fig. 3 in simplified case in which individual filament is covered by the silver sheath. R_{out} is external radius of the tape during bending, R_{sh} radius then of the sheath, while R_{fil} radius of bent filamentin 1G or film in 2G tape. Taking into account the differences between geometrical lengths of these parameters we receive slightly different values of the applied to the superconducting tape bending strain e and bending strain acting on the filament e_{filg}. This effect is mathematically described by the following relations:

$$e = 100\cdot(R_{out} - R_{fil})/(R_{out} + R_{fil}) \quad (2)$$

$$e_{filg} = 100 \cdot(R_{sh} - R_{fil})/(R_{sh} + R_{fil}) \quad (3)$$

The calculated on this base relations between the bending strain parameters e and e_{filg} for various filaments thicknesses, in the relative units are given in the Fig. 4.These results indicate on the approximately linear dependence between above both parameters, it is $e_{filg} = \gamma e$, with γcoefficient of proportionality smaller than 1, for the case shown in the Fig. 4.

2. Theoretical analysis

Theoretical model has been elaborated next describing the influence of the bending strain on the electromagnetic properties: current-voltage characteristics and critical current I_C of HTc superconducting tapes, explaining measured dependences shown in Figs. 1-2.

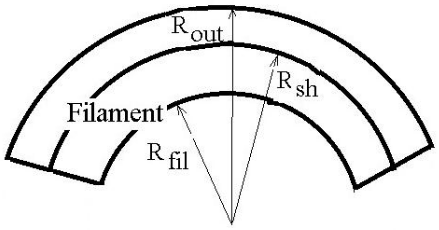

Fig. 3. Simplified view of the filament surrounded by the silver sheath in the superconducting tape at the bending strain process

In present approach analogously as in[3], it has been in details considered the subtle structure of the superconducting tape, composed from thin filaments or film immersed in silver matrix. Such theoretical analysis has important technical meaning because the effect of the bending strain appears in various applications of the superconducting tapes, especially occurs during winding process of the superconducting electromagnets. It concerns also the superconducting wires, in which filaments are usually twisted, while formed from them cables [5] can be also folded. Shown in Fig. 2 the dependence of the critical current on the bending strain e, describes the rupture probability function $G(e)$, which has been approximated here according to data of Fig. 2 through the linear relation:

$$G(e) = 1 - I_C(e)/I_C(0) = 0.96(e - e_c) \quad (4)$$

for $e > e_c = 0.3\%$. According to Fig. 2, for bending strain smaller than critical one e_c, appears in superconducting tape an elastic, reversible region, in which micro-cracks do not arise, therefore $G(e < e_c) = 0$. For higher bending strains it begins then the creation of the micro-cracks in the filaments or films, due to the breaking forces acting on the total tape and immersed in the silver matrix filaments. This effect will influence the transport of the electric current and critical current value, as shows Fig. 2. The elastic properties of silver matrix lead then to the reduction of the strain in filaments in comparison to the total applied strain. The regular ordering of the micro-cracks in the filaments allows to treat them as long line of deformed elements interlaced with the long line, which contains undeformed filaments. In resistive state it appears therefore analogy to the electrical long line of resistors as is shown in Fig. 5. R_1 in this figure, is the resistance on unit length of the undeformed filament in the resistive state, while R_2 is the resistance of the matrix and R_c is resistance on unit length of the deformed tape, by presence of micro-cracks.

Basing on the Fig. 5 it is easily to find then the simple mathematical relations describing variation with the depth of the voltage and current in such long line taking into account the leakage of the current through the normal matrix and voltage drop along the long line. For deformed by the existence of the micro-cracks long line the appropriate relations describing current and voltage variation $dV/dx = -R_c I$ and $dI/dx = -V/R_2$ lead to the following dependence:

$$\frac{\partial^2 I}{\partial x^2} = \frac{R_c}{R_2} I \quad (5)$$

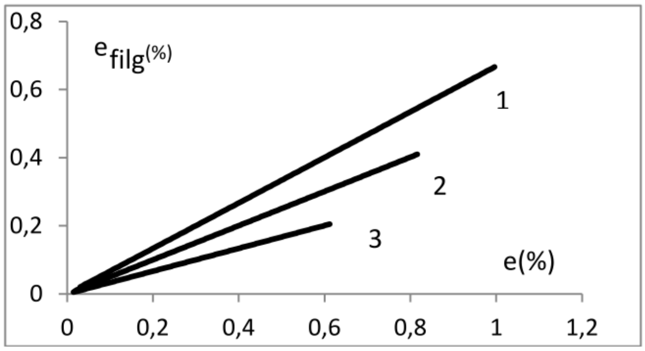

Fig. 4. Relation, following from the geometrical factor, between applied to the tape bending strain e and bending strain acting onthe filament e_{filg} calculated for various values of the filament thickness in relative units $z = (R_{out} - R_{sh})/(R_{sh} - R_{fil})$: (1) z = 0.5; (2) z = 1.0; (3)z = 2.0.

Decreasing with depth inside long line the solution of Eq. 5, describing the leakage of the current to the sheath, has been found in the exponential form:

$$I(x) = I(0)\cdot\exp\left(-\sqrt{\frac{R_c}{R_2}}x\right) \quad (6)$$

and then voltage variation has been determined:

$$V(x) = I(0)\sqrt{R_c R_2}\cdot\exp\left(-\sqrt{\frac{R_c}{R_2}}x\right) \quad (7)$$

while effective resistance per unit length of this deformed tape is:

$$R_{effd} = \sqrt{R_c \cdot R_2} \quad (8)$$

Analogously the expression for the effective resistance in resistive state per unit length of the tape, containing undeformed regions joined in parallel to the sheath, is:

$$R_{effu} = \sqrt{R_1 \cdot R_2} \quad (9)$$

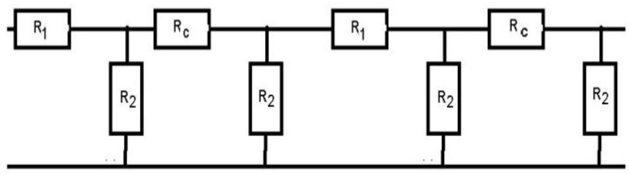

Fig. 5. Simulation of the HTc superconducting multifilamentary tape with ordered micro-cracks as the long line of resistors R_C and R_1

Similar picture has been applied next for the description of the elastic properties of the HTc superconducting tape, which determine then the micro-crack creation under bending strain process. It has been considered the relations between the elasticity spring constant k of the HTc superconducting tape and bending strain e acting on the total tape, with spring constant k_{fila} and bending strain e_{fila} in the filaments [3]. These last values due to amortizing effects of the silver sheath, expressed by the parameters k_{sh} and e_{sh} should be smaller. Additionally total bending strain acting on the filaments e_{fil} will be modified in the respect to the applied bending strain due to the geometrical reasons, finite thickness and curvature of the bended filaments, as it was described in previous chapter.

Relations between these parameters describing the elasticity properties of the deformed multifilamentary superconducting tape will be described therefore by the similar picture as in the case of the resistive long line model shown in the Fig. 5, where k_{fil} corresponds toR_1, while k_{sh} to R_2. Then as it was shown in [3] new relations arise joining the applied bending strain parameters e and acting on the filament e_{fila} with appropriate resistances in long line model approach $e/e_{fila} = R_1/R_{eff} = k_{fil}/k_{eff}$, where R_{eff} is the effective resistance on unit length of the long line shown in the Fig. 5. We should additionally introduce the condition connected with the fact that while the micro-cracks appear in filament then stress force will be directed onto the sheath, which elasticity properties are suppressed therefore, so elasticity parameter k_{sh} will decrease with enhancement of rupture probability $G(e)$. In the present paper such relation has been approximated by formula:

$$k_{sh} \approx k_{fila}\frac{1-G(e)}{1+G(e)} \tag{10}$$

Above considerations allow to determine then the bending strain acting on the filaments e_{fila}, the part connected with elasticity properties of the multifilamentary tape, as the function of the applied strain e:

$$e \approx e_{fila}\cdot\sqrt{\frac{1+G(e)}{1-G(e)}} \tag{11}$$

Eq. 11 is useful for evaluation next the length of the micro-cracks in the filament, which average value was assumed, to be determined by the difference between the applied e and acting on the filament total bending strain e_{fil}

$$e_{fil} = \gamma\cdot e\cdot e_{fila} \tag{12}$$

and is described according to the following relation:

$$l_e = \gamma(e-e_{fil})\frac{50\left(1+\frac{R_{out}-R_{sh}}{R_{sh}-R_{fil}}\right)+\frac{R_{out}-R_{sh}}{R_{sh}-R_{fil}}-\frac{1}{2}}{50\left(1+\frac{R_{out}-R_{sh}}{R_{sh}-R_{fil}}\right)+\frac{R_{out}-R_{sh}}{R_{sh}-R_{fil}}+\frac{1}{2}} \tag{13}$$

Here parameter l_e is the relative length of the microcracks in the deformed regions in the unit length of the tape, while parameters R_{sh},R_{out},R_{fil} describe the bending radius of sheath, radius of the total tape and bending radius of the filament as it was explained in the Fig. 3.The average depth of the micro-crack g is then given by the product

$$g = (R_{sh} - R_{fil})\cdot G(e) \tag{14}$$

according to the notation presented in the Fig. 3. Above equations indicate on the importance of the proper choice of the rupture probability function for determining the electric and elastic properties of the HTc superconducting tapes.

In the present paper it has been considered therefore, beside linear with bending strain form of function $G(e)$ described by Eq. 4,fractional and exponential approximations, which also correspond well to data shown in Fig. 2.

Results of calculations of the dependence of acting on filament elastic part of the bending strain as the function of applied bending strain are shown in Fig. 6 for various shapes of the $G(e)$ functions and indicate on the good agreement obtained between each of these approximations.

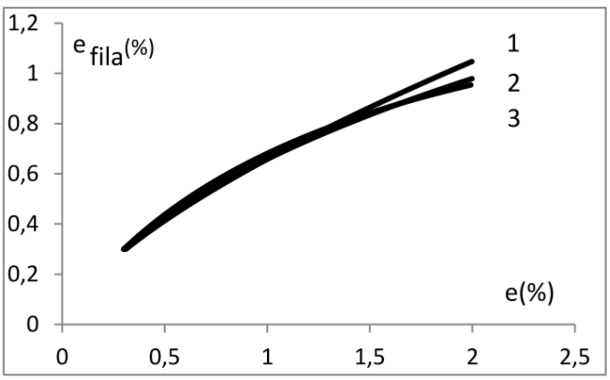

Fig. 6. Calculated dependence of the elastic part of the bending strain acting on HTc superconducting filament e_{fila} on the applied bending strain e for: (1) fractional, (2) exponential and (3) linear shape of the rupture probability function G(e)

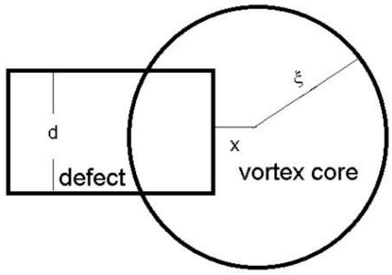

Fig. 7. Schematic view of the pancake shape magnetic vortex core interaction with the nano-defect of size d

Now we can pass therefore to the determination of the current-voltage characteristics of bended HTc superconducting tape. Effective resistance R_{eff} of the unit length of such tape is then the amount of these components given by Eqs. 8-9, with appropriate weight factor describing the relative lengths of these both regions in treated as long line superconducting tape, as it was explained previously:

$$R_{eff} = \sqrt{R_1(1-l_e)R_2}+\sqrt{R_c\cdot l_e\cdot R_2} \tag{15}$$

Existence of these two types of the regions denotes that although the same current flows through the superconducting tape others are current-voltage characteristics in both these regions: deformed and undeformed by the existence of the micro-cracks, because current density is different then. This effect concerns resistances R_1 and R_c connected with the undeformed section of the tape and the deformed one, respectively, as it follows from the relations:

$$R_1 = E(\tfrac{I}{S})/I\ , R_c = E(\tfrac{I}{S(1-G)})/I \tag{16}$$

$E(j = I/S)$ in Eq. 16 is just the current-voltage characteristic for the unit length of the superconducting tape, of the cross-section of tape S, while I is transport electric current. Right part of Eq. 16 gives the current-voltage characteristic divided on current for tape with microcrack, so with smaller cross-section, which is just described by the product S(1-G).

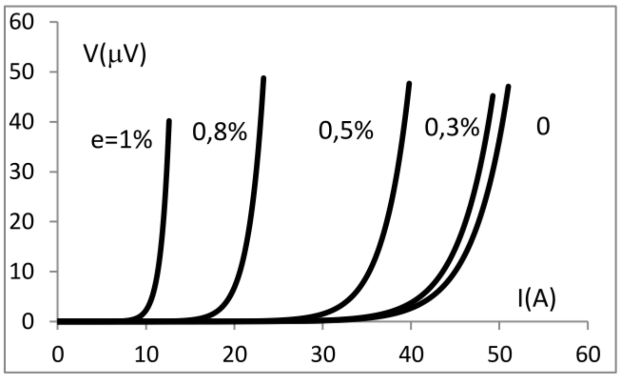

Fig. 8. Theoretically calculated influence of the bending strain e on the current-voltage characteristics of the HTc superconducting multifilamentary tape with ordered micro-cracks

As it follows from this equation16 very important function plays in the present considerations the shape of the current-voltage characteristics function $E(j)$. In the present paper theoretical model of the current-voltage characteristics has been applied, based on flux creep equation, describing flux creep forward and backward processes given by Eq. 17:

$$E = -B\omega\, a\left(e^{\frac{-\Delta U(0)(1+i)}{k_BT}} - e^{\frac{-\Delta U(i)}{k_BT}}\right) \tag{17}$$

Here $i = j/j_c$ is reduced to critical transport current density,ω is flux creep process frequency, a average distance between nano-defects acting as pinning centers, k_B means Boltzmann's constant, T temperature. Eq. 17 describes the current-voltage characteristics, which is required for solving relation 16 in the function of potential barrier for flux creep process $\Delta(i)$.

For determining the shape of this barrier detailed analysis has been performed of the capturing interaction between the pancake vortices specific for HTc multilayered superconductors with defects of rectangular shape, which correspond to micro-cracks. The geometrical scheme of such interaction shown in Fig. 7 presents the vortex core pinned on the normal state defect of the width *d* on the length x against the initial position, for which x = 0 and vortex is then half captured onto the depth of the coherence lengthξ. Various initial captured vortex positions have been considered in this analysis too. This model leads to following expression 18 for the potential barrier ΔU in the function of reduced current $i = I/I_c$ and nano-defect size *d* reduced to the coherence length ξ. H_c is critical magnetic field, *l* thickness of superconducting layer.

$$\Delta U(i) = \frac{\mu_0 H_c^2}{2} l \xi^2 \left(-\arcsin(i) + \arcsin\left(\frac{d}{2\xi}\right) + \frac{d}{2\xi}\sqrt{1-\left(\frac{d}{2\xi}\right)^2} - i\sqrt{1-i^2} \right) \tag{18}$$

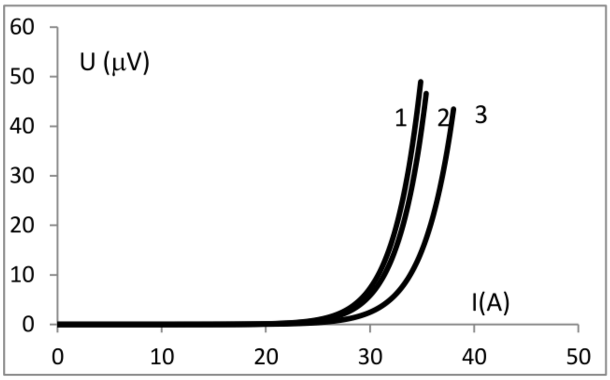

Fig. 9. Influence of the shape of the rupture probability function G(e) on the current-voltage characteristics U(I) of the HTc superconducting tape with ordered micro-cracks for e = 0.5%, B = 0.05 T at: (1) fractional approximation (2) exponential approximation (3) linear approximation

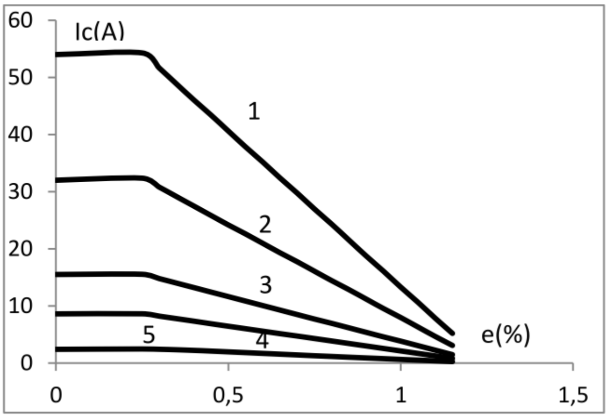

Fig. 10. Dependence of the critical current on the bending strain versus the coherence length: (1) ξ = 3 nm, (2) ξ = 3.57 nm,(3)ξ = 4 nm, (4)ξ = 5 nm, (5) ξ = 6 nm

Final results of calculations influence of bending strain on current-voltage characteristics are presented in Fig. 8for linear shape of the rupture probability function *G(e).*Results shown here well correspond qualitatively to the experimental data given in Fig. 1, which conclusion confirms validity of the presented model. On the importance of the rupture probability function *G(e)*at the critical current analysis indicates Fig. 9, in which is presented theoretically predicted influence of the form of this function *G(e)*: linear, fractional or exponential on the current-voltage characteristics of the HTc superconducting multifilamentary tape with regularly ordered micro-cracks. In Fig 10 are given the results of calculations influence of the coherence length on the dependence of the critical current versus the bending strain magnitude.

Realized work indicates on the importance of problem of deformation arising especially in the bending strain process, which influences the electrical properties of the HTc superconducting tapes, first and second generation, such as current-voltage characteristics and their critical currents.

References

[1] Drozdov A.P., Eremets M.I., Troyan I.A., Ksenofontov V., Shylin S.I.: Conventional superconductivity at 203 kelvin at high pressures in the sulfur hydride system. Nature Letter525/2015, 73–76.
[2] Gao P., Wang X.: Critical-current degeneration dependence on axial strain of Bi-based superconducting multi-filamentary composite tapes. Chinese Physics Lettersvol.31(4), 2014, 155–158.
[3] Kiss T. et al: Transport Properties of Multifilamentary Ag-Sheathed Bi-2223Tapes under the Influence of Strain. IEEE Trans. on Applied Superconductivity, vol. 11, 2001, 3888–3891.
[4] Panchal A., Bano A., Ghate M., Raj P., Pradhan S.: Indigenously developed bending strain setup for i-v characterization of superconducting tapes and wires. Journal of Physics: Conference Series, vol.823(1), 2017, 012045.
[5] Sosnowski J.: Superconducting cryocables. Book Publisher of Electrotechnical Institute, 2012.
[6] Zhou C., Yagotintsev K.A., Gao P., Haugan T.J., van Der Laan D.C., Nijhuis A.: Critical Current of Various REBCO Tapes Under Uniaxial Strain. IEEE Transactions on Applied Superconductivity, vol.26(4), 2016, 1–4.

Prof. Jacek Sosnowski
e-mail: j.sosnowski@iel.waw.pl

Prof. J. Sosnowski has graduated in the Physics Faculty of Warsaw University. Since 1980 year he is employed in the Electrotechnical Institute in Warsaw. He is specializing in the superconducting materials investigations, recently especially their electro-magnetic properties connected with the critical currents phenomena and applications of the high temperature superconductors in electric devices, ascable. In the issue of superconductivity he prepared Ph.D. and D.Sc. theses and received full professor title. He is author of about 300 papers published in polish and international Journals. He was awarded with price of International Electrotechnical Commission IEC. He teached superconductivity in Warsaw University of Technology and in Extramural PhD Course in Electrotechnical Institute. He was on the scientific stays in JINR in Russia, France, Japan, Germany.

otrzymano/received: 19.12.2017 *przyjęto do druku/accepted: 15.02.201*

DOI: 10.5604/01.3001.0010.8658

WYZNACZANIE CHARAKTERYSTYK R = F(T) TAŚM NADPRZEWODNIKOWYCH PIERWSZEJ I DRUGIEJ GENERACJI

Rafał Kwoka[1], Janusz Kozak[2], Michał Majka[1]
[1]Politechnika Lubelska, Instytut Elektrotechniki i Elektrotechnologii, [2]Instytut Elektrotechniki, Zakład Wielkich Mocy, Pracownia Technologii Nadprzewodnikowych

Streszczenie*. W artykule przedstawiono eksperymentalnie wyznaczone charakterystyki R = f(T) taśm nadprzewodnikowych pierwszej (1G) i drugiej generacji (2G). W pracy opisano sposób przygotowania próbek taśm nadprzewodnikowych 1G i 2G do badań, opisano metodę pomiarową oraz przedstawiono wyniki badań eksperymentalnych.*

Słowa kluczowe: nadprzewodnictwo, taśmy nadprzewodnikowe HTS pierwszej i drugiej generacji, nadprzewodnikowy ogranicznik prądu zwarciowego

DETERMINATION OF R = F(T) CHARACTERISTICS OF THE FIRST AND SECOND GENERATION SUPERCONDUCTING TAPES

Abstract. *The experimental characteristics R = f(T) of the first (1G) and the second (2G) generation HTS tapes are presented in this paper. The paper describes samples preparation of 1G and 2G superconducting tapes, describes the measurement method and the results of experimental studies.*

Keywords: superconductivity, 1st and 2nd generation HTS tape, superconducting fault current limiter

Wstęp

Obecnie produkowane taśmy nadprzewodnikowe pierwszej (1G) i drugiej generacji (2G) wytwarzane są w odcinkach o długości kilkuset metrów, a koszt ich wytwarzania jest coraz niższy. Taśmy nadprzewodnikowe znajdują zastosowanie w elektromagnesach, transformatorach nadprzewodnikowych, organicznikach prądów zwarciowych, silnikach elektrycznych czy też generatorach [2, 3, 4, 5, 8, 9]. Taśmy nadprzewodnikowe drugiej generacji bez stabilizatora miedzianego mają rezystancję w stanie rezystywnym wystarczająco dużą do budowy skutecznie działających ograniczników prądów zwarciowych.

Producenci taśm nadprzewodnikowych podają podstawowe parametry taśm nadprzewodnikowych takie jak szerokość taśmy, minimalną średnicę gięcia czy też wartość prądu krytycznego [4, 5, 8], nie podają jednak wartości rezystancji taśm mierzonych w różnych temperaturach. Charakterystyka $R = \mathrm{f}(T)$ taśmy nadprzewodnikowej jest niezbędna do projektowania nadprzewodnikowych ograniczników prądu zwarciowego i obliczeń modeli ograniczników metodą elementów skończonych.

1. Taśmy nadprzewodnikowe I i II generacji

Podział taśm nadprzewodnikowych na pierwszą i drugą generację wynika z różnicy w ich budowie wewnętrznej i technologii ich wytwarzania. Taśmy nadprzewodnikowe pierwszej generacji (1G) wytwarzane są metodą rurowo–proszkową [5]. Taśmy te mają budowę kompozytową i składają się z kilkudziesięciu włókien nadprzewodnika (Bi-2212 lub Bi-2223) umieszczonych wewnątrz srebrnej matrycy, rysunek 1 [5].

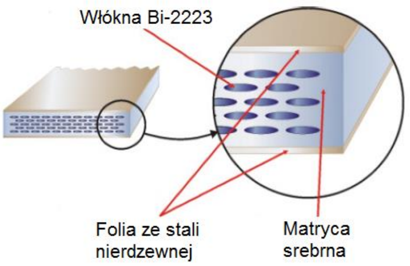

Rys. 1. Budowa taśmy nadprzewodnikowej pierwszej generacji [7]

Matrycą może być czyste srebro, stopy srebra ze złotem lub stopy innych metali [1]. Materiał matrycy ma decydujący wpływ na wytrzymałość mechaniczną taśmy. Obecnie głównym producentem taśm nadprzewodnikowych pierwszej generacji jest firma Sumitomo Electric. Parametry taśmy DI-BSCCO produkowanej przez Sumitomo zamieszczono w tabeli 1. Taśmy HTS 1G typu HT (HT–SS, HT–CA, HT–NX) charakteryzują się wzmocnioną mechaniczne konstrukcją, dzięki dwustronnemu pokryciu warstwą stali nierdzewnej, miedzi lub niklu. Dodatkowo taśma jest uszczelniona obustronnie lutem w celu ograniczenia wnikania cieczy kriogenicznej do wnętrza taśmy [11].

Tabela 1. Parametry taśm HTS pierwszej generacji DI-BSCCO produkcji Sumitomo Electric [11]

Taśmy pierwszej generacji DI-BSCCO firmy Sumitomo Electric	
Szerokość	2,8÷4,5 mm
Długość odcinkowa,	500÷1500 m
Grubość	0,23÷0,34 mm
Granica plastyczności	130÷400 MPa
Minimalna średnica gięcia	40÷80 mm
Materiał powłoki zewnętrznej	stal nierdzewna – 20 µm miedź – 50 µm nikiel – 30 µm
Prąd krytyczny $I_{C\,(77\,K)}$	60÷200 A

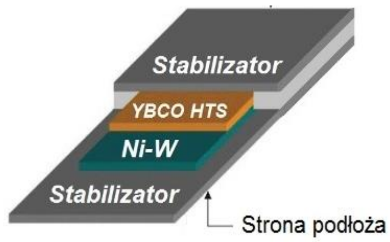

Rys. 2. Struktura taśmy HTS 2G firmy American Superconductor [10]

Tabela 2. Parametry taśm nadprzewodnikowych drugiej generacji produkowanych przez firmę American Superconductor [10]

Taśmy HTS drugiej generacji firmy American Superconductor	
Szerokość	4,24 ÷ 12,3 mm
Długość odcinkowa	300 ÷ 800 m
Grubość	0,18 ÷ 0,44 mm
Granica plastyczności, MPa	150 ÷ 200 MPa
Minimalna średnica gięcia, mm	40 ÷ 250 mm
Materiał powłoki zewnętrznej	stal nierdzewna – 25 µm miedź – 50 µm
Prąd krytyczny I_C w temp. 77 K	60 ÷ 200 A

Taśmy nadprzewodnikowe drugiej generacji (taśmy HTS 2G) składają się z szeregu warstw, z których wyróżniamy: warstwę podłoża odpowiadającą za parametry mechaniczne taśmy, kilku warstw buforowych, warstwy nadprzewodnika, warstwy srebra i warstwy stabilizatora miedzianego [2, 6, 12]. Strukturę taśm nadprzewodnikowych HTS drugiej generacji, której parametry zamieszczono w tabeli 2 i tabeli 3 przedstawiają rysunki 2 i 3.

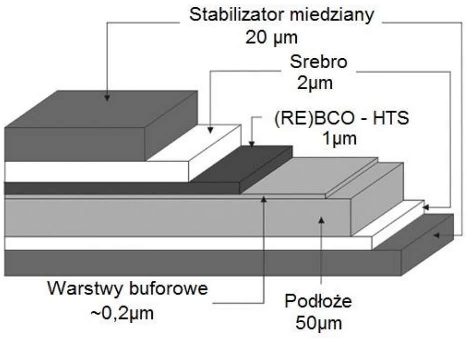

Rys. 3. Przekrój poprzeczny taśmy HTS 2G firmy SuperPower

Tabela 3. Parametry taśm nadprzewodnikowych drugiej generacji produkowanych przez firmę SuperPower [12]

Taśmy HTS drugiej generacji firmy SuperPower	
Szerokość	3÷12
Długość odcinkowa	300÷600 m
Grubość	0,055÷0,105 mm
Granica plastyczności	650÷1200 MPa
Minimalna średnica gięcia	11÷25 mm
Materiał powłoki zewnętrznej	miedź – 50 µm
Prąd krytyczny I_C w temp. 77 K	75÷300 A

2. Przygotowanie próbek taśm HTS 1G i 2G do wyznaczania charakterystyk R = f(T)

Próbka taśmy nadprzewodnikowej przygotowana do wyznaczenia charakterystyki $R = f(T)$ metodą czteroprzewodową ma przylutowane dwa doprowadzenia prądowe (I-, I+) i dwa napięciowe (V-, V+) (rys. 4). Rozstaw przewodów pomiarowych wynosi 100 mm. Lutowanie przewodów pomiarowych do taśmy nadprzewodnikowej wykonano lutownicą na gorące powietrze w temperaturze zgodnie z zaleceniami producenta taśm nadprzewodnikowych (tabela 4). Do lutowania zastosowano pastę lutowniczą Sn62Pb36Ag2 o temperaturze topnienia 179°C.

Tabela 4. Zalecenia firmy SuperPower dotyczące lutowania taśm HTS [12]

	SCS	SF
Temperatura lutowania, ºC	200	195
Max. temp. lutowania, ºC	240	240

W celu wyznaczenia charakterystyki $R = f(T)$ został wykonany uchwyt dla próbek taśm nadprzewodnikowych. Uchwyt próbki taśmy wykonany z kompozytu szklano – epoksydowego do którego zamocowane są dwa płaskowniki miedziane izolowane folią poliamidową o grubości 50 µm. W płaskownikach wykonane są rowki w miejscach, w których do próbki przylutowane są przewody pomiarowe. Po skręceniu uchwytu taśma nadprzewodnikowa przylega z obu stron do płaskowników, próbka jest izolowana elektrycznie. Temperatura taśmy nadprzewodnikowej mierzona była kriogenicznym czujnikiem temperatury Cernox umieszczonym w otworze bloku miedzianego.

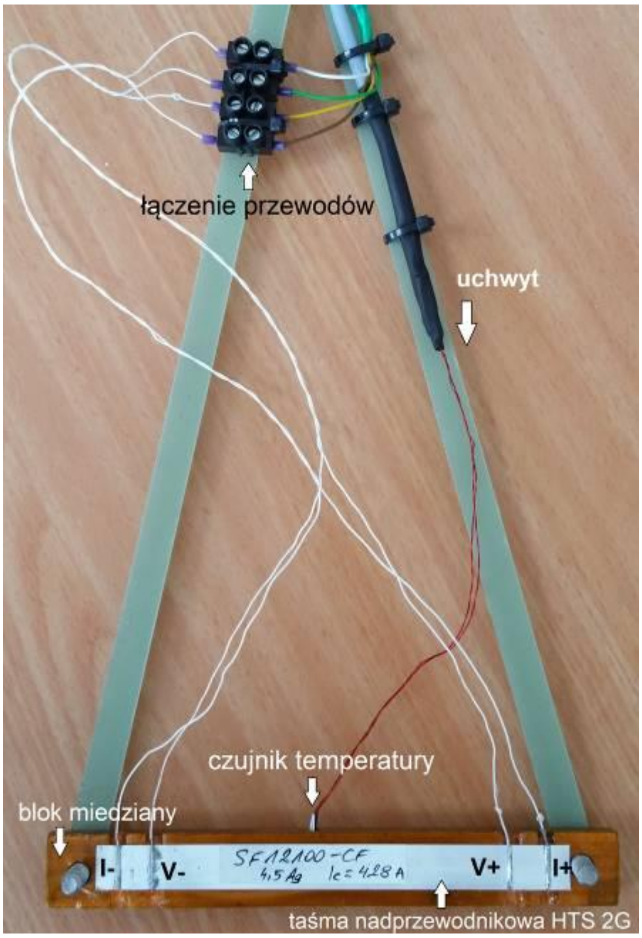

Rys. 4. Próbka taśmy HTS 2G w uchwycie

Charakterystyki wyznaczono dla kilku próbek taśm nadprzewodnikowych pierwszej i drugiej generacji. Wybrane próbki przedstawiono na rysunkach:

- 5a, 5b – taśmy 1G,
- 6c, 6d – taśmy 2G typu SCS ze stabilizatorem miedzianym,
- 7e, 7f – taśmy 2G typu SF bez stabilizatora miedzianego.

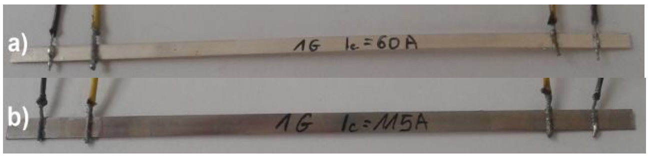

Rys. 5. Próbki taśm HTS pierwszej generacji: a) taśma typu AMSC HSW (I_c = 60 A), b) taśma typu AMSC HSPW (Ic = 115 A)

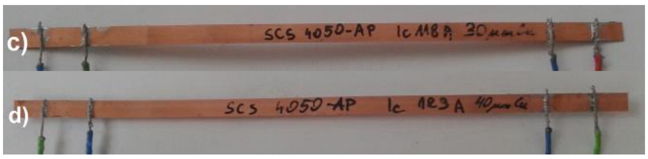

Rys. 6. Próbki taśm HTS drugiej generacji: c) taśma typu SCS (I_c = 118 A), d) taśma typu SCS (I_c = 123 A)

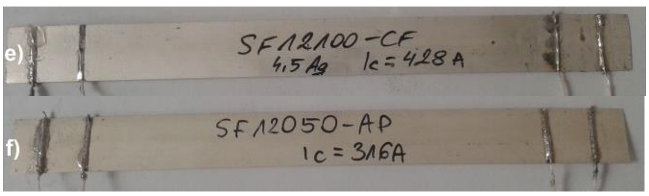

Rys. 7. Próbki taśm HTS 2G: e) typu SF12100-CF (I_c = 428 A) i f) typu SF12050-AP (I_c = 316 A)

3. Układ pomiarowy

Do wyznaczenia charakterystyk $R = f(T)$ taśm nadprzewodnikowych zaprojektowano i wykonano układ pomiarowy składający się z miernika temperatury LakeShore Model 218, układu sterowania, komputera pomiarowego z oprogramowaniem NI LabView, karty pomiarowej USB-6343 oraz kriostatu z ciekłym azotem do schłodzenia próbki (rysunek 8). Uproszczony schemat układu pomiarowego przedstawiono na rys. 9.

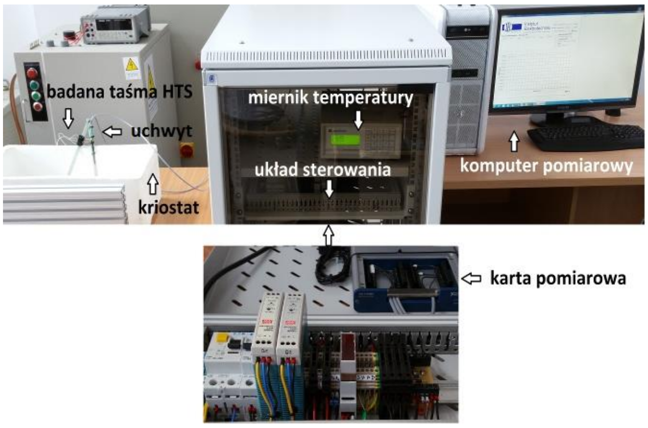

Rys. 8. Laboratoryjny układ pomiarowy

Wszystkie urządzenia laboratoryjnego układu pomiarowego są skomunikowane z komputerem. Oprogramowanie napisane w środowisku LabView umożliwia wykonanie pomiarów, wykreślenie charakterystyki oraz zapisanie rezultatów.

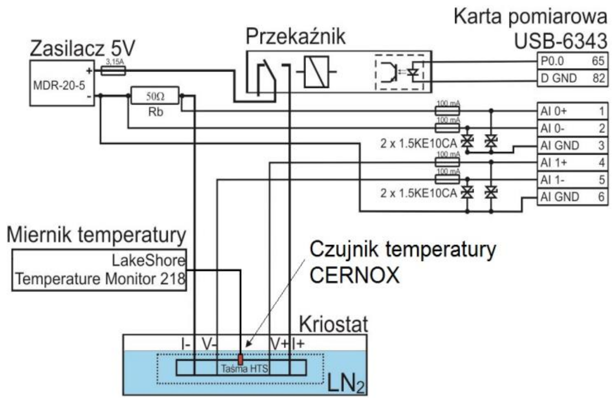

Rys. 9. Schemat układu pomiarowego

4. Wyznaczanie charakterystyk R = f(T) taśm nadprzewodnikowych 1G i 2G

Wykonano serie pomiarów taśm nadprzewodnikowych, których najważniejsze parametry zestawiono w tabeli 6.

Tabela 6. Parametry zastosowanych taśm nadprzewodnikowych HTS [10, 12]

Taśma HTS	SF 12050 AP	SF 12100 CF	SCS 4050 AP	SCS 4050 AP	AMSC HSW	AMSC HSPW
	2G	2G	2G	2G	1G	1G
Szerokość taśmy, mm	12	12	4	4	4	4
Grubość warstwy srebra, µm	2	4,5	2	2	-	-
Grubość warstwy miedzi, µm	-	-	30	40	-	-
Prąd krytyczny, A	316	428	118	123	60	118

Po schłodzeniu uchwytu z próbką taśmy nadprzewodnikowej w kąpieli ciekłym azotem do temperatury 77 K (rysunek 10) uchwyt został wyjęty z kriostatu w celu powolnego ogrzania. Schłodzoną próbkę ogrzewano do temperatury pokojowej. Podczas jej ogrzewania mierzona była jej rezystancja i temperatura w zakresie od 77 do 300 K. Wyniki pomiarów rejestrowano przy użyciu programu napisanego w środowisku LabView (rysunek 11). Program umożliwia odczyt temperatury z miernika LakeShore Temperature Monitor 218 przez port GPIB, pomiar rezystancji próbki taśmy metodą czteroprzewodową oraz zapis wyników do pliku *.xls.

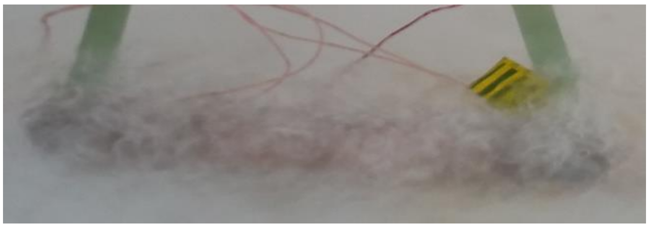

Rys. 10. Chłodzenie próbki w ciekłym azocie

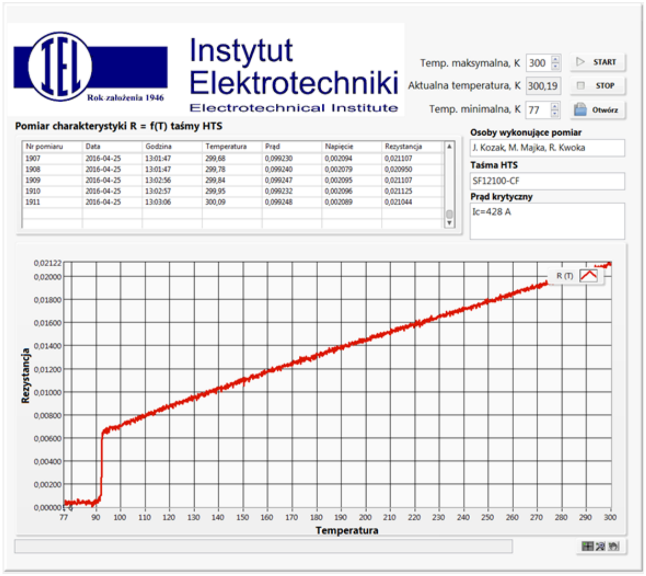

Rys. 11. Program napisany w środowisku LabView do pomiaru charakterystyki R = f(T) taśm nadprzewodnikowych

Otrzymane wyniki wyznaczonych charakterystyk $R = f(T)$ taśm nadprzewodnikowych zaprezentowano na rysunku 12. Rezystancja taśm zmierzona w temperaturze 77 K jest bliska zeru. Na charakterystyce widoczne jest przejście nadprzewodnika ze stanu nadprzewodzącego do stanu rezystywnego po przekroczeniu temperatury krytycznej. Najmniejszą rezystancję w stanie rezystywnym uzyskały taśmy 1G AMSC HSW i HSPW, taśma SF12100 ma około dwukrotnie mniejsza rezystancję od taśmy SF12050-AP, wynika to z różnicy w grubości warstwy srebra.

W obliczeniach uzwojeń w nadprzewodnikowych ogranicznikach prądu zwarciowego uwzględnia się zarówno rezystancję taśmy jak i jej pojemność cieplną. Parametry te umożliwiają obliczenie temperatury taśmy podczas zwarcia [3, 4]. Taśma SF12100-CF ma dwukrotnie grubszą warstwę podłoża w porównaniu do taśmy SF12050-AP, dzięki czemu charakteryzuje się większą pojemnością cieplną i umożliwia zaprojektowanie nadprzewodnikowego ogranicznika prądu zwarciowego na dłuższy czas zwarcia.

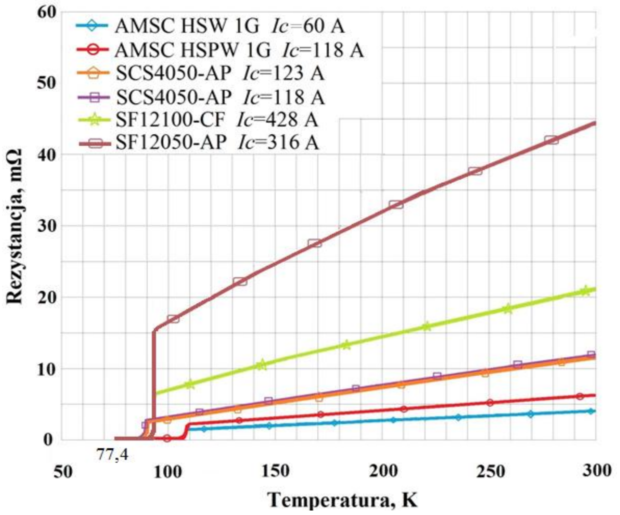

Rys. 12. Wyznaczone eksperymentalnie charakterystyki R = f(T) taśm nadprzewodnikowych pierwszej i drugiej generacji (długość próbki 100 mm)

5. Wnioski

W artykule przedstawiono sposób przygotowania próbek taśm nadprzewodnikowych do badań, opisano metodę pomiarową i sposób wyznaczania charakterystyki $R = \mathrm{f}(T)$ taśm nadprzewodnikowych. Przedstawiono unikatowe wyniki nowej, niedostępnej na rynku komercyjnym próbce taśmy nadprzewodnikowej SF 12100-CF o grubości warstwy srebra 4,5 μm.

Taśmy nadprzewodnikowe drugiej generacji bez stabilizatora miedzianego SF12050-AP oraz SF12100-CF są specjalnie zaprojektowane do zastosowania w nadprzewodnikowych ogranicznikach prądu zwarciowego. Przy prądach roboczych prąd płynący w taśmie nadprzewodnikowej jest mniejszy od prądu krytycznego taśmy I_C. W stanie nadprzewodzącym prąd płynie w warstwie nadprzewodnika REBCO z pominięciem innych warstw. Podczas zwarcia wartość prądu w taśmie kilkukrotnie przekracza wartość prądu krytycznego I_C, nadprzewodnik przechodzi do stanu rezystywnego i prąd w taśmie płynie głównie przez warstwę srebra oraz podłoże. Podczas zwarcia zarówno temperatura jak i rezystancja taśmy szybko rośnie, dlatego do prawidłowego projektowania ogranicznika konieczne jest eksperymentalne wyznaczenie charakterystyki $R = \mathrm{f}(T)$.

Literatura

[1] Baldan C.A., Oliveira U.R., Shigue C.Y., Filho E.R.: Evaluation of Electrical Properties of Lap Joints for BSCCO and YBCO Tapes. IEEE Transactions on Applied Superconductivity 3(19)/2009, 2831–2834 [DOI: 10.1109/TASC.2009.2017701].

[2] Kozak J., Majka M.: Technologia łączenia taśm HTS 2G w uzwojeniach nadprzewodnikowych urządzeń elektrycznych. Przegląd Elektrotechniczny 3(90)/2014, 157–160 [DOI: 10.12915/pe.2014.03.34].

[3] Kozak J., Majka M., Janowski T., Kozak S., Wojtasiewicz G., Kondratowicz-Kucewicz B.: Tests and performance analysis of coreless inductive HTS fault current limiters. IEEE Transactions on Applied Superconductivity 3(12)/2011, 1303–1306 [DOI: 10.1109/TASC.2010.2101033].

[4] Kozak S., Janowski T., Kondratowicz–Kucewicz B., Kozak J., Wojtasiewicz G.: Experimental and numerical analysis of energy losses in resistive SFCL. IEEE Transactions on Applied Superconductivity 2(15)/2005, 2098–2101 [DOI: 10.1109/TASC.2005.849461].

[5] Majka M., Kozak S.: Zastosowanie taśm I i II generacji do budowy nadprzewodnikowych ograniczników prądu. Przegląd Elektrotechniczny 5(89)/2009, 183–185.

[6] Nguyen N. T., Tixador P.: A YBCO-coated conductor for a fault current limiter: architecture influences and optical study. Superconductor Science and Technology 2(23)/2010 [DOI: 10.1088/0953-2048/23/2/025008].

[7] Salazar A., Pastor J. Y., Lorca J.: Fatigue behavior of multifilamentary BSCCO 2223/Ag superconducting tapes. IEEE Transactions on Applied Superconductivity 3(14)/2004, 1841–1847, [DOI: 10.1109/TASC.2004.830606].

[8] Suarez P., Alvarez A., Ceballos J. M., Perez B.: Loss and transition studies of shunted free-stabilized YBCO tape for SFCL applications. IEEE Transactions on Applied Superconductivity 2(21)/2011, 1267–1270, [DOI:10.1109/TASC.2010.2102991].

[9] Woźniak Ł., Wojtasiewicz G., Surdacki P., Komarzyniec G., Kwoka R.: Wpływ parametrów transformatora nadprzewodnikowego na ograniczenie prądu w stanach przejściowych. Przegląd Elektrotechniczny 7(92)/2016, 61–64, [DOI:10.15199/48.2016.07.12].

[10] American Superconductor, HTS Wire [17.05.2016].

[11] Sumitomo Electric, HTS Wire, www.global-sei.com [30.05.2016].

[12] SuperPower 2G HTS Wire Specifications, www.superpower-inc.com [10.05.2016].

Mgr inż. Rafał Kwoka
e-mail: rafal_kwoka@wp.pl

Ukończył studia magisterskie w 2012 roku na Wydziale Elektrotechniki i Informatyki Politechniki Lubelskiej. Obecnie doktorant w Instytucie Elektrotechniki i Elektrotechnologii na Wydziale Elektrotechniki i Informatyki Politechniki Lubelskiej. Zajmuję się badaniami taśm nadprzewodnikowych HTS stosowanych do budowy nadprzewodnikowych ograniczników prądu zwarciowego.

Dr hab. inż. Janusz Kozak, prof. IEL
e-mail: j.kozak@iel.waw.pl

Profesor nadzwyczajny w Pracowni Technologii Nadprzewodnikowych Instytutu Elektrotechniki. 2005–2007 pracował w CERN, gdzie zajmował się badaniem elektromagnesów nadprzewodnikowych dla LHC. W 2009 roku pracował w CERN przy uruchomieniu akceleratora LHC. Otrzymał Nagrodę Główną w Konkursie ABB w 2010 r. Jest współautorem ponad 50 publikacji w tym 31 z listy filadelfijskiej. Jest współtwórcą 6 patentów.

Dr inż. Michał Majka
e-mail: m.majka@pollub.pl

Adiunkt w Instytucie Elektrotechniki i Elektrotechnologii Wydziału Elektrotechniki i Informatyki Politechniki Lubelskiej, gdzie zajmuje się projektowaniem i badaniami urządzeń nadprzewodnikowych: ograniczników prądu, elektromagnesów nadprzewodnikowych, zasobników energii oraz transformatorów. Współautor dwóch monografii, kilkudziesięciu publikacji naukowych i dwóch patentów. Brał udział w realizacji kilku projektów badawczych.

otrzymano/received: 15.06.2015 *przyjęto do druku/accepted: 15.02.2018*